BODIPYs AND THEIR DERIVATIVES: THE PAST, PRESENT AND FUTURE

EDITED BY: Hua Lu and Zhen Shen
PUBLISHED IN: Frontiers in Chemistry

frontiers Research Topics

ISSN 1664-8714
ISBN 978-2-88963-786-7
DOI 10.3389/978-2-88963-786-7

About Frontiers

Frontiers is more than just an open-access publisher of scholarly articles: it is a pioneering approach to the world of academia, radically improving the way scholarly research is managed. The grand vision of Frontiers is a world where all people have an equal opportunity to seek, share and generate knowledge. Frontiers provides immediate and permanent online open access to all its publications, but this alone is not enough to realize our grand goals.

Frontiers Journal Series

The Frontiers Journal Series is a multi-tier and interdisciplinary set of open-access, online journals, promising a paradigm shift from the current review, selection and dissemination processes in academic publishing. All Frontiers journals are driven by researchers for researchers; therefore, they constitute a service to the scholarly community. At the same time, the Frontiers Journal Series operates on a revolutionary invention, the tiered publishing system, initially addressing specific communities of scholars, and gradually climbing up to broader public understanding, thus serving the interests of the lay society, too.

Dedication to Quality

Each Frontiers article is a landmark of the highest quality, thanks to genuinely collaborative interactions between authors and review editors, who include some of the world's best academicians. Research must be certified by peers before entering a stream of knowledge that may eventually reach the public - and shape society; therefore, Frontiers only applies the most rigorous and unbiased reviews.
Frontiers revolutionizes research publishing by freely delivering the most outstanding research, evaluated with no bias from both the academic and social point of view. By applying the most advanced information technologies, Frontiers is catapulting scholarly publishing into a new generation.

What are Frontiers Research Topics?

Frontiers Research Topics are very popular trademarks of the Frontiers Journals Series: they are collections of at least ten articles, all centered on a particular subject. With their unique mix of varied contributions from Original Research to Review Articles, Frontiers Research Topics unify the most influential researchers, the latest key findings and historical advances in a hot research area! Find out more on how to host your own Frontiers Research Topic or contribute to one as an author by contacting the Frontiers Editorial Office: researchtopics@frontiersin.org

BODIPYs AND THEIR DERIVATIVES: THE PAST, PRESENT AND FUTURE

Topic Editors:
Hua Lu, Hangzhou Normal University, China
Zhen Shen, Nanjing University, China

Citation: Lu, H., Shen, Z., eds. (2020). BODIPYs and Their Derivatives: The Past, Present and Future. Lausanne: Frontiers Media SA. doi: 10.3389/978-2-88963-786-7

Table of Contents

frontiers in Chemistry

EDITORIAL
published: 28 April 2020
doi: 10.3389/fchem.2020.00290

Editorial: BODIPYs and Their Derivatives: The Past, Present and Future

Hua Lu[1]* *and Zhen Shen*[2]*

[1] Key Laboratory of Organosilicon Chemistry and Material Technology, Ministry of Education, and Key Laboratory of Organosilicon Material of Zhejiang Province, Hangzhou Normal University, Hangzhou, China, [2] State Key Laboratory of Coordination Chemistry, Nanjing National Laboratory of Microstructures, Nanjing University, Nanjing, China

Keywords: BODIPY, dyes/pigments, spectroscopic properties, synthesis, borate complexes

Editorial on the Research Topic

BODIPYs and Their Derivatives: The Past, Present and Future

Over the past decades, boron-dipyrromethene (4,4-difluoro-4-bora-3a,4a-diaza-s-indacene, BODIPY) fluorescent dyes, first described by Treibs and Kreuzer, have been the focus of considerable research interest and rapidly growing (Treibs and Kreuzer, 1968). Their structural versatility makes it possible to fine-tune their spectroscopic properties, and therefore they have been used in many scientific and technological fields (Loudet and Burgess, 2007; Ulrich et al., 2008; Boens et al., 2012, 2019; Kamkaew et al., 2013; Lu et al., 2014, 2016; Ni and Wu, 2014; Kowada et al., 2015; Zhao et al., 2015; Bañuelos, 2016; Sheng et al., 2019; Turksoy et al., 2019). This Research Topic mainly focuses on the most innovative research regarding the synthesis, spectroscopic properties, theoretical calculations, and application of BODIPY dyes and their derivatives. Four reviews and six original research articles by recognized academic experts are collected, which will offer a broad perspective for BODIPY chemistry and provide powerful guidance for the future rational design of BODIPY dyes and their derivatives with properties suitable for applications. We believe this Research Topic should attract the attention of multidisciplinary researchers and continue to promote BODIPY chemistry as a vibrant and highly multidisciplinary research field.

The contribution of Miao et al. summarizes fluorescent molecular rotors based on BODIPY for viscosity detection, providing key strategies for the design of various functional BODIPYs covering the red to NIR wavelength region for biological-related viscosity imaging. Triplet photosensitizers based on BODIPYs continue to attract increasing attention due to their extensive applications in photocatalysis, photodynamic therapy and photon upconversion. The contribution from Chen et al. reviews and classifies BODIPY-derived triplet photosensitizers based on ISC mechanisms, including the heavy atom effect, exciton coupling, and charge recombination (CR)-induced ISC, using a spin converter and radical enhanced ISC. Importantly, the molecular structure factors and mechanism of ISC-efficient are analyzed in-depth. This review affords fascinating insight for the rational design of novel BODIPY-based triplet photosensitizers. Typically, BODIPY dyes demonstrate weak fluorescence in the aggregation state duo to the self-absorption and strong intermolecular interactions, which restrict their application as solid-state emitters. In recent years, a number of AIE-active BODIPYs have been reported, but there remains a lack of general guidance regarding structural design. Therefore, Liu et al. summarize the AIE-active BODIPYs, their analogs boron-complexes, and their application in fluorescent imaging, gas sensors and as mechanofluorochromic (MFC) materials. The mechanism and structural factor for the aggregated fluorescent enhancement are further discussed to facilitate their future development. This review points out broad approaches for the design and application of BODIPYs as aggregation-state emitters, thus promoting, and enriching BODIPY chemistry. In addition to the three reviews already mentioned, which focus

OPEN ACCESS

Edited and reviewed by:
Tony D. James,
University of Bath, United Kingdom

***Correspondence:**
Hua Lu
hualu@hznu.edu.cn
Zhen Shen
zshen@nju.edu.cn

Specialty section:
This article was submitted to Supramolecular Chemistry, a section of the journal Frontiers in Chemistry

Received: *10 March 2020*
Accepted: *23 March 2020*
Published: *28 April 2020*

Citation:
Lu H and Shen Z (2020) Editorial: BODIPYs and Their Derivatives: The Past, Present and Future. Front. Chem. 8:290. doi: 10.3389/fchem.2020.00290

on molecular design and application, one contribution by Gupta and Kesavan concentrates on the synthesis and spectroscopic properties of BODIPY. Gupta and Kesavan summarize and classify BODIPYs containing a carbazole ring at *alpha*, *beta*, and *meso*-positions, and carbazole based hybrid BODIPYs, carbazole linked aza-BODIPYs, as well as carbazole-fused boron-complexes. The effects of a carbazole substituent in different positions on the optical properties of the BODIPYs are presented by tabulating their spectral properties.

The six research articles, on the other hand, focus on different aspects, mainly fluorescent probe and imaging, as well as synthesis and spectroscopic properties of bis-BODIPY and its optical limiting properties. Bartelmess et al. develop a BODIPY-cobaloxime complex for the detection of H_2S in the liquid and gas phase. The selective substitution by the HS^- anion at the cobalt center releases the free BODIPY fluorophore, thus recovering the BODIPY fluorescence. The contribution by Wang et al. designs a FRET fluorescent probe for ratiometric detection of H_2S *in vitro* and *in vivo*. Monochlorinated BODIPY can react with HS^- to form HS-BODIPY, thus affording a ratiometric fluorescent change. Interestingly, NIR-II fluorescence at 920 nm is observed, making the formation mechanism worthy of further study. The work by Qu et al. investigates a NIR BODIPY probe using triphenylphosphine as a reactive site for hydroxyl radical recognition and its bioimaging in HeLa cells, providing a new way to construct a molecular recognition system for biological application. Self-assembling BODIPY nanoparticles for bioimaging remain largely unexplored. The work of Ma et al. looks into the nanoparticles containing BODIPY with spherical and rod like morphology for cell imaging. Interestingly, the rod-like nanoparticles display great potential for bioimaging in efficient delivery and imaging efficacy, affording promising information for the design of bioimaging materials.

Oliden-Sánchez et al. describe the synthesis, photophysical, and lasing properties of a serial of bis-BODIPYs with spacers consisting of urea-, thiourea-, phosphonate-, amine-, disulfur-, and ether-based linkers. The spectroscopic behavior of bis-BODIPYs can be effectively tuned by the length and/or stereoelectronic properties of the spacer. The influence of the bridging moiety, solvent-effect and mechanism are systematically studied and analyzed in-depth, thus providing powerful guidelines for the future design of tailored bis-BODIPYs for wide applications. Non-linear optical properties of BODIPY have not been as extensively studied as their linear optical properties. The work of Ngoy et al. investigates the optical limiting properties of a 3.5-styryl BODIPY dye by using the open-aperture Z-scan technique. Since transparence of optical limiting materials remains a challenge, the authors point out how the structural modification of the BODIPYs to enhance this ESA, while shifting the main spectral band to the red, is the direction of future efforts.

AUTHOR CONTRIBUTIONS

All authors listed have made a substantial, direct and intellectual contribution to the work, and approved it for publication.

ACKNOWLEDGMENTS

We acknowledge financial support by the National Natural Science Foundation of China (Nos. 21871072 and 21771102).

REFERENCES

Bañuelos, J. (2016). BODIPY dye, the most versatile fluorophore ever? *Chem. Rec.* 16, 335–348. doi: 10.1002/tcr.201500238

Boens, N., Leen, V., and Dehaen, W. (2012). Fluorescent indicators based on BODIPY. *Chem. Soc. Rev.* 41, 1130–1172. doi: 10.1039/C1CS15132K

Boens, N., Verbelen, B., Ortiz, M. J., Jiao, L., and Dehaen, W. (2019). Synthesis of BODIPY dyes through postfunctionalization of the boron dipyrromethene core. *Coord. Chem. Rev.* 399:213024. doi: 10.1016/j.ccr.2019.213024

Kamkaew, A., Lim, S. H., Lee, H. B., Kiew, L. V., Chung, L. Y., and Burgess, K. (2013). BODIPY dyes in photodynamic therapy. *Chem. Soc. Rev.* 42, 77–88. doi: 10.1039/C2CS35216H

Kowada, T., Maeda, H., and Kikuchi, K. (2015). BODIPY-based probes for the fluorescence imaging of biomolecules in living cells. *Chem. Soc. Rev.* 44, 4953–4972. doi: 10.1039/C5CS00030K

Loudet, A., and Burgess, K. (2007). BODIPY dyes and their derivatives: syntheses and spectroscopic properties. *Chem. Rev.* 107, 4891–4932. doi: 10.1021/cr078381n

Lu, H., Mack, J., Nyokong, T., Kobayashi, N., and Shen, Z. (2016). Optically active BODIPYs. *Coord. Chem. Rev.* 318, 1–15. doi: 10.1016/j.ccr.2016.03.015

Lu, H., Mack, J., Yang, Y., and Shen, Z. (2014). Structural modification strategies for the rational design of red/NIR region BODIPYs. *Chem. Soc. Rev.* 43, 4778–4823. doi: 10.1039/C4CS00030G

Ni, Y., and Wu, J. (2014). Far-red and near infrared BODIPY dyes: synthesis and applications for fluorescent pH probes and bio-imaging. *Org. Biomol. Chem.* 12, 3774–3791. doi: 10.1039/c3ob42554a

Sheng, W., Lv, F., Tang, B., Hao, E., and Jiao, L. (2019). Toward the most versatile fluorophore: direct functionalization of BODIPY dyes via regioselective C–H bond activation. *Chin. Chem. Rev.* 30, 1825–1833. doi: 10.1016/j.cclet.2019.08.004

Treibs, A., and Kreuzer, F.-H. (1968). Difluorboryl-komplexe von di- und tripyrrylmethenen. *Justus Liebigs Annalen der Chemie* 718, 208–223. doi: 10.1002/jlac.19687180119

Turksoy, A., Yildiz, D., and Akkaya, E. U. (2019). Photosensitization and controlled photosensitization with BODIPY dyes. *Coord. Chem. Rev.* 379, 47–64. doi: 10.1016/j.ccr.2017.09.029

Ulrich, G., Ziessel, R., and Harriman, A. (2008). The chemistry of fluorescent bodipy dyes: versatility unsurpassed. *Angew. Chem. Int. Ed.* 47, 1184–1201. doi: 10.1002/anie.200702070

Zhao, J., Xu, K., Yang, W., Wang, Z., and Zhong, F. (2015). The triplet excited state of bodipy: formation, modulation and application. *Chem. Soc. Rev.* 44, 8904–8939. doi: 10.1039/C5CS00364D

Conflict of Interest: The authors declare that the research was conducted in the absence of any commercial or financial relationships that could be construed as a potential conflict of interest.

frontiers in Chemistry

ORIGINAL RESEARCH
published: 28 August 2019
doi: 10.3389/fchem.2019.00598

A Highly Selective NIR Fluorescent Turn-on Probe for Hydroxyl Radical and Its Application in Living Cell Images

Xingyu Qu[1,2], *Wenting Song*[1] *and Zhen Shen*[1]*

[1] State Key Laboratory of Coordination Chemistry, Nanjing National Laboratory of Microstructures, School of Chemistry and Chemical Engineering, Nanjing University, Nanjing, China, [2] Department of Chemistry and Chemical Engineering, Jinzhong University, Jinzhong, China

A highly selective NIR fluorescent turn-on probe for hydroxyl radical (·OH) has been built up using triphenylphosphine as a reactive-site for ·OH in an energy transfer cassette **2b** consisting of 8-2′-(thiophen-2-yl) quinoline (**TQ**) as a donor and 3,5-diphenylphosphinostyryl-substituted BODIPY as an acceptor, which exhibits ca. 317 nm pseudo Stokes' shift due to efficient through-bond energy transfer (up to 169%). The triphenylphosphine substituent of **2b** selectively oxidized by ·OH over the other reactive oxygen species (ROS) and the reactive nitrogen species (RNS) resulting in fluorescence enhancement in aqueous solution and in living cells.

Keywords: NIR fluorescent probe, hydroxyl radical, living cell images, energy transfer, BODIPY

OPEN ACCESS

Edited by:
Rui Zhao,
University of Chinese Academy of Sciences, China

Reviewed by:
Weizhi Wang,
University of Chinese Academy of Sciences, China
Xiaodong Zhang,
Tianjin University, China

***Correspondence:**
Zhen Shen
zshen@nju.edu.cn

Specialty section:
This article was submitted to Chemical Biology, a section of the journal Frontiers in Chemistry

Received: *04 June 2019*
Accepted: *13 August 2019*
Published: *28 August 2019*

Citation:
Qu X, Song W and Shen Z (2019) A Highly Selective NIR Fluorescent Turn-on Probe for Hydroxyl Radical and Its Application in Living Cell Images. Front. Chem. 7:598. doi: 10.3389/fchem.2019.00598

INTRODUCTION

Free radicals that are natrually produced *in vivo*, by normal cellular metabolism or through disease process and xenobiotic activities, often cause many of the tissue changes associated with toxicities and disease processes (Dixon and Stockwell, 2014). The hydroxyl radical (·OH) is the most reactive species of oxygen in biological systems. It has a half-life about 1 ns and reacts unselectively in preferences for coreactants, resulting in a wide range of initial molecular changes, such as oxidative damage to DNA, proteins, lipids, and mediate redox alteration of cell-membrane Ca^{2+} channels (Cleveland and Kastan, 2000; Ayala et al., 2014). The difficulty in detecting such a short-lived species has made determining its involvement in toxic events difficult. Therefore, developing a rapid and sensitive method for monitoring ·OH in biological systems greatly improves our understanding of the roles of this reactive species in toxic mechanisms and disease processes (Wiseman and Halliwell, 1996; Pennathur et al., 2001). The common detection method for ·OH is the electron spin resonance (ESR). As the ESR measures the electron paramagnetic resonance spectrum of a spin adduct derivative after spin trapping, this method is insensitive and only qualitative estimates of ·OH (Valavanidis, 2000; Vidrio et al., 2008). Valavanidis to overcome these limitations, several fluorescent probes for ·OH have been developed. These probes include fluorescein with ·OH reactive-site (Zhang et al., 2016; Bai et al., 2017), cyanine dye based on a hybrid phenothiazine platform (Liu et al., 2016), a hybrid carbazole-cyanine dye (Zeng et al., 2017), fluorophore with nitroxide function group (Liras et al., 2016). However, limitation of these ·OH-responsive probes in intracellular imaging is their absorption and emission bands being situated in the Ultraviolet (UV) or Visible region, weak sensitivity or poor selectivity. Moreover, the difference in lifetimes of ROS/RNS further increases the difficulty to design

multiple probes. Up to date, the approach of a single fluorescent probe to the simultaneous detections of several ROS/RNS has still been a challenging task.

The 4,4-Difluoro-4-bora-3*a*,4*a*-diaza-*s*-indacene (BODIPY) dyes have many favorable photophysical properties, such as high extinction coefficient, high fluorescence quantum yields, facile derivatization, and good photostability (Lu et al., 2014; Kowada et al., 2015). They have been investigated intensively as labeling reagents (Cheng et al., 2017), fluorescent switches (Dolan et al., 2017), chemosensor (Ren et al., 2018), and laser dyes (Zhu et al., 2018) in the last three decades. Since the absorption and emission bands of the unmodified BODIPY lie at *ca.* 500 nm, one important approach to red shift the main BODIPY absorption band is introducing styryl-substituents at 3-, 5- and/or 1-, 7-positions on the pyrrole moieties (Patalag et al., 2017; Verwilst et al., 2017). The following characteristics are highly desirable for intracellular imaging: (i) selectivity and sensitivity toward a specific ion; (ii) fluorescence maxima appear in the near infrared (NIR) region (650–900 nm); (iii) minimize the scattering effects from the excitation source (Ali et al., 2015, 2017). Herein, we report two NIR BODIPY probes using the triphenylphosphine as substituents at 3-, 5-positions of the BODIPY core. The two probes exhibits excellent optical properties and can be used as fluorescence turn-on chemosensor for ·OH, as ·OH -trigger oxidation of the triphenylphosphine. Their sensing properties have been investigated for living cell images. To the best of our knowledge, no attempt to employ NIR probe for detection of ·OH in living cells has previously been made.

MATERIALS AND METHODS

The ^{1}H and ^{13}C NMR spectroscopic measurements were carried out on a Bruker 500 MHz spectrometer. The measurements for ^{1}H and ^{13}C NMR were performed at 500 (DRX-500), and 125 MHz (DRX-500), respectively. Mass spectra were measured on a Bruker Daltonics Autoflex II^{TM} MALDI-TOF MS spectrometer. Fluorescence spectral measurements were carried out by using a Hitachi F-4600 fluorescence spectrophotometer. Electronic absorption spectra were recorded with a Shimadzu UV-2550 spectrophotometer. Cyclic voltammograms were recorded using a platinum working electrode, a platinum wire counter electrode and an Hg/Hg_2Cl_2 reference electrode. The measurements were carried out in dichloromethane (CH_2Cl_2) solution using 0.1 M Bu_4NPF_6 as the supporting electrolyte at a scan rate of 0.1 V/s. Peak potentials were determined from differential pulse voltammetry experiments. The Fc/Fc^{+} redox couple was used as an internal standard. Unless otherwise noted, all reagents or solvents were obtained from commercial suppliers and used without further purification. All air and moisture sensitive reactions were carried out under an argon atmosphere. Dry CH_2Cl_2 was obtained by refluxing and distilling over CaH_2 under nitrogen. Dry THF was distilled from sodium/benzophenone.

X-ray crystallographic data for **ox-2a** were recorded at 100 K on a Rigaku CCD detector (Saturn 724) mounted on a Rigaku rotating anode X-ray generator (MicroMax-007HF) using Mo-Kα radiation from the corresponding set of confocal optics. The structure was solved by direct methods and refined on F^2 by full-matrix least-squares using the Crystal Clear and SHELXS-2000 programs. CCDC 875597 contains the supplementary crystallographic data for this paper. These data can be obtained free of charge from The Cambridge Crystallographic Data Center via www.ccdc.cam.ac.uk/conts/retrieving.html (or from the Cambridge Crystallographic Data Center, 12, Union Road, Cambridge CB21EZ, UK; fax: (+44) 1223-336-033; email: deposit@ccdc.cam.ac.uk).

Spectra were measured in 1 cm quartz cuvettes with spectroscopic grade solvents. The slit width was set at 5 nm for both excitation and emission measurements. Cresyl violet perchlorate in methanol ($\Phi_f = 0.55$) was used as the standard for the fluorescent quantum yield calculation using the absorption of the test sample. The emission spectra area was obtained from 550 to 800 nm. Dilute solutions (10^{-6} M) were used to minimize reabsorption effects. Fluorescence measurement were made three times for each dye and averaged. Quantum yields were determined using the following equation:

$$\Phi_{samp} = (\Phi_{stand} \times F_{samp}/F_{stand}) \times (A_{samp}/A_{stand}) \times (n_{samp}{}^2/n_{stand}{}^2)$$

F_{samp} and F_{samp} are the quantum yield of the sample and the cresyl violet perchlorate standard. F_{samp} and F_{stand} are the areas under the emission spectra of the sample and standard. A_{samp} and A_{stand} are the absorbance values for the sample and standard at the excitation wavelength. n_{samp} and n_{stand} are the refractive index values of the solvents used for the sample and standard measurements. Molar extinction coefficients were obtained from the slope of a graph of absorbance vs. concentration for each dye at five different concentrations (10^{-6} M).

The HeLa cell line was provided by the Institute of Biochemistry and Cell Biology, SIBS, CAS (China). Cells were grown in high glucose Dulbecco's Modified Eagle Medium (DMEM, 4.5 g of glucose/L) supplemented with 10% fetal bovine serum (FBS) at 37°C and 5% CO_2. Cells (5×10^8/L) were plated on 14 mm glass coverslips and allowed to adhere for 24 h. Experiments to assess phorbol myristate acetate (PMA) uptake were performed over 2 h in the same medium.

Immediately before the experiments, cells were washed with PBS buffer and then incubated with 10 μM **2b** in PBS buffer for 2 h at 37°C. Cell imaging was then carried out after washing the cells with PBS buffer. Confocal fluorescence imaging was performed with a Zeiss LSM 710 laser scanning microscope and a 63 × oil-immersion objective lens. Cells incubated with **2b** were excited at 633 nm using a multi-line argon laser.

The compounds **1a** and **1b** were synthsised according to the literature (Qu et al., 2012). **1a** was obtained as yellow solid with 38.6% yield., ^{1}H NMR($CDCl_3$, 500 MHz): 7.45 (*t*, $J = 5$ Hz, 3H), 7.27 (s, 2H), 6.95 (s, 2H), 2.53 (s, 6H), 1.34 (s, 6H).

1b was obtained as red solid with 65% yield. ^{1}H NMR($CDCl_3$, 500 MHz): 8.19 (d, 1H, $J = 10$ Hz), 8.08 (d, 1H, $J = 10.0$ Hz), 7.81 (m, 2H), 7.76 (d, 1H, $J = 3.5$ Hz), 7.71 (t, 1H, $J = 5.0$ Hz), 7.51 (t, 1H, $J = 5.0$ Hz), 7.04 (d, 1H, $J = 5.0$ Hz), 6.02 (s, 2H), 2.57 (s, 6H), 1.76 (s, 6H).

The compounds **2a** and **2b** were synthsised according to the literature (Buyukcakir et al., 2009). Compound **1a** (0.16 mmol, 50 mg) and 2-(diphenylphosphino)benzaldehyde (0.32 mmol, 100 mg) were added to a 100 mL round bottomed flask containing 50 mL acetonitrile, and then piperidine (0.4 mL) and acetic acid (0.4 mL) were added to this solution. The mixture was heated under reflux by using a Dean Stark trap and reaction was monitored by TLC in solvent CH_2Cl_2. When all the starting material had been disappeared, the mixture were cooled to room temperature and concentrated at reduced pressure. The dark brown reaction mixture was washed with 100 mL water and extracted twice with 50 mL chloroform., dried over Na_2SO_4, and concentrated at reduced pressure. The crude products were purified by silica-gel column chromatography using mixture solvent (ethyl acetate:petroleum, 1:1, v/v) as the eluant to give **2a** as a black solid with 77% yield. ^{1}H NMR (500 MHz, $CDCl_3$): 8.04 (1 H, d, J = 5.1), 8.01 (1 H, d, J = 5.2), 7.98–7.92 (2 H, m), 7.65 (1 H, s), 7.62 (1 H, s), 7.47 (3 H, d, J = 3.4), 7.42 (2 H, t, J = 7.6), 7.33 (11 H, d, J= 2.8), 7.31–7.27 (7 H, m), 7.21 (2 H, t, J = 7.5), 6.93–6.86 (2 H, m), 6.45 (2 H, s), 1.38 (6 H, s); ^{14}B NMR (160 MHz, $CDCl_3$): 1.05; ^{31}P NMR (202 MHz, $CDCl_3$): −14.29. MALDI-TOF MS: m/z: 867.6 (M^+) (**Figures S1, S2** and **S9**, ESI).

Compound **1b** (0.11 mmol, 50 mg) and 2-(diphenylphosphino)benzaldehyde (0.33 mmol, 110 mg) were added to a 100 mL round bottomed flask containing 60 mL mixture solvent (acetonitrile: 1,2-dichloroethane, 1:1, v/v), and then piperidine (0.4 mL) and acetic acid (0.4 mL) were added to this solution. The mixture was heated under reflux by using a Dean Stark trap and reaction was monitored by thin-layer chromatography (TLC) in solvent CH_2Cl_2. When all the starting material had been disappeared, the mixture were cooled to room temperature and concentrated at reduced pressure. The dark brown reaction mixture was washed with 100 mL water and extracted twice with 50 mL chloroform., dried over Na_2SO_4, and concentrated at reduced pressure. The crude products were purified by silica-gel column chromatography using mixture solvent (dichloromethane:petroleum, 1:1, v/v) as the eluant to give **2b** as a black solid with 45% yield. ^{1}H NMR (500 MHz, $CDCl_3$) 8.23–8.16 (2 H, m), 8.05 (3 H, dd, J = 15.9, 5.4), 7.99–7.93 (2 H, m), 7.82 (3 H, dd, J = 12.3, 8.3), 7.75–7.69 (2 H, m), 7.63 (2 H, d, J = 15.7), 7.55–7.49 (3 H, m), 7.44 (3 H, dd, J = 17.4, 9.7), 7.33 (12 H, d, J = 2.3), 7.29 (7 H, dd, J = 7.3, 2.4), 7.22 (2 H, t, J = 7.6), 7.06–7.00 (1 H, m), 6.90 (3 H, dd, J = 7.3, 4.9), 6.48 (2 H, s), 1.76 (6 H, s) 13C NMR (126 MHz, CDCl3) δ = 153.17, 151.57, 142.34, 140.90, 140.74, 136.85, 136.70, 136.59, 136.23, 135.05, 134.83, 134.05, 133.90, 133.68, 132.38, 131.99, 130.10, 129.34, 129.25, 128.88, 128.67, 128.63, 127.52, 127.40, 126.45, 125.78, 120.45, 118.51, 117.26, 77.27, 77.02, 76.77, 14.16, −0.00.^{31}P NMR (202 MHz, $CDCl_3$): −14.30. MALDI- TOF MS: m/z: 1002 (M^+) (**Figures S3–S5** and **S10**, ESI).

The compound **ox-2a** was synthsized according to the literature (Ali et al., 2017). Compound **2a** (0.02 mmol) and hydrogen peroxide (0.2 mmol) were added to a 100 mL round bottomed flask containing 50 mL tetrahydrofuran, and then $FeSO_4 \bullet 7H_2O$ (0.12 mmol) were added to this solution. The solution was stirred for 30 min at ambient temperature. When all the starting material had disolved, was washed with 100 mL water and extracted twice with 50 mL chloroform., dried over Na_2SO_4, and concentrated at reduced pressure. The products were the remainder that the mixture was washed with 100 mL of water to give **ox-2a** as a black solid in quantitative yield. ^{1}H NMR (500 MHz, $CDCl_3$): 8.13 (2 H, d, J = 16.1), 8.03 (2 H, dd, J = 7.7, 3.9), 7.67 (8 H, dd, J = 11.8, 7.5), 7.63–7.41 (20 H, m), 7.17 (2 H, dd, J = 14.1, 7.6), 6.28 (2 H, s), 1.33 (6 H, s); ^{13}C NMR (126 MHz, $CDCl_3$): δ 152.42, 142.30, 141.26, 139.50, 134.90, 134.31, 133.81, 133.71, 133.57, 133.23, 132.40, 132.31, 131.97, 131.90, 131.02, 130.22, 129.06, 128.69, 128.59, 128.25, 127.69, 127.58, 121.42, 118.64, 77.26, 77.01, 76.75, 14.47. ^{14}B NMR (160 MHz, $CDCl_3$): 0.95; ^{31}P NMR (202 MHz, $CDCl_3$): 31.41. MALDI- TOF MS: m/z: 800 (M^+-F) (**Figures S6–S8** and **S11**, ESI).

RESULTS AND DISCUSSIONS

Design and Synthesis

The synthesis of BODIPYs **2a** and **2b** bearing triphenylphosphine as a reactive-site for ·OH are outlined in **Scheme 1**. Compounds **1a** and **1b** were synthesized in 65 and 39% yields according to a published procedure. Using knoevenagel condensation method, the sensors **2a** and **2b** can be obtained in 77% and 45% yield by condensation of **1a** and **1b** with 2-diphenylphosphinobenzaldehyde. Oxidation reaction of **2a** with hydroxyl radical gives compound **ox-2a** in 100% yield.

The structure of compound **ox-2a** has been determined by X-ray analysis. Single crystal of **ox-2a** is obtained by slow evaporation of hexane/CH_2Cl_2 solution at ambient temperature. Similar to the previously reported structures of alkyl substituted BODIPYs (Qu et al., 2012), the *meso*-phenyl ring is virtually orthogonal to the indacene plane with the torsion angle being 87.69°. The indacene plane of BODIPY is nearly planar with the deviations from the mean plane 0.0285 Å. It is interesting to note that the dihedral angles between the neighboring phenyl in triphenylphosphine are 78.53°, 88.57°, 88.56°, respectively in the unit cell (**Figure 1** and **Table S1**).

Spectral Properties

The UV/vis absorption and emission spectra of **2a**, **2b** and **TQ** are measured in various solvents with different polarities and the photophysical properties are summarized in **Table 1**. As shown in **Figure 2**, the absorption maxima of **2a** and **2b** are centered at 628 and 650 nm, respectively, which can be ascribed to the $S_0 \rightarrow S_1$ transition of the BODIPY. The absorption band at 350 nm for **2a** and **2b** can be assigned to the intramolecular charge transfer (ICT) band due to the electron-donating 2-diphenylphosphinostyryl moiety. The absorption spectra of **2a**, **2b,** and **ox-2a** are slightly varied with increasing the solvent polarity (**Table S2**, ESI). Upon exciting 2-(thiophen-2-yl)quinoline moiety at 334 nm in **2b**, the emission from the **TQ** moiety is almost quenched completely, instead strong emission at 665 nm is observed. These results imply that efficient energy transfer from the donor to the BODIPY acceptor occurs. The energy transfer efficiency is evaluated according to the equation: $[1\text{-}I_d]/I_p \times 100\%$, where

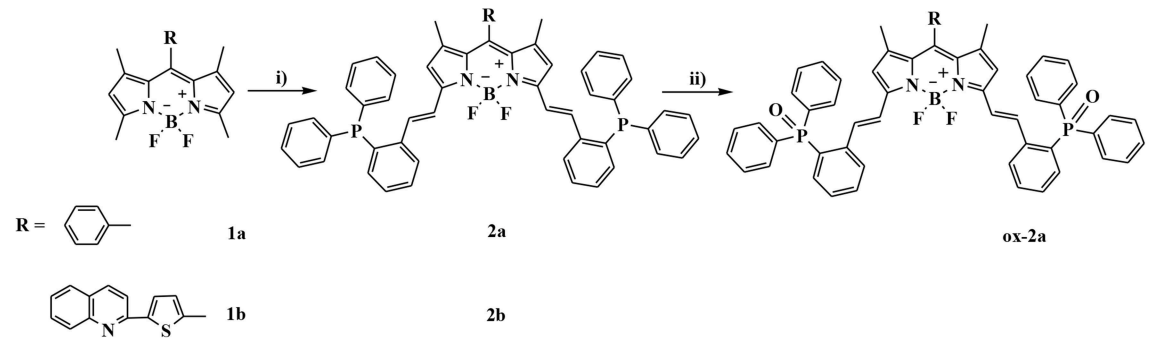

SCHEME 1 | Synthetic procedures for compounds **2a** and **2b**: (i) 2-diphenylphosphinobenzaldehyde, AcOH/piperidine, in CH_3CN, reflux, 77% for **2a** and 45% for **2b**; (ii) Fenton's reagent, in THF, rt, 100%.

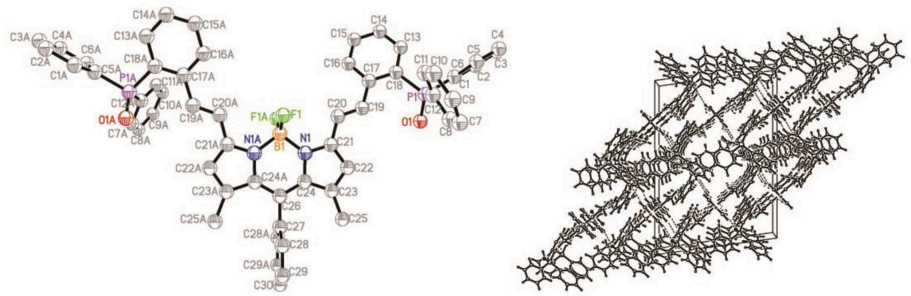

FIGURE 1 | ORTEP views of the molecular structure of **ox-2a** with the thermal ellipsoids set at 30% probability **(left)** and packing diagram **(right)**.

TABLE 1 | Optical properties of **2a**, **2b**, and **TQ** in CH_2Cl_2 at 298 K.

compounds	λ_{abs}^{max} (nm)/logε_{max}	λ_{flu} (nm)	Quasi-Stokes' shift [cm^{-1}]	$\Phi^b{}_f$ex334	$\Phi^a{}_f$ accptor	ETE[b]	τ(ns)[c]
2a	633/4.91, 577/4.58, 350/4.65	650	55,555	–	0.72	–	4.25
2b	650/5.05, 594/4.64, 350/4.65,	665	3,154	0.54	0.32	169%	4.03
TQ	334/4.27	386	19,230	0.09	–	–	–

[a] *Fluorescence quantum yield.*
[b] *Energy transfer efficiency.*
[c] *Fluorescence lifetimes.*

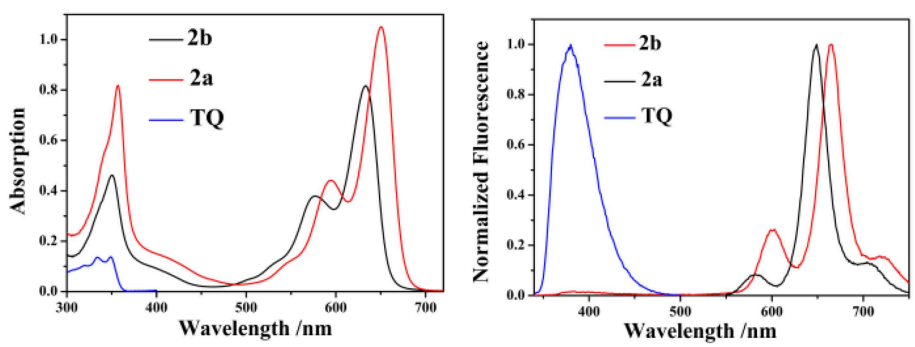

FIGURE 2 | The absorption **(left)** and emission **(right)** spectra of **2a**, **2b,** and **TQ** in CH_2Cl_2 (10 μM, λ_{ex} = 334 nm for **2b** and **TQ**, λ_{ex} = 555 nm for **2a**).

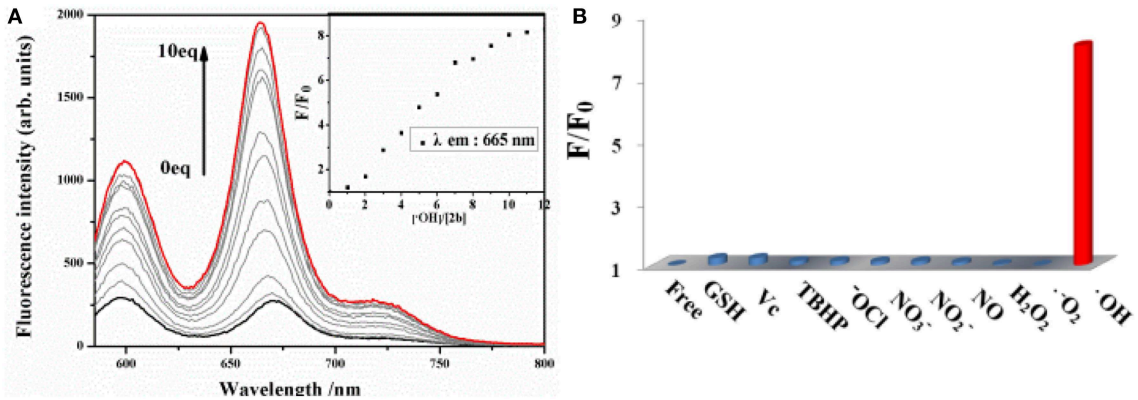

FIGURE 3 | (A) Changes in the fluorescence spectrum of **2b** (10 μM in DMSO) as the concentration of ·OH is increased upon excitation at 580 nm. **(B)** Fluorescence reactivity of **2b** (10 μM in DMSO) with various ROS/RNS species upon excitation at 580 nm (F and F_0 were the fluorescence intensity of the probe in the presence and absence of various ROS/RNS species).

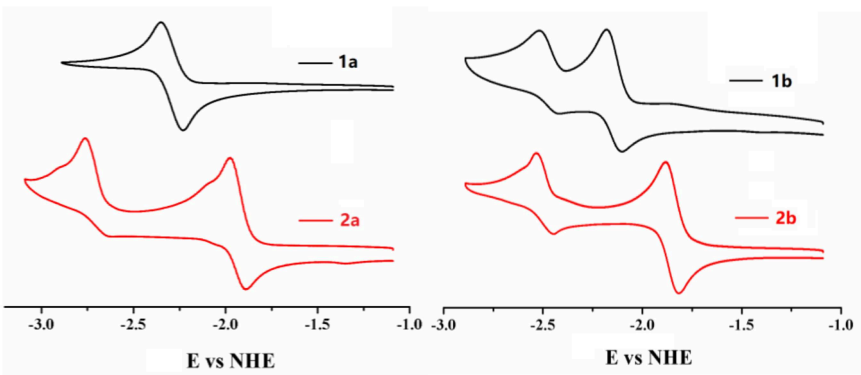

FIGURE 4 | Cyclic voltammograms of compounds **1a, 2a, 1b, 2b** (0.1 mM) in CH_2Cl_2 containing 0.1 M NBu_4PF_6 (vs. NHE). The ferrocene/ferrocenium (Fc/Fc^+) couple was used as an external standard.

I_d is the fluorescence intensity of **2b** excited at 334 nm, I_p is the fluorescence intensity of **2b** excited at 580 nm (Yan et al., 2016). In addition, due to the antenna effect (Greene et al., 2017), the fluorescence quantum yields of **2b** upon excitation of the **TQ** moiety (λ_{ex} = 334 nm) are higher than that obtained by directly excitation of the BODIPY acceptor (λ_{ex} = 580 nm) (**Table 1**). The fluorescence quantum yield of **2b** in DMSO (λ_{ex} = 580 nm; Φ = 0.08) is weak, which can be ascribed to the photo-induced electron transfer (PET) from the triarylphosphine moiety to the BODIPY fluorophore (**Table S2**, ESI).

Fluorescence Detection of ·OH

The sensitivity of probe **2b** toward ·OH is investigated by spectrometric titration in DMSO (**Figure 3**). Fenton reaction between $Co(OAc)_2$ and hydrogen peroxide was used to generate ·OH *in situ* in a sample solution. Upon addition of increasing amount of ·OH, the fluorescence intensity at 665 nm increases remarkably with a virtually unchanged peak position upon excitation at 580 nm (**Figure 3A**) or excitation at 334 nm (**Figure S12**, ESI). The titration curve of **2b** shows a quick enhancement upon addition small amount of ·OH and then reaches a plateau at 10 equiv of ·OH. The detection limit for ·OH is determined to be 10 μM based on the signal-to-noise ratio of three (**Figure S15**, ESI). A good linear relationship between the fluorescence response and concentration of ·OH is obtained with a 0.9808 correlation coefficient.

To evaluate the selectivity of **2b** for ·OH, the interference experiments in the presence of several ROS/RNS both in respective and integrated manners are carried out. Almost no change is observed in the fluorescence intensity of **2b** by adding 20 equiv. of O_2^-, 100 equiv. of other ROS/RNS species, such as H_2O_2, ClO^-, TBHP, NO, NO_2^-, NO_3^-, Vc, GSH, respectively, upon excitation at 580 nm (**Figure 3B**) or excitation at 334 nm (**Figure S13**, ESI). Moreover, the fluorescence turn-on response toward ·OH is nearly not interfered in the presence of excess amount of background containing appropriate ROS/RNS species, such as H_2O_2, ClO^-, NO_2^-, NO_3^-, GSH, and is little interfered in the background

containing NO and Vc (**Figure S14**, ESI). The above results demonstrate that **2b** is a highly selective and sensitive fluorescence turn-on probe for ·OH and its response for ·OH is not interfered in the background containing various ROS/RNS species.

Sensing Mechanism

As the most obvious explanation for the fluorescence turn-on response is that the photo-induced electron transfer (PET) from the lone pair electrons of P(III) atom of triarylphosphine to the BODIPY fluorophore is inhibited upon oxidation by ·OH to form triphenylphosphine oxide $P(V)O_2$. To further demonstrate this mechanism, the reaction mode of ·OH with **2b** is investigated by ^{31}P NMR spectroscopy (**Figure S16**, ESI). The ^{31}P NMR spectra of **2b** in the presence of different concentrations of ·OH are recorded in DMSO-d_6 and compared to the spectrum of the free probe. As shown in the ^{31}P NMR spectra of **2b**, upon addition of ·OH, the chemical shift of P(III) atom of the triarylphosphine group at −15.73 ppm is significantly down field shifted to 28.89 ppm, which is corresponding to the P(V) of triphenylphosphine oxide, indicating that ·OH oxidize the phosphorus atom of **2b** to form triphenylphosphine oxide. Furthermore, according to the database, the standard oxidation potentials of ·OH, H_2O_2, ClO^-, O_2^-, NO, NO_2^-, NO_2^- are 2.8, 1.76, 1.63, 1.59, 0.99, 0.94 V, respectively. Santhanam and Bard reported that the reduction electrode potentials of triphenylphosphine (−2.7 V vs. sce) early in 1967 year (Santhanam and Bard, 1968). Therefore, only the ·OH radical can oxide the triphenylphosphine. Electrochemical properties of **1a**, **2a**, **1b**, **2b** were studied by cyclic voltammetry measured in dry dichloromethane (**Figure 4**). Probe **2b** consists two reversible reduction potentials at −1.992 and −2.49 V vs. NHE. These results reveal that compound **2b** can be selectively oxidized by ·OH radical without interference in the background containing other RON/ROS.

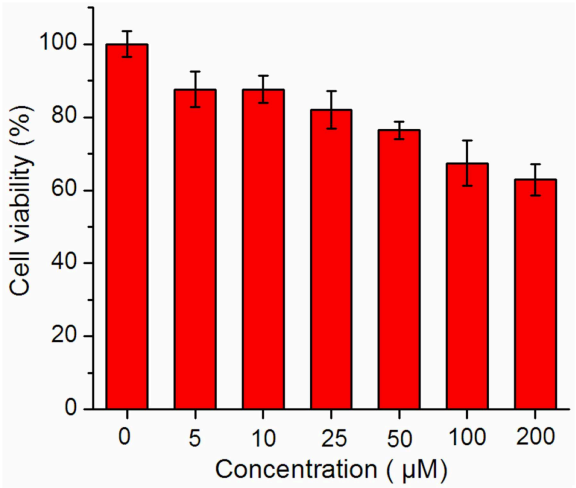

FIGURE 5 | MTT assay of **2b**.

The Cell Imaging of ·OH

Prior to assess the sensing properties of probe **2b** in a cellular environment, the cytotoxicity of **2b** was evaluated through an MTT assay in HeLa cells. As shown in **Figure 5**, more than 80% cells are viable after incubation with **2b** over a wide range of

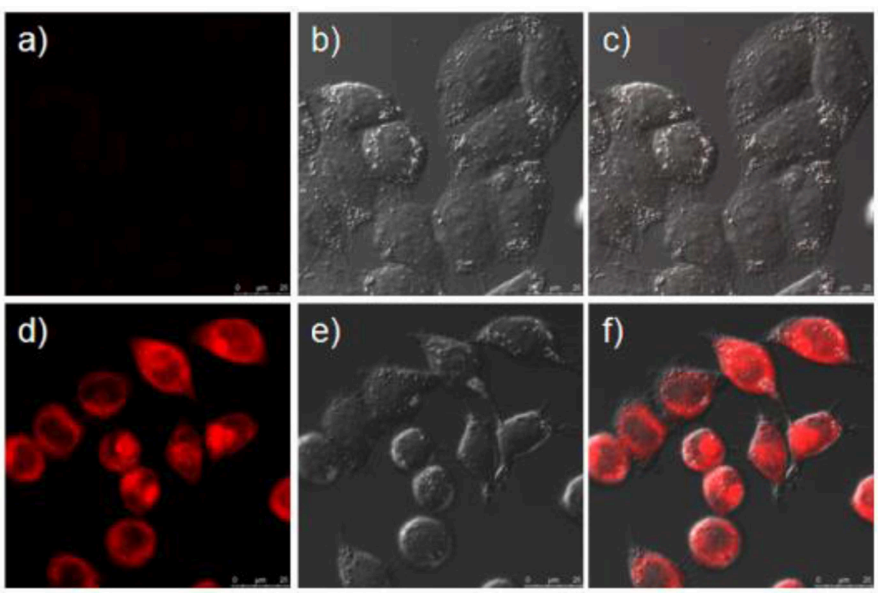

FIGURE 6 | Confocal fluorescence and brightfield images of Hela cells. **(a)** Cells incubated with 10 μM of sensor **2b** for 2 h at 37°C. **(b)** Brightfield image of cells showed in **(a)**. **(c)** One overlay image of **(a,b)**. **(d)** Cells incubated with 10 μM probe at 37°C for 2 h and then treated with phorbol myristate acetate (PMA) for 2 h. **(e)** Brightfield image of cells showed in **(d)**. **(f)** One overlay image of **(d,e)**.

concentrations (5–50 μM) for 24 h, indicating that **2b** do not negatively affect the cell viability to HeLa cells. This encouraged us to explore the potential utility of **2b** as a fluorescent probe for ·OH in living cells (**Figure 6** and **Figure S17** ESI) (Yang et al., 2017). HeLa cells were incubated with 10 μM of **2b** for 30 min at 37 °C and subsequently viewed under confocal microscope upon excitation at 633 nm as control experiments. No intracellular fluorescence was observed (**Figure 6a**). Then phorbol myristate acetate (PMA) was added in the cells for 2 h, the microscope images exhibited intense intracellular fluorescence (**Figure 6d**). Bright field measurements, after treatment with both PMA and **2b**, confirmed that the cells are viable throughout the imaging experiments (**Figures 6b,c,e,f**). Therefore, probe **2b** can clearly be used for intracellular detection of ·OH.

CONCLUSIONS

In summary, a highly selective and sensitive Near IR fluorescent turn-on probe for hydroxyl radical have been designed by utilizing triphenylphosphine as a reaction-site for ·OH in the presence of other reactive oxygen species (ROS) and reactive nitrogen species (RNS). In addition, **2b** can also be applied for bioimaging ·OH in HeLa cells with almost no cytotoxicity, thus demonstrating its application for studying the effect of ·OH in biological systems. These results point the way to a new generation of molecular recognition systems in the NIR window for biological system.

DATA AVAILABILITY

All datasets generated for this study are included in the manuscript/**Supplementary Files**.

AUTHOR CONTRIBUTIONS

XQ was responsible for carried out the experiments and performing spectroscopic measurements. WS was responsible for carrying out the cell imaging experiments. ZS was responsible for designing the project and revising the manuscript.

ACKNOWLEDGMENTS

We gratefully acknowledge the financial support provided by the National Natural Science Foundation of China (No. 21771102) to ZS, the Construction Plan of 1331 engineering Photoelectric Material Innovation Team of Jinzhong University (No. 2017007), the Shanxi 1331 project Key Innovative Research Team (No. PY201817), and the Scientific and Technological Innovation Programs of Higher Education Institutions in Shanxi (No. 2019L0879) to XQ.

SUPPLEMENTARY MATERIAL

The Supplementary Material for this article can be found online at: https://www.frontiersin.org/articles/10.3389/fchem.2019.00598/full#supplementary-material

REFERENCES

Ali, F., Anila, H. A., Taye, N., Gonnade, R. G., Chattopadhyay, S., and Das, A. (2015). A fluorescent probe for specific detection of cysteine in the lipid dense region of cells. *Chem. Commun.* 51, 16932–16935. doi: 10.1039/c5cc07450a

Ali, F., Sreedharan, S., Ashoka, A. H., Saeed, H. K., Smythe, C. G. W., Thomas, J. A., et al. (2017). A super-resolution probe to monitor HNO levels in the endoplasmic reticulum of cells. *Anal. Chem.* 89, 12087–12093. doi: 10.1021/acs.analchem.7b02567

Ayala, A., Muñoz, M. F., and Argüelles, S. (2014). Lipid peroxidation: production, metabolism, and signaling mechanisms of malondialdehyde and 4-hydroxy-2-nonenal. *Oxid. Med. Cell. Longev.* 2014, 1–31. doi: 10.1155/2014/360438

Bai, X., Huang, Y., Lu, M., and Yang, D. (2017). HKOH-1: a highly sensitive and selective fluorescent probe for detecting endogenous hydroxyl radicals in living cells. *Angew. Chem.* 129, 13053–13057. doi: 10.1002/ange.201705873

Buyukcakir, O., Bozdemir, O. A., Kolemen, S., Erbas, S., and Akkaya, E. U. (2009). Tetrastyryl-bodipy dyes: convenient synthesis and characterization of elusive near IR fluorophores. *Org. Lett.* 11, 4644–4647. doi: 10.1021/ol9019056

Cheng, M. H. Y., Savoie, H., Bryden, F., and Boyle, R. W. (2017). A convenient method for multicolour labelling of proteins with BODIPY fluorophores via tyrosine residues. *Photochem. Photobiol. Sci.* 16, 1260–1267. doi: 10.1039/c7pp00091j

Cleveland, J. L., and Kastan, M. B. (2000). A radical approach to treatment. *Nature* 407, 309–311. doi: 10.1038/35030277

Dixon, S. J., and Stockwell, B. R. (2014). The role of iron and reactive oxygen species in cell death. *Nat. Chem. Biol.* 10, 9–17. doi: 10.1038/nchembio.1416

Dolan, C., Byrne, A., Long, C., Czamara, K., Kaczor, A., Baranska, M., et al. (2017). Polypyridyl substituted BODIPY derivatives; water switchable imaging probes that exhibit halogen substituent dependent localisation in live cells. *RSC Adv.* 7, 43743–43754. doi: 10.1039/c7ra07493j

Greene, L. E., Lincoln, R., and Cosa, G. (2017). Rate of lipid peroxyl radical production during cellular homeostasis unraveled via fluorescence imaging. *J. Am. Chem. Soc.* 139, 15801–15811. doi: 10.1021/jacs.7b08036

Kowada, T., Maeda, H., and Kikuchi, K. (2015). BODIPY-based probes for the fluorescence imaging of biomolecules in living cells. *Chem. Soc. Rev.* 44, 4953–4972. doi: 10.1039/c5cs00030k

Liras, M., Simoncelli, S., Rivas-Aravena, A., García, O., Scaiano, J. C., Alarcon, E. I., et al. (2016). Nitroxide amide-BODIPY probe behavior in fibroblasts analyzed by advanced fluorescence microscopy. *Org. Biomol. Chem.* 14, 4023–4026. doi: 10.1039/c6ob00533k

Liu, F., Du, J., Song, D., Xu, M., and Sun, G. (2016). A sensitive fluorescent sensor for the detection of endogenous hydroxyl radicals in living cells and bacteria and direct imaging with respect to its ecotoxicity in living zebra fish. *Chem. Commun.* 52, 4636–4639. doi: 10.1039/c5cc10658c

Lu, H., Mack, J., Yang, Y., and Shen, Z. (2014). Structural modification strategies for the rational design of red/NIR region BODIPYs. *Chem. Soc. Rev.* 43, 4778–4823. doi: 10.1039/c4cs00030g

Patalag, L. J., Ho, L. P., Jones, P. G., and Werz, D. B. (2017). Ethylene-bridged oligo-BODIPYs: access to intramolecular J-aggregates and superfluorophores. *J. Am. Chem. Soc.* 139, 15104–15113. doi: 10.1021/jacs.7b08176

Pennathur, S., Wagner, J. D., Leeuwenburgh, C., Litwak K. N., and Heinecke, J. W. (2001). A hydroxyl radical–like species oxidizes cynomolgus monkey artery wall proteins in early diabetic vascular disease. *J. Clin. Invest.* 107, 853–856. doi: 10.1172/JCI11194

Qu, X., Liu, Q., Ji, X., Chen, H., Zhou, Z., and Shen, Z. (2012). Enhancing the Stokes' shift of BODIPY dyes via through-bond energy transfer and its application for Fe3+-detection in live cell imaging. *Chem. Commun.* 48, 4600–4602. doi: 10.1039/c2cc31011b

Ren, W., Zhang, J.-J., Peng, C., Xiang, H., Chen, J., Peng, C., et al. (2018). Fluorescent imaging of β-amyloid using BODIPY based near-infrared off-on fluorescent probe. *Bioconjug. Chem.* 29, 3459–3466.doi: 10.1021/acs.bioconjchem.8b00623

Santhanam, K. S. V., and Bard, A. J. (1968). Electrochemistry of organophosphorus compounds. II. Electroreduction of triphenylphosphine and triphenylphosphine oxide. *J. Am. Chem. Soc.* 90, 1118–1122. doi: 10.1021/ja01007a005

Valavanidis, A. (2000). Generation of hydroxyl radicals by urban suspended particulate air matter. The role of iron ions. *Atmos. Environ.* 34, 2379–2386. doi: 10.1016/s1352-2310(99)00435-5

Verwilst, P., Kim, H.-R., Seo, J., Sohn, N.-W., Cha, S.-Y., Kim, Y., et al. (2017). Rational design of *in vivo* tau tangle-selective near-infrared fluorophores: expanding the BODIPY Universe. *J. Am. Chem. Soc.* 139, 13393–13403. doi: 10.1021/jacs.7b05878

Vidrio, E., Jung, H., and Anastasio, C. (2008). Generation of hydroxyl radicals from dissolved transition metals in surrogate lung fluid solutions. *Atmos. Environ.* 42, 4369–4379. doi: 10.1016/j.atmosenv.2008.01.004

Wiseman, H., and Halliwell, B. (1996). Damage to DNA by reactive oxygen and nitrogen species: role in inflammatory disease and progression to cancer. *Biochem. J.* 313, 17–29. doi: 10.1042/bj3130017

Yan, Y., Wu, F., Qin, J., Xu, H., Shi, M., Zhou, J., et al. (2016). Efficient energy transfer in ethynyl bridged corrole–BODIPY dyads. *RSC Adv.* 6, 72852–72858. doi: 10.1039/c6ra12271j

Yang, Q., Ma, Z., Wang, H., Zhou, B., Zhu, S., Zhong, Y., et al. (2017). Rational design of molecular fluorophores for biological imaging in the NIR-II window. *Adv. Mater.* 29:1605497. doi: 10.1002/adma.201605497

Zeng, L., Xia, T., Hu, W., Chen, S., Chi, S., Lei, Y., et al. (2017). Visualizing the regulation of hydroxyl radical level by superoxide dismutase via a specific molecular probe. *Anal. Chem.* 90, 1317–1324. doi: 10.1021/acs.analchem.7b04191

Zhang, R., Zhao, J., Han, G., Liu, Z., Liu, C., Zhang, C., et al. (2016). Real-time discrimination and versatile profiling of spontaneous reactive oxygen species in living organisms with a single fluorescent probe. *J. Am. Chem. Soc.* 138, 3769–3778. doi: 10.1021/jacs.5b12848

Zhu, T., Xiong, J., Xue, Z., Su, Y., Sun, F., Chai, R., et al. (2018). A novel amphiphilic fluorescent probe BODIPY–O-CMC–cRGD as a biomarker and nanoparticle vector. *RSC Adv.* 8, 20087–20094. doi: 10.1039/c8ra02125b

Conflict of Interest Statement: The authors declare that the research was conducted in the absence of any commercial or financial relationships that could be construed as a potential conflict of interest.

frontiers in Chemistry

ORIGINAL RESEARCH
published: 20 September 2019
doi: 10.3389/fchem.2019.00641

Development of a "Turn-on" Fluorescent Probe-Based Sensing System for Hydrogen Sulfide in Liquid and Gas Phase

Juergen Bartelmess†, Virginia Valderrey† and Knut Rurack†*

Chemical and Optical Sensing Division, Bundesanstalt für Materialforschung und -prüfung (BAM), Berlin, Germany

A "turn-on" fluorescence sensing system based on a BODIPY-cobaloxime complex for the detection of H_2S in liquid and gas phase was developed. To that aim, two cobaloxime complexes bearing an axial pyridyl-BODIPY ligand were initially evaluated as sensitive fluorescent HS^- indicators in aqueous solution. The sensing mechanism involves the selective substitution of the BODIPY ligand by the HS^- anion at the cobalt center, which is accompanied by a strong fluorescence enhancement. The selection of a complex with an ideal stability and reactivity profile toward HS^- relied on the optimal interaction between the cobalt metal-center and two different pyridyl BODIPY ligands. Loading the best performing BODIPY-cobaloxime complex onto a polymeric hydrogel membrane allowed us to study the selectivity of the probe for HS^- against different anions and cysteine. Successful detection of H_2S by the fluorescent "light-up" membrane was not only accomplished for surface water but could also be demonstrated for relevant H_2S concentrations in gas phase.

Keywords: sulfide sensing, fluorescence, BODIPY, cobaloxime complex, gas sensing

OPEN ACCESS

Edited by:
Zhen Shen,
Nanjing University, China

Reviewed by:
Adarsh Nayarassery Narayanan,
Mahatma Gandhi University, India
John Mack,
Rhodes University, South Africa

***Correspondence:**
Knut Rurack
knut.rurack@bam.de

†ORCID:
Juergen Bartelmess
orcid.org/0000-0002-1977-612X
Virginia Valderrey
orcid.org/0000-0002-4444-7424
Knut Rurack
orcid.org/0000-0002-5589-5548

Specialty section:
This article was submitted to Supramolecular Chemistry, a section of the journal Frontiers in Chemistry

Received: *23 July 2019*
Accepted: *06 September 2019*
Published: *20 September 2019*

Citation:
Bartelmess J, Valderrey V and Rurack K (2019) Development of a "Turn-on" Fluorescent Probe-Based Sensing System for Hydrogen Sulfide in Liquid and Gas Phase. Front. Chem. 7:641. doi: 10.3389/fchem.2019.00641

INTRODUCTION

Hydrogen sulfide is a toxic gas of pungent odor (Malone Rubright et al., 2017; Szabo, 2018), affecting the well-being of humans and animals already at very low concentrations (Nimmermark, 2004; Godoi et al., 2018). Although the smell is usually offensive, the human olfactory system adapts rather quickly to it (ca. 1 min for a concentration of 8 ppm of H_2S in air) (Stuck et al., 2014), contributing to the gas' hazardousness. The main sources of H_2S emission are animal feeding operations and industrial livestock facilities (Blunden et al., 2008; Feilberg et al., 2017) as well as sewage, waste water treatment and storage systems (Carrera et al., 2016; Jiang et al., 2017) yet also landfills where H_2S is formed by the biodegradation of municipal solid waste (Ko et al., 2015). As a ubiquitous product of the degradation of sulfur containing matter, it can be also present in significant amounts in fossil fuels or in geothermal fluids in which it is the most dominant non-condensable gas (NCG) (Bayer et al., 2013; Marriott et al., 2016). For environmental safety and human health preservation, the monitoring of H_2S emissions is thereby crucial (Pandey et al., 2012). Although it has a major impact as an air pollutant, transit through the gas–liquid interface from a waste water reservoir into air is one of its main migration pathways in urban areas (Blunden et al., 2008; Prata et al., 2018). Monitoring of the HS^- anion, the form in which dissolved H_2S is commonly present in water, is thus also highly desirable for pollution management, for instance, in

terms of the effectiveness of biofiltration in H_2S treatment processes (Vikrant et al., 2018). Among the various sensor types that have so far been developed for H_2S determination, optical methods are particularly appealing when it comes to miniaturization, remote operation and the build-up of multipoint monitoring schemes, no matter whether for the gas or the liquid phase (Liang et al., 2004; Pandey et al., 2012). The considerable number of optical H_2S sensors reported until today basically rely on three different photochemical modes of operation. First, the reductive potential of the analyte can be exploited by reducing functional groups on fluorophores such as azide, leading to a switching on of the fluorescence of the dye (Lippert et al., 2011; Peng et al., 2011; Zhang et al., 2016). Second, metal-bound fluorophores can be modified in a way that the sulfide anion binds to the metal center, resulting in a release of the fluorophore, and thus a restoration or "turn-on" of the fluorophore's emission features upon photoexcitation. Typical metal centers are transition and heavy metals such as Cu, Zn, or Hg (Strianese and Pellecchia, 2016; Kaushik et al., 2017; El-Maghrabey et al., 2019). The third prominent approach involves the cleavage of quencher molecules, leading to the release of highly emissive fluorophores (Liu et al., 2011, 2012; Dai et al., 2014; Karakuş et al., 2016; Chen et al., 2019; Das and Sahoo, 2019; Gomathi and Viswanathamurthi, 2019). In this report, we utilize a cobalt complex, namely cobaloxime, with an axial pyridyl-BODIPY ligand as hydrogen sulfide sensitive indicator. While a focus of many previous research efforts was on hydrogen sulfide sensing in living cells (Qian et al., 2011; Yu et al., 2014; Kowada et al., 2015), our aim is to develop a chemosensing system that can be used for both, the sensitive determination of H_2S in liquid samples such as surface waters and airborne H_2S. This contribution reports the identification of a suitable fluorophore-based molecular probe and its performance both as HS^- indicator in solution and in the gas phase.

Pyridyl-BODIPY complexes were reported for the first time by one of us (Bartelmess et al., 2013b) with the purpose to create novel hydrogen evolving photocatalysts (Bartelmess et al., 2014). Other groups expanded their application to electrocatalytic hydrogen generation (Manton et al., 2014) and improved the photocatalytic efficiency as well as the turnover numbers through chemical modification of the pyridyl-BODIPY fluorophores (Luo et al., 2014, 2015). More recently, analogous BODIPYs were used for the first time as homogeneous hydrogen-generating photosensitizers under acidic aqueous conditions (Xie et al., 2019). Two features of these BODIPY-cobaloxime complexes were notable in the present context and led us to study some of those compounds in more detail for HS^- sensing: The bright emission of the BODIPY fluorophore was almost quantitatively quenched upon complexation with the cobaloxime's cobalt center and the stability of the coordinative bond could be altered by introducing pyridyl linkers with different substituents. Recent work by Strianese et al. then supported our approach. These researchers found that pyridyl-cobaloxime complexes (not bearing fluorophores) were subject to a substitution reaction of the pyridine by the hydrogen sulfide anion HS^- (Strianese et al., 2015), which is formed by dissolving H_2S in water (or, for example, dissolving the Na_2S salt, respectively).

In the present study, we combine and exploit these previous findings and present an efficient and sensitive hydrogen sulfide sensing approach based on pyridyl-BODIPY-cobaloxime complexes. First, we demonstrate a "turn-on" fluorescence behavior for HS^- detection in water. Second, we apply the pyridyl-BODIPY-cobaloxime complex to a polymeric matrix, which shows the same "turn-on" fluorescence behavior upon exposure to H_2S gas.

MATERIALS AND METHODS

BODIPY-cobaloxime complexes **1** and **2** and their precursor molecules were synthesized according to refs (Bartelmess et al., 2013a,b). Toward this, chemicals purchased from Sigma-Aldrich were used as received. Reactions and measurements were carried out under ambient conditions unless otherwise noted in the respective protocols. All solvents were of highest purity available and used as received.

NMR titration experiments were recorded on a Varian Mercury 400 NMR spectrometer (^{1}H: 400 MHz, ^{19}F: 376 MHz). A solution of complex **1** (7.0 mM) in a mixture of CD_3CN/D_2O (5%) was titrated with increasing amounts of $Na_2S \times 9\ H_2O$ in D_2O ($c[Na_2S \times 9\ H_2O] = 0.4$ M). The residual proton signal ($CHD_2CN = 1.94$ ppm) was used as standard.

Ultra-high-performance liquid chromatography electro-spray ionization mass spectrometry (UPLC-ESI-MS) was performed on a Waters Acquity UPLC (gradient mixtures of acetonitrile/water) with a Waters LCT Premier XE mass detector. Additionally, a Waters Alliance System with Waters Separations Module 2695, a Waters Diode Array Detector 996, and a Waters Mass Detector ZQ 2000 were used. Chromatographic separations were performed with a gradient of 20 to 95% acetonitrile in water.

Initial emission titration experiments were carried out in acetonitrile, using 1×10^{-7} M solutions of the respective BODIPY-cobaloxime complexes, and subsequent addition of small aliquots of an aqueous solution of $Na_2S \times 9\ H_2O$ from 0.2 to 2.0 eq. A comparable concentration range was used for kinetic studies, monitoring the development of the emission maximum of the BODIPY dye vs. time. Absorption measurements were carried out on an Analytik Jena Specord 201 Plus UV/Vis spectrophotometer; fluorescence measurements in solution were carried out on a Horiba Jobin–Yvon Fluoromax-4P. Further spectroscopic experiments were carried out in 96-well microplates, made of polystyrene, non-binding, with transparent bottom and black body, purchased from Greiner Bio-One. Initially, a small amount of HydroMed's polyurethane hydrogel D4, dissolved in 96% ethanol (0.9 g of D4 in 4.0 g of ethanol), was deposited in the well and after drying, 5×10^{-8} mmol of the respective BODIPY cobaloxime complex (as 1×10^{-6} M solution in acetonitrile) was added. After drying, 50 μL of an aqueous solution of Na_2S (of the respective concentration, indicated by the molar eq. of the analyte) was added. After an incubation time of 10 min, the wells were analyzed with a TECAN infinite 200 Pro microplate reader.

To probe interactions with different anions and a typical organic thiol, the microplate was prepared as described before.

Subsequently, 200 μL of 0.3 mM solutions of the respective analyte were added and after an incubation time of about 1.5 h, the respective fluorescence intensities were determined. In addition to the analyte solutions in DI water, also pure DI water as well as a sample of surface water, collected in June 2019 from the Müggelspree river in Berlin-Friedrichshagen, was tested in the described manner. The latter sample was also spiked with HS^- (0.3 mM) and analyzed accordingly. The extended incubation time was chosen to reach full conversion of the respective analyte, and to avoid false negative results due to possibly increased reaction times of the different anions. Relative measurement uncertainties were estimated following our previously published considerations on this topic (Rurack and Spieles, 2011; Bell et al., 2016). Major contributions came from deviations of repeat measurements of the well-plate setup with only minor processing effects, all remaining below 6.0%. Only for the slightly turbid surface water sample a larger relative uncertainty of about 22% was estimated.

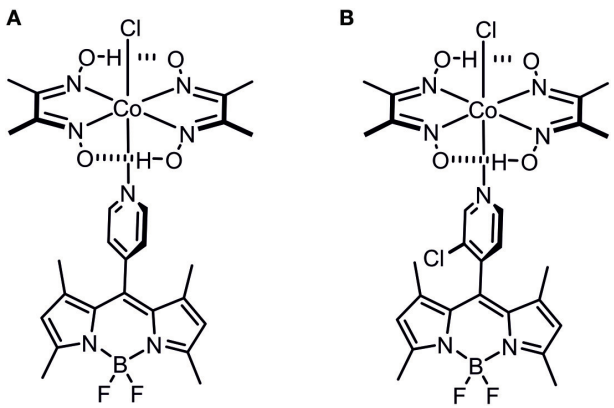

FIGURE 1 | Molecular structures of the investigated BODIPY-cobaloxime complexes **1 (A)** and **2 (B)**.

To probe the sensing of H_2S in the gas phase, the microplate was also prepared as described before and sealed with an aluminum foil sticker. The wells were exposed to H_2S gas from a H_2S gas cylinder ($C[H_2S] = 11.13$ ppm) with a 4 L h^{-1} flow rate for different periods of time.

RESULTS AND DISCUSSION

The synthesis of *meso*-pyridyl-BODIPY-cobaloxime $[Co(dmgH)_2(Cl)(BODIPY)]$ (dmgH = dimethylglyoximate anion) complexes **1** and **2** (**Figure 1**), together with their structural and photophysical characterization, was previously published (Bartelmess et al., 2013a,b). The fluorescence quantum yields of the parent BODIPY fluorophores were reported to be 0.30 in the case of BODIPY **1** and 0.90 in the case of BODIPY **2** in dichloromethane (Bartelmess et al., 2013a). By carefully evaluating the properties of BODIPY-cobaloxime complexes, especially in terms of stability, we focused our H_2S sensing studies on complexes **1** and **2**.

The stability of complex **2** is slightly lower compared with complex **1** due to the introduction of an electron withdrawing chlorine substituent on the pyridyl linker. We hypothesized that this lower complex stability of **2** will provide faster sensing responses as compared to **1**. Initial titration experiments, where the respective BODIPY-cobaloxime complexes were dissolved in acetonitrile and then titrated with an aqueous Na_2S solution, revealed promising results (**Figure 2**). Both investigated complexes showed a fluorescence enhancement upon addition of the analyte. However, a lower reaction rate was derived for complex **1**, based on the continued evolution of the fluorescence band upon addition of two eq. of the analyte. In the case of complex **2**, the system was entering a plateau after the addition of 2 eq. indicating a completion of the reaction already at lower concentrations (**Figure 2**, insets). The lower stability of complex **2** is a rational explanation for this observation. A more detailed determination of the reaction rate of complex **1**

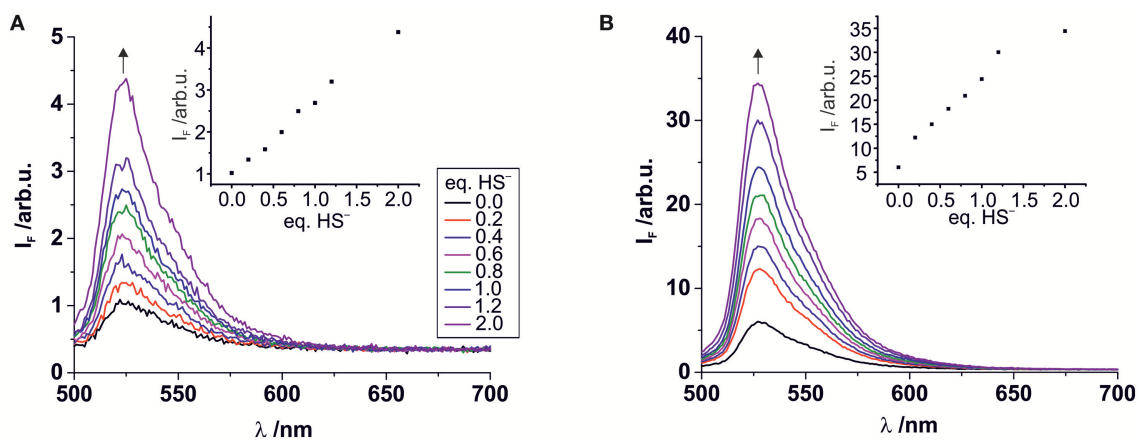

FIGURE 2 | Fluorescence titrations of 10^{-7} M solutions of complexes **1 (A)** and **2 (B)** in acetonitrile with increasing amounts of aqueous Na_2S solution. Excitation wavelength 490 nm. Insets: Plots of the fluorescence intensity at the emission maximum vs. the number of added HS^- eq., relative to the BODIPY-cobaloxime complexes (legend with color code in graph A applies to both graphs).

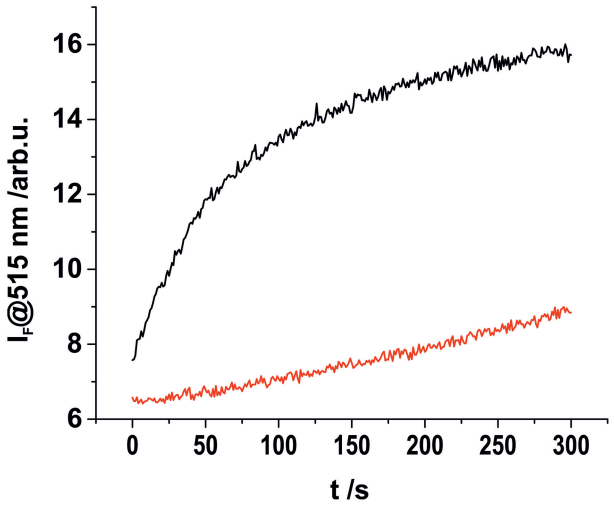

FIGURE 3 | Kinetic investigation of complex **1** in acetonitrile (2×10^{-8} M) upon addition of 1.5 eq., of aqueous HS^- solution (black), and in the absence of an analyte (red).

is shown in **Figure 3** and corroborates the initial findings of the titration experiment. The reaction of complex **2** was already completed before the measurement could be initiated, thus no results are shown here. The absorption titration spectra revealed virtually no changes upon addition of aqueous HS^- solution. The absence of absorption spectroscopic changes corroborated our earlier findings (Bartelmess et al., 2013b, 2014), that is, that the attachment of a BODIPY fluorophore to the cobaloxime metal-center through an internally orthogonally oriented and thus electronically decoupled *meso*-4-pyridyl linker does not allow for electronic coupling between BODIPY and metal ion in the ground state. The negligible shifts of ca. 4 nm only reflect the change in inductive effect at the pyridyl-*N* when the coordinative bond is cleaved.

We then performed ^{1}H-NMR titration experiments to obtain a better understanding of the mechanism behind the HS^--triggered fluorescence enhancement (**Figure 4**). To a 7.0 mM acetonitrile/5% water solution of **1** (**Figure 4A**) increasing quantities of Na_2S in water were added (**Figures 4B,C**). Initially, the addition of 0.75 eq. of Na_2S resulted in the formation of a new set of proton signals (H') which are in slow chemical exchange on the NMR time scale with the signals of complex **1** (H) (**Figure 4B**). This new set of protons signals resonate at the same chemical shift as the protons of the free BODIPY in solution (**Figure 4D**). The addition of 1.4 eq. of Na_2S then already produced the disappearance of the BODIPY-cobaloxime signals with the concomitant increase of the intensity of those signals assigned to the free BODIPY. The methyl protons (H^6) of the BODIPY-cobaloxime also vanish upon the addition of Na_2S. This is due to precipitation of the HS-cobaloxime which is insoluble in acetonitrile at these concentrations.

UPLC-MS analysis of the NMR sample containing a mixture of the BODIPY-cobaloxime complex **1** and 0.75 eq. of Na_2S was further invoked to reveal the mechanism, yielding a chromatogram with three major absorption bands at 5.15, 5.05, and 2.93 min retention times (**Supplementary Figure 2**) which were assigned to the BODIPY ligand, the BODIPY-cobaloxime complex, and HS-cobaloxime complex according to their corresponding ions $[BODIPY + H]^+$ (m/z = 326), $[[Co(dmgH)_2(Cl)(BODIPY)] + H]^+$ (m/z = 650) and $[Co(dmgH)_2(Cl)(HS)]^+$ (m/z = 356) in the ESI positive mode, respectively (see **Supplementary Figures 2–4**).

To identify a suitable solid support for further H_2S sensing studies in the gas phase, we performed more detailed spectroscopic studies loading polystyrene 96-well microplates with a thin layer of a D4 hydrogel. Subsequently, the BODIPY-cobaloxime complexes were also added to the wells. After plate preparation, aqueous HS^- solutions of different concentrations were added to the respective wells of the microplates. Fluorescence measurements were carried out through the transparent bottom of the plates (**Figure 5**) after an incubation time of 10 min. Since this time depends on the thickness of the hydrogel, reduction of the assay time is merely an engineering task.

In these experiments, the results for higher HS^- concentrations were largely comparable for the two BODIPY-cobaloxime complexes. When investigating lower HS^- concentrations, however, the decreased stability of complex **2** was obvious and no conclusive results could be obtained. Nevertheless, for complex **1** the results of the entire concentration range studied showed favorable features, that is, a pronounced response and an acceptable linearity, allowing for concentration-dependent measurements over a range from 10 μM to 1.0 mM. Complex **1** thus qualifies as a suitable fluorescent indicator for the determination of HS^- in aqueous solutions.

The effect of other, possibly competing anions which are typical constituents of drinking or surface water on the stability of **1** were studied as well. Additionally, the potential interference of biologically relevant molecules, mainly existing in the form of cysteine-containing biomolecules exhibiting free thiol groups, was also evaluated. Toward this, a microplate was loaded with the complex in the described manner and solutions containing similar anion or thiol concentrations (0.3 mM; 200 μL) of NO_3^-, SO_4^{2-}, Cl^-, CO_3^{2-}, PO_4^{3-}, OCl^-, HSO_3^-, SCN^-, and cysteine (as well as HS^-) were added. The fluorescence intensity was evaluated in the reader for up to 1.5 h of incubation. It was found that for most of the anion-containing samples the fluorescence response was low and of a similar intensity than for DI water. Solely HS^-, and to a lesser extent HSO_3^-, led to a largely increased emission of the BODIPY dye, compared to a DI water reference (**Figure 6**). In addition, a sample of surface water, collected from the Müggelspree in Berlin-Friedrichshagen was analyzed. A certain increase in fluorescence intensity was observed, which however is a matrix effect that did only marginally influence the HS^- detection performance. The latter was corroborated by analyzing a Müggelspree sample spiked with HS^-, yielding a fluorescence that amounted to the sum of the HS^-, and the matrix signal (**Figure 6**). The matrix effect of real water samples most likely stems from thiol-containing organic matter, as the moderate fluorescence response recorded for cysteine suggests. This is not surprising considering the chemical similarity of HS^- and an organic thiol group

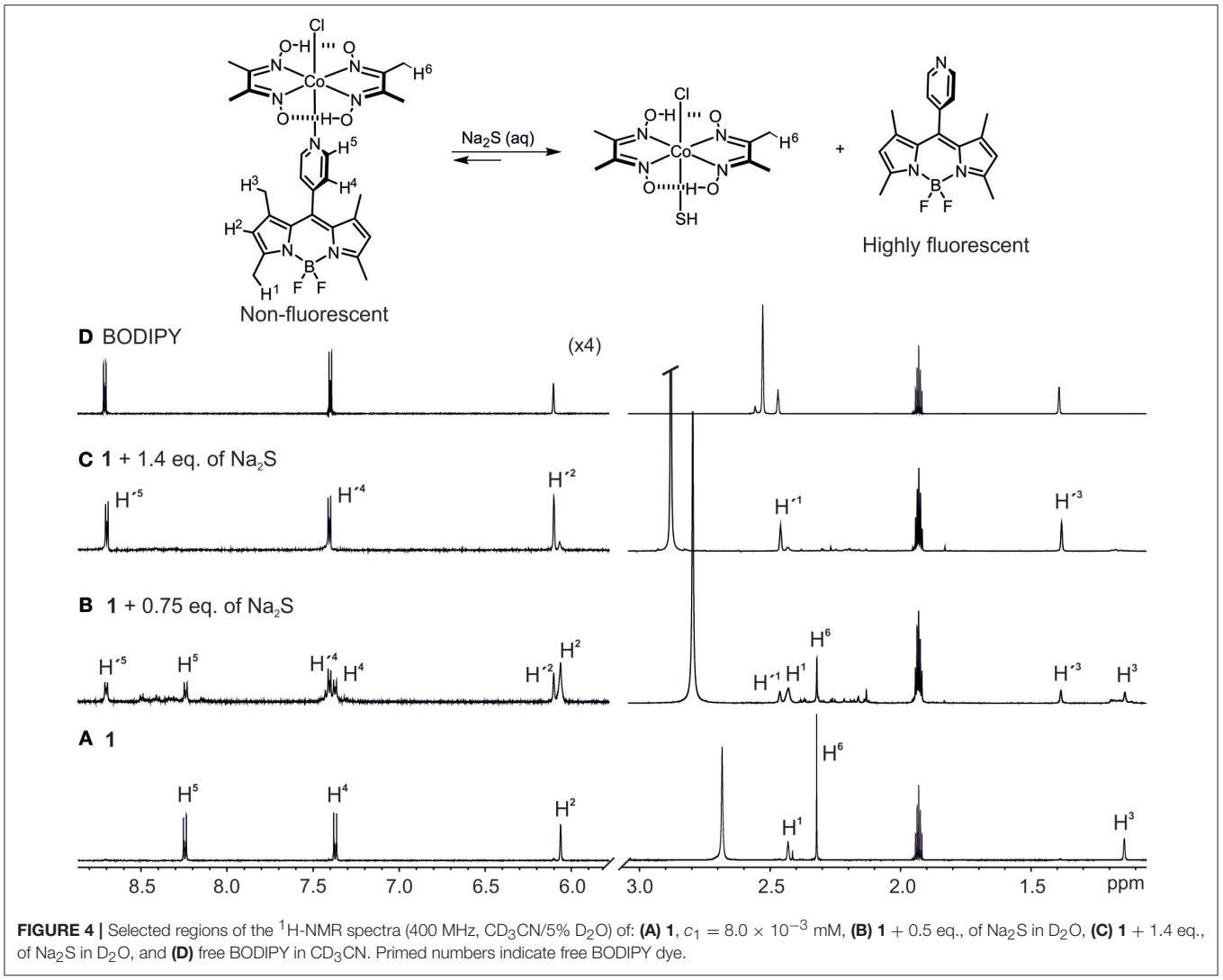

FIGURE 4 | Selected regions of the ^{1}H-NMR spectra (400 MHz, CD_3CN/5% D_2O) of: **(A) 1**, $c_1 = 8.0 \times 10^{-3}$ mM, **(B) 1** + 0.5 eq., of Na_2S in D_2O, **(C) 1** + 1.4 eq., of Na_2S in D_2O, and **(D)** free BODIPY in CD_3CN. Primed numbers indicate free BODIPY dye.

and the absence of a dedicated supramolecular binding site in complex **1**. However, such background signals can be accounted for by appropriate (automated) calibration procedures and background libraries.

Finally, a sealed microplate containing BODIPY-cobaloxime complex **1** loaded onto the hydrogel support was exposed to H_2S gas simply by flowing gas of a defined concentration though the system for different time intervals (**Figure 7**). These experiments revealed that the fluorescence response after 5 min of exposure to an atmosphere containing 11 ppm H_2S is distinctly higher compared to a reference sample which was exposed to synthetic air for 30 min. 11 ppm H_2S is a concentration that for instance workers involved in manure storage or handling on farms are frequently exposed to (Fabian-Wheeler et al., 2017). For the hydrogel film format used here, we determined that approximately 1 h is needed to achieve complete saturation of the system. Most likely, the sensing event involves first the transformation of H_2S into the anion HS^- once the gas is dissolved in the water contained in and at the surface of the hydrogel and, second the reaction of the anionic species with the BODIPY-cobaloxime indicator. Altogether, these experiments demonstrate that BODIPY-cobaloxime complex **1**, when applied to an adequate polymer matrix, can be used for the detection of H_2S gas in a straightforward manner.

CONCLUSION

In conclusion, BODIPY-cobaloxime complexes were successfully employed as fluorescent "turn on" indicators for the detection of HS^- in liquid and gas phase. Dissolving H_2S in water always leads to the formation of HS^- which reacts with the title complexes and allowed us to postulate a sensing mechanism which involves the selective replacement of the pyridyl-BODIPY dye by the HS^- anion in the cobaloxime complex via ^{1}H-NMR titration experiments. Fluorescence titration experiments indicated that both BODIPY-cobaloxime complexes **1** and **2** are in principle suitable molecules for the sensing of HS^- in liquid phase. However, the lower stability of complex **2** rendered it less applicable once the sensor dye was loaded onto a hydrogel support.

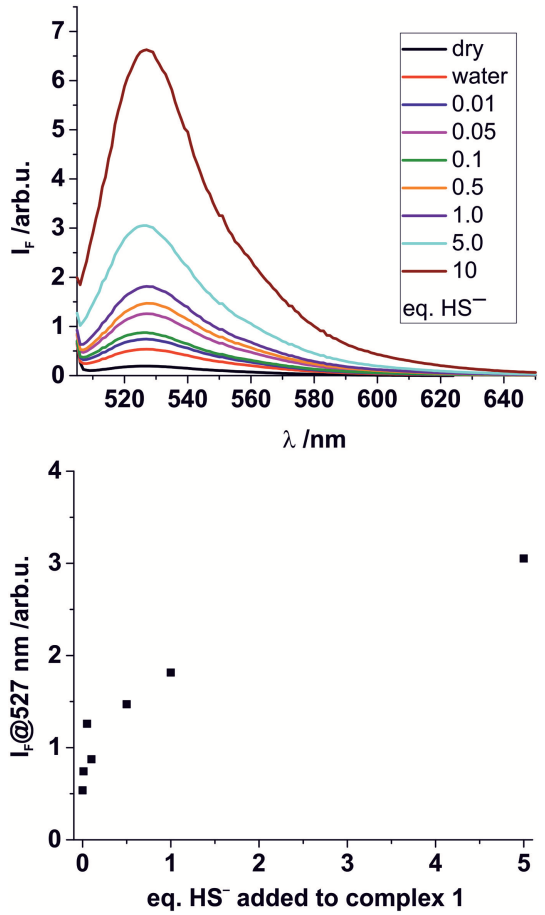

FIGURE 5 | Top: Fluorescence response of solid complex **1** (5×10^{-8} mmol per well) deposited on hydrogel D4 in a 96 well-microplate upon addition of 50 μL of aqueous Na_2S solutions of different concentrations. Eq., of Na_2S added as indicated. **Bottom:** Concentration dependency of the fluorescence response at the emission maximum.

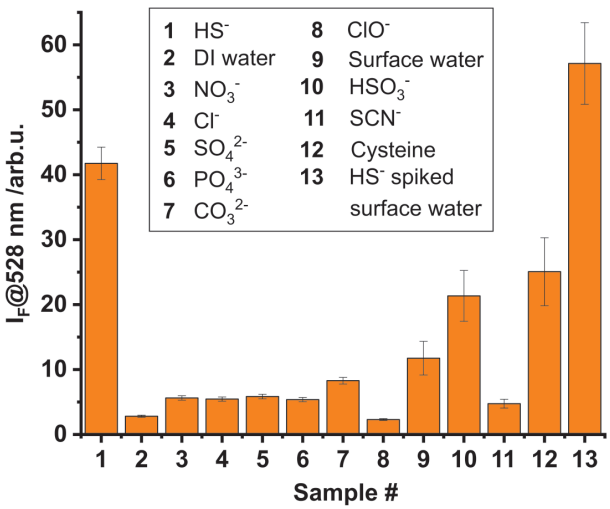

FIGURE 6 | Cross-reactivity study investigating the fluorescence response of complex **1** (5×10^{-8} mmol per well) adsorbed on hydrogel D4 upon addition of 200 μL of 0.3 mM aqueous solutions of different anions and thiols. The incubation time was 1.5 h. Sample 13 is surface water spiked with a similar amount of HS^- than sample **1**.

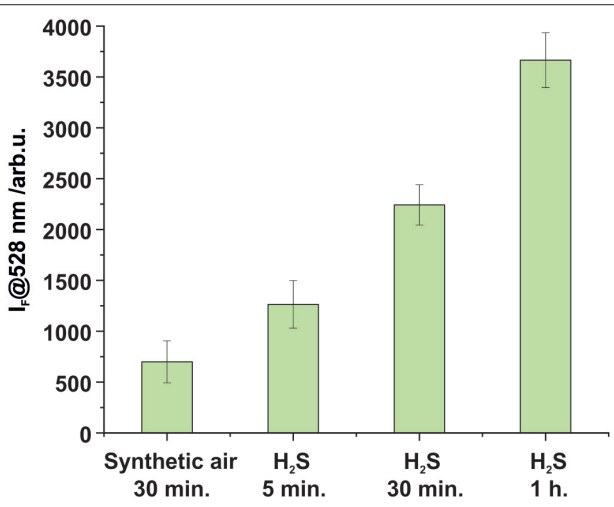

FIGURE 7 | Fluorescence enhancement observed after the exposure of complex **1** loaded on top of a hydrogel matrix (5×10^{-8} mmol per well) to synthetic air and H_2S ($c_{H2S} = 11.13$ ppm ± 0.33 Mol-ppm) for different time intervals at a 4 L h^{-1} flow rate in both cases.

BODIPY-cobaloxime complex **1** was successfully loaded onto a polymer matrix and its higher stability was suitable for using the sensory film for HS^- determination by a pronounced fluorescence response in the concentration range from 10 μM up to 1.0 mM in surface water. Cross-reactivity studies revealed that anions typically present in drinking water did not lead to a significant enhancement of fluorescence and only cysteine led to a certain background signal that has to be accounted for. Finally, we demonstrated that the combination of the BODIPY-cobaloxime complex with an adequate hydrophilic polymer matrix was suitable for H_2S gas detection at a concentration relevant in a farming context. Since cysteine and related thiol-containing compounds are non-volatile, an application in the gas phase would not suffer from these cross-reactivities.

Having successfully devised an indicator system for H_2S, we are currently integrating the sensory matrix into a dedicated measurement device to realize an automated sensor unit. The latter is the second part of a multi-gas sensing device for hazardous gases currently being developed within an interdisciplinary research project at BAM, the first target analyte having been NH_3 (Gawlitza et al., 2017). In the case of the present analyte, challenges beyond matrix integration and a unique detection mechanism are its high toxicity in combination with a pungent odor and the human olfactory system's fast adaption which do not only require the provision of a special laboratory setting but also the development of a dedicated H_2S test and reference gas generator currently being undertaken in our laboratories.

DATA AVAILABILITY STATEMENT

All datasets generated for this study are included in the manuscript/**Supplementary Files**.

AUTHOR CONTRIBUTIONS

JB, VV, and KR conceived the experiments, prepared the manuscript, discussed the results and commented on the manuscript. JB synthesized the compounds. JB and VV performed the experiments.

FUNDING

Funding was provided by the interdisciplinary Focus Area research project KonSens (Kommunizierende Sensorsysteme).

ACKNOWLEDGMENTS

Bundesanstalt für Materialforschung und -prüfung (BAM) is acknowledged for funding of the interdisciplinary Focus Area research project KonSens (Kommunizierende Sensorsysteme) within which this work was realized. Within KonSens, we thank BAM Divisions 1.2, 4.2, and 8.1 for fruitful collaboration, discussions and instrumental support. We are grateful to Carlo Tiebe (BAM Div. 8.1) for providing H_2S gas for the gas phase experiments.

SUPPLEMENTARY MATERIAL

The Supplementary Material for this article can be found online at: https://www.frontiersin.org/articles/10.3389/fchem.2019.00641/full#supplementary-material

REFERENCES

Bartelmess, J., Francis, A. J., El Roz, K. A., Castellano, F. N., Weare, W. W., and Sommer, R. D. (2014). Light-driven hydrogen evolution by BODIPY-sensitized cobaloxime catalysts. *Inorg. Chem.* 53, 4527–4534. doi: 10.1021/ic500218q

Bartelmess, J., Weare, W. W., Latortue, N., Duong, C., and Jones, D. S. (2013a). meso-Pyridyl BODIPYs with tunable chemical, optical and electrochemical properties. *New J. Chem.* 37, 2663–2668. doi: 10.1039/c3nj00426k

Bartelmess, J., Weare, W. W., and Sommer, R. D. (2013b). Synthesis, characterization and structural investigation of novel meso-pyridyl BODIPY-cobaloxime complexes. *Dalton Trans.* 42, 14883–14891. doi: 10.1039/c3dt51849c

Bayer, P., Rybach, L., Blum, P., and Brauchler, R. (2013). Review on life cycle environmental effects of geothermal power generation. *Renew. Sustain. Energy Rev.* 26, 446–463. doi: 10.1016/j.rser.2013.05.039

Bell, J., Climent, E., Hecht, M., Buurman, M., and Rurack, K. (2016). Combining a droplet-based microfluidic tubing system with gated indicator releasing nanoparticles for mercury trace detection. *ACS Sens.* 1, 334–338. doi: 10.1021/acssensors.5b00303

Blunden, J., Aneja, V. P., and Overton, J. H. (2008). Modeling hydrogen sulfide emissions across the gas–liquid interface of an anaerobic swine waste treatment storage system. *Atmos. Environ.* 42, 5602–5611. doi: 10.1016/j.atmosenv.2008.03.016

Carrera, L., Springer, F., Lipeme-Kouyi, G., and Buffiere, P. (2016). A review of sulfide emissions in sewer networks: overall approach and systemic modelling. *Water Sci. Technol.* 73, 1231–1242. doi: 10.2166/wst.2015.622

Chen, H., Wu, X., Yang, S., Tian, H., Liu, Y., and Sun, B. (2019). A visible colorimetric fluorescent probe for hydrogen sulfide detection in wine. *J. Anal. Methods Chem.* 2019:2173671. doi: 10.1155/2019/2173671

Dai, Z., Tian, L., Song, B., Ye, Z., Liu, X., and Yuan, J. (2014). Ratiometric time-gated luminescence probe for hydrogen sulfide based on lanthanide complexes. *Anal. Chem.* 86, 11883–11889. doi: 10.1021/ac503611f

Das, S., and Sahoo, P. (2019). A colorimetric sensor for hydrogen sulfide: Detection from biogas and quantitative estimation in water. *Sens. Actuators B.* 291, 287–292. doi: 10.1016/j.snb.2019.04.089

El-Maghrabey, M. H., Watanabe, R., Kishikawa, N., and Kuroda, N. (2019). Detection of hydrogen sulfide in water samples with 2-(4-hydroxyphenyl)-4,5-di(2-pyridyl)imidazole-copper(II) complex using environmentally green microplate fluorescence assay method. *Anal. Chim. Acta* 1057, 123–131. doi: 10.1016/j.aca.2019.01.006

Fabian-Wheeler, E. E., Hile, M. L., Murphy, D., Hill, D. E., Meinen, R. J., and Brandt, R. C. (2017). Operator exposure to hydrogen sulphide from dairy manure storage containing gypsum bedding. *J. Agric. Saf. Health* 23, 9–22. doi: 10.13031/jash.11563

Feilberg, A., Hansen, M. J., Liu, D., and Nyord, T. (2017). Contribution of livestock H_2S to total sulfur emissions in a region with intensive animal production. *Nat. Commun.* 8:1069. doi: 10.1038/s41467-017-01016-2

Gawlitza, K., Tiebe, C., Banach, U., Noske, R., Bartholmai, M., and Rurack, K. (2017). "Novel sensor for long-term monitoring of ammonia in gas phase," in *Proceeding of 13th Dresden Sensor Symposium* (Dresden), 272–276. doi: 10.5162/13dss2017/P4.02

Godoi, A. F. L., Grasel, A. M., Polezer, G., Brown, A., Potgieter-Vermaak, S., Scremim, D. C., et al. (2018). Human exposure to hydrogen sulphide concentrations near wastewater treatment plants. *Sci. Total Environ.* 610–611, 583–590. doi: 10.1016/j.scitotenv.2017.07.209

Gomathi, A., and Viswanathamurthi, P. (2019). Hydrogen sulfide detection by ESIPT based fluorescent sensor: potential in living cells imaging. *J. Photochem. Photobiol. A* 369, 97–105. doi: 10.1016/j.jphotochem.2018.10.013

Jiang, G. M., Melder, D., Keller, J., and Yuan, Z. G. (2017). Odor emissions from domestic wastewater: a review. *Crit. Rev. Environ. Sci. Technol.* 47, 1581–1611. doi: 10.1080/10643389.2017.1386952

Karakuş, E., Üçüncü, M., and Emrullahoglu, M. (2016). Electrophilic cyanate as a recognition motif for reactive sulfur species: selective fluorescence detection of H_2S. *Anal. Chem.* 88, 1039–1043. doi: 10.1021/acs.analchem.5b04163

Kaushik, R., Ghosh, A., and Amilan Jose, D. (2017). Recent progress in hydrogen sulphide (H_2S) sensors by metal displacement approach. *Coord. Chem. Rev.* 347, 141–157. doi: 10.1016/j.ccr.2017.07.003

Ko, J. H., Xu, Q. Y., and Jang, Y. C. (2015). Emissions and control of hydrogen sulfide at landfills: a review. *Crit. Rev. Environ. Sci. Technol.* 45, 2043–2083. doi: 10.1080/10643389.2015.1010427

Kowada, T., Maeda, H., and Kikuchi, K. (2015). BODIPY-based probes for the fluorescence imaging of biomolecules in living cells. *Chem. Soc. Rev.* 44, 4953–4972. doi: 10.1039/c5cs00030k

Liang, Y., Xin, H., Hoff, S. J., Richard, T. L., and Kerr, B. J. (2004). Performance of single point monitor in measuring ammonia and hydrogen sulfide gases. *Appl. Eng. Agric.* 20, 863–872. doi: 10.13031/2013.17712

Lippert, A. R., New, E. J., and Chang, C. J. (2011). Reaction-based fluorescent probes for selective imaging of hydrogen sulfide in living cells. *J. Am. Chem. Soc.* 133, 10078–10080. doi: 10.1021/ja203661j

Liu, C., Pan, J., Li, S., Zhao, Y., Wu, L. Y., Berkman, C. E., et al. (2011). Capture and visualization of hydrogen sulfide by a fluorescent probe. *Angew. Chem. Int. Ed.* 50, 10327–10329. doi: 10.1002/anie.201104305

Liu, C., Peng, B., Li, S., Park, C. M., Whorton, A. R., and Xian, M. (2012). Reaction based fluorescent probes for hydrogen sulfide. *Org. Lett.* 14, 2184–2187. doi: 10.1021/ol3008183

Luo, G. G., Fang, K., Wu, J. H., Dai, J. C., and Zhao, Q. H. (2014). Noble-metal-free BODIPY-cobaloxime photocatalysts for visible-light-driven hydrogen production. *Phys. Chem. Chem. Phys.* 16, 23884–23894. doi: 10.1039/c4cp03343d

Luo, G. G., Fang, K., Wu, J. H., and Mo, J. (2015). Photocatalytic water reduction from a noble-metal-free molecular dyad based on a thienyl-expanded BODIPY photosensitizer. *Chem. Commun.* 51, 12361–12364. doi: 10.1039/c5cc03897a

Malone Rubright, S. L., Pearce, L. L., and Peterson, J. (2017). Environmental toxicology of hydrogen sulfide. *Nitric Oxide* 71, 1–13. doi: 10.1016/j.niox.2017.09.011

Manton, J. C., Long, C., Vos, J. G., and Pryce, M. T. (2014). A photo- and electrochemical investigation of BODIPY-cobaloxime complexes for hydrogen production, coupled with quantum chemical calculations. *Phys. Chem. Chem. Phys.* 16, 5229–5236. doi: 10.1039/c3cp55347g

Marriott, R. A., Pirzadeh, P., Marrugo-Hernandez, J. J., and Raval, S. (2016). Hydrogen sulfide formation in oil and gas. *Can. J. Chem.* 94, 406–413. doi: 10.1139/cjc-2015-0425

Nimmermark, S. (2004). Odour influence on well-being and health with specific focus on animal production emissions. *Ann. Agric. Environ. Med.* 11, 163–173. doi: 10.15244/pjoes/29944

Pandey, S. K., Kim, K.-H., and Tang, K.-T. (2012). A review of sensor-based methods for monitoring hydrogen sulfide. *Trends Anal. Chem.* 32, 87–99. doi: 10.1016/j.trac.2011.08.008

Peng, H., Cheng, Y., Dai, C., King, A. L., Predmore, B. L., Lefer, D. J., et al. (2011). A fluorescent probe for fast and quantitative detection of hydrogen sulfide in blood. *Angew. Chem. Int. Ed.* 50, 9672–9675. doi: 10.1002/anie.201104236

Prata, A. A. Jr., Santos, J. M., Timchenko, V., and Stuetz, R. M. (2018). A critical review on liquid-gas mass transfer models for estimating gaseous emissions from passive liquid surfaces in wastewater treatment plants. *Water Res.* 130, 388–406. doi: 10.1016/j.watres.2017.12.001

Qian, Y., Karpus, J., Kabil, O., Zhang, S. Y., Zhu, H. L., Banerjee, R., et al. (2011). Selective fluorescent probes for live-cell monitoring of sulphide. *Nat. Commun.* 2:495. doi: 10.1038/ncomms1506

Rurack, K., and Spieles, M. (2011). Fluorescence quantum yields of a series of red and near-infrared dyes emitting at 600-1000 nm. *Anal. Chem.* 83, 1232–1242. doi: 10.1021/ac101329h

Strianese, M., Mirra, S., Bertolasi, V., Milione, S., and Pellecchia, C. (2015). Organometallic sulfur complexes: reactivity of the hydrogen sulfide anion with cobaloximes. *New J. Chem.* 39, 4093–4099. doi: 10.1039/c5nj00206k

Strianese, M., and Pellecchia, C. (2016). Metal complexes as fluorescent probes for sensing biologically relevant gas molecules. *Coord. Chem. Rev.* 318, 16–28. doi: 10.1016/j.ccr.2016.04.006

Stuck, B. A., Fadel, V., Hummel, T., and Sommer, J. U. (2014). Subjective olfactory desensitization and recovery in humans. *Chem. Senses* 39, 151–157. doi: 10.1093/chemse/bjt064

Szabo, C. (2018). A timeline of hydrogen sulfide (H_2S) research: from environmental toxin to biological mediator. *Biochem. Pharmacol.* 149, 5–19. doi: 10.1016/j.bcp.2017.09.010

Vikrant, K., Kailasa, S. K., Tsang, D. C. W., Lee, S. S., Kumar, P., Giri, B. S., et al. (2018). Biofiltration of hydrogen sulfide: trends and challenges. *J. Cleaner Prod.* 187, 131–147. doi: 10.1016/j.jclepro.2018.03.188

Xie, A., Pan, Z. H., Yu, M., Luo, G. G., and Sun, D. (2019). Photocatalytic hydrogen production from acidic aqueous solution in BODIPY-cobaloxime-ascorbic acid homogeneous system. *Chin. Chem. Lett.* 30, 225–228. doi: 10.1016/j.cclet.2018.05.003

Yu, F., Han, X., and Chen, L. (2014). Fluorescent probes for hydrogen sulfide detection and bioimaging. *Chem. Commun.* 50, 12234–12249. doi: 10.1039/c4cc03312d

Zhang, R., Liu, S., Wang, J., Han, G., Yang, L., Liu, B., et al. (2016). Visualization of exhaled hydrogen sulphide on test paper with an ultrasensitive and time-gated luminescent probe. *Analyst* 141, 4919–4925. doi: 10.1039/c6an00830e

Conflict of Interest: The authors declare that the research was conducted in the absence of any commercial or financial relationships that could be construed as a potential conflict of interest.

The handling editor declared a past co-authorship with one of the authors KR.

frontiers in Chemistry

REVIEW
published: 25 October 2019
doi: 10.3389/fchem.2019.00712

Recent Progress of BODIPY Dyes With Aggregation-Induced Emission

Zhipeng Liu[2,3]*, *Zhiyong Jiang*[2,3], *Ming Yan*[1] and *Xiaoqing Wang*[1]*

[1] College of Science, Nanjing Forestry University, Nanjing, China, [2] College of Materials Science and Engineering, Nanjing Forestry University, Nanjing, China, [3] Key Laboratory of Flexible Electronics (KLOFE) & Institute of Advanced Materials (IAM), Jiangsu National Synergetic Innovation Center for Advanced Materials (SICAM), Nanjing Tech University (NanjingTech), Nanjing, China

With the development of organic optoelectronic materials and bioimaging technology, to exploit organic luminescent materials with high luminescent efficiency in aggregation-state has become a research hotspot. BODIPYs have become one of the research objects of this kind of material because of their obvious advantages. This review focuses on the design and synthesis of AIE-type BODIPYs, the mechanism of AIE properties and their applications in recent years. Through classification, analysis, and summary, this review aims to explore the structure-activity relationship of AIE-type BODIPYs and to provide ideas for the further design and potential applications of AIE-active fluorescent materials.

Keywords: BODIPY, aggregation-induced emission, fluorescence, bioimaging, sensor

OPEN ACCESS

Edited by:
Hua Lu,
Hangzhou Normal University, China

Reviewed by:
Shaomin Ji,
Guangdong University of Technology, China
Wanhua Wu,
Sichuan University, China

***Correspondence:**
Zhipeng Liu
zpliu@njfu.edu.cn
Xiaoqing Wang
xqwang@njfu.edu.cn

Specialty section:
This article was submitted to Supramolecular Chemistry, a section of the journal Frontiers in Chemistry

Received: *02 August 2019*
Accepted: *09 October 2019*
Published: *25 October 2019*

Citation:
Liu Z, Jiang Z, Yan M and Wang X (2019) Recent Progress of BODIPY Dyes With Aggregation-Induced Emission. Front. Chem. 7:712. doi: 10.3389/fchem.2019.00712

INTRODUCTION

Organic luminescent materials (OLMs) are widely used in chemo/biosensors and light-emitting devices in light of their rich advantages, which include great diversity, easily modified structures, rich colors, and low environmental pollution (Chan et al., 2012; Uoyama et al., 2012; Yan et al., 2018). Since most of these applications heavily depend on their luminescent capabilities in the condensed state, the development of luminophores with excellent photophysical properties in the aggregation state is highly required. Traditional organic fluorescent dyes with a π-conjugated structure show excellent luminescent properties in dilute solution but become weakly or non-emissive in high concentration solutions or the aggregation-state, which is called the aggregation-caused emission quenching (ACQ) effect (Förster and Kasper, 1954). This effect is due to the collision between the ground state and the excited state of the fluorescent molecule at high concentration, which leads to the non-radiation deactivation process, or because the strong interaction between the planar π-conjugated structures leads the formation of excimers or exciplexes, and the energy of the excited state decays through the non-radiative form. The ACQ effect greatly limits the practical application of OLMs because the aggregated states are unavoidable for both light-emitting devices and fluorescent sensors.

Aggregation-induced emission (AIE), which was first introduced by Tang et al. has been widely accepted as a novel strategy to mitigate the ACQ effect on OLMs (Mei et al., 2015). Generally, AIE molecules such as 1,1,2,3,4,5-hexaphenylsilole (HPS, **Figure 1**) and tetraphenylethylene (TPE, **Figure 1**) usually possess highly twisted structures and show weak fluorescence in diluted solutions due to non-radiative transition induced by intramolecular motion (IM) in their excited state. In the aggregation state, such IM progress is effectively suppressed, resulting in their enhanced emission. Additionally, the highly twisted structure can effectively inhibit the π-π interactions between AIE molecules, which is conducive to improving their solid-state luminescence efficiency. Based on the

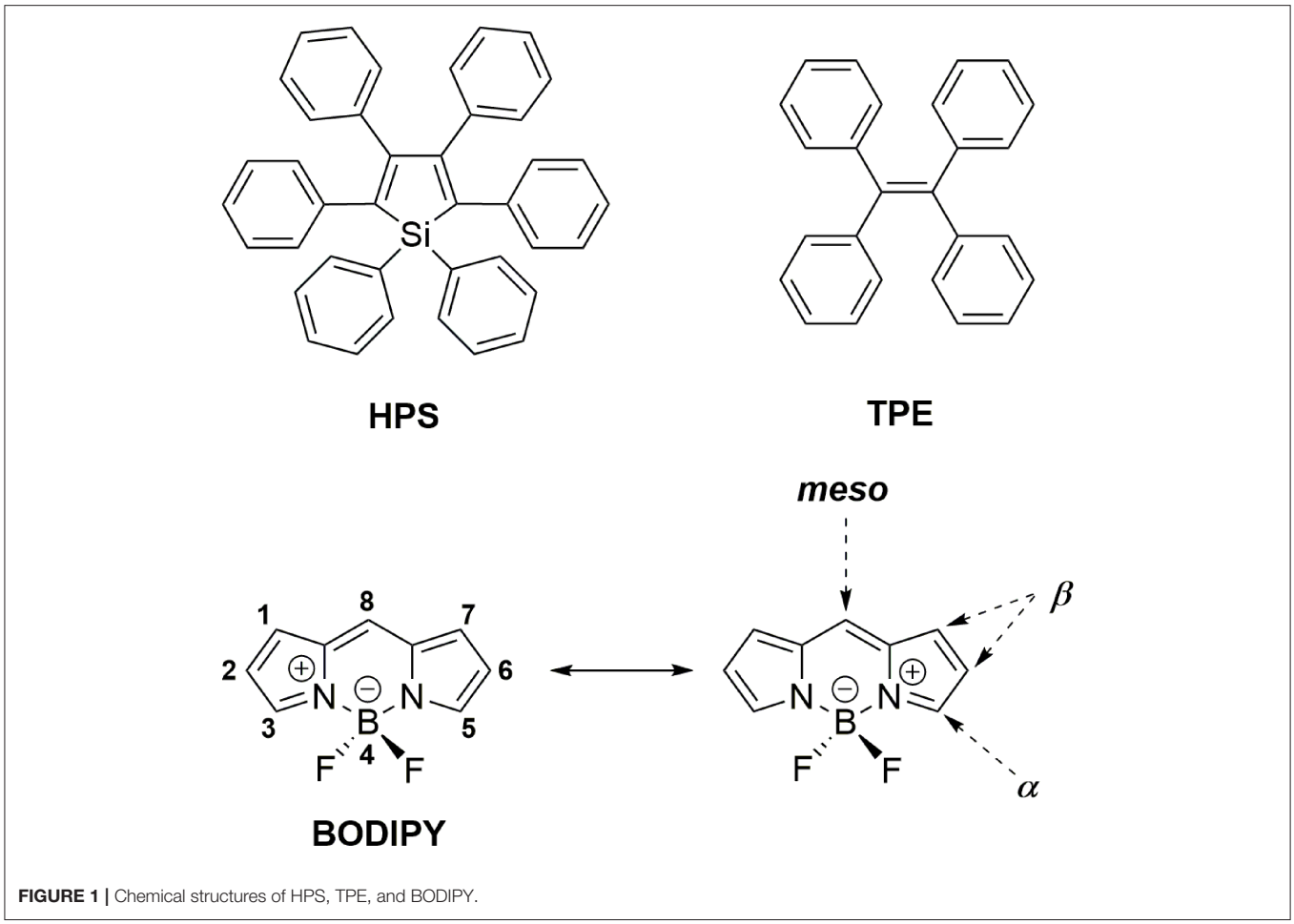

FIGURE 1 | Chemical structures of HPS, TPE, and BODIPY.

widely accepted restriction of intramolecular motion (RIM) mechanism, AIE materials, including not only various newly designed molecules but also classical fluorophores including coumarins, pyrene, squaraines, cyanies, perleneimides, and BODIPYs, have been developed and applied in bioimaging, data encryption/decryption, OLEDs, and stimuli-responsive materials (Mei et al., 2015; Kokado and Sada, 2019).

As a classical luminophore, BODIPY dyes (boron dipyrromethene and its analogs, **Figure 1**) have achieved great development in the field of fluorescent sensing and bioimaging because of their excellent photophysical properties, including large molar extinction coefficients, high fluorescence quantum yields, tunable emission from visible light to near-infrared (NIR), and high photo- and chemical-stability (Loudet and Burgess, 2007; Boens et al., 2012; Lu et al., 2014; Kowada et al., 2015; Fan et al., 2016; Ge and O'shea, 2016; Wang et al., 2017). Unfortunately, in contrast to their excellent luminescence in a solution, most BODIPYs suffer from the ACQ effect and show weak fluorescence in the aggregation state. This is mainly because of the self-absorption and strong intermolecular interactions (π-π stacking, etc.) induced by their small Stokes shift and planar π-conjugated structures. These problems greatly restrict the further applications of BODIPYs as solid-state emitters. Therefore, the development of BODIPYs with aggregation-state fluorescence has received intense attention in the past decades.

AIE has been proved to be an efficient strategy for the construction of BODIPYs with efficient fluorescence in the aggregation state. A number of AIE-active BODIPYs have been rationally designed by various strategies, such as the direct integration of AIE molecules with the BODIPY skeleton (Hu et al., 2012; Gomez-Duran et al., 2015), J-type aggregation (Choi et al., 2014; Kim et al., 2015), and dipyrromethene bidentate ligand modification (Yang et al., 2012; Wang et al., 2015b). Taking the advantages of AIE, the intense aggregation-state fluorescence of BODIPYs has been successfully achieved. Moreover, their application as aggregation-state emitters for bioimaging, stimuli-response switches as well as OLEDs has been demonstrated (Mei et al., 2015; Baysec et al., 2018; Che et al., 2019). This mini review focuses on providing an overview of the design, mechanism and application of AIE-active BODIPYs and BODIPY analogs so as to facilitate their future application in the solid-state luminescence field. For the convenience of explanation, AIE-active BODIPYs are divided into two categories: one is based on the boron dipyrromethene platform (classical BODIPYs); the other is BODIPY analogs based on heterocycle-based bidentate chelates. The key photophysical data of each compound discussed are listed in **Table 1**. Moreover, boron difluoride complexes based on β–diketonate,

TABLE 1 | Compilation of the photophysical data of BODIPY dyes with AIE.

	In solution			In H_2O-THF mixture		In solid-state	
Dye	**solvent**	**λ_{abs} (nm)[a] (ε/M^{-1} cm^{-1})**	**λ_{em}[b] (nm)**	**Φ_f (%)**	**λ_{em} (nm)[b] (f_w)**	**Φ_f (%)**	**λ_{em}[b] (nm)**	**Φ_f (%)**
1	THF	-	650	0.2	618 (90)	-	-	5
2	THF	-	640	0.3	640 (90)	-	-	27
3	THF	-	529	0.1	600 (90)	-	-	7.5
4	THF	536	567	59	569 (80)	53	-	-
5	THF	572 (54600)	630	2.9	630 (90)	3.9	642	10
6	THF	619 (26400)	697	6.4	697 (90)	2.32	706	6.9
7	THF	665 (80100)	690	42	690 (90)	-	690	1.3
8	THF	513	663	6.1	645 (99)	-	-	-
9	THF	498	586	0.74	700 (95)	-	-	-
10	THF	515	688	1.1	658 (99)	-	-	-
11	THF	501	754	0.27	-	-	-	-
12	THF	540	641	3	-	4	-	-
13	THF	513	633	4	-	10	-	-
14	THF	536	636	5	-	5	-	-
15a	CH_2Cl_2	550 (50000)	592	80	-	-	630 ± 4	-
15b	CH_2Cl_2	587 (48000)	618	81	-	-	636 ± 4	-
15c	CH_2Cl_2	589 (54000)	618	86	-	-	636 ± 4	-
15d	CH_2Cl_2	589 (47000)	619	87	-	-	636 ± 4	-
16	THF	514.5	525	-	-	-	537[g]	-
17a	CH_3CN	549 (46310)	620	0.3	625 (99)[d]	6	-	-
17b	CH_3CN	509 (87180)	535	0.3	587 (99)[d]	7	-	-
17c	CH_3CN	509 (92160)	537	0.4	594 (99)[d]	-	-	-
17d	CH_3CN	501 (85070)	536	0.8	557 (99)[d]	1.57	-	-
18a	EA[c]	503 (84000)	511.5	94	-	-	-	-
18b	EA[c]	503 (80000)	511	90	-	-	-	-
18c	EA[c]	503 (86000)	511	90	-	-	-	-
19a	EA[c]	503 (69000)	514.5	89	-	-	-	-
19b	EA[c]	503.5 (53000)	516.5	98	-	-	-	-
20a	CH_2Cl_2	507	514	2	575 (45)[e]	6.6	592	3
20b	CH_2Cl_2	502	515	2	-	-	595	5
21a	CH_2Cl_2	506	512	75	565 (50)[e]	32	609	16
21b	CH_2Cl_2	501	512	22	-	-	576	18
22a	CH_2Cl_2	508	515	40	545 (75)[e]	3.2	585	13
22b	CH_2Cl_2	502	515	13	-	-	590	28
23	$CHCl_3$	484 (12882)	515	5	515 (96)	23	515[g]	14
24	THF	668 (128000)	683	0.8	683 (90)[f]	21.9	-	-
25	THF	677 (115000)	697	1.1	697 (90)[f]	18.8	-	-
26	THF	440	473	12	610 (90)	-	540[g]	-
27a	CH_2Cl_2	432	538	7	-	-	525[g]	20
27b	CH_2Cl_2	413	512	6	-	-	497[g]	52
27c	CH_2Cl_2	404	497	4	-	-	508[g]	19
27d	CH_2Cl_2	408	506	4	-	-	49 [g]	5
27e	CH_2Cl_2	384	545	3	-	-	515[g]	6
28a	THF	434 (47000)	514	<1	549 (90)	<1	573	2
28b	THF	398 (57000)	524	<1	564 (90)	1	543	1
29a	THF	305 (33000), 420 (76000)	506	<1	523 (90)	1	541	10
29b	THF	292 (35000), 394 (41000)	556	<1	562 (90)	<1	560	1
30a	hexane	380 (43700)	440	<1	495 (80)	-	495	26
30b	hexane	402 (25800)	499	41	-	-	503	60

(Continued)

TABLE 1 | Continued

Dye	In solution				In H_2O-THF mixture		In solid-state	
	solvent	λ_{abs} (nm)[a] (ε/M^{-1} cm^{-1})	λ_{em}[b] (nm)	Φ_f (%)	λ_{em} (nm)[b] (f_w)	Φ_f (%)	λ_{em}[b] (nm)	Φ_f (%)
31a	CH_2Cl_2	391 (33300)	429	2	-	-	525	13
31b	CH_2Cl_2	388 (24000)	426	1	-	-	488	15
31c	CH_2Cl_2	459 (70800)	529	78	-	-	629	20
32a	CH_2Cl_2	362 (16000)	450	<1	450 (90)	1	460	53
32b	CH_2Cl_2	387 (12000)	471	<1	475 (90)	1	494	46
33a	THF	373 (140000)	462	3	463 (90)	13	498	10
33b	THF	348 (370000)	441	1	443(90)	9	459	44
33c	THF	350 (310000)	437	2	440 (90)	23	463	38
33d	THF	367 (390000)	522	10	524 (90)	15	491	37
34a	$CHCl_3$	459 (25119)	475	92	-	-	580	2
34b	$CHCl_3$	452 (15848)	467	81	-	-	537	9.1
34c	$CHCl_3$	510 (39810)	605	30	-	-	624	1.8
34d	$CHCl_3$	466 (25119)	482	78	-	-	523	22
34e	$CHCl_3$	525 (39810)	617	10	-	-	620	9.3
35a	THF	392 (19000)	447	1	480 (99)	7	494	29
35b	THF	397 (19300)	438	3	576 (99)	16	547	27
35c	THF	409 (37700)	485	1	521 (80)	7	506	21
35d	THF	408 (35500)	448	2	545 (90)	20	555	23
35e	CH_2Cl_2	395 (34200)	458	<1	-	-	473	0.60
35f	CH_2Cl_2	409 (43800)	522	<1	-	-	518	0.27
36a	CH_2Cl_2	407 (20000)	471	<1	471 (99)	14	481	12
36b	CH_2Cl_2	416 (21000)	464	<1	518 (90)	<1	534	20
36c	CH_2Cl_2	448 (11000)	522	<1	522 (90)	35	538	26
36d	CH_2Cl_2	461 (14000)	513	<1	583 (90)	<1	577	10

[a] *Longest absorption band.*
[b] *Longest emission band.*
[c] *EA, ethyl acetate.*
[d] *Measured in CH_3CN/H_2O mixture.*
[e] *Measured in methanol/H_2O mixture.*
[f] *Measured in CH_2Cl_2/Hexane mixture.*
[g] *Measured in the film state.*

ketoiminate, and diiminate will not be discussed in this review. A review that summarizes the photophysical properties and applications of these complexes would be helpful to readers (Tanaka and Chujo, 2015).

CLASSICAL BODIPYS WITH AIE

AIE-Active BODIPYs Based on TPE

Due to the planar π-conjugated structure of boron dipyrromethene core, strong intermolecular interactions such as π-π stacking and hydrogen bonds are usually observed in the aggregation state of BODIPYs, leading to distinct emission quenching. In order to suppress the strong intermolecular interactions, the well-known AIE luminescent element, TPE, has been successfully integrated with BODIPYs; thus, both AIE and intense aggregation-state emission were achieved. Tang et al. first reported TPE-containing BODIPYs (**1**–**3**, **Figure 2**) with AIE effect (Hu et al., 2012). In compounds **1**–**3**, TPE was simply introduced to the *meso*-position of the BODIPY core *via* a palladium-catalyzed cross-coupling reaction. In tetrahydrofuran (THF)-water mixture, both locally excited (LE) state, and twisted intramolecular charge transfer (TICT) state emission bands were observed in the emission spectra of compounds **1**–**3**. Compound **1** showed ACQ with the increment of the fraction of water (f_w) in THF. In contrast, the intensity of the TICT emission band of compounds **2** and **3** was increased dramatically and accompanied by the decrement of the LE emission band. Meanwhile, the fluorescence quantum yields (Φ_f) of compounds **2** and **3** in the solid state were determined to be 27 and 7.5%, respectively, which are higher than those of obtained in THF solution (Φ_f < 1%). Clearly, the relative stronger TICT effect of compounds **2** and **3** compared to compound **1** should be responsible for their different AIE and ACQ behavior.

The AIE behavior of TPE-BODIPY is highly dependent on the position and the number of TPE units attached to the BODIPY core. For example, Wu et al. (Chua et al., 2015), Scherf et al. (Baysec et al., 2018), and Atilgan et al. (Baglan et al., 2013) have reported that BODIPY derivatives with TPE or triphenylethene units at 2,6- or 2,6,8-positions

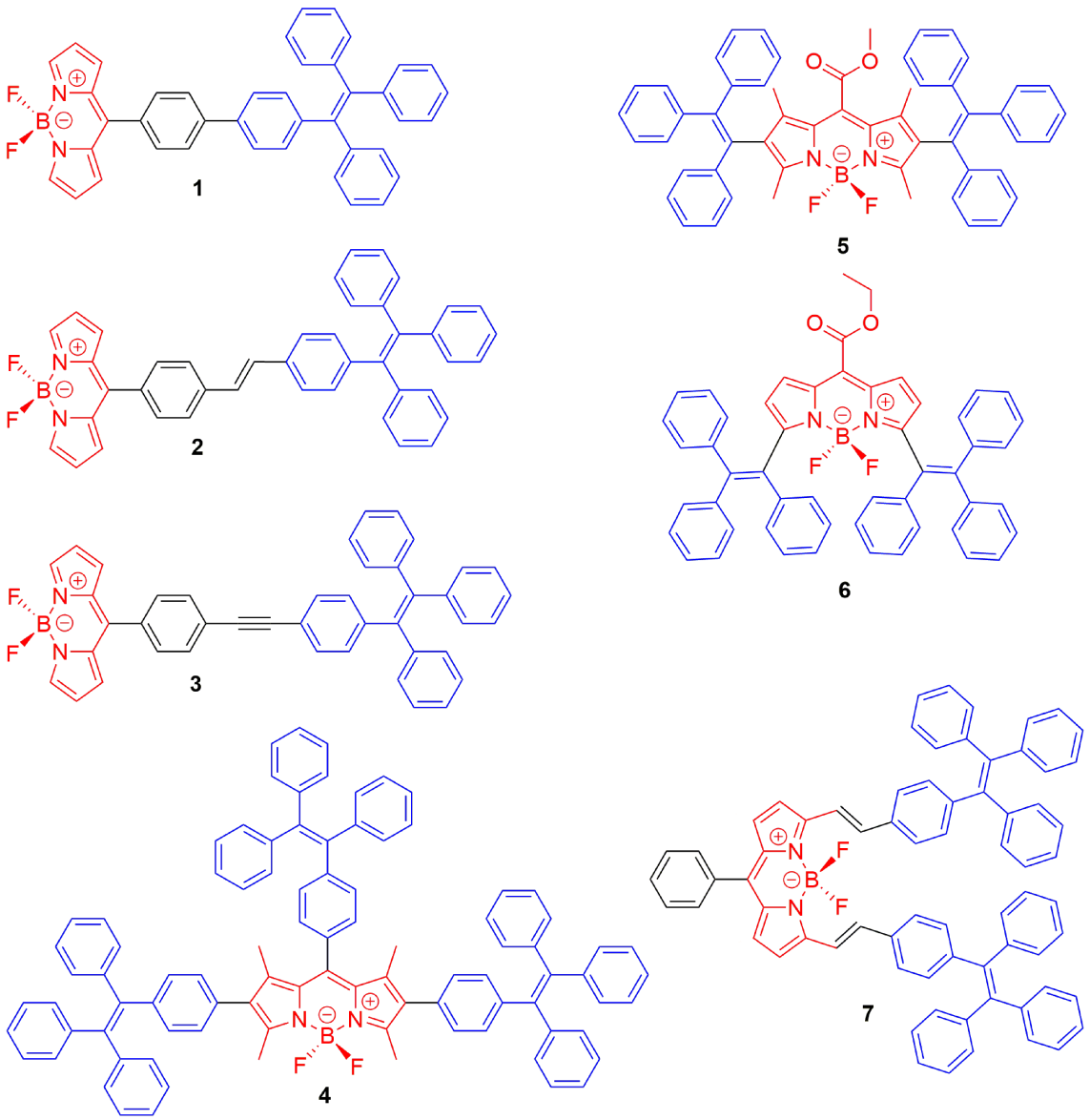

FIGURE 2 | Chemical structures of compounds **1**–**7**.

(**4**–**5**, **Figure 2**) could effectively inhibit ACQ and act as aggregation-induced emission enhancement (AIEE). However, the conjugating of TPE at 3,5-position of the BODIPY core resulted in large π-conjugated structures with ACQ (**6**–**7**) (Gomez-Duran et al., 2015).

AIE-Active BODIPYs Based on Triphenylamine (TPA)

Designing the propeller-shaped BODIPY molecules to consist of electron donor (D) and acceptor (A) units is another method to hinder the ACQ effect. Tang et al. developed a group of AIE-active BODIPYs with a D-A structure (**8**–**11**, **Figure 3**). Due to the strong electronic interaction between TPA (D) and BODIPY (A), compounds **8**–**11** displayed TICT and AIE properties. When the water was added to the THF solution of **8**–**11**, the LE emission intensity decreased with an increment of f_w, accompanied by the red-shift of emission. This progress is mainly dominated by the polarity effect. However, when the f_w reached the point of aggregation, the rotation of the aromatic rings was efficiently restricted, resulting in blue-shifted emission, and AIE (**Figure 4**) (Hu et al., 2009; Lager et al., 2009). Moreover, compounds **12**–**14** with TPA unit incorporated into the 2-, 2,6-, 2,6,8-positions showed more enhanced TICT effect than compounds **8**–**11**, and only aggregation-induced emission enhancement of TICT was observed (Bui et al., 2019).

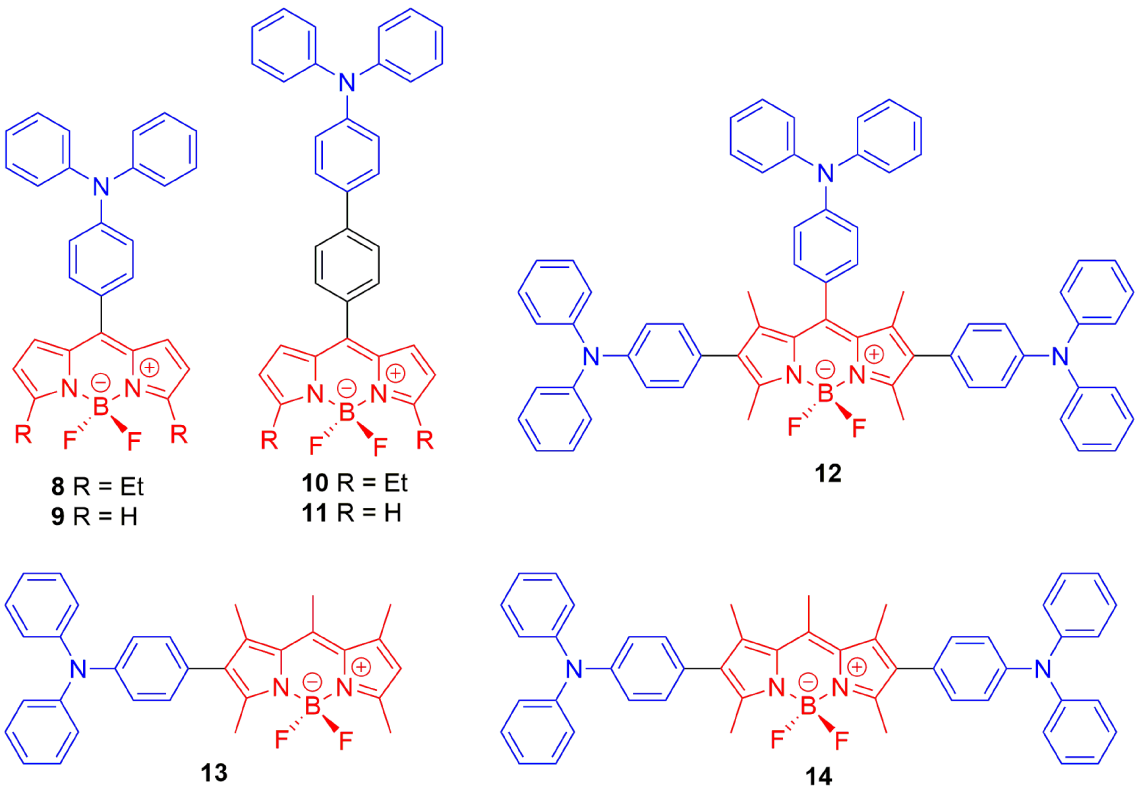

FIGURE 3 | Chemical structures of compounds **8**–**14**.

AIE-Active BODIPYs Based on J-aggregation

Most BODIPYs tend to form H-type (face to face) aggregates in the aggregated state, which leads to fluorescence quenching. Recent studies indicated that the packing of BODIPYs could be engineered to favor the formation of J-type (head to tail) aggregates, and they would then give out red-shifted emission in comparison to their respective monomers in solution. Under this aggregation, the transition dipoles of the monomers aligned in a coplanar inclined way with a slip angle $<54.7^{\circ}$ to form dimers, trimers or even larger J-aggregates (Wurthner et al., 2011; Choi et al., 2014; Tian et al., 2018).

Johansson et al. first evidenced the formation of non-fluorescent BODIPY H-dimers in double-labeled proteins and emissive J-dimers in labeled lipid vesicles (Bergström et al., 2002). Vu et al. found that bulky substituents at the 3- and 5-positions of the BODIPY core, such as paracyclophane (**15**, **Figure 5**) (Vu et al., 2009) and the adamantyl group (**16**) (Vu et al., 2013), could facilitate the formation of emissive J-aggregates in the aggregation state. To elucidate the factors that govern the formation of emissive J-aggregates of BODIPYs, Kim et al. carried out a systematic study of the substitution effect on the *meso*-position (Choi et al., 2014; Kim et al., 2015). For 1,3,5,7-tetramethyl derivatives, the *meso*-substituents **17**, that are $-CF_3$, -COOMe, $-COO^tBu$, and $-^iPr$, demonstrably formed emissive J-aggregates. Meanwhile, other *meso*-substituents, such as $-CH_3$, -CHO, -CN, and -Cl, exhibited the ACQ effect or were fluorescent in the solid state without forming J-aggregates (**Figure 6**). The formation of emissive J-aggregates is quite sensitive to minute structural changes. J-aggregations were not encountered in the closely related 3,5-dimethyl derivatives. Both the electron-withdrawing *meso*-substituents and flanking methyl groups are necessary for the formation of emissive BODIPY J-aggregates. Moreover, by using the AIEE-type *meso*-ester-substituted BODIPY probe **17b**, they realized the need to detect specifically HOBr generated by eosinophil peroxidase (EPO) for a clean turn-on signal: the red emissive (621 nm) J-aggregates of 2,6-dibrominated **17b** self-assembled into orange emissive (581 nm) J-aggregates (Kim et al., 2018).

Besides the abovementioned J-aggregation tuning tuned *via* variation the *meso*-substitutions, the modification of BF_2 moiety with a diacyloxyl or diaryl substituent should be another potential strategy. For example, AIE behavior induced by J-aggregation of BODIPY in pure organic solvents was described by Chiara et al. in *O*-BODIPYs with a B-spiranic 4,4-diacyloxyl substitution pattern (**18**, **19**, **Figure 5**). The high conformational rigidity of this design along with the orthogonal disposition of the B-diacyloxyl substituent and the *meso*-aryl group were analyzed to be the key factors of the J-aggregation process (Manzano et al., 2016). Wang et al. investigated spiro-BODIPYs with a diaryl chelate unit that

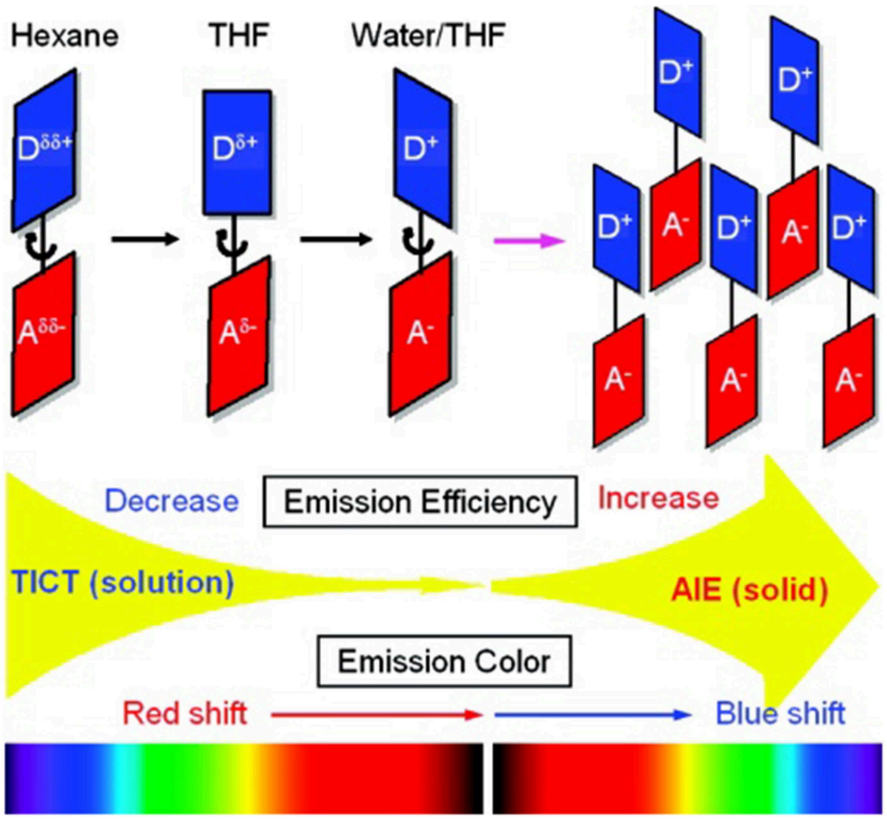

FIGURE 4 | Proposed mechanism for TICT and AIE behaviors in AIE-active BODIPYs based on TPA (Reprinted from Hu et al., 2009. Copyright 2009 American Chemical Society).

could form J-aggregates in the alcohol-water mixture. The J-aggregates of **20a** showed increased emission efficiency while those of **21a** and **22a** indicated decreased emission efficiency, suggesting that the change in emission intensity is not a reliable indicator for the formation of J-aggregates. An important detail to mention is that similar structures substituted by phenyl at *meso*-position (**20b**–**22b**) were not observed in the J-aggregation formation of the alcohol-water mixture or in the tetrahydrofuran-water mixture (Yuan et al., 2017).

BODIPY ANALOGS WITH AIE

AIE strategy, relying on the RIM, has produced numerous systems with high emission in the aggregation state. Except for classical BODIPYs, the development of new members of BODIPYs family viz. BODIPY analogs with AIE-active will undoubtedly contribute to a better understanding of the phenomena and lead to novel applications.

In the process of elucidating the optical properties of benzo[*c*, *d*]indole-containing aza-BODIPYs, Kobayashi et al. found that the photophysical property of aza-BODIPYs could be tuned by incorporating heteroaromatic moieties in place of pyrrole or isoindole rings. Moreover, they reported the first aza-BODIPY (**23**, **Figure 7**) exhibiting AIEE behavior. Compound **23** showed weak fluorescence in a diluted solution (Φ_f = 2% in THF solution), however, fluorescence enhancement was observed both in film-state (drop-cast film, Φ_f = 14%) and aggregation-state (f_w = 90%, Φ_f = 23%). Clearly, the restricted molecular dynamics induced by the non-conjugated moiety should be responsible for such AIEE phenomenon (Shimizu et al., 2015).

Similar to the strategy mentioned in section AIE-active BODIPYs Based on TPE, the AIE property of NIR-emissive aza-BODIPYs based on a diketopyrrolopyrrole-benzo[*d*]thiazole ligand was realized by linking one or two TPE moieties to its planar π-conjugated structure (Li et al., 2017). Compounds **24** and **25** showed weak fluorescence with Φ_f of 0.7 and 0.4% in diluted dichloromethane solution. After the adding of hexane as a poor solvent to the dichloromethane solution, great fluorescence enhancement of around 690 nm was observed (21.9% for compound **24**, and 18.8% for compound **25**) due to the formation of high emissive aggregates. Moreover, the imaging ability of **25**-NPs, which was prepared from compound **25** and Pluronics 127, has been proved in HeLa cells.

By incorporating two phenothiazine units into the biquinoline-based ligand, an AIE-active aza-BODIPY with

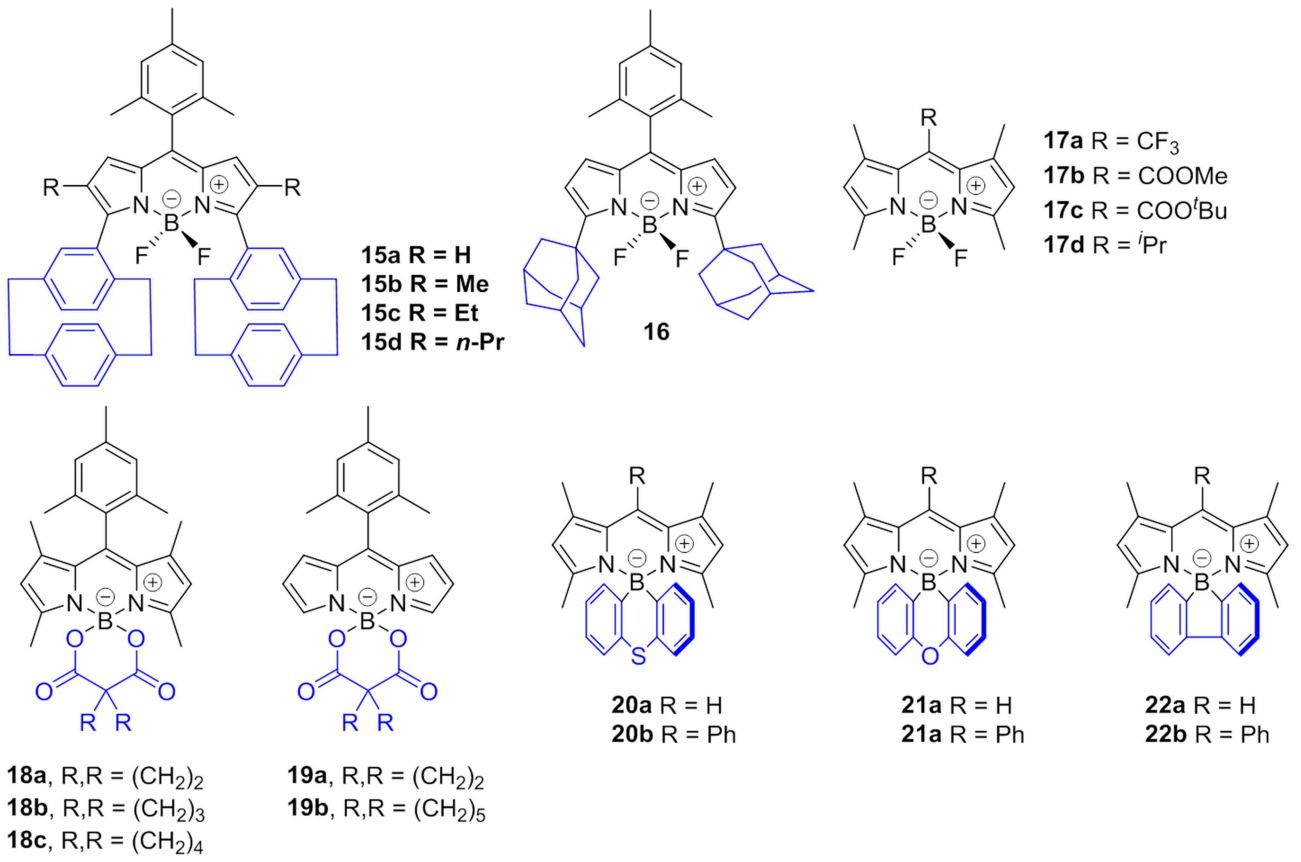

FIGURE 5 | Chemical structures of compounds **15**–**22**.

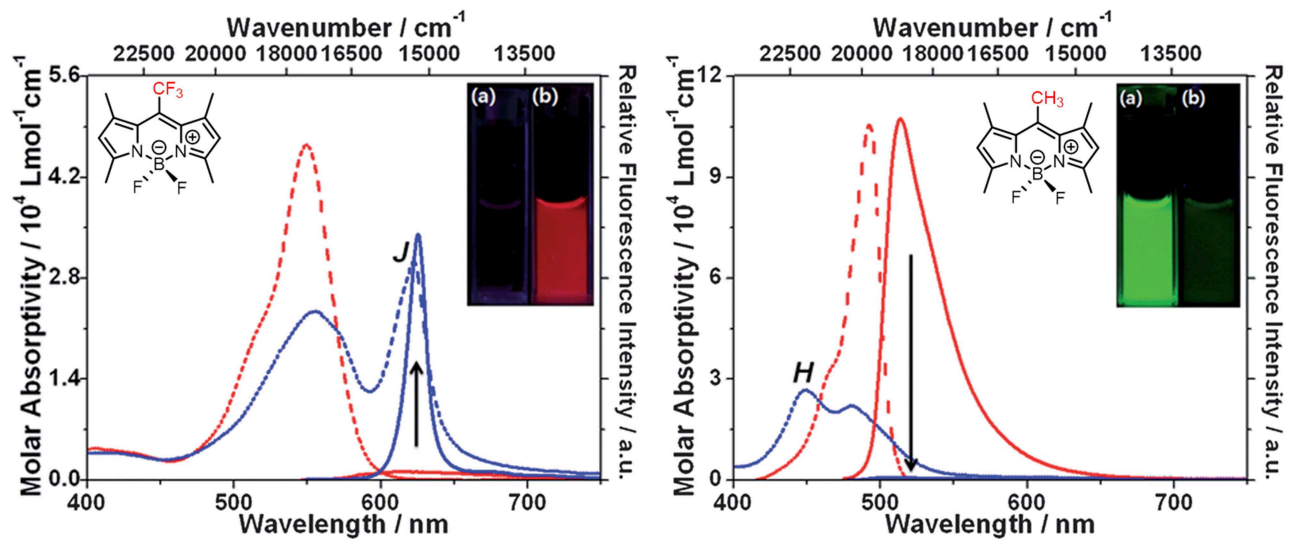

FIGURE 6 | Different aggregation behavior of **17a** (2×10^{-5} mol L^{-1}) and it's analog with a methyl group at the *meso*-position in acetonitrile and acetonitrile-water mixtures (1:99, v: v). Dotted and solid lines refer to the absorption and emission spectra of BODIPYs, respectively (adapted with permission from Choi et al., 2014, Copyright 2014, Royal Chemistry Society).

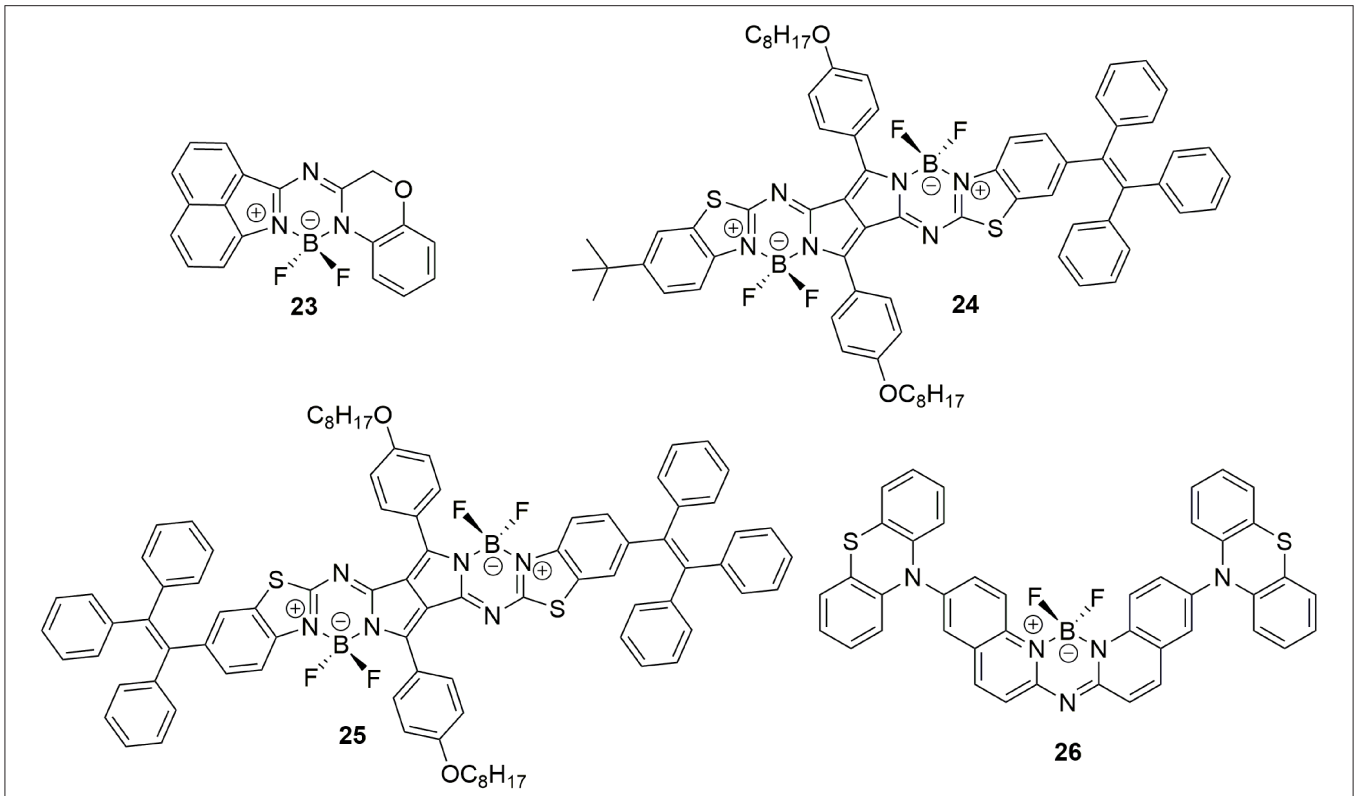

FIGURE 7 | Chemical structures of compounds **23**–**26**.

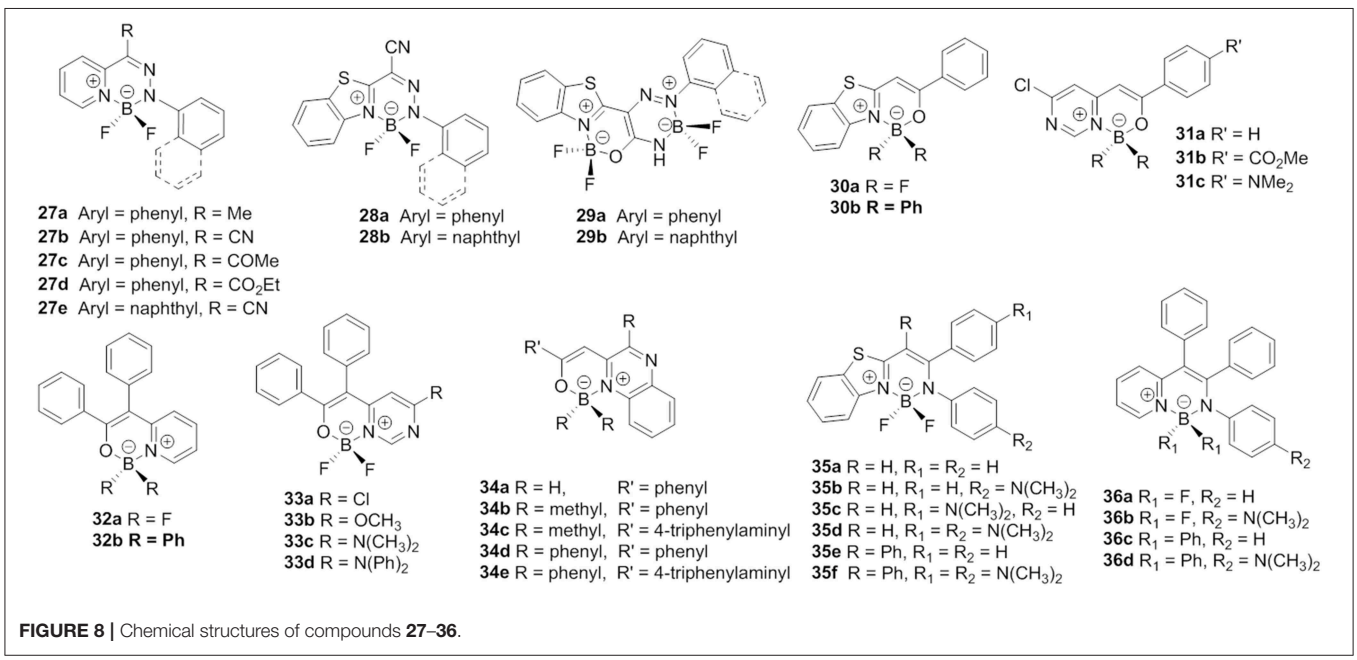

FIGURE 8 | Chemical structures of compounds **27**–**36**.

highly twisted structure (**26**, **Figure 7**) was reported by Zhu et al. (2014). Compound **26** showed weak blue emission at 480 nm in THF solution. The addition of water to the THF solution ($f_w \leq 50\%$) first induced emission quenching due to the enhanced TICT effect. Then, great red-shifted emission from 480 to 610 nm accompanied by emission enhancement was observed because of the formation of aggregates.

Besides the strategies of incorporation of AIE units into the BODIPY core and J-aggregation engineering, modification of the dipyrromethene bidentate to give BODIPY analogs with desymmetrized and propeller-shaped structure has also proved to be an efficient method to achieve AIE-active BODIPYs with high aggregation-state Φ_f. Generally, these BODIPY analogs usually show a larger Stokes shift than classical BODIPY, which is helpful for suppressing the self-absorption in the condensed phase. Moreover, as a benefit of their high twisted structure, the strong π-π interaction can be efficiently avoided. Based on the above conception, various AIE-active BODIPY analogs with the propeller-shaped structure have been developed by replacing the dipyrrole units to various heterocycles such as pyridine, benzo[*d*]thiazole, quinoline, *etc*.

Heterocycle-hydrazone-based boron difluoride complexes, which were first reported by Aprahamian et al. are a new class of AIE-active BODIPY analogs (**27**, **Figure 8**) (Yang et al., 2012). Due to the desymmetrized and propeller-shaped structure, compound **27a** showed weak fluorescence at 512 nm ($\Phi_f < 10\%$) with a large Stokes shift (101,010 cm^{-1}) in dichloromethane. After restricting the intramolecular rotations, enhanced emission both in the film and crystalline state was observed. Most importantly, the AIE mechanism of pyridine-hydrazone-based boron difluoride complexes was rationalized by TD-DFT calculations (Qian et al., 2017). The calculated results demonstrated that the emission of these compounds was not generated from the S_1 state but from the other excited states with higher energy ($>S_1$). The authors also suggested that suppression of Kasha's rule should be the real mechanism responsible for emission in the solid state.

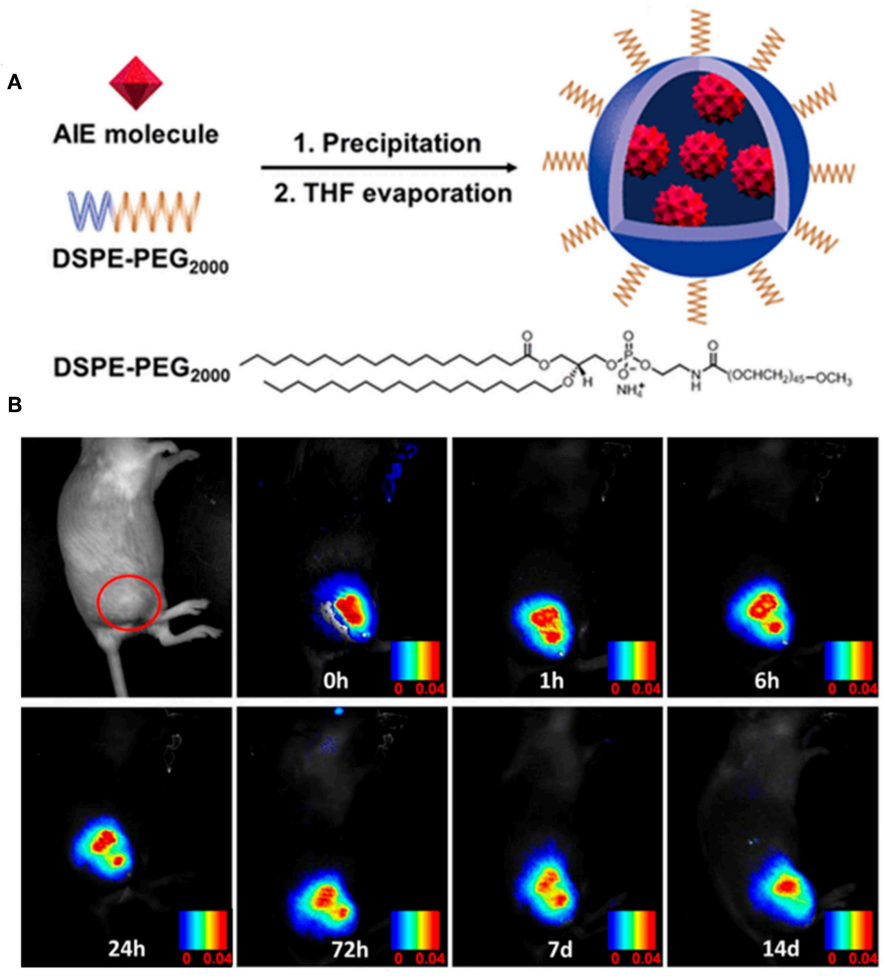

FIGURE 9 | (A) Preparation of the AIE NPs of compound **12**. **(B)** *In vivo* confocal images of the tumor-bearing mouse with AIE NPs of compound **12** from day 0 to day 14 (adapted with permission from Che et al., 2019, Copyright 2019, Royal Chemistry Society).

Inspired by the AIE-active BOIDPY analogs based on pyridine-hydrazone ligands, a group of new AIE-active monoboron (**28**) and bisboron (**29**) difluoride complexes was developed by adopting benzo[*d*]thiazole-hydrozone as the chelates (Duan et al., 2018). Similar to compound **27a**, these complexes showed weak emission ($\Phi_f < 1\%$) and large Stokes shifts (up to 7,400 cm^{-1}) in a diluted solution and AIEE in the aggregation state. The AIE behavior of these complexes was investigated and found to be closely related to the RIR of the aromatic rings.

In consideration of the attractive properties of heterocycle-amidine and heterocycle-hydrazone ligands based BODIPY analogs, it is worth to further expand the family of these BODIPY analogs so as to develop more AIE-active functional materials. In this case, various BODIPY analogs based on heterocycle-enolate ligands have been successfully developed. Matsui et al. synthesized a boron difluoride complexes derivate from βbenzo[*d*]thiazole-enolate ligands (**30**, **Figure 8**) (Kubota et al., 2012). The desymmetrized structure and AIEE effect make these complexes show high emission with Φ_f up to 60% in the solid state. Based on this pioneering work, Matsui et al. also investigated the photophysical and AIE properties of monoboron and bisboron complexes based on pyrimidine-enolate ligands (**31**, **Figure 8**) (Kubota et al., 2013). By tuning the CT and conjugation effect, an intense solid-state emission maximum from 488 to 641 nm was achieved ($\Phi_f = 7–20\%$). Next, a number of propeller-shaped BODIPY analogs based on pyridine- (Wu et al., 2015), quinoxaline- (Liao et al., 2015), pyrimidine- (Qi et al., 2016), and benzo[*d*]thiazole-enolate (Gong et al., 2015) ligands (**32–34**, **Figure 8**) were reported by different groups. Like HPS and TPE, the propeller-shaped structure quenched the emission of these complexes in a diluted solution, and, after restricting the intramolecular rotations by aggregation, distinct AIE behavior was observed.

By reacting pyridine- and benzo[*d*]thiazole-enolate ligands with arylamine, our group developed a series of pyridyl- and benzothiazole-enamide *N^N*-bidentate ligands, which facilitated the generation of a new family of propeller-shaped BODIPY analogs (Liu et al., 2015; Wang et al., 2015a,b). Similarly to the abovementioned compounds **27–34**, compounds **35** and **36** showed very weak emission in low-viscosity solvents and displayed AIE in the aggregation state. All of these compounds showed large Stokes shifts and very weak intermolecular interactions in the aggregation state, resulting in high Φ_f. Moreover, the applications of these compounds as solid-emitters for acid gas and pressure sensing were also demonstrated.

APPLICATIONS OF AIE-ACTIVE BODIPYS

Although BODIPYs have gained great success in biological sensing and imaging, their application as the emitter in the aggregation state was rarely reported in the past decades. This obstacle would be well-solved by the rational designing of aggregation-state emissive BODIPYs and their analogs. Indeed, taking the advantages of AIE, the

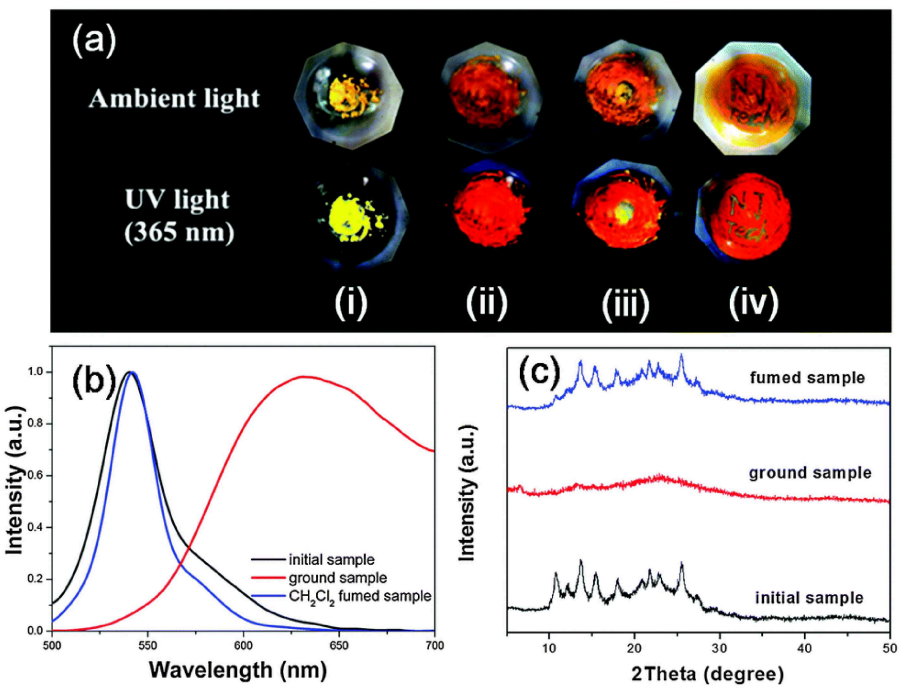

FIGURE 10 | (a) Photographs of the powder of compound **26** before and after grinding under ambient and light UV light (365 nm): (i) crystalline powder, (ii) ground powder, (iii) ground powder upon adding of a drop of CH_2Cl_2, and (iv) the letters "NJ Tech" were written on the ground powder using CH_2Cl_2. **(b)** Emission spectra and **(C)** PXRD patterns of the powder, after being ground and CH_2Cl_2-fumed (Reprinted from Zhu et al., 2014, Copyright 2014, Royal Chemistry Society).

application scope of BODIPYs has been successfully expanded from solution state to aggregation state in recent years.

Fluorescent Imaging

Fluorescence imaging technology has been demonstrated as a powerful tool for investigating biological processes in living

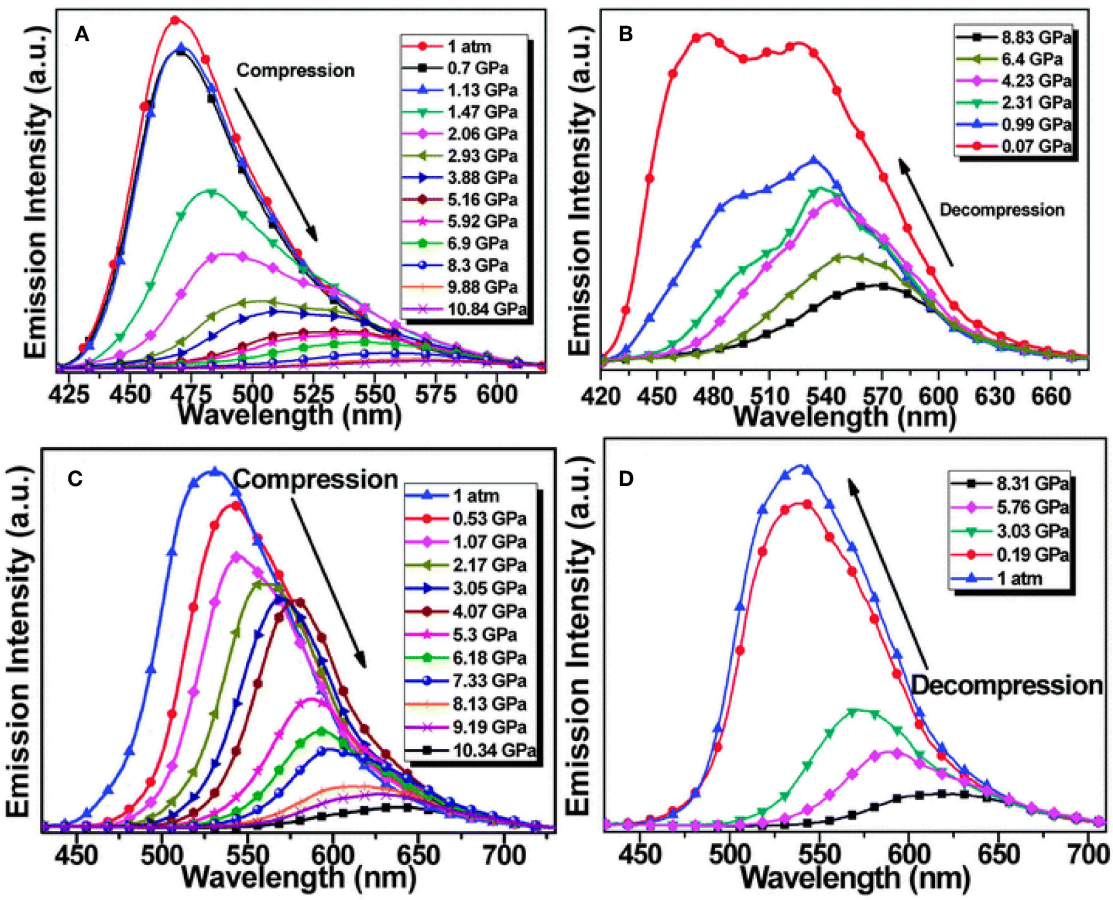

FIGURE 11 | Emission spectra of compounds **35e (A,B)** and **35f (C,D)** upon the compressing **(A,C)** and following decompressing processes **(B,D)** (Reprinted from Wang et al. (2015a), Copyright 2015, Royal Chemistry Society).

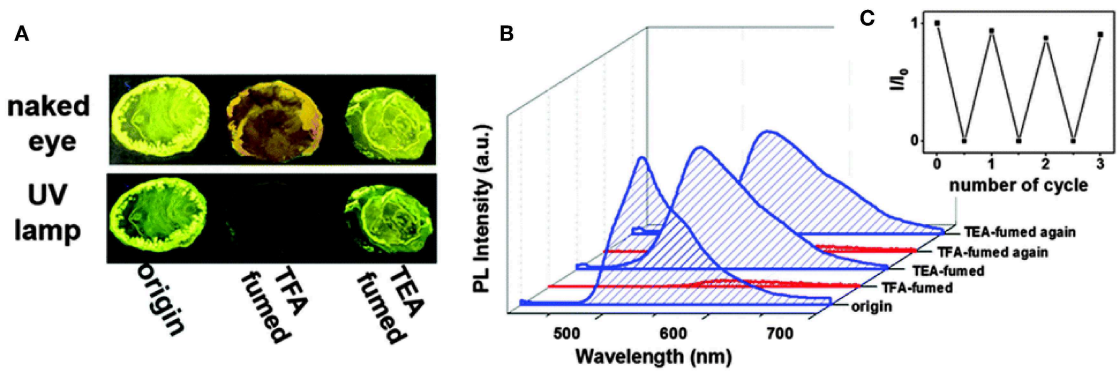

FIGURE 12 | (A) Photographs of compound **34d** on sliding glass taken under ambient and UV light (λ_{ex} = 365 nm). **(B)** Emission spectra of compound **34d** after treating with TEA–TFA vapors in solid-state. **(C)** Recycling of the emission switching of the power of compound **34d** upon fuming with TFA and TEA vapors (Reprinted from Liao et al., 2015, Copyright 2015, Royal Chemistry Society).

cells and clinical diagnostics because of its high specificity and sensitivity, high resolution, and its nondestructive properties (Johnson and Spence, 2010). Numerous fluorescent materials such as fluorescent proteins, quantum dots, polymer dots, and small organic fluorescent molecules with photo-active or photoswitch properties have been developed (Lavis and Raines, 2008; Chan et al., 2012; Li et al., 2014). Compared with the above fluorescent materials, AIE materials have distinct advantages, including high emission at high concentration or in the aggregation state, low toxicity and good anti-photobleaching ability, which make them hold great potential as candidates for fluorescent imaging (Chen et al., 2016). As an important member of AIE materials, AIE-active BODIPYs have been employed as imaging agents in biological sensing and imaging.

Tang et al. first used the aggregates of compound **3** for fluorescence imaging in living HeLa cells. After staining living cells with the aggregates, both the LE emission, and TICT emission were detected (Hu et al., 2012). After that, the biocompatible AIE dots that were prepared from AIE-active BODIPY molecules were applied for intracellular fluorescent imaging. For example, red emissive nanoparticles of compound **4** were obtained by encapsulating compound **4** with 1,2-sistearoyl-sn -glycero-3-phosphoethanolamine-N-[methoxy(polyethylene glycol)-2000] (DSPE-PEG_{2000}). Benefitting from their good biocompatibility and two-photon absorption and excited fluorescence (TPEF), these AIE NPs were further applied in TPEF cellular imaging and mouse brain blood vascular visualization, suggesting their potential application in TPEF sensing and imaging (Zhao et al., 2014).

Very recently, the efficient imaging capabilities of TPA- and carbazoyl-based AIE-active BODIPYs have also been reported by Tang and Su. After fabricating in the presence of DSPE-PEG_{2000}, the NPs of compound **12** were obtained with intense far-red emission (around 650 nm) and excellent photostability. Moreover, these NPs showed an ultrafast cell staining time of a few seconds and excellent cell imaging ability. More importantly, these NPs can be used for long term imaging both *in vitro* and *in vivo* (**Figure 9**), demonstrating their great potential imaging abilities in the practical biological applications (Che et al., 2019).

Mechanofluorochromic (MFC) Materials

MFC materials that change their luminescence upon mechanical grinding/shearing have been attracting a great deal of interest owing to their promising applications (Sagara et al., 2016). Generally, AIE molecules with a strong twisted skeleton with rotatable aryl units, resulting in the stacking of loose molecules in the crystal state, can be easily destroyed by mechanical stimulation, resulting in a change of luminescence color. Thus, twisted π-conjugated AIE-active BODIPY analogs have been used as potential candidates for promising MFC materials. For example, the yellow powder of compound **26** showed bright fluorescence with λ_{em} at 540 nm. After grinding with the motor, the yellow emissive powder immediately changed its emission color to red (λ_{em} = 635 nm), resulting in a 95 nm red-shift of emission. Moreover, the mechanic-induced color change can be switched back via dichloromethane fuming. The crystalline-amorphous-crystalline state transformation of **26** during the grinding and fuming stimuli processes has been demonstrated by powder X-ray diffraction (PXRD) (**Figure 10**) (Zhu et al., 2014).

Upon mechanical grinding or hydrostatic compression, compounds **35e** and **35f** displayed red-shift emission under high pressure, while **35f** with ICT effects showed a more sensitive piezochromic response at low pressure (<1.5 GPa), which implied that the pressure-dependent π-π intermolecular interaction and the intramolecular CT effect were efficient in inducing piezochromic luminescence (**Figure 11**) (Wang et al., 2015a). The distinct piezochromic effect of **35f** at low compression pressure suggested that the propeller-shaped AIE luminophore with the ICT effect could be a valuable basis upon which to design MFCs with high sensitivity. In the process of studying pyrimidine-based BF_2 complexes, **33a–d**, we found that only **33d** showed distinct luminescence change upon mechanical stimuli. **33d** underwent red-shift from 491 to 509 nm on mechanical grinding, while it recovered to the original state when exposed to dichloromethane vapor for 10 min. In addition to the XRD characteristic, we rationalized that the mechanochromism is attributed to the desymmetric propeller-shaped configuration and donor-acceptor character of **33d** (Qi et al., 2016).

Gas Sensors

Due to their strong fluorescent properties in the solid state, AIE-active BODIPYs and their analogs are proposed to be an ideal candidate for gas sensing. A number of compounds have been reported as the fluorescent switch for organic solvent, acid and base gases. For example, compounds **34a–e** possessed unusual acidochromic behavior triggered by acid vapor (Liao et al., 2015). After exposure to trifluoroacetic acid (TFA) vapors, the colors of **34a-e** turned obscure, and absorption spectra were red-shifted and accompanied by strong quenching of luminescence. The effect of fluorescence quenching upon acid fuming should be attributed to the synergistic effects of the protonation of nitrogen resulting from the pyrazine segment-induced push-pull effect and the changes of intermolecular packing and molecular conformation upon acid protonation (**Figure 12**).

Another example is that the intense solid-state emission of compound **26** could be switched by multiple external stimuli, including grinding, organic solvent vapors as well as acid and base vapors (Zhu et al., 2014). Fumigation of **26** with HCl–TEA vapors exhibited an off/on switching fluorescence effect. Based on the protonation–deprotonation stimuli luminescence property of **26**, a simple, convenient and efficient piece of technology for data encryption and decryption was designed. All these comprehensive investigations suggested that complex **26** was a very promising candidate for application in sensing, detection, and security protection.

The introduction of the *N,N*-dimethylamino group as an acid-sensitive group to the π-conjugated structure of AIE-active BODIPYs has been demonstrated to be an efficient strategy for achieving highly sensitive acidic vapor sensing. Taking compound **35b** as an example, when exposed to HCl vapors for a few seconds, **35b** exhibited blue-shifted emission with the color

changing from yellow to cyan (547–518 nm). The protonated powder samples gradually recovered their original color and fluorescence when they were treated with NH_3 vapor for a few minutes. Such an acidic/basic gas-triggered solid-state emission change was also observed in compounds **35d**, **36b,** and **36d** (Liu et al., 2015; Wang et al., 2015b).

SUMMARY AND OUTLOOK

Among many organic fluorescent molecules, the synthesis of BODIPY fluorescent molecules and their analogs is relatively simple, and the advantages of photophysical properties are prominent, such as a high molar extinction coefficient, high quantum yield, tunable emission wavelength, and high stability. The methods of achieving AIE activity of classical BODIPY and BODIPY analogs mainly include linking AIE-active molecules on the chromophore core, the J-aggregation method, and designing fluorescent molecules into propeller-shaped structures. Because of their high luminescence efficiency in aggregates and solid-state, these molecules have been successfully applied to bioimaging, solid-state stimulus-responsive materials, OLEDs and other fields. However, some challenges still exist for the design and application of the AIE-active BODIPYs.

Fundamental understanding of the aggregation effect on photophysical property is not yet satisfactory. Mechanisms based on RIM and J-aggregation are generally applied in molecular design, and in some cases they do not work as well as expected yet. For example, integrating the TPE unit to BODIPY is generally thought to induce AIE, but ACQ behavior toward some BODIPYs bearing TPE units was reported (Gomez-Duran et al., 2015). On the other hand, J-aggregation of BODIPYs should result in emissive J-aggregates in the aggregation state; however, we recently demonstrated that the J-aggregation could generate multiple emissions across the red to NIR region (Tian et al., 2018).

Improving the fluorescent efficiency in the aggregation state is highly required. Although the ACQ effect of BODIPYs was suppressed by introducing an AIE unit, the aggregation-state Φ_f for most of AIE-active BODIPYs remained low, which restricted their further applications. Exploring a new strategy or a proper platform to achieve intense aggregation-state emission of BODIPYs remains a challenge.

There is huge scope in exploring AIE-active BODIPYs with NIR emission (700–1,700 nm). Compared to the large number of AIE-active BODIPYs with a short emission wavelength, successful examples of NIR emission are rather limited. Exploring the suitable building block and fine-tuning of the π-conjugated structures should be helpful for achieving NIR aggregation-state emission. Aggregation-state emissive BODIPYs, especially those with NIR-II (1,000–1,700 nm) emission, could have a bright future for *in vivo* and clinical imaging (Zhu et al., 2019).

Taken together, under the guidance of AIE, efficient aggregation-state emissive BODIPYs with diverse chemical structures and intriguing photophysical properties will be developed. These BODIPY derivatives will undoubtedly show their capabilities in various application fields.

AUTHOR CONTRIBUTIONS

ZL and XW designed this proposal, revised the manuscript, and determined the contents. ZJ and MY drew the chemical structures and prepared the figures. All authors contributed to the writing of the manuscript.

FUNDING

This research was funded by the National Natural Science Foundation of China (21971115 and 21501085) and the Key University Science Research Project of Jiangsu Province (17KJA150004).

ACKNOWLEDGMENTS

We thank the National Natural Science Foundation of China and the Key University Science Research Project of Jiangsu Province.

REFERENCES

Baglan, M., Ozturk, S., Gur, B., Meral, K., Bozkaya, U., Bozdemir, O. A., et al. (2013). Novel phenomena for aggregation induced emission enhancement: highly fluorescent hydrophobic tpe-bodipy couples in both organic and aqueous media. *RSC Adv.* 3, 15866–15874. doi: 10.1039/c3ra40791h

Baysec, S., Minotto, A., Klein, P., Poddi, S., Zampetti, A., Allard, S., et al. (2018). Tetraphenylethylene-bodipy aggregation-induced emission luminogens for near-infrared polymer light-emitting diodes. *Sci. China Chem.* 61, 932–939. doi: 10.1007/s11426-018-9306-2

Bergström, F., Mikhalyov, I., Hägglöf, P., Wortmann, R., Ny, T., and Johansson, L. B. (2002). Dimers of dipyrromethene boron difluoride (bodipy) with light spectroscopic applications in chemistry and biology. *J. Am. Chem. Soc.* 124, 196–204. doi: 10.1021/ja010983f

Boens, N., Leen, V., and Dehaen, W. (2012). Fluorescent indicators based on bodipy. *Chem. Soc. Rev.* 41, 1130–1172. doi: 10.1039/C1CS15132K

Bui, H. T., Mai, D. K., Kim, B., Choi, K. H., Park, B. J., Kim, H. J., et al. (2019). Effect of substituents on the photophysical properties and bioimaging application of bodipy derivatives with triphenylamine substituents. *J. Phys. Chem. B* 123, 5601–5607. doi: 10.1021/acs.jpcb.9b04782

Chan, J., Dodani, S. C., and Chang, C. J. (2012). Reaction-based small-molecule fluorescent probes for chemoselective bioimaging. *Nat. Chem.* 4, 973–984. doi: 10.1038/nchem.1500

Che, W., Zhang, L., Li, Y., Zhu, D., Xie, Z., Li, G., et al. (2019). Ultrafast and non-invasive long-term bioimaging with highly stable red aggregation-induced emission nanoparticles. *Anal. Chem.* 91, 3467–3474. doi: 10.1021/acs.analchem.8b05024

Chen, S. J., Wang, H., Hong, Y. N., and Tang, B. Z. (2016). Fabrication of fluorescent nanoparticles based on aie luminogens (aie dots) and their applications in bioimaging. *Mater. Horiz.* 3, 283–293. doi: 10.1039/C6MH00060F

Choi, S., Bouffard, J., and Kim, Y. (2014). Aggregation-induced emission enhancement of a meso-trifluoromethyl bodipy via j-aggregation. *Chem. Sci.* 5, 751–755. doi: 10.1039/C3SC52495G

Chua, M. H., Ni, Y., Garai, M., Zheng, B., Huang, K. W., Xu, Q. H., et al. (2015). Towards meso-ester bodipys with aggregation-induced emission properties: the effect of substitution positions. *Chem. Asian J.* 10, 1631–1634. doi: 10.1002/asia.201500420

Duan, W., Liu, Q., Huo, Y., Cui, J., Gong, S., and Liu, Z. (2018). Aie-active boron complexes based on benzothiazole-hydrazone chelates. *Org. Biomol. Chem.* 16, 4977–4984. doi: 10.1039/C8OB00755A

Fan, C., Wu, W., Chruma, J. J., Zhao, J., and Yang, C. (2016). Enhanced triplet-triplet energy transfer and upconversion fluorescence through host-guest complexation. *J. Am. Chem. Soc.* 138, 15405–15412. doi: 10.1021/jacs.6b07946

Förster, T., and Kasper, K. (1954). Ein konzentrationsumschlag der fluoreszenz des pyrens. *Z. Phys. Chem.* 1, 275–277. doi: 10.1524/zpch.1954.1.5_6.275

Ge, Y., and O'shea, D. F. (2016). Azadipyrromethenes: from traditional dye chemistry to leading edge applications. *Chem. Soc. Rev.* 45, 3846–3864. doi: 10.1039/C6CS00200E

Gomez-Duran, C. F., Hu, R., Feng, G., Li, T., Bu, F., Arseneault, M., et al. (2015). Effect of aie substituents on the fluorescence of tetraphenylethene-containing bodipy derivatives. *ACS Appl Mater Interfaces* 7, 15168–15176. doi: 10.1021/acsami.5b05033

Gong, S., Liu, Q., Wang, X., Xia, B., Liu, Z., and He, W. (2015). Aie-active organoboron complexes with highly efficient solid-state luminescence and their application as gas sensitive materials. *Dalton Trans.* 44, 14063–14070. doi: 10.1039/C5DT01525A

Hu, R., Gomez-Duran, C. F., Lam, J. W., Belmonte-Vazquez, J. L., Deng, C., Chen, S., et al. (2012). Synthesis, solvatochromism, aggregation-induced emission and cell imaging of tetraphenylethene-containing bodipy derivatives with large stokes shifts. *Chem. Commun.* 48, 10099–10101. doi: 10.1039/c2cc35188a

Hu, R. R., Lager, E., Aguilar-Aguilar, A., Liu, J. Z., Lam, J. W. Y., Sung, H. H. Y., et al. (2009). Twisted intramolecular charge transfer and aggregation-induced emission of bodipy derivatives. *J. Phys. Chem. C* 113, 15845–15853. doi: 10.1021/jp902962h

Johnson, I., and Spence, M. T. Z. (2010). *The Molecular Probes Hand-Book: A Guide to Fluorescent Probes and Labeling Technologies*. Grand Island, NE: Life Technologies Corporation.

Kim, S., Bouffard, J., and Kim, Y. (2015). Tailoring the solid-state fluorescence emission of bodipy dyes by meso substitution. *Chem. Eur. J.* 21, 17459–17465. doi: 10.1002/chem.201503040

Kim, T. I., Hwang, B., Lee, B., Bae, J., and Kim, Y. (2018). Selective monitoring and imaging of eosinophil peroxidase activity with a j-aggregating probe. *J. Am. Chem. Soc.* 140, 11771–11776. doi: 10.1021/jacs.8b07073

Kokado, K., and Sada, K. (2019). Consideration of molecular structure in the excited state to design new luminogens with aggregation-induced emission. *Angew. Chem. Int. Ed.* 58, 8632–8639. doi: 10.1002/anie.201814462

Kowada, T., Maeda, H., and Kikuchi, K. (2015). Bodipy-based probes for the fluorescence imaging of biomolecules in living cells. *Chem. Soc. Rev.* 44, 4953–4972. doi: 10.1039/C5CS00030K

Kubota, Y., Ozaki, Y., Funabiki, K., and Matsui, M. (2013). Synthesis and fluorescence properties of pyrimidine mono- and bisboron complexes. *J. Org. Chem.* 78, 7058–7067. doi: 10.1021/jo400879g

Kubota, Y., Tanaka, S., Funabiki, K., and Matsui, M. (2012). Synthesis and fluorescence properties of thiazole-boron complexes bearing a beta-ketoiminate ligand. *Org. Lett.* 14, 4682–4685. doi: 10.1021/ol302179r

Lager, E., Liu, J., Aguilar-Aguilar, A., Tang, B. Z., and Pena-Cabrera, E. (2009). Novel meso-polyarylamine-bodipy hybrids: synthesis and study of their optical properties. *J. Org. Chem.* 74, 2053–2058. doi: 10.1021/jo802519b

Lavis, L. D., and Raines, R. T. (2008). Bright ideas for chemical biology. *ACS Chem Biol* 3, 142–155. doi: 10.1021/cb700248m

Li, L., Wang, L., Tang, H., and Cao, D. (2017). A facile synthesis of novel near-infrared pyrrolopyrrole aza-bodipy luminogens with aggregation-enhanced emission characteristics. *Chem. Commun.* 53, 8352–8355. doi: 10.1039/C7CC04568A

Li, X., Gao, X., Shi, W., and Ma, H. (2014). Design strategies for water-soluble small molecular chromogenic and fluorogenic probes. *Chem. Rev.* 114, 590–659. doi: 10.1021/cr300508p

Liao, C. W., Rao, M. R., and Sun, S. S. (2015). Structural diversity of new solid-state luminophores based on quinoxaline-beta-ketoiminate boron difluoride complexes with remarkable fluorescence switching properties. *Chem. Commun.* 51, 2656–2659. doi: 10.1039/C4CC08958H

Liu, Q., Wang, X., Yan, H., Wu, Y., Li, Z., Gong, S., et al. (2015). Benzothiazole-enamide-based bf_2 complexes: luminophores exhibiting aggregation-induced emission, tunable emission and highly efficient solid-state emission. *J. Mater. Chem. C* 3, 2953–2959. doi: 10.1039/C4TC02876G

Loudet, A., and Burgess, K. (2007). Bodipy dyes and their derivatives: syntheses and spectroscopic properties. *Chem. Rev.* 107, 4891–4932. doi: 10.1021/cr078381n

Lu, H., Mack, J., Yang, Y., and Shen, Z. (2014). Structural modification strategies for the rational design of red/nir region bodipys. *Chem. Soc. Rev.* 43, 4778–4823. doi: 10.1039/C4CS00030G

Manzano, H., Esnal, I., Marqués-Matesanz, T., Bañuelos, J., López-Arbeloa, I., Ortiz, M. J., et al. (2016). Unprecedented j-aggregated dyes in pure organic solvents. *Adv. Funct. Mater.* 26, 2756–2769. doi: 10.1002/adfm.201505051

Mei, J., Leung, N. L., Kwok, R. T., Lam, J. W., and Tang, B. Z. (2015). Aggregation-induced emission: together we shine, united we soar! *Chem. Rev.* 115, 11718–11940. doi: 10.1021/acs.chemrev.5b00263

Qi, F., Lin, J., Wang, X., Cui, P., Yan, H., Gong, S., et al. (2016). New aie-active pyrimidine-based boronfluoride complexes with high solid-state emission and reversible mechanochromism luminescence behavior. *Dalton Trans.* 45, 7278–7284. doi: 10.1039/C6DT00292G

Qian, H., Cousins, M. E., Horak, E. H., Wakefield, A., Liptak, M. D., and Aprahamian, I. (2017). Suppression of kasha's rule as a mechanism for fluorescent molecular rotors and aggregation-induced emission. *Nat. Chem.* 9, 83–87. doi: 10.1038/nchem.2612

Sagara, Y., Yamane, S., Mitani, M., Weder, C., and Kato, T. (2016). Mechanoresponsive luminescent molecular assemblies: an emerging class of materials. *Adv. Mater.* 28, 1073–1095. doi: 10.1002/adma.201502589

Shimizu, S., Murayama, A., Haruyama, T., Iino, T., Mori, S., Furuta, H., et al. (2015). Benzo[c,d]indole-containing aza-bodipy dyes: asymmetrization-induced solid-state emission and aggregation-induced emission enhancement as new properties of a well-known chromophore. *Chem. Eur. J.* 21, 12996–13003. doi: 10.1002/chem.201501464

Tanaka, K., and Chujo, Y. (2015). Recent progress of optical functional nanomaterials based on organoboron complexes with β-diketonate, ketoiminate and diiminate. *NPG Asia Mater.* 7:e223. doi: 10.1038/am.2015.118

Tian, D., Qi, F., Ma, H., Wang, X., Pan, Y., Chen, R., et al. (2018). Domino-like multi-emissions across red and near infrared from solid-state 2-/2,6-aryl substituted bodipy dyes. *Nat. Commun.* 9:2688. doi: 10.1038/s41467-018-05040-8

Uoyama, H., Goushi, K., Shizu, K., Nomura, H., and Adachi, C. (2012). Highly efficient organic light-emitting diodes from delayed fluorescence. *Nature* 492, 234–238. doi: 10.1038/nature11687

Vu, T. T., Badré, S., Dumas-Verdes, C. C., Vachon, J.-J., Julien, C., and Audebert, P., et al. (2009). New hindered bodipy derivatives: solution and amorphous state fluorescence properties. *J. Phys. Chem. C* 113, 11844–11855. doi: 10.1021/jp9019602

Vu, T. T., Dvorko, M., Schmidt, E. Y., Audibert, J.-F., Retailleau, P., Trofimov, B. A., et al. (2013). Understanding the spectroscopic properties and aggregation process of a new emitting boron dipyrromethene (bodipy). *J. Phys. Chem. C* 117, 5373–5385. doi: 10.1021/jp3097555

Wang, X., Liu, Q., Yan, H., Liu, Z., Yao, M., Zhang, Q., et al. (2015a). Piezochromic luminescence behaviors of two new benzothiazole-enamido boron difluoride complexes: intra- and inter-molecular effects induced by hydrostatic compression. *Chem. Commun.* 51, 7497–7500. doi: 10.1039/C5CC01902H

Wang, X., Wu, Y., Liu, Q., Li, Z., Yan, H., Ji, C., et al. (2015b). Aggregation-induced emission (aie) of pyridyl-enamido-based organoboron luminophores. *Chem. Commun.* 51, 784–787. doi: 10.1039/C4CC07451C

Wang, Z., Zhao, J., Barbon, A., Toffoletti, A., Liu, Y., An, Y., et al. (2017). Radical-enhanced intersystem crossing in new bodipy derivatives and application for efficient triplet-triplet annihilation upconversion. *J. Am. Chem. Soc.* 139, 7831–7842. doi: 10.1021/jacs.7b02063

Wu, Y., Li, Z., Liu, Q., Wang, X., Yan, H., Gong, S., et al. (2015). High solid-state luminescence in propeller-shaped aie-active pyridine-ketoiminate-boron complexes. *Org. Biomol. Chem.* 13, 5775–5782. doi: 10.1039/C5OB00607D

Wurthner, F., Kaiser, T. E., and Saha-Moller, C. R. (2011). J-aggregates: from serendipitous discovery to supramolecular engineering of functional dye materials. *Angew. Chem. Int. Ed.* 50, 3376–3410. doi: 10.1002/anie.201002307

Yan, J., Lee, S., Zhang, A., and Yoon, J. (2018). Self-immolative colorimetric, fluorescent and chemiluminescent chemosensors. *Chem. Soc. Rev.* 47, 6900–6916. doi: 10.1039/C7CS00841D

Yang, Y., Su, X., Carroll, C. N., and Aprahamian, I. (2012). Aggregation-induced emission in bf_2-hydrazone (bodihy) complexes. *Chem. Sci.* 3, 610–613. doi: 10.1039/C1SC00658D

Yuan, K., Wang, X., Mellerup, S. K., Kozin, I., and Wang, S. (2017). Spiro-bodipys with a diaryl chelate: impact on aggregation and luminescence. *J. Org. Chem.* 82, 13481–13487. doi: 10.1021/acs.joc.7b02602

Zhao, Z. J., Chen, B., Geng, J. L., Chang, Z. F., Aparicio-Ixta, L., Nie, H., et al. (2014). Red emissive biocompatible nanoparticles from tetraphenylethene-decorated bodipy luminogens for two-photon excited fluorescence cellular imaging and mouse brain blood vascular visualization. *Part. Part. Syst. Charact.* 31, 481–491. doi: 10.1002/ppsc.201300223

Zhu, S., Tian, R., Antaris, A. L., Chen, X., and Dai, H. (2019). Near-infrared-ii molecular dyes for cancer imaging and surgery. *Adv. Mater.* 31, e1900321. doi: 10.1002/adma.201900321

Zhu, X., Liu, R., Li, Y., Huang, H., Wang, Q., Wang, D., et al. (2014). An aie-active boron-difluoride complex: multi-stimuli-responsive fluorescence and application in data security protection. *Chem. Commun.* 50, 12951–12954. doi: 10.1039/C4CC05913A

Conflict of Interest: The authors declare that the research was conducted in the absence of any commercial or financial relationships that could be construed as a potential conflict of interest.

frontiers in Chemistry

ORIGINAL RESEARCH
published: 31 October 2019
doi: 10.3389/fchem.2019.00740

Optical Limiting and Femtosecond Pump-Probe Transient Absorbance Properties of a 3,5-distyrylBODIPY Dye

Bokolombe P. Ngoy[1,2], *Aviwe K. May*[1], *John Mack*[1]* *and Tebello Nyokong*[1]

[1] *Department of Chemistry, Institute for Nanotechnology Innovation, Rhodes University, Makhanda, South Africa,*
[2] *Département de Chimie, Université de Kinshasa, Kinshasa, Democratic Republic of the Congo*

The optical limiting (OL) properties of a 3,5-di-*p*-benzyloxystyrylBODIPY dye with an *p*-acetamidophenyl moiety at the *meso*-position have been investigated by using the open-aperture Z-scan technique at 532 nm with 10 ns laser pulses. There is a ca. 140 nm red shift of the main spectral band to 644 nm relative to the corresponding BODIPY core dye, due to the incorporation of *p*-benzyloxystyryl groups at the 3,5-positions. As a result, there is relatively weak absorbance across most of the visible region under ambient light conditions. Analysis of the observed reverse saturable absorbance (RSA) profiles demonstrates that the dye is potentially suitable for use in optical limiting applications as has been reported previously for other 3,5-distyrylBODIPY dyes. Time-resolved transient absorption spectroscopy and kinetic studies with femtosecond and nanosecond scale laser pulses provide the first direct spectral evidence that excited state absorption (ESA) from the S_1 state is responsible for the observed OL properties.

Keywords: BODIPY dyes, optical limiting, knoevenagel condensation, Z-scan, transient absorbance spectroscopy

OPEN ACCESS

Edited by:
Zhen Shen,
Nanjing University, China

Reviewed by:
Chengbao Yao,
Harbin Normal University, China
Xiaodong Zhuang,
Shanghai Jiao Tong University, China
Hua Lu,
Hangzhou Normal University, China

***Correspondence:**
John Mack
j.mack@ru.ac.za

Specialty section:
This article was submitted to Supramolecular Chemistry, a section of the journal Frontiers in Chemistry

Received: *08 August 2019*
Accepted: *16 October 2019*
Published: *31 October 2019*

Citation:
Ngoy BP, May AK, Mack J and Nyokong T (2019) Optical Limiting and Femtosecond Pump-Probe Transient Absorbance Properties of a 3,5-distyrylBODIPY Dye. Front. Chem. 7:740. doi: 10.3389/fchem.2019.00740

INTRODUCTION

Non-linear optics (NLO) is a field that focuses on changes in the optical properties of materials upon interacting with intense incident laser pulses. One aspect of NLO that has gained considerable interest over the past few decades is the development of optical limiting (OL) materials that are capable of significantly attenuating the transmittance of light at high incident intensities while remaining optically transparent under ambient light conditions. This normally involves multiphoton processes such as two-photon absorption (2PA), a third-order non-linear process of materials. Since nanosecond laser pulses are used in this study, excited state absorption (ESA) from either the S_1 or T_1 states can also result in an OL response. If the ESA is more intense than absorption from the ground state at the wavelength of the incident pulsed laser beam, a solution of the molecular dye absorbs more strongly once the S_1 and/or T_1 states are populated after it has interacted with an incident laser pulse (Saleh and Teich, 1991; Tutt and Boggess, 1993; de la Torre et al., 2004). Optical limiting materials can be formed using molecular dyes and other materials that can be used to protect light-sensitive objects such as the human eye and optical sensors by attenuating intense incident laser beams (Dini and Hanack, 2003; Chen et al., 2005). The molecular dyes that have been used as optical limiters typically have a delocalized π-conjugation system which is highly polarizable when interacting with intense laser light (Kandasamy et al., 1997; Ogawa et al., 2002; de la Torre et al., 2004). Phthalocyanines and porphyrins have been the main compounds of

interest in this context (Calvete et al., 2004; Chen et al., 2005; Senge et al., 2007), while until recently there had been relatively little research reported on boron-dipyrromethene (BODIPY) dyes in this context (Zhu et al., 2008; Zheng et al., 2009, 2018; Frenette et al., 2014; Kulyk et al., 2016, 2017; Thakare, 2017). Over the past 2 years, we have demonstrated that 3,5-distyrylBODIPY dyes exhibit strong OL responses on the nanosecond timescale (Ndebele et al., 2019).

BODIPY dyes are structural analogs of the porphyrins and consist of two pyrrole units linked by a methene bridge and a BF_2 moiety. These dyes are structurally versatile due to the stability of the highly robust BODIPY core, allowing facile structural modification for the enhancement of selected properties depending on the potential application of the dye (Loudet and Burgess, 2007; Ulrich et al., 2008; Lu et al., 2014). The second harmonic for Nd:YAG laser beams lies at 532 nm and is particularly important with respect to OL applications given challenges in fields such as aviation safety due to the ever-growing irresponsible use of laser pointers (Harris et al., 2017). The optical properties of the BODIPY dyes must be modified to be useful in OL applications at 532 nm, since this lies close to the main BODIPY spectral band of BODIPY core dyes. One of the most widely used methods to achieve a red shift of the main BODIPY spectral band toward the NIR region is the introduction of styryl groups at the 3,5-positions (Loudet and Burgess, 2007; Ulrich et al., 2008; Lu et al., 2014). Dyes modified in this fashion have an extended degree of π-conjugation and this results in a shift of the main absorption and fluorescence bands to longer wavelengths, hence achieving two of the necessary requirements for NLO studies at 532 nm: a π-conjugation system that results in high polarizability and a main absorption band that lies well to the red of the second harmonic wavelength for Nd:YAG lasers at 532 nm with minimal absorption across most of the visible region.

The main aim of this study is to further investigate the mechanism that is responsible for the observed NLO properties of 3,5-divinyl- and 3-5-distyrylBODIPY dyes at 532 nm on the nanosecond timescale (Harris et al., 2017; Kubheka et al., 2017, 2018; May et al., 2018; Ngoy et al., 2018). Since these dyes possess an extended π-system, an enhanced NLO response has been reported even in the absence of heavy atoms that promote intersystem crossing to the triplet manifold, in contrast with what has been found with phthalocyanines where the incorporation of heavy atoms has been found to significantly enhance the optical limiting properties in the context of nanosecond laser pulses (Dini and Hanack, 2003). For this reason, we report the first study of the femtosecond pump-probe transient absorbance properties of a novel 3,5-distyrylBODIPY dye (**Figure 1A**), so that the ESA properties of the singlet manifold can be explored.

METHODS

Materials

4-Acetamidobenzaldehyde, 4-bromobenzaldehyde, N-bromosuccinimide (NBS), boron trifluoride diethyl etherate ($BF_3{\cdot}OEt_2$), 2,4-dimethylpyrrole, glacial acetic acid, piperidine, Rhodamine 6G, anhydrous sodium sulfate (Na_2SO_4), tetrachloro-1,4-benzoquinone (*p*-chloranil), triethylamine (TEA), trifluoroacetic acid (TFA), and zinc phthalocyanine were purchased from Sigma-Aldrich. Spectroscopic grade solvents were used for the photophysical and the open aperture Z-scan studies.

Instrumentation

^{1}H NMR data were measured on a Bruker AMX 600 NMR instrument. Mass spectral data were recorded with a Bruker AutoFLEX III Smart beam TOF/TOF Mass spectrometer. The spectra were acquired using α-cyano-4-hydroxycinnamic acid as the MALDI matrix, and a 355 nm Nd:YAG laser as the ionizing source. UV-visible absorption spectra were recorded on a Shimadzu UV-2550 spectrophotometer, and infrared spectra were measured with a Perkin Elmer Spectrum 100 FT-IR spectrometer. Fluorescence emission spectra were recorded with a Varian Eclipse instrument, while fluorescence lifetime (τ_F) values were calculated by using a Picoquant FluoTime 200 time-correlated single-photon counting instrument. Fluorescence quantum yield (Φ_F) values were calculated by using the comparative method (Ogunsipe et al., 2004). Standard and sample solutions with identical optical densities were excited at the same wavelength in DMSO, with zinc phthalocyanine used as the standard. Triplicate measurements were made to ensure accuracy.

A frequency-doubled Quanta-Ray Nd:YAG laser was used in a near Gaussian transverse mode to carry out open aperture Z-scan measurements on BODIPY dyes (Ndebele et al., 2019) using an instrumental setup that has been described previously (Neethling, 2005). The 532 nm beam was spatially filtered with Glan Thompson GTH10M polarizers to remove higher-order modes and was tightly focused with a plano-convex Thorlabs LA1433 lens with a 15 cm focal length. To enable the Z-scan measurement the sample was translated along the z-axis direction parallel to the incident laser beam with a Newport M-ILS250CCL translation stage in 0.5 mm steps over a total 80 mm path centered on the focal point of the lens. Coherent J5-09 energy detectors (energy ranges of 0.1 μJ−0.1 mJ) and a Coherent EPM2000 energy meter were used to determine normalized transmittance values. A Thorlabs BSW07 beam splitter enables the measurement of both the incident intensity and that transmitted through the sample. Normalized transmittance values determined for 32 consecutive laser pulses were averaged to obtain a value at each z value during the Z-scan measurements. A 2 mm optical glass cuvette was used to obtain the Z-scan data for BODIPY **2** in CH_2Cl_2 solution.

Femtosecond transient absorption measurements were made with a Clark MXR CPA2001 titanium-sapphire (Ti/Sa) laser system with a pulse energy of 0.9 mJ, and a full width at half-maximum (FWHM) of 150 fs, and an operating frequency of 426 Hz as has been reported previously (Klíčová et al., 2012) with slight modifications. The pump-supercontinuum probe technique was implemented. Since BODIPY **2** does not absorb in the near infrared region, the output of the Ti/Sa laser at 775 nm was directly frequency-doubled by a β-barium borate (BBO) crystal to 387.5 nm to generate the pump beam. The energy of the laser pulses were 1 μJ energy in this context, while the pulse width was kept below 150 fs. The probe beam was generated

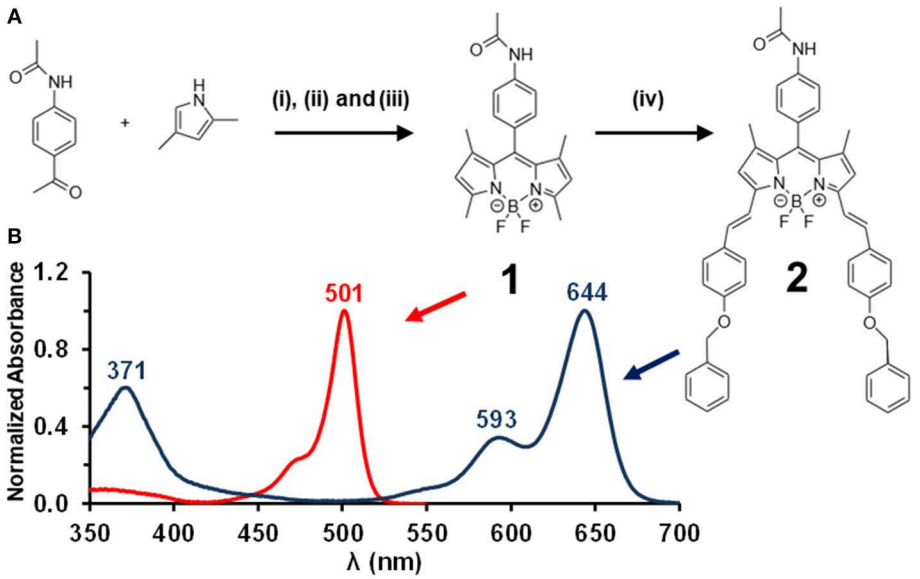

FIGURE 1 | The synthesis of BODIPY dyes **1** and **2 (A)**. Reagents and conditions: (i) TFA at r.t. in dry CH_2Cl_2, (ii) *p*-chloranil at 0°C in dry CH_2Cl_2, (iii) $BF_3{\cdot}OEt_2$ and TEA at 0°C in dry CH_2Cl_2, and (iv) p-benzyloxybenzaldehyde, piperidine, acetic acid in benzene at reflux with a fitted Dean-Stark trap. Normalized absorption spectra for **1** (red) and **2** (blue) in CH_2Cl_2 **(B)**.

by focusing a 2 mm CaF_2 plate in front of the 775 nm beam to produce a 270–690 nm supercontinuum span. The CH_2Cl_2 solution of BODIPY **2** was passed through an optical flow cell with a thickness of 0.4 mm, and the probe and pump beams were focused onto a 0.2 mm spot. The pump beam and a reference signal that was also passed through the solution in the absence of the probe beam were dispersed spectrally and recorded with two 512 pixel photodiode arrays. The ratio of the intensities of the two beams was used to generate the transient absorption spectra. The pump-probe cross-correlation was determined to be <100 fs across the whole spectrum. Measurements on time scales below 50 ps were corrected for chirp in the manner described previously (Klíčová et al., 2012). Data were averaged over three pump-probe scans with 400 shots per temporal point to lower the signal-to-noise ratio.

Nanosecond laser flash photolysis kinetics were studied with an Ekspla NT 342B-20-AW laser that contains an Nd:YAG (355 nm, 78 mJ/7 ns, 20 Hz) pumping a 420–2,300 nm range optical parametric oscillator (8 mJ/7 ns, 20 Hz) to provide the pump beam for an Edinburgh Instruments LP980 transient absorption spectrometer. A 150 W Xe arc lamp provided the probe beam and was used in its continuous mode. The LP980 instrument is fitted with a Quantum Composers 9512+ pulse generator and a Tektronix TDS 3012C oscilloscope to collect data under the control of Edinburgh Instruments' L900 software. The spectrometer contains 500 nm blazed gratings for both excitation and emission and is fitted with a PMT-LP (Hamamatsu R928P) and an ICCD camera (Andor DH320T-25F03). The CH_2Cl_2 solution of **2** was excited with the pump beam at the band maximum of the main BODIPY spectral band at 644 nm. Samples were deoxygenated with inert nitrogen gas.

Synthesis

An adapted version of the conventional 1-pot 3-step reaction procedure for BODIPY synthesis (Yogo et al., 2005) was used to prepare BODIPY **1** (**Figure 1A**). BODIPY **1** was then used as a precursor to form 3,5-distyryl BODIPY **2** (**Figure 1A**) through a Knoevenagel condensation reaction (Rurack et al., 2001) by introducing the *p*-benzyloxystyryl groups by reacting **1** with *p*-benzyloxybenzaldehyde. TLC plates were used to verify the completion of the reaction through the absence of unreacted BODIPY core **1**, and to confirm after purification of **2** by column chromatography that other side products are not present. No additional UV-visible absorption bands were observed due to unwanted side products. The MALDI-TOF MS data for **2** and ^{1}H NMR spectra obtained for **1** and **2** were found to be fully consistent with the anticipated structures.

4,4′-Difluoro-8-(4-acetamidophenyl)-1,3,5,7-tetramethyl-4-bora-3a,4a-diaza-s-indacene (1)

A solution of 2,4-dimethylpyrrole (2 eq) and 4-acetamidobenzaldehyde (1 eq) was prepared in dry CH_2Cl_2 (50 mL) under inert Ar gas. Two to three drops of TFA were added, followed by stirring at room temperature. TLC was used to confirm the complete consumption of the aldehyde. A *p*-chloranil solution (1.2 eq) in dry CH_2Cl_2 (10 mL) was then added at 0°C, and the reaction mixture was stirred for 30 min at room temperature under Ar gas. A deep purple color was observed, and TLC confirmed the synthesis of the dipyrromethene. TEA (7 eq) was added dropwise at 0°C and $BF_3{\cdot}OEt_2$ (11 eq) was then added in a similar manner, followed by stirring for 12 h at room temperature. The reaction mixture was filtered, washed with water (100 mL), and dried over anhydrous Na_2SO_4. Silica gel column chromatography with

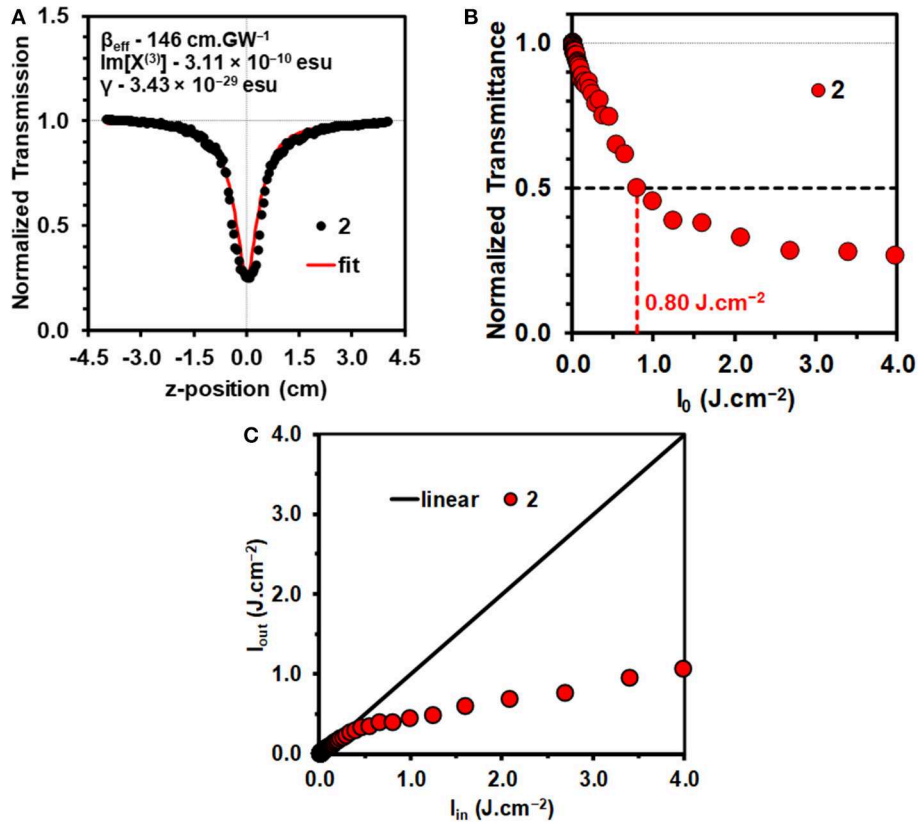

FIGURE 2 | Open-aperture Z-scan for a 4.9 × 10^{-6} M solution of **2** in CH_2Cl_2 at an input intensity of 32 μJ with the calculated NLO parameters **(A)**. Normalized transmittance vs. input fluence (I_{in}) curve for **2** in CH_2Cl_2 **(B)**. The calculation of the I_{lim} value is shown with horizontal and vertical lines. Output fluence (I_{out}) vs. input fluence (I_{in}) curves for **2 (C)**. Details of the optical limiting parameters are provided in **Table 1**.

ethyl acetate:petroleum ether (1:4) as the eluent provided the pure target compound in 33% yield. ^{1}H NMR (600 MHz, $CDCl_3$) δ_H, ppm 7.70 (d, J = 7.9 Hz, 2H), 7.47 (s, 1H), 7.24 (d, J = 7.9 Hz, 2H), 6.00 (s, 2H), 2.57 (s, 6H), 2.25 (s, 3H), 1.44 (s, 6H). FT-IR: ν, cm^{-1} 3,368 (N-H amide stretch), 2,920 (C-H stretch), 2,852 (C-H stretch), 1,529 (N-H amide bend), 1,459, 1,399 (C-N stretch), 1,186 (C-N stretch), 967 (=C-H bend), 470 (C-H).

4,4′-Difluoro-8-(4-acetamidophenyl)-1,7-dimethyl-3,5-di-(4-benzyloxy)styryl-4-bora-3a,4a-diaza-s-indacene (2)

Piperidine (1 mL) and glacial acetic acid (1 mL) were added to a solution of 4-benzyloxybenzaldehyde (2 eq) and **1** (1 eq) in benzene (50 mL). The reaction mixture was heated at reflux for several hours, and water was removed with a Dean-Stark trap. The solvent was removed under vacuum on a rotary evaporator and the crude product was diluted in CH_2Cl_2, washed with water and then dried over anhydrous Na_2SO_4. The solvent was removed under vacuum and pure target compound was obtained in 32% yield by silica gel column chromatography with ethyl acetate:petroleum ether (1:4) as the eluent. ^{1}H NMR (600 MHz, $CDCl_3$) δ_H, ppm 7.70 (d, J = 7.9 Hz, 2H), 7.64–7.58 (m, 6H), 7.51–7.46 (m, 5H), 7.46–7.42 (m, 4H), 7.39–7.35 (m, 2H), 7.27–7.21 (m, 4H), 7.02 (d, J = 8.2 Hz, 4H), 6.62 (s, 2H), 5.13 (s, 4H), 2.24 (s, 3H), 1.48 (s, 6H). FT-IR: ν, cm^{-1} 3,377 (N-H amide stretch), 2,916 (C-H stretch), 2,853 (C-H stretch), 1,471 (N-H

TABLE 1 | Photophysical data for BODIPYs **1** and **2** in CH_2Cl_2, and optical limiting parameters for **2** in CH_2Cl_2.

Photophysical properties					
	λ_{Abs} (nm)	λ_{ex} (nm)	λ_{em} (nm)	Φ_F	τ_F (ns)
1	501	500	514	0.50	3.3
2	644	644	660	0.40	4.6

Optical limiting properties						
	Energy (μJ)	α (cm^{-1})	β_{eff} (cm.GW^{-1})	Im[$\chi^{(3)}$] (esu)	γ (esu)	I_{lim} (J.cm^{-2})
2	30	0.78	145.5	3.17 × 10^{-10}	3.25 × 10^{-29}	0.80

amide bend), 1,368 (C-N stretch), 1,103 (C-N stretch), 1,154 (C-O-C), 979 (=C-H bend). MS (MALDI-TOF): m/z 769.30 (calc. for $[M]^+$ 769.86).

RESULTS AND DISCUSSION

A typical 3,5-distyrylBODIPY dye was synthesized so that its photophysical and optical limiting properties could be investigated. A *p*-acetamidophenyl group was introduced at the *meso*-position to form a novel BODIPY core dye **1** (**Figure 1A**) and benzyloxystyryl moieties were added at the 3,5-positions to form a novel 3,5-distyrylBODIPY dye **2**. We have previously reported the optical limiting properties of 3,5-di-*p*-benzyloxystyrylBODIPY dyes with a range of different *meso*-substituents (Ngoy et al., 2018; Ndebele et al., 2019). The results were found to be broadly similar and to suggest that these dyes are potentially suitable for use as OL materials. In this study, transient absorbance spectroscopy and kinetic studies with femtosecond and nanosecond laser pulses are used to investigate the role of ESA from the S_1 state in the context of 3,5-distyrylBODIPY dyes. Since there are no heavy atoms incorporated, these dyes are not expected to undergo significant intersystem crossing to the triplet manifold.

Optical Spectroscopy and Photophysical Properties

The UV-visible absorption spectra of **1** and **2** (**Figure 1B**) are typical of what is normally observed for a 1,3,5,7-tetramethylBODIPY core dye and its 3,5-distyryl derivative (Lu et al., 2014). Since the BODIPY chromophore lacks a macrocycle, the visible region is dominated by a single intense spectral band and does not give rise to the Q and B bands that dominate the optical spectra of porphyrins and phthalocyanines (Lu et al., 2014). The main absorption band of BODIPY core dye **1** lies at 501 nm in CH_2Cl_2, while that of **2** lies at 644 nm with a log ε value of 5.56 in CH_2Cl_2. The main emission bands of **1** and **2** lie at 514 and 660 nm, respectively, and were found to have Φ_F values of 0.50 and 0.40 and τ_F values of 3.3 and 4.6 ns (**Table 1**). **2** is hence moderately fluorescent, in a similar manner to what has previously been observed for a wide range of BODIPY dyes that have extended π-systems with co-planar styryl or vinylene substituents (Ndebele et al., 2019). Theoretical calculations have demonstrated that the large red shift of the main BODIPY spectral band of 3,5-distyrylBODIPY dyes upon styrylation results primarily from a relative destabilization of the HOMO (Lu et al., 2014; Ndebele et al., 2019), which has larger MO coefficients at the 3,5-positions at the LUMO. This results in a significant narrowing of the HOMO–LUMO gap. Since a relatively large energy gap is predicted between the S_1 and S_2 excited states of 3,5-distyrylBODIPY dyes (Ndebele et al., 2019), these dyes exhibit only relatively weak absorbance under ambient light conditions across most of the visible region (**Figure 1B**). These properties make 3,5-distyrlBODIPY dyes suitable for use in OL applications in the context of visible region laser pulses.

Optical Limiting Properties

The mechanisms that can result in an optical limiting effect are non-linear absorption (NLA), non-linear refraction (NLR), and non-linear scattering (NLS). Since a solution of a molecular dye is involved in the context of this study, NLA is the dominant mechanism. Z-scan measurements were carried out for **2** in a 4.9×10^{-6} M CH_2Cl_2 solution (**Figure 2A**) with 10 ns laser pulses. The concentration used lies within the linear range according to the Beer-Lambert law. This prevents aggregation that can result in significant NLS.

Since nanosecond laser pulses were used in this study, the concave downward dipping reverse saturable absorption (RSA) response (**Figure 2A**) that is observed for **2** in the open aperture Z-scan data is unlikely to arise exclusively from multiphoton processes such as 2PA. ESA from the S_1 or T_1 state can result in an RSA response when the ESA is more intense than the ground state absorbance, due to the effect of depopulating the ground state (Saleh and Teich, 1991; Tutt and Boggess, 1993; de la Torre et al., 2004), so only a β_{eff} value can be quantified for the non-linear absorption coefficient rather than the intrinsic β value that is associated with 2PA. There have been a limited number of studies of the intrinsic β values of BODIPY dyes in femtosecond pump-probe studies (Wang et al., 2010; Kim et al., 2015; Zheng et al., 2018).

The normalized transmittance values at each z-axis position [T(z)] were analyzed as the sample is translated through the focal point of the lens used in the Z-scan measurements by using the approach developed by Sheik-Bahae et al. (1989, 1990) and Sheik-Bahae and Van Stryland (1998) (Equations 1–4):

$$T(z) = \frac{1}{\sqrt{\pi} q_0(z)} \int_{-\infty}^{\infty} \ln[1 + q_0(z) e^{-\tau^2}] d\tau \quad (1)$$

where the size of the non-linear response is described by $q_0(z)$. For a circular beam, the $q_0(z)$ value is described by Equation 2:

$$q_0(z) = \frac{2\beta_{eff} P_0 l_{eff}}{\pi w(z)^2} \quad (2)$$

where P_0 is the peak power of the laser pulse, β_{eff} is the effective non-linear absorption coefficient, and l_{eff} is the effective pathlength, given by Equation 3:

$$l_{eff} = \frac{1 - e^{(-\alpha L)}}{\alpha} \quad (3)$$

where L is the pathlength. The linear absorption coefficient, α, is described by Equation 4:

$$\alpha = \frac{2.303 \cdot OD}{L} \quad (4)$$

where OD is the optical density of the solution at 532 nm. The beam width [w(z)], in Equation 2 can be described as a function of sample position using Equation 5:

$$w(z) = w_0 \sqrt{1 + \left(\frac{z}{z_0}\right)^2} \quad (5)$$

where z is the translation distance of the sample from the laser focal point, and z_0 is the Rayleigh length that is defined as $\pi w_0^2/\lambda$ where λ is the wavelength of the laser, w_0 is the beam waist value at the focal point ($z = 0$) of the laser beam which describes the distance where there is $1/e^2$ intensity relative to the on axis value.

Although the effective non-linear absorption coefficient, β_{eff}, can be described using Equations 1–5, the $q_0(z)$ value is usually derived from the normalized transmittance data by applying an analytical version of Equation 1 (Ndebele et al., 2019):

$$T(z) = 0.363e^{\left(\frac{-q_0(z)}{5.60}\right)} + 0.286e^{\left(\frac{-q_0(z)}{1.21}\right)} + 0.213e^{\left(\frac{-q_0(z)}{24.62}\right)} + 0.096e^{\left(\frac{-q_0(z)}{115.95}\right)} + 0.038e^{\left(\frac{-q_0(z)}{965.08}\right)} \quad (6)$$

When Equation 2 is substituted into Equation 5, the $q_0(z)$ value can be described as:

$$q_0(z) = \frac{Q_0}{1+\frac{z^2}{z_0^2}} \quad (7)$$

where Q_0 is given as:

$$Q_0 = \frac{2\beta_{eff} P_0 l_{eff}}{\pi w_0^2} \quad (8)$$

The FWHM and peak maximum values for the Gaussian curve that is defined by Equation 1 are proportional to the z_0 and Q_0 values as defined by Equations 7, 8. Equation 9 is used to determine the β_{eff} value, which is dependent on the population of molecules in the excited state. The magnitude of the β_{eff} value provides an indication of how suitable materials are for use in optical limiting applications:

$$\beta_{eff} = \frac{\lambda z_0 Q_0}{2 P_0 l_{eff}} \quad (9)$$

The imaginary component of the third-order non-linear susceptibility, $Im[\chi^{(3)}]$, provides a measure of how rapidly an OL material responds to perturbations that are initiated by intense incident laser pulses (Sheik-Bahae and Van Stryland, 1998; Dini and Hanack, 2003). The relationship between the $Im[\chi^{(3)}]$ and β_{eff} values is described by Equation 10:

$$Im\left[\chi^{(3)}\right] = \frac{\eta^2 \varepsilon_0 c \lambda \beta_{eff}}{2\pi} \quad (10)$$

Where ε_0, η, and c are the permittivity of free space, the linear refractive index and speed of light, respectively.

The interaction between the permanent dipole of molecules with incident laser beams of high intensity can modulate the average orientation of the molecules in a manner that also induces second-order hyperpolarizability, γ. The relationship between the γ and $Im[\chi^{(3)}]$ values is shown in Equation 11:

$$\gamma = \frac{Im\left[\chi^{(3)}\right]}{f^4 C_{mol} N_A} \quad (11)$$

where N_A, f, and C_{mol} are Avogadro's constant, the Lorentz local field factor ($f = (\eta^2+2)/3$), and the molar concentration of the active species, respectively.

The data were analyzed in a similar manner to what has been described previously (Harris et al., 2017; Kubheka et al., 2018; Ngoy et al., 2018, 2019; Ndebele et al., 2019) to determine the β_{eff}, $Im[\chi^{(3)}]$, and γ values. A linear absorption coefficient, α, of 0.78 cm^{-1} was obtained at 532 nm for the 4.9×10^{-6} M CH_2Cl_2 solution of **2** that was studied (**Table 1**), so the S_1 state is likely to be populated primarily by linear absorption rather than through multiphoton processes. The β_{eff} value obtained for **2** (**Figure 2A** and **Table 1**) provides a measure of the magnitude of the non-linear absorptivity, and lies within the range previously reported for other organic compounds (Dini and Hanack, 2003; Sutherland et al., 2003). OL materials have positive β_{eff} values since there is a marked decrease in transmittance at the focal point of the Z-scan instrument.

The γ and $Im[\chi^{(3)}]$ values that were obtained (**Table 1**) confirm that BODIPY **2** has promising OL properties, since they lie in the 10^{-29}–10^{-34} and 10^{-9}–10^{-15} esu ranges (Dini and Hanack, 2003; Sutherland et al., 2003), respectively, that have previously been reported to be favorable for use in optical limiting in the context of molecular dyes, such as porphyrins and phthalocyanines (de la Torre et al., 2004; Senge et al., 2007; Dini et al., 2016). A review was recently published that provides the β_{eff}, γ and $Im[\chi^{(3)}]$ values for 17 different π-expanded BODIPY dyes on the nanosecond timescale at 532 nm (Ndebele et al., 2019). No comparison can be made with femtosecond timescale data for BODIPYs, since a multiphoton absorption mechanism is involved in that context in the absence of ESA (Wang et al., 2010; Kim et al., 2015; Zheng et al., 2018). The γ value is the most useful parameter for making direct comparisons between the OL properties, since Equation 11 includes the concentration, while Equations 9 and 10 do not since the β_{eff} and $Im[\chi^{(3)}]$ values are concentration dependent. The γ value for **2** (3.25×10^{-29}) is one of the highest we have reported to date for a 3,5-distyryl- or 3,5-divinyleneBODIPY and is comparable in magnitude to the value of 9.6×10^{-30} esu that was recently reported for a 3,5-di-*p*-benzyloxystyrylBODIPY with a *p*-hydroxyphenyl group at the *meso*-position (Ngoy et al., 2018). The γ values of most 3,5-distyrylBODIPYs have been reported to lie in the 10^{-30} esu range (Ndebele et al., 2019).

For a material to be considered to be viewed as suitable for OL applications, the transmittance should decrease by over 50% as is the case with dye **2** (**Figure 2B**). It is important to be able to determine the input energy at which this happens. Irradiance has units of $W.cm^{-2}$, with the maximum value, I_{00}, occurring at the focus ($z = 0$), determined by Equation 12.

$$I_{00} = \frac{E}{\tau \pi w_0^2} \quad (12)$$

where w_0 is the beam waist (cm), τ is the laser pulse length (s), and E is the energy of the laser pulse (J). The maximum irradiance values can be expressed in units of $W.cm^{-2}$, since $1\ J.s^{-1} = 1\ W$. Since the energy of the laser pulses is kept constant during the Z-scan measurements, the overall power of the laser

beam is also constant throughout, but the irradiance value will change with the beam width as the sample is moved into and out of focus along the z-axis direction, w(z). The area of the beam is circular and hence equal to $\pi w(z)^2$. Multiplying the circular cross-sectional beam area, $\pi w(z)^2$, by the irradiance gives the laser power, P, at the focal point (z = 0), Equation 13:

$$P = I_{00}\pi w_0^2 \tag{13}$$

At other z positions, P can be expressed by Equation 14.

$$P = I_{in}(z)\pi w(z)^2 \tag{14}$$

Since P is kept constant, Equations 13 and 14 can be combined to provide the input fluence value, Equation 15:

$$I_{in}(z) = I_{00}\left(\frac{w_0}{w(z)}\right)^2 \tag{15}$$

Since the transmittance provides the percentage of light that passes through the material, values for output fluence can be determined from the product of T(z) and $I_{in}(z)$ at each z position, Equation 16.

$$I_{out}(z) = I_{in}(z)T(z) \tag{16}$$

The limiting threshold fluence (I_{lim}) can be defined as the input fluence value at which the output fluence (I_{out}) is decreased to 50% of the input fluence (I_{in}), and this can be readily determined using a plot of normalized transmittance vs. input fluence (**Figure 2B**). A relatively low I_{lim} value of 0.80 J.cm^{-2} was obtained in CH_2Cl_2 solution (**Table 1**). This provides further evidence that 3,5-distyrylBODIPYs are potentially suitable for use in OL applications. A wide range of different π-expanded BODIPY dyes have provided broadly similar I_{lim} values (Ndebele et al., 2019). Since the limiting threshold can be lowered by increasing the concentration of the solution, I_{lim} values reported in the literature cannot be readily compared. The International Commission on Non-Ionizing Radiation Protection has published a guideline (International Commission on Non-Ionizing Radiation Protection (ICNIRP), 2000) for exposure to a variety of lasers, which has been determined to provide a limit of 0.95 J.cm^{-2} for the 0.25 s exposure time for the normal human blink reflex to prevent significant damage to the human eye (Harris et al., 2017). Plotting I_{out} against I_{in} (**Figure 2C**) can be used to demonstrate whether the I_{out} values approach a plateau as the I_{in} value increases, which is the type non-linear response that would normally be expected for an OL material that is suitable for practical applications (Dini and Hanack, 2003; Sutherland et al., 2003).

Pump-Probe Transient Spectroscopy Studies

BODIPY **2** is not halogenated and contains no other heavy atom. BODIPY dyes of this type usually have very low triplet state and singlet oxygen quantum yields in the absence of heavy atoms (Yogo et al., 2005; Jiao et al., 2011; Yang et al., 2013; Frenette et al., 2014), so the S_1 state is believed to be involved with the ESA of non-halogenated 3,5-distyrylBODIPY dyes (Harris et al., 2017; Kubheka et al., 2018; Ngoy et al., 2018, 2019). This was confirmed in this study by carrying out the femtosecond and nanosecond pump-probe spectroscopy and kinetic studies. A time-resolved transient spectroscopic study was carried out for solutions of BODIPY dye **2** (ca. 5.0 × 10^{-3} M) in CH_2Cl_2 with a femtosecond laser at 387.5 nm in order to study what happens during Z-scan measurements when the S_1 state is populated upon electronic excitation (**Figure 3A**). As would normally be anticipated, intense ground state depletion peaks are observed at 371, 596, and 645 nm, which correspond to the main absorption bands of **2** (**Figures 1B**, **3B**). These signals decay on a nanosecond timescale (**Figure 3A**) in a manner that is consistent with the observed fluorescence lifetime of 4.6 ns (**Table 1**), since the decay of the ESA and fluorescence intensities are both dependent upon changes in the population of the S_1 state after its initial population by an incident laser pulse. An intense broad peak is observed due to ESA across most of the visible region between 400 and 580 nm with a maximum at 481 nm (**Figure 3B**). When attempts were made

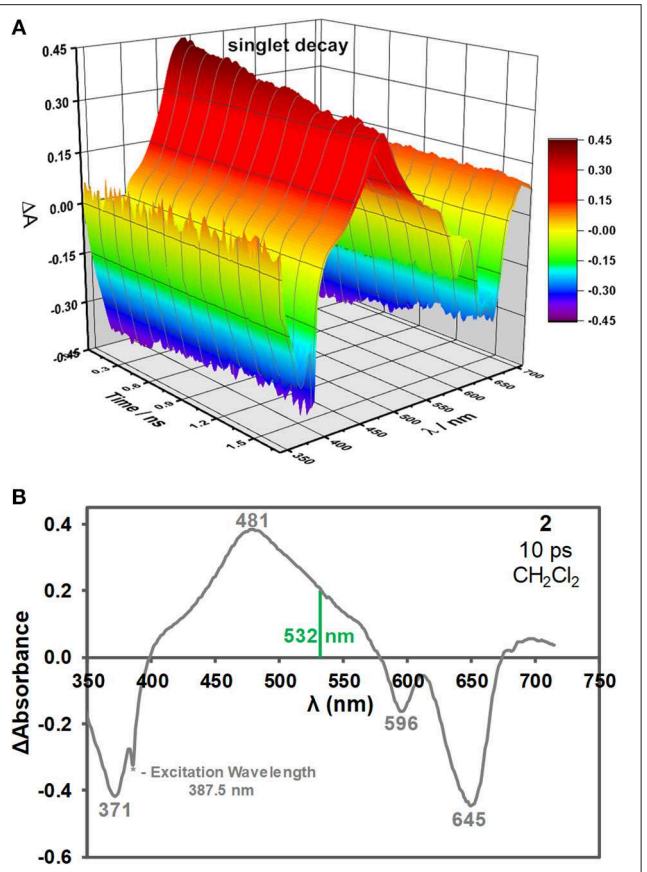

FIGURE 3 | Time-resolved transient absorption spectra of **2** in CH_2Cl_2 after a 150 fs laser pulse at an excitation wavelength of 387.5 nm **(A)**. The transient absorption spectrum of **2** at 10 ps after a 150 fs laser pulse at 387.5 nm in CH_2Cl_2 **(B)**. The 532 nm wavelength used for the open-aperture Z-scan measurement is highlighted with a green vertical line.

to measure transient absorption spectra and decay curves on the microsecond timescale for the T_1 state of **2** using 7 ns laser pulses to excite at the band maximum at 644 nm (**Figure 1B**), no decay curve was observed for **2** in degassed CH_2Cl_2 solutions. In contrast, data could be readily measured with comparable solutions of halogenated BODIPYs using a similar approach, since the rate of intersystem crossing is greatly enhanced by the heavy atom effect. This demonstrates that ESA associated with the T_1 state does not play a significant role in the optical limiting properties of **2**.

CONCLUSIONS

The open aperture Z-scan study on a 3,5-di-*p*-benzyloxystyrylBODIPY dye at 532 nm on the nanosecond timescale demonstrates that dyes of this type have favorable OL properties as has been reported previously. Time-resolved transient-absorption spectra were recorded after a 150 fs laser pulse to provide further insights into the mechanism of the observed optical limiting response. A broad and intense band is observed between 400 and 580 nm due to ESA from the S_1 state, which is consistent with the observed strong RSA response at the 532 nm. In contrast, no triplet decay curve was observed on the microsecond timescale for **2** when 7 ns laser pulses were used instead. This provides the first direct spectroscopic evidence that the OL effects that have consistently been observed at 532 nm for 3,5-divinyl- and 3,5-distyrylBODIPY dyes that contain no heavy halogen atoms at the 2,6-positions are due primarily to ESA from the S_1 state to higher energy states in the singlet manifold. The key to further enhancing the reverse saturable absorbance response that is observed for nanosecond laser pulses in the visible region is to further enhance this ESA. Since it is usually important that optical limiting materials remain transparent under ambient light conditions, the goal in future will be to identify how the structure of the BODIPY chromophore can be modified in a rational manner to further enhance this ESA, while also shifting the main spectral band of the BODIPY chromophore to the red so that there is minimal absorbance across the entire visible region. The use of hybrid materials in which BODIPY dyes are conjugated with nanomaterials in a similar manner to what has been reported previously for porphyrins and phthalocyanines (Dini et al., 2016) also merits in depth investigation in the years ahead.

DATA AVAILABILITY STATEMENT

The key data sets that support the conclusions reported in this manuscript will be made available by the corresponding author to any qualified researcher without undue reservation.

AUTHOR CONTRIBUTIONS

BN synthesized BODIPYs **1** and **2** and carried out the femtosecond timescale kinetic measurements. AM carried out the Z-scan measurements, the photophysical studies, and the nanosecond timescale kinetic measurements. JM conceptualized the research and was the lead author in preparing the manuscript. TN provided the resources for the project and also assisted with the writing of the manuscript.

FUNDING

Funding was provided by the National Research Foundation (NRF) and Department of Science and Technology (DST) of South Africa through the DST/NRF South African Research Chairs Initiative for Professors of Medicinal Chemistry and Nanotechnology to TN (uid: 62620), and NRF CSUR and IPRR grants to JM (uids: 93627 & 119259). Photophysical measurements were enabled by the Laser Rental Pool Programme of the Council for Scientific and Industrial Research (CSIR) of South Africa. The Z-scan instrument was provided by Armscor of South Africa.

ACKNOWLEDGMENTS

We thank Prof. Petr Klan of Masaryk University in Brno, in the Czech Republic for help with the femtosecond measurements. This aspect of the research was supported by the RECETOX Research Infrastructure (LM2015051 and CZ.02.1.01/0.0/0.0/16_013/0001761).

REFERENCES

Calvete, M., Yang, G. Y., and Hanack, M. (2004). Porphyrins and phthalocyanines as materials for optical limiting. *Synth. Met.* 141, 231–243. doi: 10.1016/S0379-6779(03)00407-7

Chen, Y., Hanack, M., Araki, Y., and Ito, O. (2005). Axially modified gallium phthalocyanines and naphthalocyanines for optical limiting. *Chem. Soc. Rev.* 34, 517–529. doi: 10.1039/b416368k

de la Torre, G., Vazquez, P., Agullo-Lopez, F., and Torres, T. (2004). Role of structural factors in the non-linear optical properties of phthalocyanines and related compounds. *Chem. Rev.* 104, 3723–3750. doi: 10.1021/cr030206t

Dini, D., Calvete, M. J. F., and Hanack, M. (2016). Non-linear optical materials for the smart filtering of optical radiation. *Chem. Rev.* 116, 13043–13233. doi: 10.1021/acs.chemrev.6b00033

Dini, D., and Hanack, M. (2003). "Physical properties of phthalocyanine-based materials", in *The Porphyrin Handbook*, eds K. M. Kadish, K. M. Smith, and R. Guilard (Cambridge, MA: Academic Press), 1–36. doi: 10.1016/B978-0-08-092391-8.50007-8

Frenette, M., Hatamimoslehabadi, M., Bellinger-Buckley, S., Laoui, S., La, J., Bag, S., et al. (2014). Shining light on the dark side of imaging: excited state absorption enhancement of a *bis*-styryl BODIPY photoacoustic contrast agent. *J. Am. Chem. Soc.* 136, 15853–15856. doi: 10.1021/ja508600x

Harris, J., Gai, L., Kubheka, G., Mack, J., Nyokong, T., and Shen, Z. (2017). Optical limiting properties of 3,5-dithienylenevinylene BODIPY dyes at 532 nm. *Chem. Eur. J.* 23, 14507–14514. doi: 10.1002/chem.201702503

International Commission on Non-Ionizing Radiation Protection (ICNIRP) (2000). Revision of guidelines on limits of exposure to laser radiation of wavelengths between 400 nm and 1.4 μm. *Health Phys.* 79, 431–440. doi: 10.1097/00004032-200010000-00013

Jiao, L., Pang, W., Zhou, J., Wei, Y., Mu, X., Bai, G., et al. (2011). Regioselective stepwise bromination of boron dipyrromethene (BODIPY) dyes. *J. Org. Chem.* 76, 9988–9996. doi: 10.1021/jo201754m

Kandasamy, K., Shetty, S. J., Puntambekar, P. N., Srivastava, T. S., Kundu, T., and Singh, B. P. (1997). Non-resonant third-order optical non-linearity of porphyrin derivatives. *Chem. Commun.* 33, 1159–1160. doi: 10.1039/a702098h

Kim, B., Yue, X., Sui, B., Zhang, X., Xiao, Y., Bondar, M. V., et al. (2015). Near-infrared fluorescent 4,4-difluoro-4-bora-3a,4a-diaza-*s*-indacene probes for one- and two-photon fluorescence bio-imaging. *Eur. J. Org. Chem.* 2015, 5563–5571. doi: 10.1002/ejoc.201500664

Kličová, L., Šebej, P., Šolomek, T., Hellrung, B., Slavíček, P., Klán, P., et al. (2012). Adiabatic triplet state tautomerization of *p*-hydroxyacetophenone in aqueous solution. *J. Phys. Chem. A* 116, 2935–2944. doi: 10.1021/jp3011469

Kubheka, G., Mack, J., Kobayashi, N., Kimura, M., and Nyokong, T. (2017). Optical limiting properties of 2,6-dibromo-3,5-distyrylBODIPY dyes at 532 nm. *J. Porphyrins Phthalocyanines* 21, 523–531. doi: 10.1142/S1088424617500511

Kubheka, G., Sanusi, K., Mack, J., and Nyokong, T. (2018). Optical limiting properties of 3,5-dipyrenylvinyleneBODIPY dyes at 532 nm. *Spectrochim. Acta A* 191, 357–364. doi: 10.1016/j.saa.2017.10.021

Kulyk, B., Taboukhat, S., Akdas-Kilig, H., Fillaut, J.-L., Boughaleb, Y., and Sahraoui, B. (2016). Non-linear refraction and absorption activity of dimethylaminostyryl substituted BODIPY dyes. *RSC Adv.* 6, 84854–84859. doi: 10.1039/C6RA19023E

Kulyk, B., Taboukhat, S., Akdas-Kilig, H., Fillaut, J. L., Karpierz, M., and Sahraoui, B. (2017). Tuning the non-linear optical properties of BODIPYs by functionalization with dimethylaminostyryl substituents. *Dyes Pigments* 137, 507–511. doi: 10.1016/j.dyepig.2016.10.045

Loudet, A., and Burgess, K. (2007). BODIPY dyes and their derivatives: syntheses and spectroscopic properties. *Chem. Rev.* 107, 4891–4932. doi: 10.1021/cr078381n

Lu, H., Mack, J., Yang, Y., and Shen, Z. (2014). Structural modification strategies for the rational design of red/NIR region BODIPYs. *Chem. Soc. Rev.* 43, 4778–4823. doi: 10.1039/C4CS00030G

May, A. K., Stone, J., Ngoy, B. P., Mack, J., Nyokong, T., Kimura, M., et al. (2018). Photophysical and optical limiting properties of a novel distyryl-BODIPY with fused crown ether moieties. *J. Porphyrins Phthalocyanines* 21, 832–843. doi: 10.1142/S1088424617500869

Ndebele, N., Hlatshwayo, Z., Ngoy, B. P., Kubheka, G., Mack, J., and Nyokong, T. (2019). Optical limiting properties of BODIPY dyes substituted with styryl or vinylene groups on the nanosecond timescale. *J. Porphyrins Phthalocyanines* 23, 701–717. doi: 10.1142/S108842461930009X

Neethling, P. (2005). *Determining Non-Linear Optical Properties with the Z-scan Technique* (M.Sc thesis). University of Stellenbosch, Stellenbosch, South Africa.

Ngoy, B. P., Hlatshwayo, Z., Nwaji, N., Fomo, G., Mack, J., and Nyokong, T. (2018). Photophysical and optical limiting properties at 532 nm of BODIPY dyes with *p*-benzyloxystyryl groups at the 3,5-positions. *J. Porphyrins Phthalocyanines* 22, 413–422. doi: 10.1142/S1088424617500857

Ngoy, B. P., May, A. K., Mack, J., and Nyokong, T. (2019). Effect of bromination on the optical limiting properties at 532 nm of BODIPY dyes with *p*-benzyloxystyryl groups at the 3,5-positions. *J. Mol. Struct.* 1175, 745–753. doi: 10.1016/j.molstruc.2018.08.012

Ogawa, K., Zhang, T., Yoshihara, K., and Kobuke, Y. (2002). Large third-order optical non-linearity of self-assembled porphyrin oligomers. *J. Am. Chem. Soc.* 124, 22–23. doi: 10.1021/ja0169015

Ogunsipe, A., Chen, J., and Nyokong, T. (2004). Photophysical and photochemical studies of zinc(II) phthalocyanine derivatives–effects of substituents and solvents. *New J. Chem.* 28, 822–827. doi: 10.1039/B315319C

Rurack, K., Kollmannsberger, M., and Daub, J. (2001). Molecular switching in the near infrared (NIR) with a functionalized boron-dipyrromethene dye. *Angew. Chem. Int. Ed.* 40, 385–87. doi: 10.1002/1521-3773(20010119)40:2<385::AID-ANIE385>3.0.CO;2-F

Saleh, B. E. A., and Teich, M. C. (1991). *Fundamentals of Photonics*. New York, NY: Wiley. doi: 10.1002/0471213748

Senge, M. O., Fazekas, M., Notaras, E. G. A., Blau, W. J., Zawadzka, M., Locos, O. B., et al. (2007). Non-linear optical properties of porphyrins. *Adv. Mater.* 19, 2737–2774. doi: 10.1002/adma.200601850

Sheik-Bahae, M., Said, A. A., and Van Stryland, E. W. (1989). High-sensitivity, single-beam n2 measurements. *Opt. Lett.* 14, 955–957. doi: 10.1364/OL.14.000955

Sheik-Bahae, M., Said, A. A., Wei, T.-H., Hagan, D. J., and Van Stryland, E. W. (1990). Sensitive measurement of optical non-linearities using a single beam. *IEEE J. Quantum Electron.* 26, 760–769. doi: 10.1109/3.53394

Sheik-Bahae, M., and Van Stryland, E. (1998). "Z-scan measurements of optical nonlinearities," in *Characterization Techniques and Tabulations for Organic Non-linear Materials*, eds M. G. Kuzyk and C. W. Dirk (New York, NY: Marcel Dekker), 655–692.

Sutherland, R. L., Mclean, D. G., and Kirkpatrick, S. (2003). *Handbook of Non-linear Optics*. New York, NY: CRC Press. doi: 10.1201/9780203912539

Thakare, S. S., Sreenath, M. C., Chitrambalam, S., Joe, I. H., and Sekar, N. (2017). Non-linear optical study of BODIPY-benzimidazole conjugate by solvatochromic, Z-scan and theoretical methods. *Opt. Mater.* 64, 543–460. doi: 10.1016/j.optmat.2017.01.020

Tutt, L., and Boggess, T. (1993). A review of optical limiting mechanisms and devices using organics, fullerenes, semiconductors and other materials. *Prog. Q. Electron.* 17, 299–338. doi: 10.1016/0079-6727(93)90004-S

Ulrich, G., Ziessel, R., and Harriman, A. (2008). The chemistry of fluorescent BODIPY dyes: versatility unsurpassed. *Angew. Chem. Int. Ed.* 47, 1184–1201. doi: 10.1002/anie.200702070

Wang, Y., Zhang, D., Zhou, H., Ding, J., Chen, Q., Xiao, Y., et al. (2010). Non-linear optical properties and ultrafast dynamics of three novel boradiazaindacene derivatives. *J. Appl. Phys.* 108:033520. doi: 10.1063/1.3457859

Yang, Y., Guo, Q., Chen, H., Zhou, Z., Guo, Z., and Shen, Z. (2013). Thienopyrrole-expanded BODIPY as a potential NIR photosensitizer for photodynamic therapy. *Chem. Commun.* 49, 3940–3942. doi: 10.1039/c3cc40746b

Yogo, T., Urano, Y., Ishitsuka, Y., Maniwa, F., and Nagano, T. (2005). Highly efficient and photostable photosensitizer based on BODIPY chromophore. *J. Am. Chem. Soc.* 127, 12162–12163. doi: 10.1021/ja0528533

Zheng, Q., He, G. S., and Prasad, P. N. (2009). A novel near IR two-photon absorbing chromophore : optical limiting and stabilization performances at an optical communication wavelength. *Chem. Phys. Lett.* 475, 250–255. doi: 10.1016/j.cplett.2009.05.040

Zheng, X., Du, W., Gai, L., Xiao, X., Li, Z., Xu, L., et al. (2018). Disilanylene-bridged BODIPY-based D–σ–A architectures: a novel promising series of NLO chromophores. *Chem. Commun.* 54, 8834–8837. doi: 10.1039/C8CC04962A

Zhu, M., Jiang, L., Yuan, M., Liu, X., Ouyang, C., Zheng, H., et al. (2008). Efficient tuning non-linear optical properties: synthesis and characterization of a series of novel poly(aryleneethynylene)s co-containing BODIPY. *J. Polym. Sci. A* 46, 7401–7410. doi: 10.1002/pola.23045

Conflict of Interest: The authors declare that the research was conducted in the absence of any commercial or financial relationships that could be construed as a potential conflict of interest.

frontiers in Chemistry

ORIGINAL RESEARCH
published: 15 November 2019
doi: 10.3389/fchem.2019.00765

Comparing the Rod-Like and Spherical BODIPY Nanoparticles in Cellular Imaging

Chong Ma[1], Jianxu Zhang[2,3], Tao Zhang[1], Haojie Sun[1], Jing Wu[4], Jingwei Shi[5] and Zhigang Xie[2]**

[1] Department of Gastrointestinal Colorectal and Anal Surgery, China-Japan Union Hospital of Jilin University, Changchun, China, [2] State Key Laboratory of Polymer Physics and Chemistry, Changchun Institute of Applied Chemistry, Chinese Academy of Sciences, Changchun, China, [3] University of Chinese Academy of Sciences, Beijing, China, [4] International Journal of Geriatrics, Jilin University, Changchun, China, [5] Department of Clinical Laboratory, China-Japan Union Hospital of Jilin University, Changchun, China*

To design efficient nanoparticles for bioimaging, it is necessary to obtain nanoparticles with desired cellular uptake and biofunction. There are many studies have shown that cellular uptake largely depends on the geometric properties of nanoparticles. In this work, the organic nanoparticles with rod-like and spherical shapes were fabricated, and their cellular behaviors were studied and compared in detail via cellular uptake and bioimaging effect. The nanoparticles with spherical and rod-like morphology both can be internalized by HeLa and HepG2 cells, but the rod-like nanoparticles showed better imaging performance than their spherical counterpart. Above results presented that the rod-like nanoparticles possess great potential for bioimaging in efficient delivery and ideal imaging efficacy. Our studies may provide useful and fundamental information for designing efficient bioimaging systems.

Keywords: BODIPY, imaging, nanoparticles, rod, spherical

OPEN ACCESS

Edited by:
Zhen Shen,
Nanjing University, China

Reviewed by:
Wei Zhang,
Chongqing Institute of Green and Intelligent Technology (CAS), China
Jiangli Fan,
Dalian University of Technology, China

****Correspondence:***
Jingwei Shi
shi123jingwei@163.com
Zhigang Xie
xiez@ciac.ac.cn

Specialty section:
This article was submitted to Supramolecular Chemistry, a section of the journal Frontiers in Chemistry

Received: *28 August 2019*
Accepted: *24 October 2019*
Published: *15 November 2019*

Citation:
Ma C, Zhang J, Zhang T, Sun H, Wu J, Shi J and Xie Z (2019) Comparing the Rod-Like and Spherical BODIPY Nanoparticles in Cellular Imaging. Front. Chem. 7:765. doi: 10.3389/fchem.2019.00765

INTRODUCTION

Nanomedicines are very important for various biomedical applications because if the prolong circulation times, overcome biological barriers, and reduce system side effects (Lee et al., 2012; Kunjachan et al., 2015). More importantly, nanomedicines have the capacity to design their physicochemical parameters such as surface charge, shape, size, and surface functionalization to achieve desired properties (Biju, 2014; Aula et al., 2015). In the past decade, many studies have shown that physicochemical parameters of nanomedicines could extremely impact their functions (Zhang et al., 2015; Kinnear et al., 2017). For example, particles with diameter in 50–100 nm show a suitable size range for maximizing tumor accumulation and minimizing the ensuing clearance (Black et al., 2014). Besides the size, another important parameter is the morphology of nanomedicines (Herd et al., 2013; Blanco et al., 2015). As a matter of fact, some microorganisms with non-spherical morphologies, such as rod bacteria or polygonal adenovirus, have great capabilities to infect specific cell types (Geisbert and Jahrling, 2004). Rencently, researchers have systematically studied the different of nanomedicines with various shapes on cellular internalization (Alemdaroglu et al., 2008; Chauhan et al., 2011). Compared to their spherical counter parts, the rod-like nanoparticles have more advantages in their cellular behaviors. However, the vast majority of nanomedicines in lab studies or clinical trials are spherical because of their ease of preparation (Yan et al., 2016; Zhang et al., 2016). To date, the development of progress in morphology control

has resulted in preparing kinds of non-spherical inorganic nanoparticles, and study of specific structure-function relationships between morphology and their biological behaviors had been extensively explored (Burda et al., 2005; Ni et al., 2008). Compared to the successful studies of non-spherical inorganic nanoparticles, there are few researches on the construct of non-spherical organic nanoparticles on account of the flexibility and variability of organic molecules. Moreover, it is difficult to generate organic nanostructures with the same size but different shapes. While some researches partially studied the cellular behaviors of organic nanoparticles with different shapes, more comprehensive understanding of this issue will be pivotal to design efficient, optimal nanosystems for bioimaging applications.

Among various bioimaging techniques, fluorescence imaging attracted much attention due to its numerous advantages including high sensitivity, minimal invasiveness, good temporal resolution, high contrast, and ease of use (Zhang et al., 2015; Guo et al., 2016). In particular, organic nanomaterials are advantageous for real-time cell visualizations, diagnosis, and treatment of diseases (Chen et al., 2016). While nanoparticles bioimaging indicates a interdependent role of shape, size, and surface chemistry, how to adjust the relevant parameters to obtain better imaging results is very important.

In this paper, rod-like organic nanoparticles were synthesized by self-assembling of small molecules borondipyrromethene (BDP), and their spherical counterpart was prepared by traditional polymeric micelles. Then their ability of imaging was compared in detail (**Scheme 1**). BDP have attracted much attention in bioimaging because of excellent optoelectronic properties and easy of functionalization (Liu et al., 2019; Zhang T. et al., 2019). To overcome the poor water-solubility, some nanomaterials containing BDP have been prepared by physical capsulation and chemical covalent connection (Kamkaew and Burgess, 2015; Zhang W. et al., 2019). Herein, BDP was encapsulated by Pluronic F127 to acquire spherical micelles, while the corresponding rod-like nanoparticles were prepared according to our previous study. The rod-like BDP nanoparticles showed good stability and biocompatibility. Importantly, the rod-like nanoparticles showed better imaging performance than their spherical counterpart. Our studies may provide useful and fundamental information for designing efficient bioimaging systems.

MATERIALS AND METHODS

Materials

BDP was synthesized based on the protocol reported in earlier studies. Pluronic F127 was purchased from Shanghai Yuanye Biological Technology Co., Ltd. The detailed description of the synthesis of BPF NPs and BSA NRs is shown in the **Supporting Information**.

Characterization Techniques

Dynamic light scattering, transmission electron microscopy (TEM), UV-vis absorption spectra, fluorescence emission spectra, cell confocal laser microscope (CLSM), and flow cytometry were used to determine the characterization of BPF NPs and BSA NRs. Test parameters and experimental procedures are shown in the **Supporting Information**.

Measurement of Fluorescence Quantum Yield

We firstly detected the concentration of BDP in BPF NPs and BSA NRs by absorbance curve, respectively. Then we adjusted them with the same concentration of BDP and also prepared BDP acetone solution with the same concentration. Fluorescence quantum efficiency was obtained on a Hamamatsu Absolute PL Quantum Yield Measurement System C9920-02.

Cell Culture

HeLa cells and HepG2 cells were purchased from the Institute of Biochemistry and Cell Biology, Chinese Academy of Sciences, Shanghai, China. The cells were propagated to confluence in Dulbecco's modified Eagle's medium (DMEM, GIBCO) supplemented with 100 U/mL penicillin, 100 μg/mL streptomycin (Sigma) and heat-inactivated fetal bovine serum (FBS, GIBCO), and maintained at 37°C in a humidified atmosphere of 5% CO_2 for further cell experiments.

Biocompatibility of Pluronic F127, BDP, BPF NPs and BSA NRs *in vitro* by MTT Assay

Cells harvested in a logarithmic growth phase were seeded in 96-well plates at a density of 8×10^3 cells per well and incubated in DMEM for 24 h. The medium was then replaced by 200 μL of cell culture medium within various concentrations of Pluronic F127. After incubation for 24 h, the MTT assays were used to measure the live cells. Untreated cells served as a control group. The cell survival rates (%) = A sample/A control ×100%. We also detected the cytotoxicity of Pluronic F127 for different culture time. The procedures were the same for that of BDP, BPF NPs, and BSA NRs.

Cellular Uptake and Tracking *in vitro*

The Cellular uptake of BPF NPs and BSA NRs was detected using CLSM and flow cytometry. Test parameters and detailed experimental procedures are shown in the **Supporting Information**.

Studies on Endocytosis Pathway

After cells in six-well plates reaching the required density, sucrose (clathrin-mediated endocytosis, 450 mM), genistein (caveolin-dependent endocytosis, 100 μM), Amiloride (micropinocytosis, 13.3 μg mL^{-1}) were used in FBS-free DMEM for 1 h and 4°C culturing was used to inhibit energy-dependent mechanisms. Then, change the culture solution within BPF NPs or BSA NRs for 4 h incubation at normal cell culture conditions. Untreated cells served as a control group. After collecting and re-suspending the cells in 0.5 mL PBS 7.4, flow cytometry analysis was performance. Test parameters and detailed experimental procedures are shown in the **Supporting Information**.

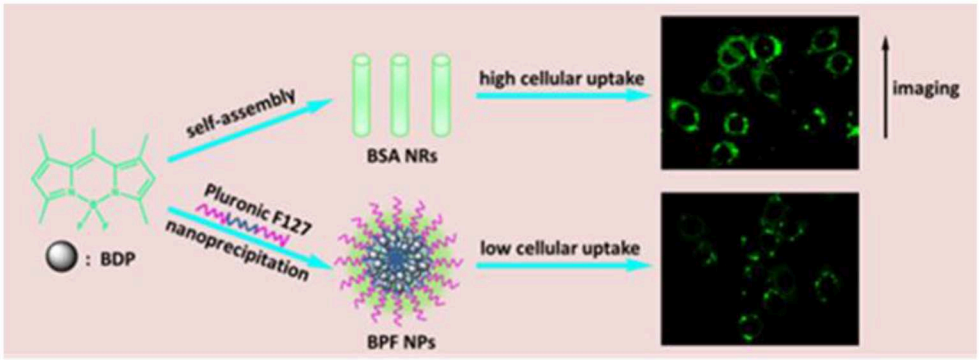

SCHEME 1 | Illustration showing the preparation of spherical and rod-like nanoparticles from BDP, and comparison of cellular imaging in cancer cells.

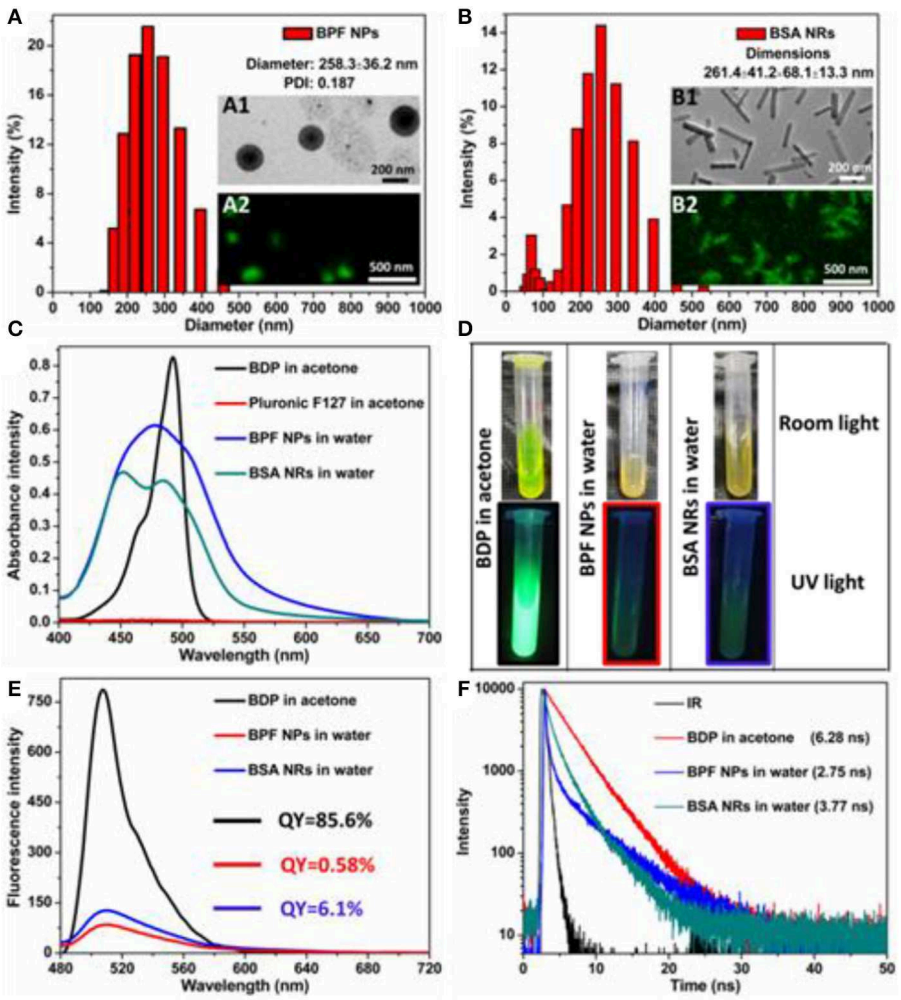

FIGURE 1 | Size distribution of **(A)** BPF NPs and **(B)** BSA NRs measured by DLS in aqueous solution. Insets: TEM image and CLSM image of BPF NPs or BSA NRs. Scale bars in all TEM images are 200 nm. Scale bars in all CLSM images are 500 nm. **(C)** UV-vis absorption spectra of BDP or Pluronic F127 in acetone and BPF NPs or BSA NRs in aqueous solution, respectively. **(D)** Photos of BDP, BPF NPs, and BSA NRs in room light field and under 365 nm light irradiation, respectively. **(E)** Fluorescence spectra of BDP, BPF NPs, and BSA NRs, respectively. **(F)** Time-resolved decay profiles of BDP, BPF NPs, and BSA NRs, respectively.

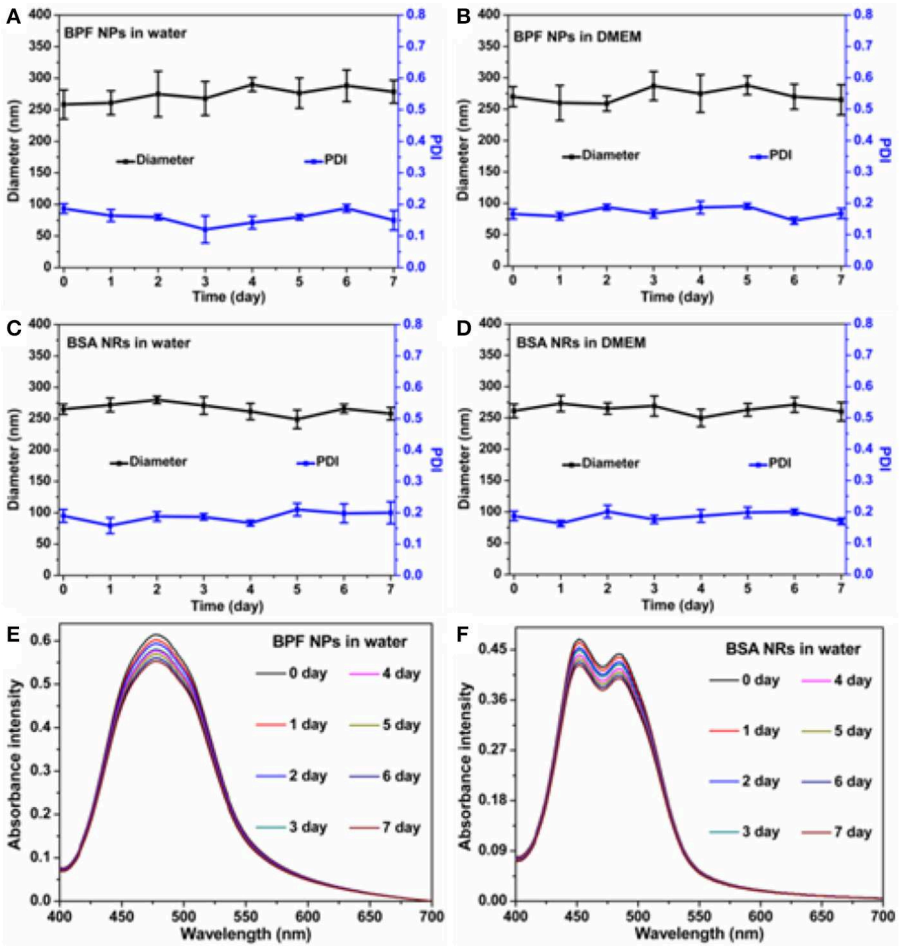

FIGURE 2 | Average size changes of BPF NPs **(A,B)**, BSA NRs **(C,D)** during 7 days in different solutions. The data are shown as the mean values ± standard deviation (SD) ($n = 3$). The absorbance intensity of **(E)** BPF NPs and **(F)** BSA NRs during 7 days.

RESULTS AND DISCUSSION

Preparation and Characterizations of BDP Nanoparticles

According to our previous work, BDP could self-assemble into rod-like nanoparticles (BDP self-assembly, BSA NRs). Then we used Pluronic F127 to make spherical BDP nanoparticles (BDP@Pluronic F127, BPF NPs) for comparison. The size distribution and morphology of BSA NRs/BPF NPs were well-characterized by dynamic light scattering (DLS), transmission electron microscopy (TEM), and confocal fluorescence microscopy (CLSM). As shown in **Figures 1A,B**, the average diameters were 258.3 nm for BPF NPs and 261.4 nm for BSA NRs. TEM images revealed spherical morphology of BPF NPs (inset A1), while the BSA NRs (inset B1) was rod-like with smooth surface. These structures were further confirmed by CLSM. The BPF NPs and BSA NRs exhibited spherical and rod-like morphology with green fluorescence, respectively (inset A2 and B2). These results indicate that fluorescence BDP nanoparticles have been successfully prepared. The UV-Vis absorption of free BDP, Pluronic F127, BPF NPs, and BSA NRs were shown in **Figure 1C**. To compare their spectra, the concentration of BDP in all samples was same, which was adjusted according to UV-Vis standard curves (**Figure S1**). After the formation of nanoparticles, the UV-Vis spectra of both BPF NPs and BSA NRs showed a broad spectrum with blue-shifted absorption relative to that of BDP. Photographs of BDP in acetone, BPF NPs and BSA NRs in water (from left to right) under room light and UV light (365 nm) were shown in **Figure 1D**. Interestingly, compared to BDP solution, the color of BPF NPs and BSA NRs produced remarkable changes, which was consistent with spectral changes in **Figure 1C**. The green fluorescence of BDP was quenched after formation of BPF NPs and BSA NRs due to the typical aggregation induced quenching effect (**Figures 1D,E**). The quantum yield of BSA NRs was 6.1% and higher than that of BPF NPs (0.58%), which was in favor of imaging. The fluorescence lifetime (**Figure 1F**) of BPF NPs and BSA NRs was 2.75 and 3.77 ns, respectively, which were both shorter than that of free BDP (6.28 ns). It is well-known lifetime of fluorophores would greatly reduce when fluorescence

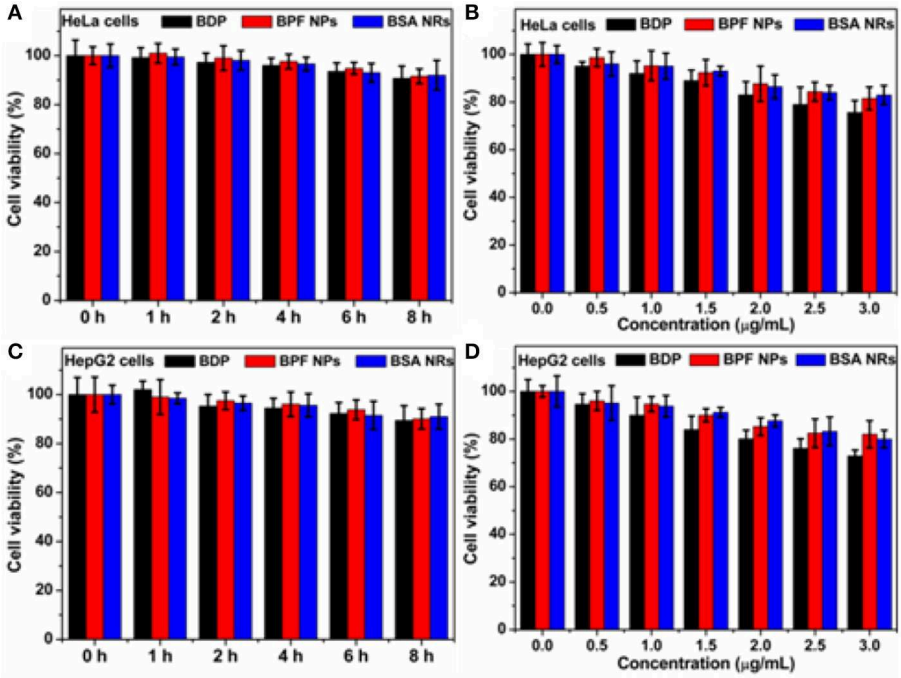

FIGURE 3 | (A) Cell survival rate of HeLa cells after incubation with BDP, BPF NPs, and BSA NRs for different hours, respectively. **(B)** Cell survival rate of HeLa cells after incubation with various concentrations of BDP, BPF NPs, and BSA NRs for 24 h, respectively. **(C)** Cell survival rate of HepG2 cells after incubation with BDP, BPF NPs, and BSA NRs for different hours, respectively. **(D)** Cell survival rate of HepG2 cells after incubation with various concentrations of BDP, BPF NPs, and BSA NRs for 24 h, respectively. Data represent mean values ± standard deviation, $n = 3$.

quenching occurs. All above results further confirm that BPF NPs and BSA NRs have been successfully prepared.

Stability of BPF NPs and BSA NRs

To investigate the stability of BDP nanoparticles, we monitored the size distribution and absorbance spectra of nanoparticles at various time points, and visual comparisons were made between the freshly prepared nanoparticles and the nanoparticles stored for 7 days. As shown in **Figure S2**, all solutions remained clear without aggregation and precipitation in 1 week. The mean sizes and size distributions of the BPF NPs (**Figures 2A,B**) and BSA NRs (**Figures 2C,D**) dispersed in aqueous solution and cell culture medium (DMEM) with 10% fetal calf serum and 1% penicillin/streptomycin changed negligibly for the whole period of time tested. Moreover, the absorbance spectra of BPF NPs and BSA NRs in water were collected during 7 days. As displayed in **Figures 2E,F**, the absorbance of both BPF NPs and BSA NRs declined slightly and kept more than 90% of the initial value within 7 days. These results suggest that the BPF NPs and BSA NRs possess excellent physical and optical stability, which is conducive to their application in biomedicine.

Biocompatibility of BDP Nanoparticles

The biocompatibility of nanoparticles is important for their biomedical applications. We firstly studied the biocompatibility of Pluronic F127 in living cells by the standard thiazolyblue tetrazolium bromide (MTT) proliferation test. As shown in **Figure S3**, little cytotoxicity of Pluronic F127 had been observed against Human cervical carcinoma (HeLa) cells and Liver hepatocellular carcinoma (HepG2), and more than 90% of those cells were alive at different incubation time or concentrations. In addition, both BPF NPs and BSA NRs showed very low cytotoxicity (90% viability) toward HeLa (**Figures 3A,B**) and HepG2 cells (**Figures 3C,D**). Therefore, the two nanoparticles are suitable for further biological research.

Comparing Cellular Imaging Between BPF NPs and BSA NRs

CLSM was used to study the cellular uptake of BPF NPs/BSA NRs on HeLa and HepG2 cells. After incubation with BPF NPs or BSA NRs for 2 h at 37°C, the nucleus was stained by 4, 6-diamidino-2-phenylindole (DAPI). As shown in **Figure S4**, the bright green fluorescence appeared in the cytoplasm, suggesting that both BPF NPs and BSA NRs could be effective endocytosis by cancer cells. The intracellular fluorescence increased with the increase of BDP concentration, indicating concentration-dependent cellular uptake.

To further compare the cellular imaging capacity between BPF NPs and BSA NRs, the HeLa and HepG2 cells were incubated with the BPF NPs and BSA NRs (BDP: 3 μg/mL), respectively. As shown in **Figure 4A**, the green fluorescence intensity increased with the incubation time from 0.5 to 2 h, suggesting time-dependent endocytosis. BSA NRs exhibited stronger green fluorescence than that of BPF NPs under the same experiment conditions. Moreover, flow cytometry was carried out to further compare the cellular imaging capacity

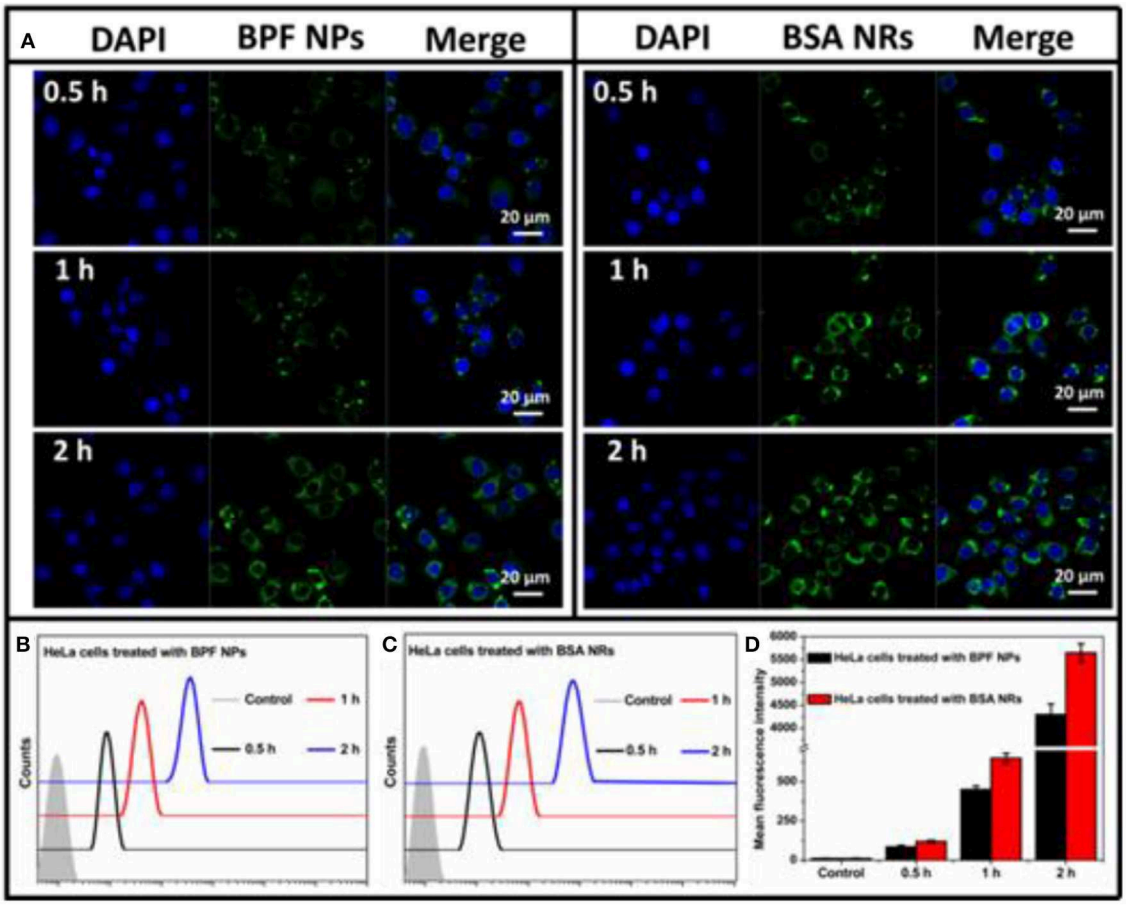

FIGURE 4 | (A) CLSM images of HeLa cells incubated with BPF NPs or BSA NRs for 0.5, 1, and 2 h at 37°C, respectively. Cells are viewed in the blue channel for DAPI, the green channel for BDP. Scale bars represent 20 μm in all images. **(B)** Flow cytometry histograms of HeLa cells treated with BPF NPs and without treatment (control) for different hours, respectively. **(C)** Flow cytometry histograms of HeLa cells treated with BSA NRs and without treatment (control) for different hours, respectively. **(D)** Quantitative analysis of **(B,C)**. The data are presented as the mean values ± standard deviation, $n = 3$.

of the two BDP nanoparticles. As reported in **Figures 4B,C**, the endocytosis of the two nanoparticles was time-dependent, and the BSA NRs showed higher imaging efficiencies than BPF NPs (**Figure 4D**). These results are consistent with the CLSM results. Similar results were obtained in HepG2 cells (**Figure S5**). One possible trigger for higher imaging performance of BSA NRs is that rod-shaped nanoparticles have more contact sites with the cell membranes, leading to stronger adhesions and endocytosis with respect to spheres, which theoretically have only one contact point with a single cancer cell.

Pathways of Endocytosis

To determine endocytosis pathway of BDP nanoparticles, different inhibitors were selected, sucrose for clathrin-mediated endocytosis, genistein for caveolae-mediated endocytosis, and amiloride for macropinocytosis, respectively. Moreover, the endocytosis was studied by low temperature (4°C) treatment to see if it is energy dependent. To reduce the side effects of inhibitors on cancer cells, we optimized the experiment conditions according to previous reports. The CLSM images of HeLa and HepG2 cells pretreated with inhibitors are shown in **Figures 5A,B** and the relative uptake rates are displayed in **Figures 5C,D**. The flow cytometry results are shown in **Figure S6**. The low temperature treatment groups all showed a sharp reduction in endocytosis of the nanoparticles, confirming endocytosis is energy dependent. The internalization of BPF NPs by HeLa cells is mainly through the clathrin-mediated endocytosis and micropinocytosis. The cellular internalization of BSA NRs through mutiple endocytosis pathways may lead to more rod-like nanoparticles internalized. Nevertheless, BSA NRs was uptaken by HepG2 cells mainly through pathway of micropinocytosis. Thus, we deduced that the endocytosis pathway varied significantly on the basis of both the physical properties of nanoparticle and the cell type, and internalization of nanoparticles with different morphologies seems to be mediated by different pathways.

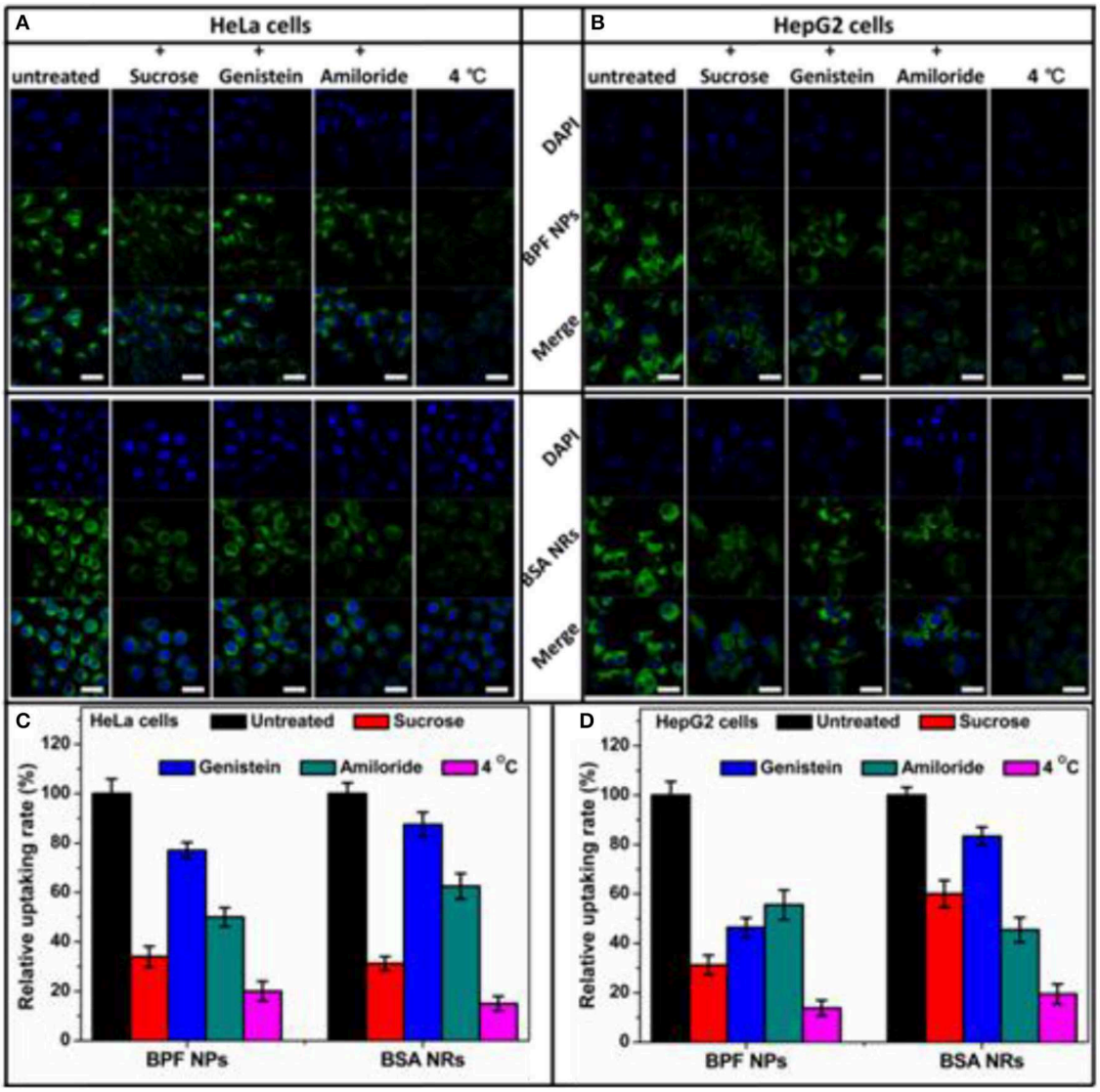

FIGURE 5 | Flow cytometry histograms of **(A)** HeLa cells and **(B)** HepG2 cells treated with BPF NPs, BSA NRs and control pretreated with various endocytic inhibitors, respectively. **(C)** Quantitative analysis of **(A)**. **(D)** Quantitative analysis of **(B)**. The data are presented as the mean values ± standard deviation, $n = 3$.

CONCLUSION

Herein, rod-like organic nanosystems have been rationally designed and prepared. BDP nanoparticles showed robust stability in aqueous media. *In vitro* studies have confirmed that these tailored nanosystems are biocompatible and could be uptake by living cells. Intriguingly, we found that the imaging capacity of the rod-like nanoparticles were better than their spherical nanoparticles. These results suggested a special role associated with the physical property of the particles. Our work demonstrates high-performance organic nanomaterial with ideal biological geometries for tumor imaging *in vitro*. This work highlights the potential of rational design to develop functional nanoparticles for tumor imaging.

DATA AVAILABILITY STATEMENT

All datasets generated for this study are included in the article/**Supplementary Material**.

AUTHOR CONTRIBUTIONS

CM designed the experiments, participated in all the experiments, analyzed the data, and wrote the draft of the manuscript. JZ and TZ provided assistance to the entire experimental section and contributed in the discussion. HS and JW were mainly responsible for cellular uptake and imaging experiments. ZX and JS conceived the idea and supervised the research project.

FUNDING

Financial support was provided by the National Natural Science Foundation of China (Project No. 81601756) and China Postdoctoral Science Foundation (2017M611328).

SUPPLEMENTARY MATERIAL

The Supplementary Material for this article can be found online at: https://www.frontiersin.org/articles/10.3389/fchem.2019.00765/full#supplementary-material

REFERENCES

Alemdaroglu, F. E., Alemdaroglu, N. C., Langguth, P., and Herrmann, A. (2008). A very useful redox initiator for aqueous RAFT polymerization of N-isopropylacrylamide and acrylamide at room temperature. *Macromol. Rapid Commun.* 29, 326–329. doi: 10.1002/marc.200700823

Aula, S., Lakkireddy, S., Jamil, K., Kapley, A., Swamy, A. V. N., and Lakkireddy, H. R. (2015). Biophysical, biopharmaceutical and toxicological significance of biomedical nanoparticles. *RSC Adv.* 5, 47830–47859. doi: 10.1039/C5RA05889A

Biju, V. (2014). Chemical modifications and bioconjugate reactions of nanomaterials for sensing, imaging, drug delivery and therapy. *Chem. Soc. Rev.* 43, 744–764. doi: 10.1039/C3CS60273G

Black, K. C. L., Wang, Y., Luehmann, H. P., Cai, X., Xing, W., Pang, B., et al. (2014). Radioactive ^{198}Au-doped nanostructures with different shapes for *in vivo* analyses of their biodistribution, tumor uptake, and intratumoral distribution. *ACS Nano* 8, 4385–4394. doi: 10.1021/nn406258m

Blanco, E., Shen, H., and Ferrari, M. (2015). Principles of nanoparticle design for overcoming biological barriers to drug delivery. *Nat. Biotechnol.* 33, 941–951. doi: 10.1038/nbt.3330

Burda, C., Chen, X., Narayanan, R., and El-Sayed, M. A. (2005). Chemistry and properties of nanocrystals of different shapes. *Chem. Rev.* 105, 1025–1102. doi: 10.1021/cr030063a

Chauhan, V. P., Popovic, Z., Chen, O., Cui, J., Fukumura, D., Bawendi, M. G., et al. (2011). Fluorescent nanorods and nanospheres for real-time *in vivo* probing of nanoparticle shape-dependent tumor penetration. *Angew. Chem. Int. Ed. Engl.* 50, 11417–11420. doi: 10.1002/anie.201104449

Chen, L., Chen, B., Liu, X., Xu, Y., Zhang, L., Cheng, Z., et al. (2016). Real-time monitoring of a controlled drug delivery system *in vivo*: construction of a near infrared fluorescence monomer conjugated with pH-responsive polymeric micelles. *J. Mater. Chem. B.* 4, 3377–3386. doi: 10.1039/C6TB00315J

Geisbert, T. W., and Jahrling, P. B. (2004). Exotic emerging viral diseases: progress and challenges. *Nat. Med.* 10, S110–S121. doi: 10.1038/nm1142

Guo, C., Hu, J., Kao, L., Pan, D., Luo, K., Li, N., et al. (2016). Pepetide dendron-functionalized mesoporous silica nanoparticle-based nanohybrid: biocompatibility and its potential as imaging probe. *ACS Biomater. Sci. Eng.* 2, 860–870. doi: 10.1021/acsbiomaterials.6b00093

Herd, H., Daum, N., Jones, A. T., Huwer, H., Ghandehari, H., and Lehr, C. M. (2013). Nanoparticle geometry and surface orientation influence mode of cellular uptake. *ACS Nano* 7, 1961–1973. doi: 10.1021/nn304439f

Kamkaew, A., and Burgess, K. (2015). Aza-BODIPY dyes with enhanced hydrophilicity. *Chem. Commun.* 51, 10664–10667. doi: 10.1039/C5CC03649F

Kinnear, C., Moore, T. L., Rodriguez-Lorenzo, L., Rothen-Rutishauser, B., and Petri-Fink, A. (2017). form follows function: nanoparticle shape and its implications for nanomedicine. *Chem. Rev.* 117, 11476–11521. doi: 10.1021/acs.chemrev.7b00194

Kunjachan, S., Ehling, J., Storm, G., Kiessling, F., and Lammers, T. (2015). Noninvasive imaging of nanomedicines and nanotheranostics: principles, progress, and prospects. *Chem. Rev.* 115, 10907–10937. doi: 10.1021/cr500314d

Lee, D. E., Koo, H., Sun, I. C., Ryu, J. H., Kim, K., and Kwon, I. C. (2012). Multifunctional nanoparticles for multimodal imaging and theragnosis. *Chem. Soc. Rev.* 41, 2656–2672. doi: 10.1039/C2CS15261D

Liu, Z., Jiang, Z., Yan, M., and Wang, X. (2019). Recent progress of BODIPY dyes with aggregation-induced emission. *Front. Chem.* 7:712. doi: 10.3389/fchem.2019.00712

Ni, W., Kou, X., Yang, Z., and Wang, J. (2008). Tailoring longitudinal surface plasmon wavelengths, scattering and absorption cross sec-tions of gold nanorods. *ACS Nano* 2, 677–686. doi: 10.1021/nn7003603

Yan, L., Zhang, Y., Xu, B., and Tian, W. (2016). Fluorescent nanoparticles based on AIE fluorogens for bioimaging. *Nanoscale* 8, 2471–2487. doi: 10.1039/C5NR05051K

Zhang, J., Chen, R., Zhu, Z., Adachi, C., Zhang, X., and Lee, C. S. (2015). Highly stable near-infrared fluorescent organic nanoparticles with a large stokes shift for noninvasive long-term cellular imaging. *ACS Appl. Mater. Interfaces* 7, 26266–26274. doi: 10.1021/acsami.5b08539

Zhang, J., Liu, S., Hu, X., Xie, Z., and Jing, X. (2016). Cyanine-curcumin assembling nanoparticles for near-infrared imaging and photothermal therapy. *ACS Biomater. Sci. Eng.* 2, 1942–1950. doi: 10.1021/acsbiomaterials.6b00315

Zhang, T., Ma, C., Sun, T., and Xie, Z. (2019). Unadulterated BODIPY nanoparticles for biomedical application. *Coord. Chem. Rev.* 390, 76–85.doi: 10.1016/j.ccr.2019.04.001

Zhang, W., Lin, W., Wang, X., Li, C., Liu, S., and Xie, Z. (2019). Hybrid nanomaterials of conjugated polymers and albumin for precise photoerhmal therapy. *ACS Appl. Mater. Interfaces* 11, 278–287. doi: 10.1021/acsami.8b17922

Conflict of Interest: The authors declare that the research was conducted in the absence of any commercial or financial relationships that could be construed as a potential conflict of interest.

frontiers in Chemistry

ORIGINAL RESEARCH
published: 25 November 2019
doi: 10.3389/fchem.2019.00778

A Förster Resonance Energy Transfer Switchable Fluorescent Probe With H_2S-Activated Second Near-Infrared Emission for Bioimaging

Rongchen Wang[1†], Wei Gao[1†], Jie Gao[2†], Ge Xu[1], Tianli Zhu[1], Xianfeng Gu[2] and Chunchang Zhao[1*]*

[1] *Key Laboratory for Advanced Materials and Feringa Nobel Prize Scientist Joint Research Center, School of Chemistry and Molecular Engineering, Institute of Fine Chemicals, East China University of Science and Technology, Shanghai, China,*
[2] *Department of Medicinal Chemistry, School of Pharmacy, Fudan University, Shanghai, China*

Real-time and accurate detection of endogenous hydrogen sulfide is of great biomedical significance. Here, a FRET-based fluorescent probe for ratiometric detection of H_2S was designed to comprise an AIE luminophore TPE as an energy donor and a monochlorinated BODIPY dye as an energy acceptor and H_2S-responsive site. Such a designed probe showed H_2S-dependent ratiometric and light-up NIR-II emission, enabling accurate imaging of H_2S-rich cancer cells and identification of H_2S-rich tumors with high resolution.

Keywords: ratiometric, light up, FRET, AIE, NIR-II imaging

OPEN ACCESS

Edited by:
Zhen Shen,
Nanjing University, China

Reviewed by:
Chusen Huang,
Shanghai Normal University, China
Shaomin Ji,
Guangdong University of Technology, China

***Correspondence:**
Xianfeng Gu
xfgu@fudan.edu.cn
Chunchang Zhao
zhaocchang@ecust.edu.cn

[†]These authors have contributed equally to this work

Specialty section:
This article was submitted to Supramolecular Chemistry, a section of the journal Frontiers in Chemistry

Received: *30 July 2019*
Accepted: *28 October 2019*
Published: *25 November 2019*

Citation:
Wang R, Gao W, Gao J, Xu G, Zhu T, Gu X and Zhao C (2019) A Förster Resonance Energy Transfer Switchable Fluorescent Probe With H_2S-Activated Second Near-Infrared Emission for Bioimaging. Front. Chem. 7:778. doi: 10.3389/fchem.2019.00778

INTRODUCTION

Endogenous hydrogen sulfide is an important signaling molecule, mainly derived from the enzymatic hydrolysis of L-cysteine (Chiku et al., 2009; Singh et al., 2009). Studies have found that H_2S is associated with many pathological processes, while an abnormal level of H_2S may associated with some diseases, such as Alzheimer's disease, hypertension, and cardiac ischemia disease (Eto et al., 2002; Zhao et al., 2015; Shi et al., 2017). Therefore, real-time and accurate detection of hydrogen sulfide is of great biomedical significance. Until now, many fluorescence-based H_2S probes have been reported (Jin et al., 2016; Wang et al., 2018, 2019b); however, the fluorescence of many probes generally locates in the visible or the near-infrared I region (650–900 nm), inevitably leading to some drawbacks of poor tissue penetration, severe background interference from living tissue (Zhou et al., 2014). Compared with the traditional NIR-I imaging (650–900 nm) (Li et al., 2018), fluorescent imaging in the second near-infrared window (NIR-II, 1,000–1,700 nm) has attracted more and more attention due to lower tissue absorption, stronger tissue penetration, and reduced autofluorescence (Hong et al., 2012; Dang et al., 2016; Shi et al., 2018; Xu et al., 2018). Another issue is the hydrophobic nature of most traditional fluorescent dyes, which generally triggers the aggregation in physiological conditions due to π-π stacking. Such a process can give rise to aggregation-caused quenching (ACQ) (Sun et al., 2014; Yuan et al., 2015) and thus compromise the accuracy of bioimaging. In comparison, fluorogens with AIE characteristics show enhanced fluorescence in the aggregate states, thus providing an alternative strategy for the design of fluorescent light up probes (Zhao et al., 2012; Mei et al., 2014, 2015; Zhang et al., 2015; Fu et al., 2019). Since the hydrophobic fluorescent probes undergo the intrinsic aggregation process in aqueous media, it is desirable to develop H_2S-activatable probes with AIE characteristic for *in vivo* imaging.

Herein, we reported a H_2S-responsive probe that showed ratiometric fluorescence and NIR-II emission light-up upon activation for *in vitro* and *in vivo* imaging (**Scheme 1**). Such a probe was designed by appending an AIE luminophore TPE, as an energy donor, to a monochlorinated BODIPY dye as an energy acceptor and H_2S-responsive site. As compared to conventional intensity-based fluorescent probes (Huang et al., 2014; Tang et al., 2016), this Förster resonance energy transfer (FRET)-based ratiometric probe can enable accurate detection through elimination of the limitations of experimental conditions including probe concentration, light source, and background interference effects (Wang et al., 2019a). Such a design strategy is applicable to the design of various ratiometric probes for different targets. As expected, in the absence of H_2S, due to the good spectral overlap between the emission spectra of the TPE and the absorption spectra of the BODIPY, efficient FRET occurs. In contrast, in the presence of H_2S, the absorption spectra of BODIPY undergo an obvious red shift, resulting in a significant reduction of the overlap with the TPE emission. Correspondingly, the FRET process is significantly attenuated. More importantly, upon activation by H_2S, the probe produces a new fluorescence light-up at 920 nm with the fluorescence tail

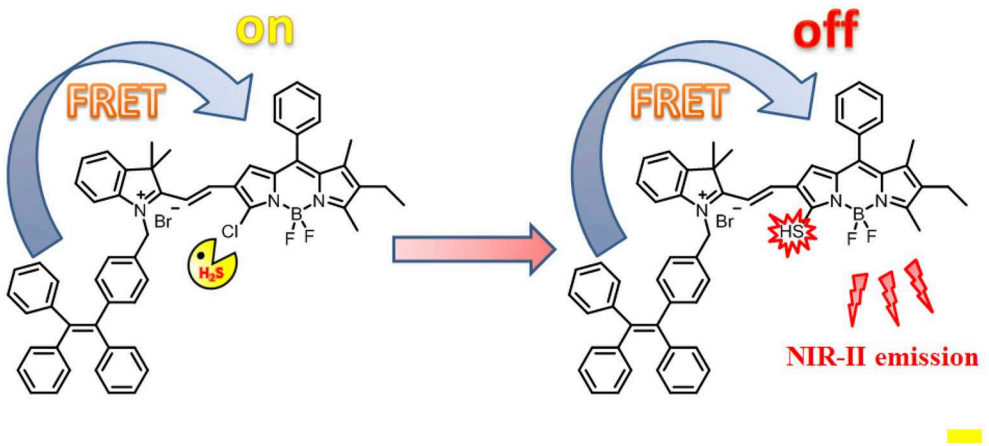

SCHEME 1 | Schematic illustration of the design of probe TPE-BODIPY-Cl and the mechanism for H_2S-mediated ratiometric and NIR fluorescence light up.

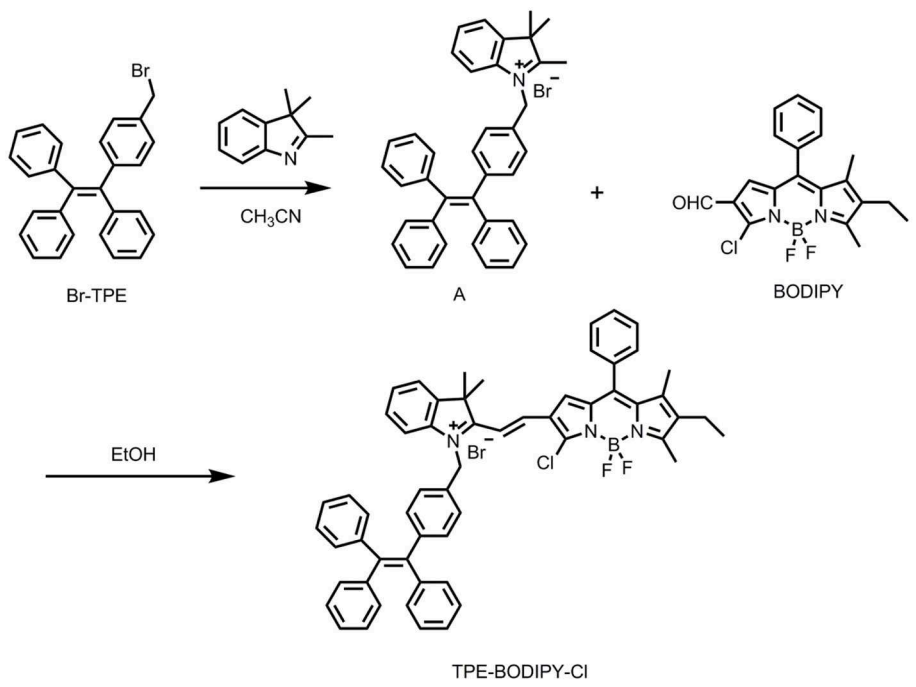

SCHEME 2 | Synthesis of the target compound TPE-BODIPY-Cl.

extending to 1,300 nm, indicative of the suitability for fluorescent imaging in the second near-infrared (NIR-II).

EXPERIMENTAL

Synthesis

The TPE-BODIPY-Cl was obtained from the synthetic route of **Scheme 2**. Br-TPE and BODIPY were synthesized according to the literature procedure (Zhao et al., 2013, 2014). Animal experiments were performed in compliance with Chinese legislation on the Use and Care of Research Animals and guidelines by Fudan University Animal Studies Committee for the Care and Use of Laboratory Animals. All experimental procedures were approved by this committee.

Synthesis of Compound A

Br-TPE (165 mg, 0.39 mmol) and 2,3,3-trimethyl-3H-indole (62 mg, 0.39 mmol) were dissolved in 25 mL CH_3CN and refluxed for 10 h. Then, the solvent was removed under reduced pressure, and the crude product was dissolved in CH_2Cl_2. The mixture was dropped into the ether solvent to precipitate white solid, which was used for next reaction without further purification. HRMS (ESI, m/z): calculated for $C_{38}H_{34}N$ $[M\text{-}Br]^+$: 504.2691, found: 504.2699.

Synthesis of Compound TPE-BODIPY-Cl

Compound A (100 mg, 0.17 mmol) and BODIPY (80 mg, 0.21 mmol) were dissolved in dry ethanol and refluxed for 4 h. Then, EtOH was evaporated and the crude product was purified by a silica gel column with CH_2Cl_2/MeOH (20/1, v/v) as eluent to give TPE-BODIPY-Cl (90 mg, 56%). ^{1}H NMR (400 MHz, $CDCl_3$) δ 8.00 (d, 1H, J = 12.00 Hz), 7.63–7.55 (m, 2H), 7.52–7.46 (m, 4H), 7.43–7.36 (m, 2H), 7.09–7.06 (m, 7H), 7.03–7.00 (m, 3H), 6.98–6.96 (m, 4H), 6.95–6.92 (m, 4H), 6.87–6.85 (m, 4H), 6.08 (s, 2H), 2.71 (s, 3H), 2.44-2.39 (q, 2H, J = 6.67 Hz), 1.78 (s, 6H), 1.52 (s, 3H), 1.09–1.05 (t, 3H, J = 8.00 Hz). ^{13}C NMR (101 MHz, $CDCl_3$) δ 144.43, 144.21, 143.73, 143.25, 143.06, 142.64, 141.75, 141.48, 139.85, 132.12, 131.79, 131.20, 130.44, 129.50, 129.38, 129.06, 128.96, 127.76, 127.68, 127.61, 126.62, 126.52, 126.39, 122.35, 115.31, 51.90, 31.94, 29.71, 29.67, 29.37, 27.60, 22.71, 17.29, 14.14, 13.94, 13.90, 12.81. HRMS (ESI, m/z): calculated for $C_{58}H_{50}BF_2N_3Cl$ $[M\text{-}Br]^+$: 872.3754, found: 872.3750.

RESULTS AND DISCUSSION

TPE-BODIPY-Cl was prepared via a Knoevenagel condensation reaction. The synthesis and characterization are outlined in **Scheme 2** and **Supporting Information**.

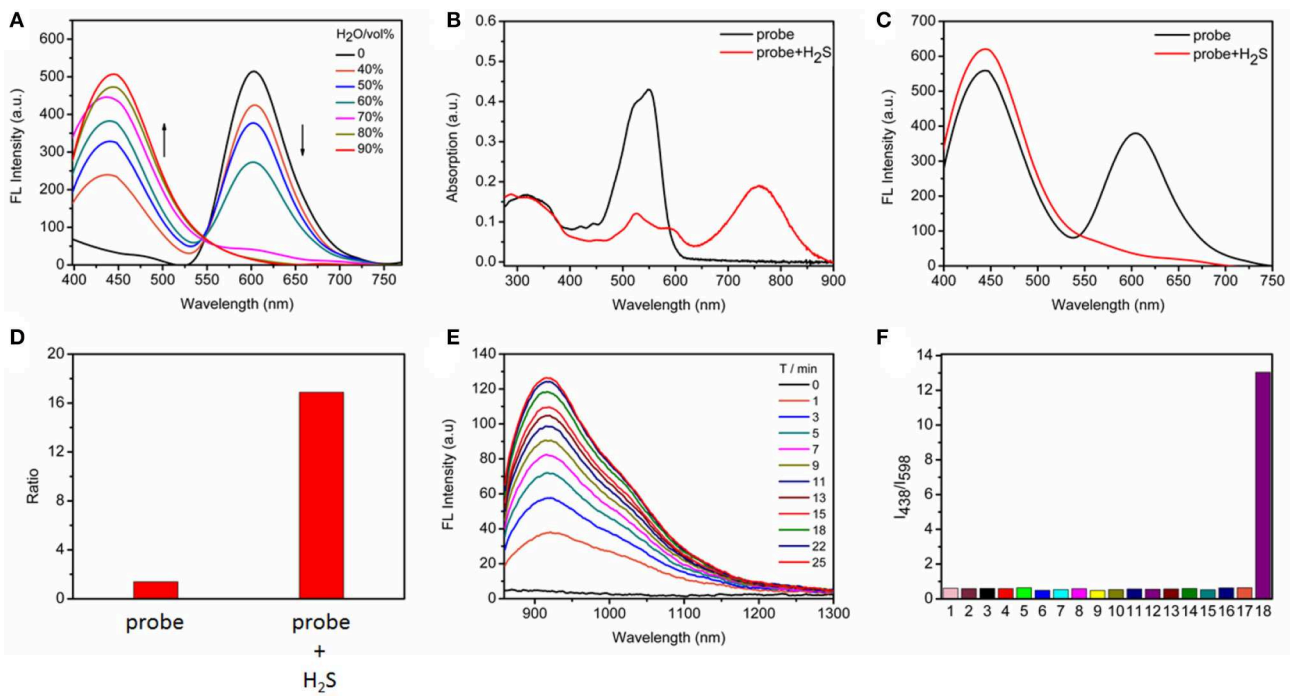

FIGURE 1 | (A) Fluorescence changes of TPE-BODIPY-Cl (10 μM) in Tris/CH_3CN mixtures with different water fractions. **(B)** Absorption and **(C)** fluorescence spectra in the absence and presence of 100 μM NaHS in Tris/CH_3CN buffer solution (0.5 M Tris-HCl, 40% CH_3CN, pH = 7.4), λ_{ex} = 360 nm. **(D)** The fluorescence intensity ratio (I_{438}/I_{598}) in the absence and presence of 100 μM NaHS. **(E)** Time-dependent NIR-II emission spectra upon addition of 100 μM NaHS, λ_{ex} = 760 nm. **(F)** Ratiometric fluorescence changes of TPE-BODIPY-Cl in the presence of 100 μM NaHS and other biologically relevant reactive sulfur and anions (1 mM) in Tris/CH_3CN buffer solution (0.5 M Tris-HCl, 40% CH_3CN, pH = 7.4): (1) Free; (2) F^-; (3) Cl^-; (4) Br^-; (5) I^-; (6) NO_2^-; (7) N_3^-; (8) HCO_3^-; (9) SO_4^{2-}; (10) HPO_4^{2-}; (11) ClO^-; (12) H_2O_2; (13) ^-OAc; (14) $S_2O_3^{2-}$; (15) GSH; (16) Cys; (17) Hcy; (18) NaHS.

Spectroscopic Studies of TPE-BODIPY-Cl

With the probe in hand, we initially evaluated the photophysical properties. Because the probe contains the TPE AIEgen, we explored the AIE performance of the probe to obtain the best test conditions. As shown in **Figure 1A**, we tested the FRET process of the probe under different ratios of H_2O/CH_3CN. With the increasing water content, the degree of aggregation of the probe intensifies, accompanying the increase of TPE fluorescence while the occurrence of ACQ for BODIPY chromophore. As is well-known, a ratiometric fluorescence mode has higher accuracy than turn-on or turn-off fluorescence detection mode (Wang et al., 2015; Zhang et al., 2019), we here selected Tris/CH_3CN buffer solution (0.5 M Tris, 40% CH_3CN, pH = 7.4) as the next testing condition in order to obtain the ratiometric fluorescent responsiveness. The aggregation of our probe under this buffer solution was proven by dynamic light scattering (**Figure S1**).

Next, we evaluated the response capability of TPE-BODIPY-Cl toward H_2S (**Figure 1** and **Figure S2**). As shown in **Figure 1B**, the free probe showed strong absorption at 550 nm. The typical absorption band of the TPE around 300–360 nm was also noted. In the fluorescence spectrum, due to FRET process, we can observe two strong fluorescence peaks with maxima at 438 and 598 nm, corresponding to TPE and BODIPY, respectively. When treated with 100 μM H_2S, the absorption band at 550 nm decreased significantly and a new absorption band appeared at 760 nm with a red-shift of 220 nm due to the formation of TPE-BODIPY-SH that was proven by HRMS analysis (**Figure S3**). Such treatment with NaHS attenuated the FRET, thus affording an enhancement of the fluorescence intensity ratio (I_{438}/I_{598}) by 12 times. This indicated that TPE-BODIPY-Cl was indeed a ratiometric fluorescent probe for H_2S. Most importantly, H_2S-triggered a new NIR-II fluorescence light up with a maximum emission of 920 nm (λ_{ex} = 760 nm). These results demonstrated that TPE-BODIPY-Cl could be used as a H_2S-activatable NIR-II fluorescent probe to enable high-resolution bioimaging with deep-tissue penetration. Utilizing the linear relation of fluorescence intensity ratio at 438 and 598 nm with H_2S concentration (0–50 μM) (**Figure S4**), the detection limit was determined to be 6.5×10^{-7} M, indicating that TPE-BODIPY-Cl has high sensitivity for H_2S detection. Of note, the probe exhibits minimal optical responsiveness to biologically related reactive sulfur (RSS), oxygen (ROS), and nitrogen species (RNS) and some ions, showing its high selectivity for H_2S (**Figure 1F** and **Figure S5**). In addition, the good photostability of probe TPE-BODIPY-Cl, evidenced by minimal optical changes under continuous irradiation with light irradiation (**Figure S6**), indicated its suitability for bioimaging.

Imaging of H_2S in Living Cells

Inspired by the promising response to H_2S, we then assessed the ability of TPE-BODIPY-Cl for fluorescence imaging in living HCT116 cells that express high levels of H_2S [20–100 μM, Szabo et al., 2013]. As shown in **Figure 2**, the incubation of HCT116 cells and 10 μM TPE-BODIPY-Cl for 30 min afforded the bright and stable fluorescence signal in the green channel and relatively weak fluorescence in the red channel. The ratio of the green to red channel is ∼2.82. When a CBS inhibitor aminooxyacetic acid (AOAA) which can inhibit the H_2S production was added,

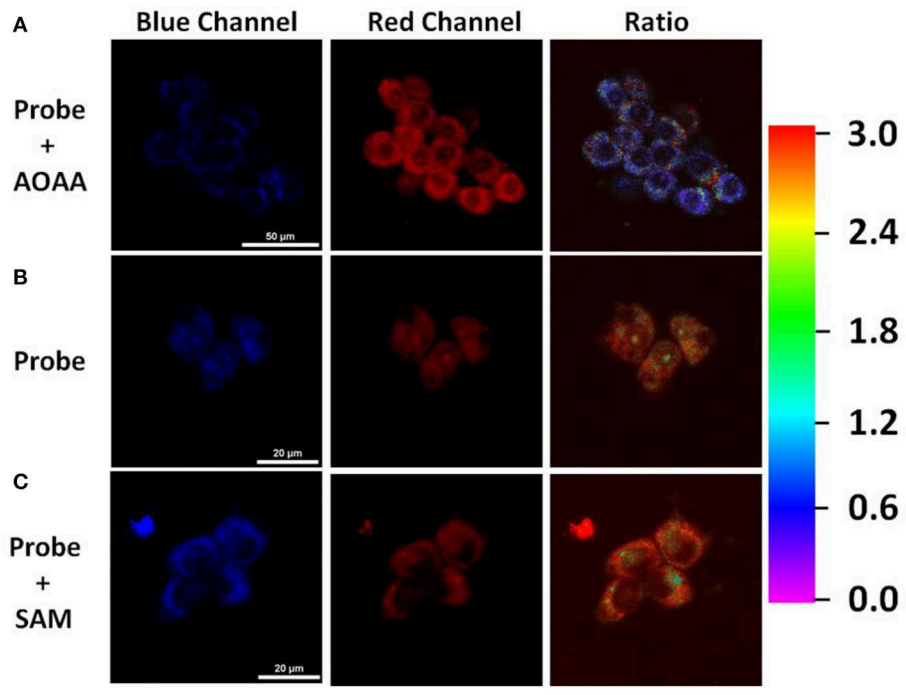

FIGURE 2 | (A) HCT116 cells pretreated with 1 mM AOAA for 1 h, followed by incubation with TPE-BODIPY-Cl (10 μM) for 30 min. **(B)** HCT116 cells incubated with TPE-BODIPY-Cl for 30 min. **(C)** HCT116 cells pretreated with SAM (3 mM) for 1 h, followed by loading with TPE-BODIPY-Cl for 30 min.

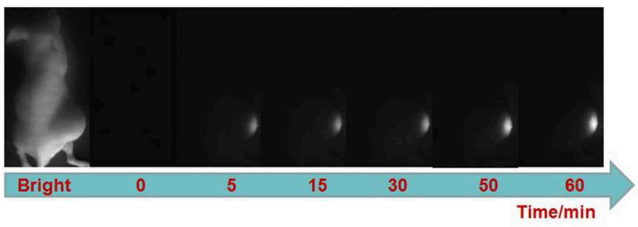

FIGURE 3 | NIR-II fluorescent images of HCT116 subcutaneous xenograft nude mice. Images were taken at various time points after subcutaneous injection of TPE-BODIPY-Cl into tumor region.

the ratio dropped to 0.70. In contrast, with the addition of an allosteric CBS activator S-adenosyl-L-methionine (SAM) to promote the production of H_2S, the ratio increased to 3.59. These results indicated that TPE-BODIPY-Cl can efficiently enter living cells and serve as a potential sensor to detect endogenous hydrogen sulfide rapidly and specifically.

Imaging of H_2S *in vivo*

Finally, we explored the ability of the probe for visualizing H_2S-rich cancers using HCT116 subcutaneous xenograft nude mice. TPE-BODIPY-Cl was administrated to nude mice through intratumoral injection. As shown in **Figure 3**, after the injection, obvious NIR-II fluorescence in the tumor region was observed and the signals gradually increased over time, producing a 14.8-fold enhancement at the time point of 60 min (**Figure S7**). These results indicated that the TPE-BODIPY-Cl could be activation of NIR-II fluorescence in H_2S-rich colorectal cancers.

CONCLUSION

In summary, we have designed a FRET based probe through appending the AIE luminophore TPE to the monochlorinated BODIPY dye for imaging of H_2S-rich cancer cells and tumors, wherein TPE serves as an energy donor and BODIPY dye as an energy acceptor. This probe showed H_2S-dependent FRET process, thus enabling the selective visualization of endogenous H_2S in HCT116 cells. Furthermore, this probe displayed H_2S specific activation of NIR II emission light up. By using this activatable NIR II emission, accurate identification of colorectal tumors was realized. We expect our design strategy here can help the development of a new activatable probe.

DATA AVAILABILITY STATEMENT

The raw data supporting the conclusions of this manuscript will be made available by the authors, without undue reservation, to any qualified researcher.

ETHICS STATEMENT

The animal study was reviewed and approved by Fudan University.

AUTHOR CONTRIBUTIONS

CZ and XG conceived the project and wrote the manuscript. RW conceived the molecule design. RW and WG prepared and characterized the small molecule. RW, TZ, and GX performed the optical characterization. RW and JG performed the living cells imaging, *in vivo* imaging, and analyzed the data.

ACKNOWLEDGMENTS

We gratefully acknowledge the financial support by the National Natural Science Foundation of China (21672062, 21874043, and 21572039).

SUPPLEMENTARY MATERIAL

The Supplementary Material for this article can be found online at: https://www.frontiersin.org/articles/10.3389/fchem.2019.00778/full#supplementary-material

REFERENCES

Chiku, T., Padovani, D., Zhu, W., Singh, S., Vitvitsky, V., and Banerjee, R. J. (2009). H_2S biogenesis by human cystathionine γ-lyase leads to the novel sulfur metabolites lanthionine and homolanthionine and is responsive to the grade of hyperhomocysteinemia. *Biol. Chem.* 284, 11601–11612. doi: 10.1074/jbc.M808026200

Dang, X., Gu, L., Qi, J., Correa, S., Zhang, G., Belcher, A. M., et al. (2016). Layer-by-layer assembled fluorescent probes in the second near-infrared window for systemic delivery and detection of ovarian cancer. *Proc. Natl. Acad. Sci. U.S.A.* 113, 5179–5184. doi: 10.1073/pnas.1521175113

Eto, K., Asada, T., Arima, K., Makifuchi, T., and Kimura, H. (2002). Brain hydrogen sulfide is severely decreased in Alzheimer's disease. *Biochem. Biophys. Res. Commun.* 293, 1485–1488. doi: 10.1016/S0006-291X(02)00422-9

Fu, W., Yan, C., Zhang, Y., Ma, Y., Guo, Z., and Zhu, W.-H. (2019). Near-infrared aggregation-induced emission-active probe enables *in situ* and long-term tracking of endogenous b-galactosidase activity. *Front. Chem.* 7:291. doi: 10.3389/fchem.2019.00291

Hong, G., Lee, J. C., Robinson, J. T., Raaz, U., Xie, L., Huang, N. F., et al. (2012). Multifunctional *in vivo* vascular imaging using near-infrared II fluorescence. *Nat. Med.* 18, 1841–1846. doi: 10.1038/nm.2995

Huang, C., Jia, T., Tang, M., Yin, Q., Zhu, W., Zhang, C., et al. (2014). Selective and ratiometric fluorescent trapping and quantification of protein vicinal dithiols and *in situ* dynamic tracing in living cells. *J. Am. Chem. Soc.* 136, 14237–14244. doi: 10.1021/ja5079656

Jin, X., Wu, S., She, M., Jia, Y., Hao, L., Yin, B., et al. (2016). A novel fluorescein-based fluorescent probe for detecting H_2S and its real applications in blood plasma and biological imaging. *Anal. Chem.* 88, 11253–11260. doi: 10.1021/acs.analchem.6b04087

Li, H., Yao, Q., Xu, F., Xu, N., Sun, W., Long, S., et al. (2018). Lighting-up tumor for assisting resection via spraying NIR fluorescent probe of g-glutamyltranspeptidas. *Front. Chem.* 6:485. doi: 10.3389/fchem.2018.00485

Mei, J., Hong, Y., Lam, J. W., Qin, A., Tang, Y., and Tang, B. Z. (2014). Aggregation-induced emission: the whole is more brilliant than the parts. *Adv. Mater.* 26, 5429–5479. doi: 10.1002/adma.201401356

Mei, J., Leung, N. L., Kwok, R. T., Lam, J. W., Tang, B. Z. (2015). Aggregation-induced emission: together we shine, united we soar!. *Chem. Rev.* 115, 11718–11940. doi: 10.1021/acs.chemrev.5b00263

Shi, B., Gu, X., Fei, Q., and Zhao, C. (2017). Photoacoustic probes for real-time tracking of endogenous H_2S in living mice. *Chem. Sci.* 8, 2150–2155. doi: 10.1039/C6SC04703C

Shi, B., Yan, Q., Tang, J., Xin, K., Zhang, J., Zhu, Y., et al. (2018). Hydrogen sulfide-activatable second near-infrared fluorescent nanoassemblies for targeted photothermal cancer therapy. *Nano Lett.* 18, 6411–6416. doi: 10.1021/acs.nanolett.8b02767

Singh, S., Padovani, D., Leslie, R. A., Chiku, T., and Banerjee, R. J. (2009). Relative contributions of cystathionine β-synthase and γ-cystathionase to H_2S biogenesis via alternative trans-sulfuration reactions. *Biol. Chem.* 284, 22457–22466. doi: 10.1074/jbc.M109.010868

Sun, X., Xu, Q., Kim, G., Flower, S. E., Lowe, J. P., Yoon, J., et al. (2014). A water-soluble boronate-based fluorescent probe for the selective detection of peroxynitrite and imaging in living cells. *Chem. Sci.* 5, 3368–3373. doi: 10.1039/C4SC01417K

Szabo, C., Coletta, C., Chao, C., Módis, K., Szczesny, B., Papapetropoulos, A., et al. (2013). Tumor-derived hydrogen sulfide, produced by cystathionine-β-synthase, stimulates bioenergetics, cell proliferation, and angiogenesis in colon cancer. *Proc. Natl. Acad. Sci. U.S.A.* 110, 12474–12479. doi: 10.1073/pnas.1306241110

Tang, M., Wu, L., Wu, D., Huang, C., Zhu, W., Xu, Y., et al. (2016). An "off–on" fluorescent probe for the detection of cysteine /homocysteine and its imaging in living cells. *RSC Adv.* 6, 34996–35000. doi: 10.1039/C6RA00832A

Wang, F., Xu, G., Gu, X., Wang, Z., Wang, Z., Shi, B., et al. (2018). Realizing highly chemoselective detection of H_2S *in vitro* and *in vivo* with fluorescent probes inside core-shell silica nanoparticles. *Biomaterials* 159, 82–90. doi: 10.1016/j.biomaterials.2018.01.009

Wang, F., Zhu, Y., Zhou, L., Pan, L., Cui, Z., Fei, Q., et al. (2015). Fluorescent *in situ* targeting probes for rapid imaging of ovarian-cancer-specific g-glutamyltranspeptidase. *Angew. Chem. Int. Ed.* 54, 7349–7353. doi: 10.1002/anie.201502899

Wang, R., Chen, J., Gao, J., Chen, J.-A., Xu, G., Zhu, T., et al. (2019a). A molecular design strategy toward enzymeactivated probes with near-infrared I and II fluorescence for targeted cancer imaging. *Chem. Sci.* 10, 7222–7227. doi: 10.1039/C9SC02093D

Wang, R., Dong, K., Xu, G., Shi, B., Zhu, T., Shi, P., et al. (2019b). Activatable near-infrared emission-guided on-demand administration of photodynamic anticancer therapy with a theranostic nanoprobe. *Chem. Sci.* 10, 2785–2790. doi: 10.1039/C8SC04854A

Xu, G., Yan, Q., Lv, X., Zhu, Y., Xin, K., Shi, B., et al. (2018). Imaging of colorectal cancers using activatable nanoprobes with second near-infrared window emission. *Angew. Chem. Int. Ed.* 57, 3626–3630. doi: 10.1002/anie.201712528

Yuan, Y., Zhang, C.-J., Gao, M., Zhang, R., Tang, B. Z., and Liu, B. (2015). Specific light-up bioprobe with aggregation-induced emission and activatable photoactivity for the targeted and image-guided photodynamic ablation of cancer cells. *Angew. Chem. Int. Ed.* 54, 1780–1786. doi: 10.1002/anie.201408476

Zhang, W., Kang, J., Li, P., Wang, H., and Tang, B. (2015). Dual signaling molecule sensor for rapid detection of hydrogen sulfide based on modified tetraphenylethylene. *Anal. Chem.* 87, 8964–8969. doi: 10.1021/acs.analchem.5b02169

Zhang, X., Zhang, L.i., Ma, W.-W., Zhou, Y., Lu, Z.-N., and Xu, S. (2019). A near-infrared ratiometric fluorescent probe for highly selective recognition and bioimaging of cysteine. *Front. Chem.* 7:32. doi: 10.3389/fchem.2019.00032

Zhao, C., Zhang, J., Wang, X., and Zhang, Y. (2013). Pyridone fused boron-dipyrromethenes: synthesis and properties. *Org. Biomol. Chem.* 11, 372–377. doi: 10.1039/C2OB26791H

Zhao, C., Zhang, X., Li, K., Zhu, S., Guo, Z., Zhang, L., et al. (2015). FRET-switchable self-assembled micellar nanoprobe: ratiometric fluorescent trapping of endogenous H_2S generation via fluvastatin-stimulated upregulation. *J. Am. Chem. Soc.* 137, 8490–8498. doi: 10.1021/jacs.5b03248

Zhao, Y., Wu, Y., Yan, G., and Zhang, K. (2014). Aggregation-induced emission block copolymers based on ring-opening metathesis polymerization. *RSC Adv.* 4, 51194–51200. doi: 10.1039/C4RA08191A

Zhao, Z., Lam, J. W. Y., and Tang, B. Z. (2012). Tetraphenylethene: a versatile AIE building block for the construction of efficient luminescent materials for organic light-emitting diodes. *J. Mater. Chem.* 22, 23726–23740. doi: 10.1039/c2jm31949g

Zhou, L., Zhang, X., Wang, Q., Lv, Y., Mao, G., Luo, A., et al. (2014). Molecular engineering of a TBET-based two-photon fluorescent probe for ratiometric imaging of living cells and tissues. *J. Am. Chem. Soc.* 136, 9838–9841. doi: 10.1021/ja504015t

Conflict of Interest: The authors declare that the research was conducted in the absence of any commercial or financial relationships that could be construed as a potential conflict of interest.

frontiers in Chemistry

MINI REVIEW
published: 26 November 2019
doi: 10.3389/fchem.2019.00825

Functionalized BODIPYs as Fluorescent Molecular Rotors for Viscosity Detection

*Wei Miao, Changjiang Yu, Erhong Hao and Lijuan Jiao**

The Key Laboratory of Functional Molecular Solids, Ministry of Education, Anhui Laboratory of Molecule-Based Materials, School of Chemistry and Materials Science, Anhui Normal University, Wuhu, China

Abnormal changes of intracellular microviscosity are associated with a series of pathologies and diseases. Therefore, monitoring viscosity at cellular and subcellular levels is important for pathological research. Fluorescent molecular rotors (FMRs) have recently been developed to detect viscosity through a linear correlation between fluorescence intensity or lifetime and viscosity. Recently, 4,4-difluoro-4-bora-3a,4a-diaza-*s*-indacene (boron dipyrrins or BODIPY) derivatives have been widely used to build FMRs for viscosity probes due to their high rotational ability of the rotor and potentially high brightness. In this minireview, functionalized BODIPYs as FMRs for viscosity detection were collected, analyzed and summarized.

Keywords: viscosity, BODIPY, fluorescent molecular rotor, viscosimeter, fluorescent probe, dyes

OPEN ACCESS

Edited by:
Zhen Shen,
Nanjing University, China

Reviewed by:
Hua Lu,
Hangzhou Normal University, China
Jiangli Fan,
Dalian University of Technology, China
John Mack,
Rhodes University, South Africa

****Correspondence:***
Lijuan Jiao
jiao421@ahnu.edu.cn

Specialty section:
This article was submitted to Supramolecular Chemistry, a section of the journal Frontiers in Chemistry

Received: *31 July 2019*
Accepted: *13 November 2019*
Published: *26 November 2019*

Citation:
Miao W, Yu C, Hao E and Jiao L (2019) Functionalized BODIPYs as Fluorescent Molecular Rotors for Viscosity Detection. Front. Chem. 7:825. doi: 10.3389/fchem.2019.00825

INTRODUCTION

The viscosity of cells is an important parameter of the cellular microenvironment, which influences the interaction and transport of biological molecules and signals in living cells (Minton, 2001). Abnormal changes of intracellular microviscosity are associated with a series of pathologies and diseases (Nadiv et al., 1994). Thus, the development of suitable imaging tools to monitor and detect cellular microviscosity is important to study cellular function in both health and disease. Fluorescent molecular rotors (FMRs) are established as tools for monitoring cellular and subcellular viscosity changes because of their high sensitivity, fast-response and non-invasive testing of targets in biological systems. A common feature of FMR is that it consists of two moieties, which are connected by a single bond. One moiety with a large moment of inertia is considered to be fixed, called the stator, and the other moiety with a smaller moment of inertia is called the rotor (**Figure 1A**). In a low viscosity medium, the rotor rotates freely, and the energy of excitation is dissipated with non-radiative energy. However, in a high viscosity medium, rotation through the C-C bond is constrained, and the excitation energy is released as emission with enhanced fluorescence intensity and lifetime (Uzhinov et al., 2011; Lee et al., 2018). Therefore, the physical mechanism of viscosity dependence of fluorescence quantum yield and lifetime is caused by the steric hindrance of intramolecular rotation. Recently, FMRs have been widely used to measure viscosity of local environment using their changes in fluorescence intensity and lifetime (Kuimova, 2012). From a practical point of view, FMR with high extinction coefficients, long (NIR) excitation wavelength, and potentially high brightness would be desirable (Ning et al., 2017; Hou et al., 2018).

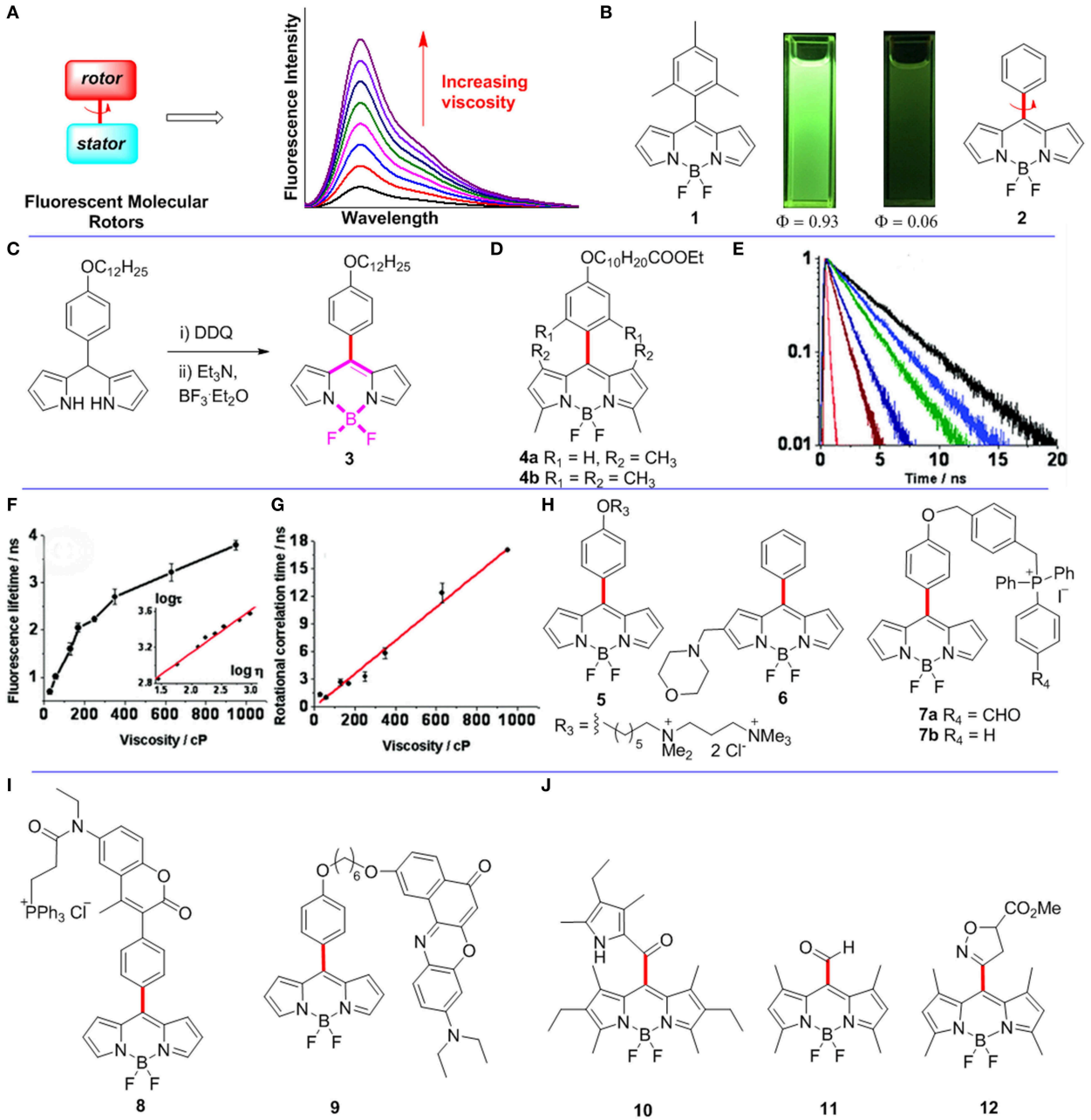

FIGURE 1 | (A) The working principle of FMRs. **(B)** Pictures of BODIPYs **1-2** in dichloromethane under 365 nm UV-light irradiation. **(C)** Synthetic route for *meso*-functionalized BODIPY **3**. **(D)** *Meso*-functionalized BODIPYs **4**. **(E–G)** Fluorescence lifetime and rotational correlation time recorded for BODIPY **3** in solvents of various viscosities. Reproduced with permission from Kuimova et al. (2008), Copyright 2008 American Chemical Society. **(H–J)** *Meso*-functionalized BODIPYs **5-12** as FMRs.

Recently, 4,4-difluoro-4-bora-3a,4a-diaza-*s*-indacenes (BODIPYs) and their derivatives have been paid much attention because of their excellent chemical and physical properties (Loudet and Burgess, 2007; Lu et al., 2014), such as easy functionalization, high molar extinction coefficients, tunable visible to red excitation wavelength, tunable fluorescence quantum yields, as well as excellent photostabilities (Miao et al., 2019; Wang et al., 2019). Not surprisingly, BODIPY derivatives are widely used as imaging probes, fluorescent organic devices, chemical sensors, and as photosensitizers (Cui et al., 2014, 2015; Peterson et al., 2018; Turksoy et al., 2019).

The fluorescence quantum yield of *meso*-(2,4,6-trimethylphenyl)BODIPY **1** is 0.93 in toluene. However, the fluorescence quantum yield of *meso*-phenylBODIPY **2** is only 0.06 in toluene (**Figure 1B**; Kee et al., 2005). The difference results from free rotations of the *meso*-phenyl group of BODIPY

2 causing energy dissipations as non-radiative. The rotation of its *meso*-phenyl group is constrained by increasing the viscosity of local environment around BODIPY **2**. Therefore, *meso*-phenylBODIPY **2** has the potential to be used as a FMR for viscosity detection. Subsequently, various BODIPY derivatives have indeed been developed as FMRs for viscosity sensors, and the rotor-moiety is mainly attached at the *meso*-position and 2,6-position of the BODIPY scaffold (Dziuba et al., 2016). In this minireview, functionalized BODIPYs as FMRs for viscosity detection are collected, analyzed, and summarized.

Meso-Functionalized BODIPYs as FMRs

In biological systems, changes in viscosity at the cellular level are associated with diseases and pathologies, such as diabetes, infarction, and hypertension. Initially, FMRs were designed to detect cellular viscosity through fluorescence intensity (Haidekker and Theodorakis, 2007). However, measurements based on fluorescence intensity are affected by intracellular uncertainty concentrations. To overcome the problem, Kuimova et al. reported a first *meso*-functionalized BODIPY **3** as a FMR, which detects intracellular viscosity by using fluorescence lifetime instead of fluorescence intensity (Kuimova et al., 2008). As shown in **Figure 1C**, BODIPY **3** was synthesized through oxidation of the corresponding dipyrromethane with DDQ followed by addition of excess amounts of base and $BF_3.OEt_2$. The authors measured the fluorescence of BODIPY **3** at various viscosities, and indicated that both the fluorescence quantum yield and lifetime (from 0.7 ± 0.05 to 3.8 ± 0.1 ns; **Figure 1E**) increased dramatically when increasing of the viscosity between 28 and 950 cP. Importantly, the plot of log τ (τ is fluorescence lifetime) vs. log η (η *is* viscosity) was fitted by a straight line (**Figure 1F**). Control BODIPYs **4a-b** (**Figure 1D**) were also studied. Since free rotations of the phenyl groups of BODIPYs **4a-b** are restricted, the non-radiative decay process in both dyes is thus prevented. As expected, BODIPYs **4a-b** have fluorescent quantum yields of close to unity in solvents. No apparent viscosity induced fluorescent intensity or lifetime was observed for both **4a** and **4b**. Subsequently, the fluorescence lifetime imaging (FLIM) using **3** was carried out to study intracellular viscosity, and the results indicated that the average viscosity of SK-OV-3 cells was 140 ± 40 cP. Time-resolved fluorescence anisotropy decays with various viscosities were recorded to confirm that the above high viscosity value didn't result from the binding of the rotor to the intracellular targets. The results showed that the rotational correlation time (θ) of BODIPY **3** increased linearly with solvent viscosity (**Figure 1G**). Finally, the viscosity in SK-OV-3 cells was also measured by using polarization-resolved time correlated single photon counting (TCSPC), and found that the average viscosity of SK-OV-3 cells is 80 cP according to a linear relationship between rotational correlation time θ and viscosity η. The average viscosity of SK-OV-3 cells measured by the two methods is compatible, which shows that the rotor does not combine to intracellular targets. Therefore, the FLIM method using BODIPY based on FMRs is a versatile and also practical method for detecting intracellular viscosity.

Viscosity changes in membranes are associated with various intracellular physiological processes, particularly with various diseases. A few FMRs have successfully detected the viscosity of model lipid bilayers (Hosny et al., 2013; Wu et al., 2013). However, it is difficult to detect viscosity of plasma membranes because of possible effective endocytosis of the probe. For example, BODIPY **3** was only reported to detect viscosity of the lipid membranes of internal cellular organelles. López-Duarte et al. reported a *meso*-functionalized BODIPY **5** to selectively detect viscosity of plasma membranes by adding a double positive charge to the hydrocarbon tail of BODIPY **3** (López-Duarte et al., 2014), which could prevent enucleation and maintain rotor function at the same time (**Figure 1H**). The fluorescence intensity and lifetime measurements of rotor **5** were studied in solvents of various viscosities. As expected, the gradual increase of the viscosity from 0.6 to 930 cP gave a continuous enhancement of both its fluorescence emission intensity and lifetime. In order to illustrate that this dye is mainly distributed on the cell membrane, the uptake experiments of **5** (8.9 μM) were carried out at 4°C with Mg^{2+} and Ca^{2+} free medium in SK-OV-3 cells. The colocalization results indicated **5** exclusively stained the plasma membranes of SK-OV-3 cells after incubation for more than 30 min. The internal staining of the cells became obvious after incubation time of 55 min. In addition, the FLIM of **5**, measured in SK-OV-3 cells, showed that some staining of internal organelles for an incubation time of 40 min. The lifetimes obtained from this lifetime histogram (40 min) were lower than that obtained after only 10 min incubation. The lifetime histogram for the 40 min image is more adequately fitted with a bimodal Gaussian peak fit, and individual peaks are centered at 1.9 ns (organelles, 200 cP) and 2.2 ns (plasma membrane, 270 cP).

The lysosomal viscosity reflects the microscopic state and function of this organelle. When lysosomal function is impaired, especially through lysosomal storage disease caused by single lysosomal enzymes deficiency, macromolecular substances cannot be decomposed and accumulate in lysozyme. Therefore, it is important to monitor the changes of lysosomal viscosity in real time. In this respect, Wang et al. reported BODIPY **6** with a morpholine moiety at the 2-position of *meso*-phenyl-BODIPY as a FMR to detected viscosity of lysosome by using the FLIM method (**Figure 1H**; Wang et al., 2013). Morpholine unit was used as an excellent lysosomal localization group according to previous reports (Yu et al., 2012). Indeed, colocalization experiments showed that **6** can selectively strain cell lysosome. At first, they measured the fluorescence intensity of **6** in different pH at a particular viscosity, and revealed that fluorescence intensity of **6** was disturbed by pH changes. In contrast, the lifetimes of **6** at different pH were very similar. Next, they measured fluorescence lifetime of **6** in a series of buffers with different viscosities (from 0.6 to 359.6 cP), and the results showed that its fluorescence lifetimes (log τ) have a strong linear relationship with viscosities (log η). Subsequently, the FLIM of **6** was recorded in MCF-7 cells, and suggested that the average viscosity was ∼65 cP in lysosome of MCF-7 cells according to the linear relationship of lifetime against viscosity. Finally, the FLIM of **6** was successfully monitored the dynamic changes of lysosomal

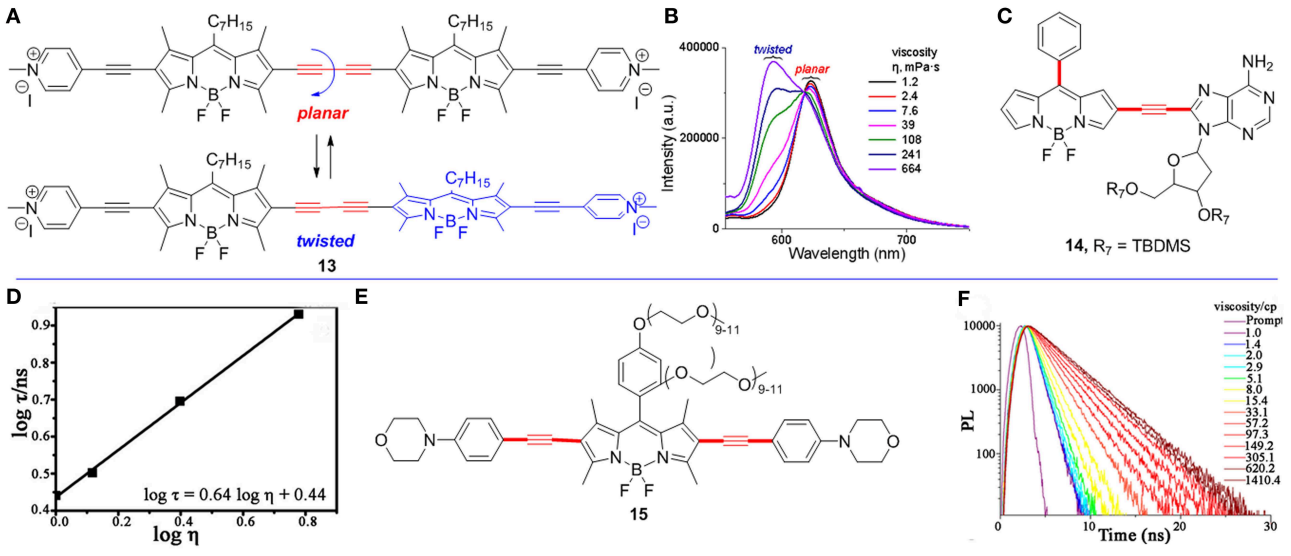

FIGURE 2 | (A) Conformational extremes of BODIPY dimer **13**. **(B)** The fluorescence spectra of BODIPY **13** in solvent of various viscosities. **(C)** 2,6-Functionalized BODIPY **14** as a FMR. **(D)** The fluorescence lifetime measurements of BODIPY **14** (3.0 μM) with different viscosities. Reproduced with permission from Li et al. (2016), Copyright 2016 American Chemical Society. **(E)** 2,6-Functionalized BODIPY **15** as a FMR. **(F)** Fluorescence lifetime spectra of BODIPY **15** (0.5 μM at 590 nm) in various viscosities (pH = 1). Reproduced with permission from Li et al. (2018), Copyright 2018 American Chemical Society.

viscosity in both dexamethasone and chloroquine stimulated MCF-7 cells.

Mitochondria, as a membrane-bound subcellular organelle, have been found in almost all eukaryotic cells. Mitochondrial viscosity deviations from normal levels will affect the respiratory state of mitochondria, and induce cell dysfunction or even death. Song et al. reported BODIPY **7a** as a novel fixable sensor for detecting mitochondrial viscosity of living cells by the FLIM method (Song et al., 2017). Initially, they synthesized two mitochondrial-localized BODIPYs **7a** and **7b** as showed in **Figure 1H**. Fluorescence lifetimes (log τ) of both dyes have excellent linear relationships with viscosities (log η) from 0.6 to 360 cP. Moreover, colocalization studies confirmed that both **7a** (Pearson's coefficient 0.92) and **7b** (Pearson's coefficient 0.97) can specially localized in the mitochondria of the SMMC7721 cells. Another set of colocalization imaging experiments of **7a** and **7b** with Mito Tracker Deep Red were recorded under extreme condition (4% formaldehyde solution treatment). Interestingly, **7a** exhibited strong intracellular fluorescence before and after the formaldehyde treatment. In contrast, **7b** only showed strong fluorescence before formaldehyde treatment, however, its fluorescence was remarkably decreased after formaldehyde treatment. These data showed that BODIPY **7a** was immobilized in the mitochondria. Next, the mitochondrial FLIM of BODIPYs **7a-b** suggested that the average viscosity around BODIPYs **7a-b** in the mitochondria of the SMMC7721 cells is 95 and 63 cP, respectively. Similar results were also found in other types of cells, e.g., MCF-7 cells. The authors explained that these different values are due to the different locations of probes: **7a** is mainly immobilized on proteins of the mitochondria, while **7b** is freely distributed in the mitochondria. The larger viscosity value measured by **7a** may be the contribution of the macromolecule of the protein. Finally, the authors further monitored the viscosity changes in abnormal mitochondria (stimulated with rotenone) using BODIPY **7a**. The fluorescence lifetime of BODIPY **7a** was increased from 2.0 to 2.45 ns after stimulated for 8.5 h, and further increased to 2.73 ns after stimulated for 18 h. Thus, **7a**, as a fixable and mitochondria selective FMR, shows a great potential for monitoring mitochondrial viscosity in real time (Zhang et al., 2019).

The second approach for quantitatively determining viscosity through FMRs is based on ratiometric fluorescence measurements. The ratiometric fluorescence probes have a self-calibration effect, which overcomes the uncertainty associated photobleaching, microenvironments, and local probe concentration for conventional fluorescence probes based on intensity changes. Yang et al. reported a fluorescence ratiometry viscosity probe **8** containing a coumarin unit, a BODIPY unit, and a mitochondria selective triphenylphosphonium group (**Figure 1I**; Yang et al., 2013). The fluorescence changes of **8** in a series of viscosities (from 0.59 to 945.35 cP) revealed that the emission intensities at 427 nm (the emission of the coumarin moiety) and 516 nm (the emission of the BODIPY moiety) both increased with increased viscosity. A strong linear relationship between fluorescence intensity ratio (I_{516}/I_{427}) and viscosity (η) was obtained. In addition, fluorescence lifetimes (log τ) also have a good linear relationship with viscosities (log η). According to the above linear relationships, the mitochondrial viscosity in HeLa cells is 62.8 and 67.5 cP, respectively, by using both fluorescence ratiometry and FLIM. Using similar strategy, Yang et al. also reported BODIPY **9 to** detect microviscosity of the endoplasmic reticulum by using both fluorescence

ratiometry and the FLIM method (**Figure 1I**; Yang et al., 2014).

The BODIPY based FMRs described above all contain rotable *meso*-phenyl groups, while BODIPY **4b** (**Figure 1**) containing substituents on the 1,7-positions of the BODIPY fluorophore is not suitable to be used as FMRs because the *meso*-aromatic group is restricted by the substituents on the 1,7-positions. Thus, it is possible that a less bulky group (than phenyl) on *meso*-position of BODIPY with substituents on the 1,7-positions may allow the rotation in non-viscous media and thus might provide an alternative strategy for designing BODIPY based efficient micro-viscosity probes. Indeed, Yu et al. recently reported a *meso*-2-ketopyrrolyl-derived BODIPY **10** as a new FMR containing substituents on the 1,7-positions (**Figure 1J**; Yu et al., 2019). The fluorescence lifetime (log τ) of BODIPY **10** has a linear relationship with viscosity (log η). Subsequently, this probe was used to detect viscosity changes during the pathological processes using the FLIM in MCF-7 cells. Moreover, a "distorted-BODIPY"-based viscosity probe **11** with *meso*-CHO group was reported by Zhu et al. (**Figure 1J**; Zhu et al., 2014). Zatsikha et al. reported a five-membered ring substituted BODIPY **12**, in which the fluorescence intensity (log *I*) has a linear relationship with viscosity (log η) (**Figure 1J**; Zatsikha et al., 2019).

2,6-Functionalized BODIPYs as FMRs

In comparison with the *meso*-functionalized BODIPYs, only a few 2,6-functionalized BODIPYs have been reported to be used as FMRs to detect viscosity. They typically built through the alkyne bridged rotor and BODIPY core. Recently, Zhang et al. reported a ratiometric fluorescence probe **13** with the two BODIPY units linked by butadiyne group (**Figure 2A**; Zhang et al., 2017). The fluorescence spectra of **13** at different viscosities (from 1.2 to 664 mPa.s) were measured, and its fluorescent emission maximum peaks gradually shifted from 624 to 593 nm with the increase of viscosities (**Figure 2B**). These two fluorescence emission peaks may be contributed by two extreme conformers of **13** with planar or twisted orientations of the two BODIPY units.

Li et al. reported a RNA-targeted BODIPY **14** as a new FMR to detect intracellular viscosity (**Figure 2C**; Li et al., 2016). FMR **14** showed two different maximum wavelengths at 496 and 565 nm, respectively. Similar to most fluorescent ratiometry probes, fluorescence measurements of BODIPY **14** showed two different emitted wavelengths (496 and 565 nm), and both fluorescence intensity (log F_{565}/F_{496}) and lifetime (log τ) have a linear relationship with and viscosity (log η) (**Figure 2D**). In addition, the colocalization experiments of BODIPY **14** and commercial RNA dye revealed that BODIPY **14** mainly distributed in cytoplasmic RNA (Pearson's correlation 0.96). This result was further supported by imaging of BODIPY **14** in four blood cell types. There was strong fluorescence in reticulocytes (contain RNA), but no fluorescence in red blood cells and other cells (without RNA).

Another FMR **15** (**Figure 2E**; Li et al., 2018) with two morpholine moieties selectively detected lysosomal viscosity using FLIM. Similar to BODIPY **6**, the fluorescence lifetime (log τ) of BODIPY **15** linearly increased with the increased viscosity (**Figure 2F**, pH = 1). Moreover, the colocalization experiments indicated that BODIPY **15** mainly distributed in lysosome in Hela cells (Pearson's coefficient 0.95). Next, they monitored the viscosity changes in abnormal mitochondria using BODIPY **15** by treating Hela cells with dexamethasone. Without treating dexamethasone, the histogram of BODIPY **15** indicated the viscosity of the lysosome is 15 cP in Hela cells. However, the viscosity of the lysosome becomes 159 cP after treating with dexamethasone for 1 h according to the linear relationship of lifetime-viscosity.

CONCLUSION

In summary, functionalized BODIPYs have recently been developed as novel FMRs for viscosity detection by fluorescence intensity and fluorescence lifetime, in which the rotor-moieties are mainly attached at the *meso*-position and 2/6-positions of the BODIPY scaffold. Those BODIPY based FMRs can be used to detect the subcellular viscosity by introducing a localization group, such as a pyridinium salt, triphenylphosphine salt or morpholine, through fluorescence ratiometry and FLIM methods. By taking advantage of the rapid development of BODIPY synthesis and post-functionalization, we can anticipate that more exciting BODIPY based FMRs decorated with various functional groups with red to near infrared absorption and emission will be developed. BODIPY based FMRs with rotation around other positions (B position, especially) will also be highly anticipated.

AUTHOR CONTRIBUTIONS

All authors listed have made a substantial, direct and intellectual contribution to the work, and approved it for publication.

ACKNOWLEDGMENTS

We thank the National Nature Science Foundation of China (Grants Nos. 21672006, 21672007, and 21871006) for supporting this work.

REFERENCES

Cui, X., Zhang, X., Xu, K., and Zhao, J. (2015). Application of singlet energy transfer in triplet state formation: broadband visible light-absorbing triplet photosensitizers, molecular structure design, related photophysics and applications. *J. Mater. Chem. C* 3, 8735–8759. doi: 10.1039/C5TC01401H

Cui, X., Zhao, J., Zhou, Y., Ma, J., and Zhao, Y. (2014). Reversible photoswitching of triplet-triplet annihilation upconversion using dithienylethene photochromic switches. *J. Am. Chem. Soc.* 136, 9256–9259. doi: 10.1021/ja504211y

Dziuba, D., Jurkiewicz, P., Cebecauer, M., Hof, M., and Hocek, M. (2016). A rotational BODIPY nucleotide: an environment-sensitive fluorescence-lifetime

probe for DNA interactions and applications in live-cell microscopy. *Angew. Chem. Int. Ed.* 55, 174–178. doi: 10.1002/anie.201507922

Haidekker, M. A., and Theodorakis, E. A. (2007). Molecular rotors—fluorescent biosensors for viscosity and flow. *Org. Biomol. Chem.* 5, 1669–1678. doi: 10.1039/B618415D

Hosny, N. A., Mohamedi, G., Rademeyer, P., Owen, J., Wu, Y., Tang, M.-X., et al. (2013). Mapping microbubble viscosity using fluorescence lifetime imaging of molecular rotors. *Proc. Natl. Acad. Sci. U.S.A.* 110, 9225–9230. doi: 10.1073/pnas.1301479110

Hou, L., Ning, P., Feng, Y., Ding, Y., Bai, L., Li, L., et al. (2018). Two-photon fluorescent probe for monitoring autophagy via fluorescence lifetime imaging. *Anal. Chem.* 90, 7122–7126. doi: 10.1021/acs.analchem.8b01631

Kee, H. L., Kirmaier, C., Yu, L., Thamyongkit, P., Youngblood, W. J., Calder, M. E., et al. (2005). Structural control of the photodynamics of boron-dipyrrin complexes. *J. Phys. Chem. B* 109, 20433–20443. doi: 10.1021/jp0525078

Kuimova, M. K. (2012). Molecular rotors image intracellular viscosity. *Chimia* 66, 159–165. doi: 10.2533/chimia.2012.159

Kuimova, M. K., Yahioglu, G., Levitt, J. A., and Suhling, K. J. (2008). Molecular rotor measures viscosity of live cells via fluorescence lifetime imaging. *J. Am. Chem. Soc.* 130, 6672–6673. doi: 10.1021/ja800570d

Lee, S. C., Heo, J., Woo, H. C., Lee, J. A., Seo, Y. H., Lee, C. L., et al. (2018). Fluorescent molecular rotors for viscosity sensors. *Chem. Eur. J.* 24, 13706–13718. doi: 10.1002/chem.201801389

Li, J., Zhang, Y., Zhang, H., Xuan, X., Xie, M., Xia, S., et al. (2016). Nucleoside-based ultrasensitive fluorescent probe for the dual-mode imaging of microviscosity in living cells. *Anal. Chem.* 88, 5554–5560. doi: 10.1021/acs.analchem.6b01395

Li, L. L., Li, K., Li, M. Y., Shi, L., Liu, Y. H., Zhang, H., et al. (2018). BODIPY-based two-photon fluorescent probe for real-time monitoring of lysosomal viscosity with fluorescence lifetime imaging microscopy. *Anal. Chem.* 90, 5873–5878. doi: 10.1021/acs.analchem.8b00590

López-Duarte, I., Vu, T. T., Izquierdo, M. A., Bull, J. A., and Kuimova, M. K. (2014). A molecular rotor for measuring viscosity in plasma membranes of live cells. *Chem. Commun.* 50, 5282–5284. doi: 10.1039/C3CC47530A

Loudet, A., and Burgess, K. (2007). BODIPY dyes and their derivatives: syntheses and spectroscopic properties. *Chem. Rev.* 107, 4891–4932. doi: 10.1021/cr078381n

Lu, H., Mack, J., Yang, Y., and Shen, Z. (2014). Structural modification strategies for the rational design of red/NIR region BODIPYs. *Chem. Soc. Rev.* 43, 4778–4823. doi: 10.1039/C4CS00030G

Miao, W., Feng, Y., Wu, Q., Sheng, W., Li, M., Liu, Q., et al. (2019). Phenanthro[*b*]-fused BODIPYs through tandem Suzuki and oxidative aromatic couplings: synthesis and photophysical properties. *J. Org. Chem.* 84, 9693–9704. doi: 10.1021/acs.joc.9b01425

Minton, A. P. (2001). The influence of macromolecular crowding and macromolecula confinement on biochemical reactions in physiological media. *J. Biol. Chem.* 276, 10577–10580. doi: 10.1074/jbc.R100005200

Nadiv, O., Shinitzky, M., Manu, H., Hecht, D., Roberts, C., LeRoith, D., et al. (1994). Elevated protein tyrosine phosphatase activity and increased membrane viscosity are associated with impaired activation of the insulin receptor kinase in old rats. *Biochem. J.* 298, 443–450. doi: 10.1042/bj2980443

Ning, P., Dong, P., Geng, Q., Bai, L., Ding, Y., Tian, X., et al. (2017). A two-photon fluorescent probe for viscosity imaging *in vivo*. *J. Mater. Chem. B* 5, 2743–2749. doi: 10.1039/C7TB00136C

Peterson, J. A., Wijesooriya, C., Gehrmann, E. J., Mahoney, K. M., Goswami, P. P., Albright, T. R., et al. (2018). Family of BODIPY photocages cleaved by single photons of visible/near-infrared light. *J. Am. Chem. Soc.* 140, 7343–7346. doi: 10.1021/jacs.8b04040

Song, X., Li, N., Wang, C., and Xiao, Y. (2017). Targetable and fixable rotor for quantifying mitochondrial viscosity of living cells by fluorescence lifetime imaging. *J. Mater. Chem. B* 5, 360–368. doi: 10.1039/C6TB02524B

Turksoy, A., Yildiz, D., and Akkaya, E. U. (2019). Photosensitization and controlled photosensitization with BODIPY dyes. *Coord. Chem. Rev.* 379, 47–64. doi: 10.1016/j.ccr.2017.09.029

Uzhinov, B. M., Ivanov, V. L., and Melnikov, M. Y. (2011). Molecular rotors as luminescence sensors of local viscosity and viscous flow in solutions and organized systems. *Russ. Chem. Rev.* 80, 1179–1190. doi: 10.1070/RC2011v080n12ABEH004246

Wang, L., Xiao, Y., Tian, W., and Deng, L. (2013). Activatable rotor for quantifying lysosomal viscosity in living cells. *J. Am. Chem. Soc.* 135, 2903–2906. doi: 10.1021/ja311688g

Wang, Z., Cheng, C., Kang, Z., Miao, W., Liu, Q., Wang, H., et al. (2019). Organotrifluoroborate salts as complexation reagents for synthesizing BODIPY dyes containing both fluoride and an organo substituent at the boron center. *J. Org. Chem.* 84, 2732–2740. doi: 10.1021/acs.joc.8b03145

Wu, Y., Štefl, M., Olzyńska, A., Hof, M., Yahioglu, G., Yip, P., et al. (2013). Molecular rheometry: direct determination of viscosity in L_o and L_d lipid phases via fluorescence lifetime imaging. *Phys. Chem. Chem. Phys.* 15, 14986–14993. doi: 10.1039/c3cp51953h

Yang, Z., He, Y., Lee, J. H., Chae, W. S., Ren, W. X., Lee, J. H., et al. (2014). A Nile Red/BODIPY-based bimodal probe sensitive to changes in the micropolarity and microviscosity of the endoplasmic reticulum. *Chem. Commun.* 50, 11672–11675. doi: 10.1039/C4CC04915B

Yang, Z., He, Y., Lee, J. H., Park, N., Suh, M., Chae, W. S., et al. (2013). A self-calibrating bipartite viscosity sensor for mitochondria. *J. Am. Chem. Soc.* 135, 9181–9185. doi: 10.1021/ja403851p

Yu, C., Huang, Z., Gu, W., Wu, Q., Hao, E., Xiao, Y., et al. (2019). Uncommon *meso*-2-ketopyrrolylBODIPYs with AIE-active features for real-time quantitative viscosity mapping via fluorescence lifetime imaging microscopy. *Mater. Chem. Front.* 3, 1823–1832. doi: 10.1039/C9QM00154A

Yu, H., Xiao, Y., and Jin, L. (2012). A lysosome-targetable and two-photon fluorescent probe for monitoring endogenous and exogenous nitric oxide in living cells. *J. Am. Chem. Soc.* 134, 17486–17489. doi: 10.1021/ja308967u

Zatsikha, Y. V., Didukh, N. O., Swedin, R. K., Yakubovskyi, V. P., Blesener, T. S., Healy, A. T., et al. (2019). Preparation of viscosity-sensitive isoxazoline/isoxazolyl-based molecular rotors and directly linked BODIPY-fulleroisoxazoline from the stable *meso*-(nitrile oxide)-substituted BODIPY. *Org. Lett.* 21, 5713–5718. doi: 10.1021/acs.orglett.9b02082

Zhang, W., Sheng, W., Yu, C., Wei, Y., Wang, H., Hao, E., et al. (2017). One-pot synthesis and properties of well-defined butadiynylene-BODIPY oligomers. *Chem. Commun.* 53, 5318–5321. doi: 10.1039/C7CC02393F

Zhang, X., Sun, Q., Huang, Z., Huang, L., and Xiao, Y. (2019). Immobilizable fluorescent probes for monitoring the mitochondria microenvironment: a next step from the classic. *J. Mater. Chem. B* 7, 2749–2758. doi: 10.1039/C9TB00043G

Zhu, H., Fan, J., Li, M., Cao, J., Wang, J., and Peng, X. (2014). A "distorted-BODIPY"-based fluorescent probe for imaging of cellular viscosity in live cells. *Chem. Eur. J.* 20, 4691–4696. doi: 10.1002/chem.201304296

Conflict of Interest: The authors declare that the research was conducted in the absence of any commercial or financial relationships that could be construed as a potential conflict of interest.

frontiers in Chemistry

ORIGINAL RESEARCH
published: 03 December 2019
doi: 10.3389/fchem.2019.00801

Tuning the Photonic Behavior of Symmetrical bis-BODIPY Architectures: The Key Role of the Spacer Moiety

Ainhoa Oliden-Sánchez[1], Rebeca Sola-Llano[1], Jorge Bañuelos[1], Inmaculada García-Moreno[2], Clara Uriel[3], J. Cristobal López[3] and Ana M. Gómez[3]**

[1] Molecular Spectroscopy Laboratory, Science and Technology Faculty, Physical Chemistry Department, Basque Country University (UPV/EHU), Bilbao, Spain, [2] Laser Materials Laboratory, "Rocasolano" Physical Chemistry Institute, Department of Low-Dimension Systems, Surfaces and Condensed Matter, CSIC, Madrid, Spain, [3] Bioorganic Chemistry Department, Instituto de Química Orgánica General (IQOG-CSIC), Madrid, Spain

Herein we describe the synthesis, computationally assisted spectroscopy, and lasing properties of a new library of symmetric bridged bis-BODIPYs that differ in the nature of the spacer. Access to a series of BODIPY dimers is straightforward through synthetic modifications of the pending *ortho*-hydroxymethyl group of readily available C-8 (*meso*) *ortho*-hydroxymethyl phenyl BODIPYs. In this way, we have carried out the first systematic study of the photonic behavior of symmetric bridged bis-BODIPYs, which is effectively modulated by the length and/or stereoelectronic properties of the spacer unit. The designed bis-BODIPYs display bright fluorescence and laser emission in non-polar media. The fluorescence response is governed by the induction of a non-emissive intramolecular charge transfer (ICT) process, which is significantly enhanced in polar media. The effectiveness of the fluorescence quenching and also the prevailing charge transfer mechanism (from the spacer itself or between the BODIPY units) rely directly on the electron-releasing ability of the spacer. Moreover, the linker moiety can also promote intramolecular excitonic interactions, leading to excimer-like emission characterized by new spectral bands and the lengthening of lifetimes. The substantial influence of the bridging moiety on the emission behavior of these BODIPY dyads and their solvent-sensitivity highlight the intricate molecular dynamics upon excitation in multichromophoric systems. In this regard, the present work represents a breakthrough in the complex relationship between the molecular structure of the chromophores and their photophysical signatures, thus providing key guidelines for rationalizing the design of tailored bis-BODIPYs with potential advanced applications.

Keywords: dye chemistry, charge transfer, excimers, lasers, BODIPY-dimers

OPEN ACCESS

Edited by:
Zhen Shen,
Nanjing University, China

Reviewed by:
Lijuan Jiao,
Anhui Normal University, China
Hua Lu,
Hangzhou Normal University, China
John Mack,
Rhodes University, South Africa

****Correspondence:***
Jorge Bañuelos
jorge.banuelos@ehu.es
Ana M. Gómez
ana.gomez@csic.es

Specialty section:
This article was submitted to Supramolecular Chemistry, a section of the journal Frontiers in Chemistry

Received: *29 July 2019*
Accepted: *06 November 2019*
Published: *03 December 2019*

Citation:
Oliden-Sánchez A, Sola-Llano R, Bañuelos J, García-Moreno I, Uriel C, López JC and Gómez AM (2019) Tuning the Photonic Behavior of Symmetrical bis-BODIPY Architectures: The Key Role of the Spacer Moiety. Front. Chem. 7:801. doi: 10.3389/fchem.2019.00801

INTRODUCTION

Modern avenues in dye chemistry are not only oriented to the development of single fluorophores with tailor-made molecular structures (De Moliner et al., 2017) but are also focused on the rational design of multichromophoric architectures where the fluorophores are linked through covalent bonds (Ahrens et al., 2013; Fan et al., 2013). The proximity of the chromophoric subunits enables

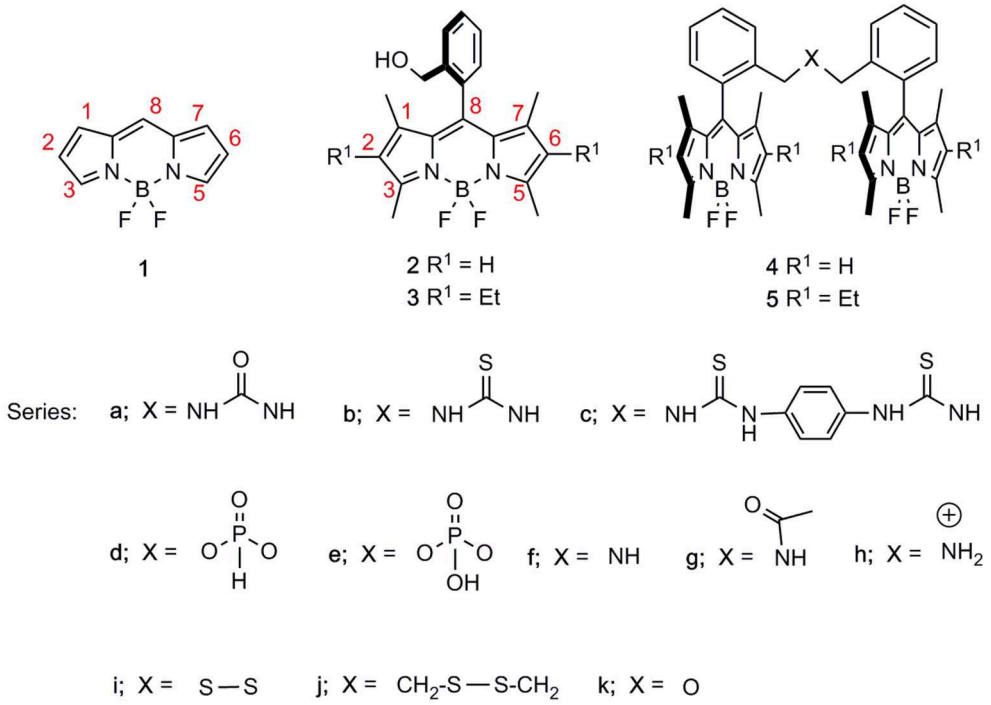

FIGURE 1 | Basic molecular structure of BODIPY (**1**), our BODIPY starting materials (**2** and **3**), and all BODIPY dimers synthesized therefrom, i.e., **4** and **5**, with spacers consisting of urea-, thiourea-, phosphonate-, amine-, disulfur-, and ether-based linkers, differing in length and/or stereoelectronic properties.

intramolecular interactions, giving rise to new photophysical phenomena ranging from a wide assortment of excitonic interactions (H- and/or J-aggregates, excimers) (Alamiry et al., 2011; Ahrens et al., 2016; Patalag et al., 2017) to charge (Zhao et al., 2013; Liu et al., 2018) and/or energy transfer (Speiser, 1996; Avellanal-Zaballa et al., 2017) processes. The balance between them or the promotion of one of them determines the final photonic performance of the multichromophoric system and, consequently, its potential field of application. It is well-established that the photonic behavior of fluorescent molecular assemblies becomes effectively modulated through a rational election of the chromophoric building blocks and the tether between them (Wang et al., 2017; Zhang, 2017; Blázquez-Moraleja et al., 2018). However, understanding and unraveling the impact of the molecular structure into the dynamics of their excited state remains a challenge owing to the complexity of multichromophoric dyes and the coexistence of several deactivation pathways competing at the same time and showing also a marked dependence on the solvent properties (Thakare et al., 2016). This knowledge becomes critical for designing straightforward and low-cost synthesis routes for smart dyes with multifunctional properties, fulfilling the tight requirements of the most advanced technological applications (Alberto et al., 2018).

Toward this aim, boron-dipyrromethene (BODIPY) scaffolds, e.g., **1** in **Figure 1**, are ideal candidates as building blocks owing to the chemical versatility of the chromophoric core (Loudet and Burgess, 2007; Ulrich et al., 2008). The boron-dipyrrin backbone is ready amenable to a wide range of post-functionalization routes (Boens et al., 2015), which might allow its ulterior covalent linkage to additional chromophoric units (Dumas-Verdes et al., 2010; Misra et al., 2014; Gartzia-Rivero et al., 2015; Kesavan et al., 2015; Arroyo-Córdoba et al., 2018; Xu et al., 2018; Zhang et al., 2018). Such tailoring of the molecular structure being available enables the modulation of the spectral bands of the BODIPY, leading to stable and bright dyes along the whole visible spectrum and even reaching the near-infrared region (Lu et al., 2014; Bañuelos, 2016). Multichromophoric dyes based on the BODIPY core are currently being intensively applied in various technological fields such as photovoltaics (Galateia et al., 2015), photosynthetic antennae (Ke et al., 2017), sensing and electronics (Squeo et al., 2017), electrochemistry (Qi et al., 2013), near-infrared emitters (Sakamoto et al., 2012), and as photosensitizers and labeling tools in biomedicine (Turksoy et al., 2019).

In this context, we have recently reported a straightforward synthetic approach from *ortho*-functionalized 8-aryl-BODIPYs, e.g., **2** and **3** (Del Río et al., 2017), to stable and luminescent urea-bridged symmetric bis-BODIPYs, i.e., **4a** and **5a** (López et al., 2017) (**Figure 1**). The fluorescence response of this covalent molecular assembly was sensible to the properties of the environment owing to the capability of the spacer moiety to induce "through-space" intramolecular charge transfer (ICT) processes. Herein, to achieve deeper insight into this ICT mechanism, which triggers the fluorescence efficiency of the whole molecular entanglement, we have synthesized a new battery of bis-BODIPYs, where the length and stereoelectronic properties of the spacer unit have been systematically modified (**Scheme 1**). Accordingly, the impact of the electron-releasing ability of the urea spacer was assessed by replacing the urea

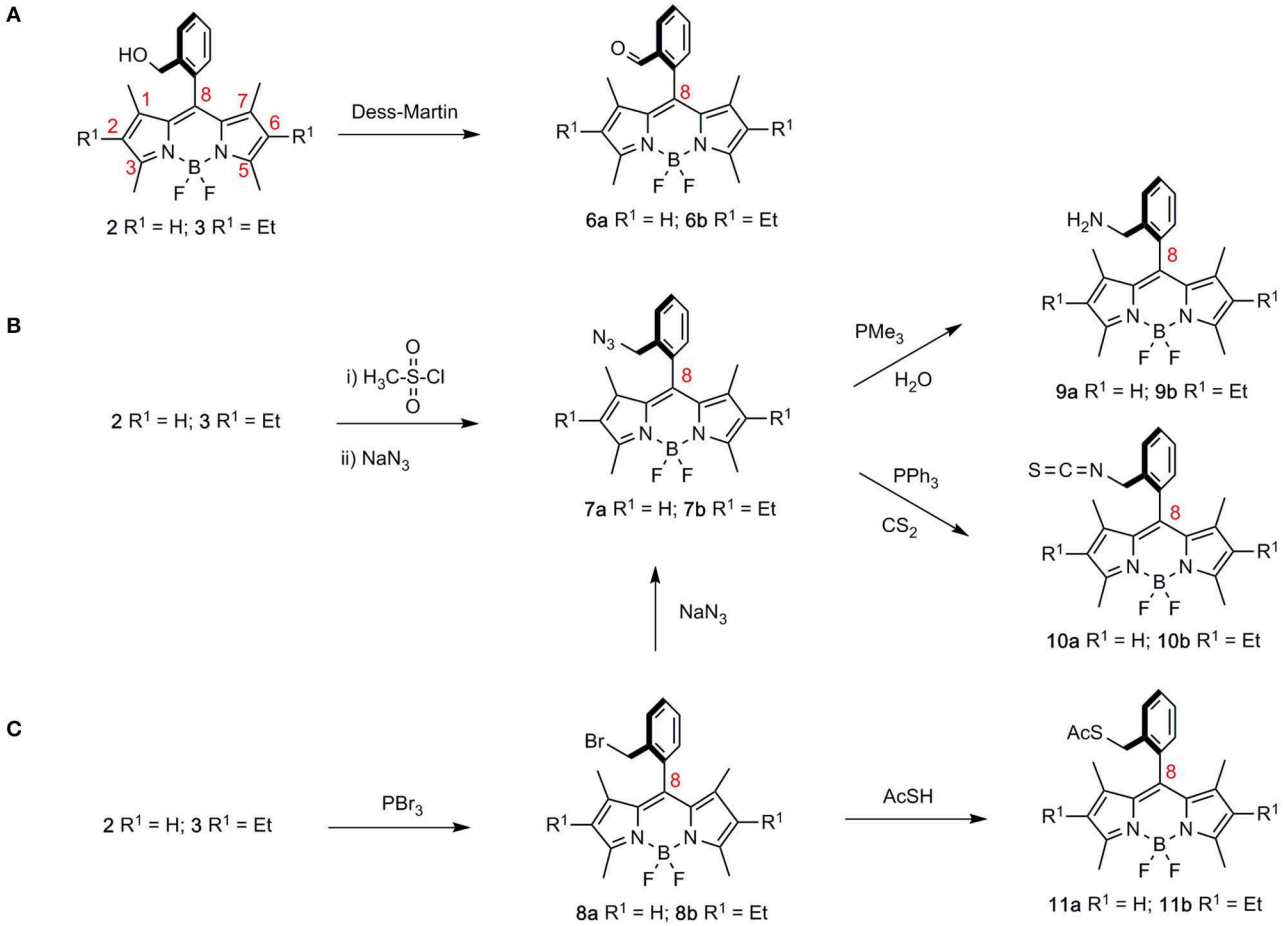

SCHEME 1 | Derivatization of the hydroxymethyl group in BODIPYs **2** and **3**, leading to differently functionalized BODIPYs. **(A)** oxidation to formyl-BODIPYs **6**; **(B)** obtention of azidomethyl BODIPYs **7** as precursors of aminomethyl derivatives **9** and isothiocyanyl-BODIPYs **10**; **(C)** preparation of bromomethyl-BODIPYs **8** and their conversion to BODIPY thiolacetates **11**.

oxygen by a less electronegative moiety such as a sulfur atom (thiourea-bridged, i.e., **4b** and **5b**, **Scheme 1**). On the other hand, the effect of the distance between BODIPY subunits has been studied by incorporating a phenyl tether in bis-thiourea-derived BODIPYs, e.g., **4c** (**Figure 1**). Furthermore, by taking advantage of the synthetic potential of the *ortho*-hydroxymethyl group in BODIPYs **2** and **3**, an additional collection of dimers with spacers that incorporate phosphorous, i.e., **4e** and **5d**, nitrogen, i.e., **4f**, **5f**, **4g**, **5g**, and **4h**, sulfur, i.e., **4i**, **5i**, and **4j**, and oxygen, i.e., **4k** and **5k**, atoms, which differed in their electronic properties and/or the tether lengths have also been efficiently obtained (**Figure 1**). The computationally aided photophysical and laser study of this new set of bis-BODIPYs have contributed to the understanding of the structural controls behind the fluorescence response of these multichromophoric laser dyes.

RESULTS AND DISCUSSION

Synthesis of Bridged bis-BODIPYs

As previously mentioned, symmetric bis-BODIPYs **4a–k** and **5a–k** were prepared from BODIPYs **2** and **3**, respectively, following standard synthetic procedures that are highlighted in **Schemes 1**–**3** (see also **Supplementary Material** for detailed experimental conditions). In this context, the divergent sequences to all of the BODIPY dimers used in this study serve to illustrate the synthetic potential of *ortho*-hydroxymethyl 8-aryl BODIPYs **2** and **3**, available through a one-pot transformation from phthalide and differently substituted pyrroles (Del Río et al., 2017).

Accordingly, synthetic transformations on the hydroxymethyl group in BODIPYs **2**, **3** gave access to a "second generation" of BODIPY derivatives comprising formyl-BODIPYs **6a** and **6b** (**a** R^1 = H, **b** R^1 = Et, throughout the series; **Scheme 1A**) (Dess and Martin, 1983), azidomethyl-BODIPYs **7a** and **7b**, (**Scheme 1B**), and bromomethyl-BODIPYs **8a** and **8b** (Godoy et al., 2015) (**Scheme 1C**). The latter was also a precursor of azidomethyl BODIPYs **7a** and **7b** by nucleophilic displacement with sodium azide.

Azidomethyl and bromomethyl BODIPYs **7** and **8**, respectively, were next used as starting materials for a "third generation" of *ortho*-methyl functionalized BODIPYs, **9**–**11**. Accordingly, azidomethyl-BODIPYs **7a** and **7b** could be transformed into aminomethyl derivatives **9a** and **9b** (PMe_3,

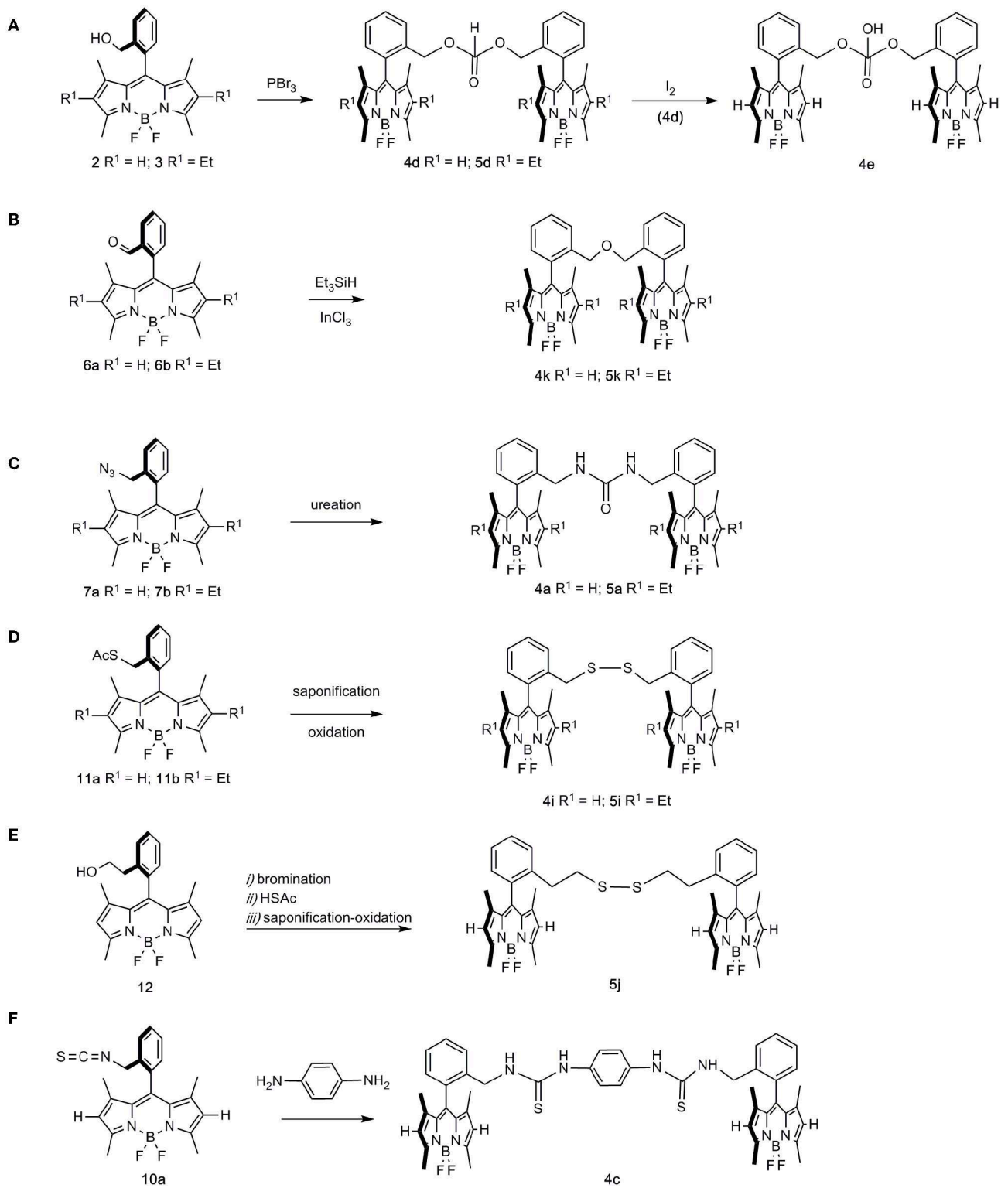

SCHEME 2 | Generation of dimeric BODIPY species from single BODIPY units. **(A)** esterification of PBr3 by hydroxymethyl BODIPYs to dialkyl H-phosphonates **4d** and **5d**, followed by oxidation to phosphate **4e**; **(B)** triethylsilane-mediated reductive etherification of formyl-BODIPYs **6a** and **6b** to ether-linked dimers **4k** and **5k**; **(C)** ureation-dimerization of azidomethyl BODIPYs **7a** and **7b**, to urea-bridged bis-BODIPYs **4a** and **5a**; **(D)** saponification-oxidation on thiolacetates **11a** and **11b**, to disulfide-bridged bis-BODIPYs **4i** and **5i**; **(E)** access to "homologated" bis-disulfide **5j** from BODIPY **12**; **(F)** coupling reaction of isothiocyanyl-BODIPY **10a** with 1,4-phenylenediamine, leading to bis-thiourea derivative **4c**.

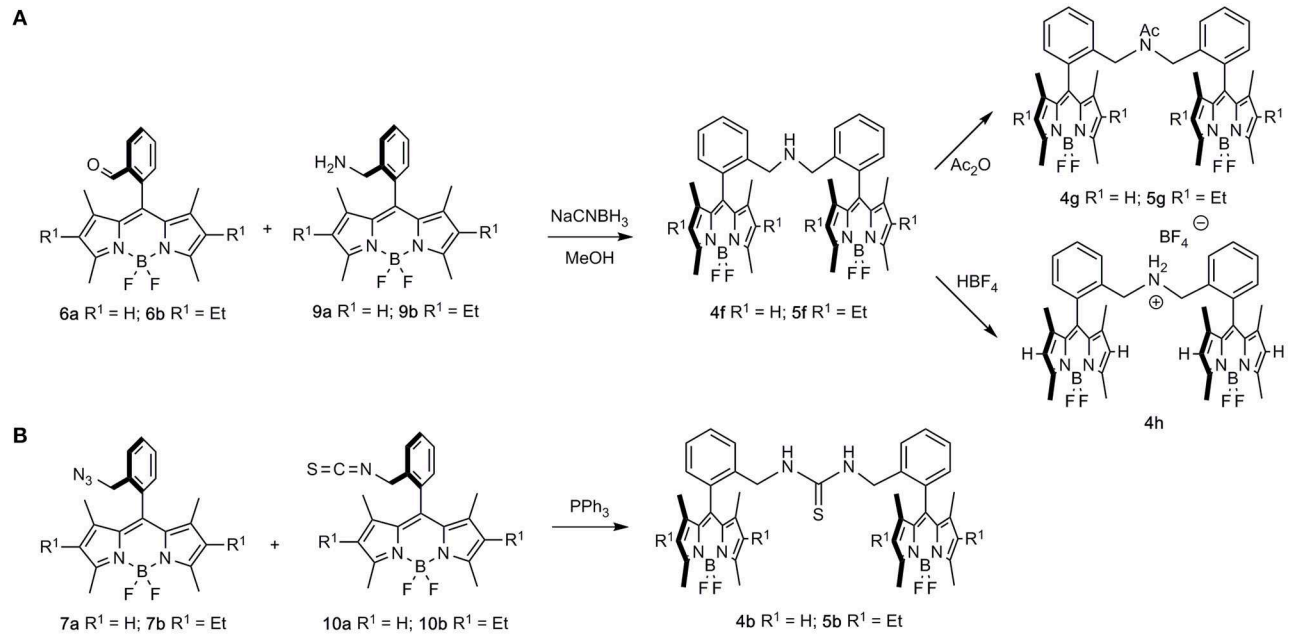

SCHEME 3 | Combination of two BODIPY units leading to symmetrical bis-BODIPYs. **(A)** Reductive amination of formyl-BODIPYs **6** with aminomethyl-BODIPYs **9**, leading to bridged-aminomethyl dimers **4f** and **5f**, and their transformation to acetamido-BODIPYs **4g** and **5g** or ammonium-bridged BODIPY **4h**; **(B)** combination of azidomethyl BODIPYs **7a** and **7b** with isothiocyanyl-BODIPYs **10a** and **10b**, respectively, leading to thiourea-bridged BODIPY dimers **4b** and **5b**.

H_2O) or isothiocyanyl-BODIPYs **10a** and **10b** (PPh_3, CS_2) by way of reactions that involved BODIPY-iminophosphorane intermediates (**Scheme 1B**). Alternatively, nucleophilic displacement on bromomethyl-BODIPYs **8a** and **8b** with thiolacetic acid led to BODIPY thiolacetates **11a** and **11b**, respectively (**Scheme 1C**).

Regarding the formation of the dimeric structures, some were produced by dimerization of these BODIPY monomers (**Scheme 2**), whereas the rest of the dimers were obtained by a combination of two differently functionalized BODIPYs (**Scheme 3**).

Thus, hydroxymethyl-BODIPYs **2** and **3** were efficiently transformed into H-phosphonate-bridged bis-BODIPYs **4d** and **5d**, respectively, upon treatment with PBr_3 (Kotlarska et al., 2013) (**Scheme 2A**). The oxidation of phosphonate **4d** (I_2) (Li et al., 2014) then paved the way to phosphate-bridged bis-BODIPY **4e** (**Scheme 2A**). On the other hand, triethylsilane-mediated reductive etherification of formyl-BODIPYs **6a** and **6b** (Huo et al., 2018) was used in the preparation of ether-linked dimers **4k** and **5k**, respectively (**Scheme 2B**). Urea-bridged bis-BODIPYs **4a** and **5a** were conveniently prepared by a ureation-dimerization protocol from azidomethyl BODIPYs **7a** and **7b** (Del Río et al., 2017) (**Scheme 2C**). A saponification-oxidation protocol on thiolacetates **11a** and **b** allowed the synthesis of disulfide-bridged bis-BODIPYs **4i** and **5i** (**Scheme 2D**). Likewise, the "homologated" bis-disulfide **5j** was prepared via an intermediate thiolacetate obtained from *ortho*-hydroxyethyl BODIPY **12,** followed by a synthetic sequence related to that mentioned above (**Scheme 2E**).

Finally, the "elongated" 1,1′-(1,4-phenylene)-bis-(3-BODIPY-thiourea) derivative **4c**, was prepared by reaction of isothiocyanyl-BODIPY **10a** with 1,4-phenylenediamine (**Scheme 2F**).

Alternatively, the combination of aminomethyl-BODIPYs **9** with formyl-BODIPYs **6** (reductive-amination conditions) led to bridged-aminomethyl dimers **4f** and **5f**, which were uneventfully transformed into the corresponding acetamido- (**4g** and **5g**) or ammonium-bridged (**4h**) BODIPYs (**Scheme 3A**). Along this line, the combination of azidomethyl BODIPYs **7a** and **7b** with isothiocyanyl-BODIPYs **10a** and **10b** led to thiourea-bridged BODIPY dimers **4b** and **5b** (**Scheme 3B**).

Photophysical Properties of Bridged bis-BODIPYs

The conducted and joined computational-spectroscopic characterization revealed that the spacer bridging the chromophoric cores in the designed library of bis-BODIPYs played a key role in the final photophysical properties of the dyads. Therefore, hereafter, we thoroughly describe the interplay between the molecular structure and the photophysical signatures, with special attention to the fluorescence response and the ongoing non-radiative channels related to intramolecular charge transfer and excitonic couplings. Toward this aim, the photophysical properties of the new symmetric bis-BODIPYs (whose structures are shown in **Figure 1**) were systematically analyzed in dilute solutions (see details in experimental section Spectroscopic Properties) in polar (dimethylformamide (DMF),

TABLE 1 | Photophysical properties of the bis-BODIPYs based on **2** and **3** as building blocks and linked through different bridges (urea, thiourea, phosphonate, amine, acetylamine, ammonium, and disulfur) in an apolar solvent (cyclohexane, except those not soluble, marked as *, whose data are provided in diethyl ether).

	λ_{ab} (nm)	$\varepsilon_{max} \cdot 10^{-4}$ (M^{-1} cm^{-1})	λ_{fl} (nm)	φ	τ (ns)
4a	502.5	13.4	515.0	0.83	5.66
4b	503.5	10.0	517.5	0.51	1.86 (46%)–6.29 (54%)
4c	504.5	16.0	511.0	0.40	0.22 (31%)–1.86 (12%)–5.12 (57%)
4e*	500.5	13.3	514.0	0.43	0.55 (28%)–6.41 (72%)
4f	501.5	14.0	517.5	0.50	2.34 (56%)–6.59 (44%)
4g	499.0	12.3	522.5	0.89	7.51
4h	504.5	11.5	513.0	0.90	4.98
4i*	503.0	21.0	524	0.85	6.76
4j	503.5	14.5	518.0	0.92	6.68
5a	525.5	16.2	540.5	0.98	6.76
5b	525.5	15.5	540.0	0.76	6.79
5d	526.5	22.6	542.5	0.79	7.28
5f	526.0	15.9	540.5	0.77	7.22
5g	524.5	13.2	544.0	0.90	8.37
5i	527.0	19.6	542.5	0.84	7.04

*Full data in more solvents of different polarities are listed in **Tables S1**, **S2**. Absorption (λ_{ab}) and fluorescence (λ_{fl}) wavelength, molar absorption at the maximum (ε_{max}), fluorescence quantum yield (φ), and lifetime (τ).*

acetonitrile, and ethanol) and apolar (cyclohexane) solvents (**Table 1**; **Tables S1**, **S2**). With the exception of the ether-bridged dyads, whose particular photophysics will be discussed in detail below (section Excitonic Coupling Induced by an Ether Spacer), the spectral absorption and emission properties of all the other dyes followed a common behavior, which was also similar to that previously described for urea-based derivatives (López et al., 2017). The absorption profile of these dyads peaked at wavelengths similar to those of the corresponding single counterpart precursors (**2** and **3**, Del Río et al., 2017), while the absorption probability increased significantly (up to 23×10^4 M^{-1} cm^{-1}), becoming roughly twice that of each single chromophore (**Figure 2**, **Table 1**). Indeed, the theoretical simulation revealed that the absorption transition resulted from the contribution of two configurations that were energetically close (just separated by 0.03 eV), with the electronic density allocated on each dipyrrin chromophoric unit. Moreover, after molecular assembly, both BODIPY subunits were held apart (the distance between the center of masses range from merely 8 Å to around 20 Å, depending on the kind of spacer bridging the chromophores), hampering any intramolecular interaction between them. In this configuration, each BODIPY moiety was electronically decoupled, retaining its identity, and photophysical properties and contributing additionally to the global transition. Furthermore, the orthogonal disposition between the 8-aryl unit and the BODIPY core (≈90° twisting dihedral angle) owing to the steric hindrance exerted by its *ortho*-substituent and the methyl groups at C1 and C7 avoids any resonant interaction among the building blocks of these bridged bis-BODIPYs. The absorption and fluorescence spectral band positions became hypsochromically shifted by increasing the solvent polarity (**Tables S1**, **S2**), according to the behavior of the corresponding parent monomeric dyes.

Regarding the emission, and owing to the claimed electronic isolation of the chromophoric units in the dyads, the high fluorescence efficiency distinctive of BODIPY dyes was retained by these bis-BODIPYs built from scaffolds **2** and **3** in apolar media (**Table 1**). Unlike the parent dyes, whose fluorescence was nearly solvent-independent (Bañuelos, 2016), the emission efficiency from the new dyads was markedly influenced by the solvent (discussed below in detail in sections Effect of Solvent Polarity on ICT Stabilization and The Special Case of DMF). As previously stated, while analyzing the photophysics behavior of the urea-bridged BODIPY dyes (López et al., 2017), the emission process in these dyads took place by an effective "*through-space*" ICT mechanism, with the urea spacer acting as donor unit and the BODIPY core behaving as the electron acceptor. In fact, the computed molecular electrostatic potential surfaces (MEP in **Figure 3**) placed remarkable negative charge at the oxygen atom of the urea bridge, showing its electron donor ability, which was even amplified by the flanking amines as well as by its proximity to the dipyrrin planes of the BODIPY skeleton. Consequently, the fluorescence emission from the herein-synthetized dyads became markedly dependent on the polarity of the media, and, even more interestingly, this solvent dependence was unambiguously modulated by the alkylation of the BODIPY core and especially by the length and the stereoelectronic properties of the spacer unit.

Spacer Effect on ICT Mechanism and Probability

Actually, the photophysical signatures of the new dyads, even in an apolar solvent such as cyclohexane (**Table 1**), were determined

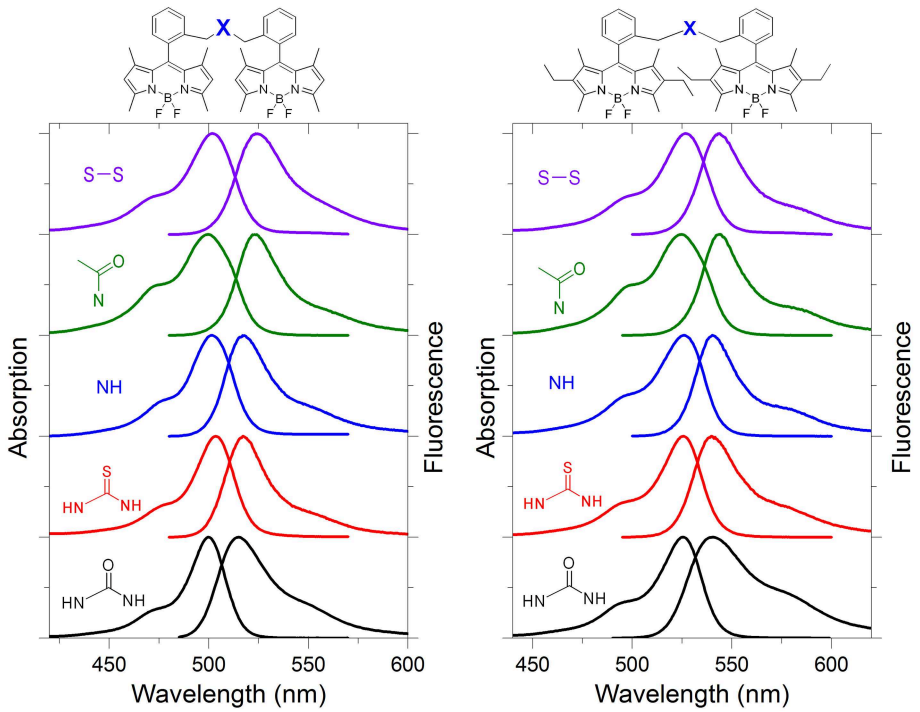

FIGURE 2 | Normalized absorption and fluorescence spectra of representative bis-BODIPYs derived from building blocks **2** and **3** and linked by urea (**4a** and **5a**), thiourea (**4b** and **5b**), amino (**4f** and **5f**), acetylamino (**4g** and **5g**), and disulfur (**4i** and **5i**) bridges in an apolar environment. All the spectra in different solvents are collected in **Figures S60**, **S61**.

by this ongoing ICT mechanism, with the spacer playing a key role:

i) The higher the electron donor ability of the linker, the lower became the fluorescence efficiency. Thus, the mere replacement of the urea moiety (**4a** and **5a**) by a thiourea bridge (**4b** and **5b**) reduced the fluorescence quantum yield (i.e., from 83 to 51% in **Table 1**). The phosphorous-bridged dyads based on two different oxidation states (valence III in **5d** with a "pendant" hydrogen atom and valence V in **4e** with a "pendant" hydroxyl group) further supported this behavior. With respect to the urea linker, the phosphorous was less electronegative than the nitrogen, therefore increasing the negative charge on the oxygen atoms, as reflected in the corresponding MEP maps (more intense red color around the phosphonyl in **Figure 3**). This was especially noticeable for the spacer bearing a "pendant" hydroxyl group in dyad **4e**, where its higher electron-donor ability enhanced the ICT probability even more, leading consequently to one of the lowest fluorescence quantum yields recorded in cyclohexane (43% in **Table 1**).

ii) Following the same argument, reducing the electron-releasing ability of the spacer enhanced the fluorescence efficiency of the bis-BODIPY dyes significantly. Trying to nullify the contribution of the spacer-induced ICT, we designed BODIPY dyads with the chromophoric units linked through electronically inert moieties such as disulfur groups (**4i**, **5i**, and **4j**), which led to one of the highest fluorescence efficiencies recorded herein (up to 92% in **Table 1**). Similar behavior was observed on the ammonium salt-linked BODIPYdyad **4h**, which exhibited a 90% fluorescence efficiency. Thus, the ammonium salt in **4h** acted as an effective electron-withdrawing moiety according to the MEP, which located a high positive charge on the spacer (**Figure 4**).

iii) The smaller the distance between the BODIPY cores interposed by the spacer, the lower became the fluorescence performance, even reducing the electron-releasing ability of the connector. This dependence was well-illustrated by analyzing the behavior of the bis-BODIPYs linked through the shortest bridges tested herein, such as the amino-linked (**4f** and **5f**) and *N*-acetylamino-linked (**4g** and **5g**) dyads. Thus, the connection of the 8-benzyl groups of the BODIPYs through an amine group implied a shortening of the spacer length and hence the disposition of the electronic clouds of the BODIPY subunits closer than in other synthetized dyads. In spite of this geometrical arrangement, no evidence of excitonic interaction was detected in the ground state, as supported by the unaltered profile of the absorption spectra (**Figure 2**), but it led to an effective deactivation on the fluorescence emission (down to 50% **Table 1**). This trend could be understood in terms of a higher probability of the spacer-induced ICT owing to the closer proximity of the electron-donor amine to the electron-acceptor BODIPY subunits (**Figure 4**). Nevertheless, this drastic decrease of the fluorescence signal could demonstrate an additional pathway of non-radiative deactivation, since an ICT could also be

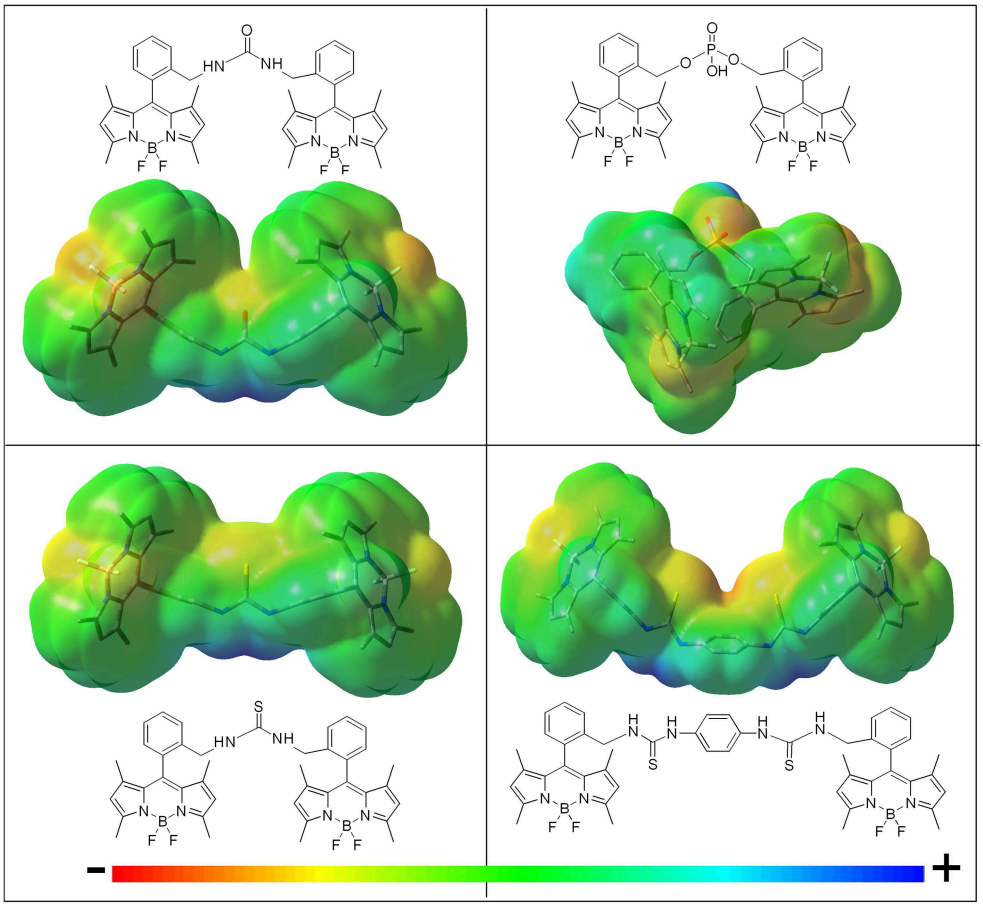

FIGURE 3 | Molecular electrostatic potential (MEP) maps of the bis-BODIPYs derived from building block **2** bearing different urea-based and phosphonate-based spacers (negative charge in red and positive charge in blue). Similar MEPs are computed for the corresponding analogs built on scaffold **3**.

promoted between the electronic clouds of the BODIPYs (Yu et al., 2015; Li et al., 2016) due to the mentioned proximity imposed by the amine-based spacers. This intramolecular deactivation process was what is known as photoinduced symmetry-breaking charge transfer (SBCT). According to the literature focusing on ICT processes in BODIPY dimers (Cakmak et al., 2011; Whited et al., 2012; Zou et al., 2017), the SBCT pathway has been seen to be characteristic of orthogonally disposed and directly linked BODIPY dyads, but also took place in non-orthogonal and electronically decoupled subunits through sterically hindered phenyl spacers (Liu et al., 2018). Moreover, these authors claimed that SBCT in bridged dimers did not lead to a triplet state population, as in directly linked and orthogonal dimers. In fact, no singlet oxygen generation from the triplet state of the bridged bis-BODIPYs tested herein was detected under any experimental conditions. Collectively, all these strands of evidence allowed us to state that the fluorescence deactivation in the amine-bridged bis-BODIPYs could be driven by the spacer-mediated ICT mechanism along with the aforementioned SBCT process.

iv) The insertion of more than one electron-donor group in the linker quenched the fluorescence more effectively, even if the connector imposed the highest distance between BODIPYs among all the structures synthesized herein. Accordingly, the increase in the number of thiourea groups at the linker on going from **4b** to **4c** reinforced the extension and effectiveness of the spacer-induced ICT process, reducing the fluorescence quantum yield from 51 to 40% (**Table 1**), in spite of the consequent lengthening of the linking unit, which separates the BODIPY electronic clouds further (the distance between molecular centers in the optimized geometries increased from 13.5 to 20.5 Å; **Figure 3**).

v) Compared to the dyads arising from the C2,C6-non-alkylated BODIPY **2**, the alkylation (ethylation) at positions C2 and C6 of each dipyrrin unit promoted a further enhancement of the fluorescence efficiency [e.g., dyads linked by thiourea moieties (**4b** vs. **5b**), from 51% on the non-ethylated derivatives (**4b**) to 76% for the fully substituted (**5b**) derivatives; **Table 1**]. In the dyads derived from the C2,C6-diethyl scaffold **3**, all the decay curves are properly analyzed as monoexponentials. Conversely, in the bis-BODIPYs based

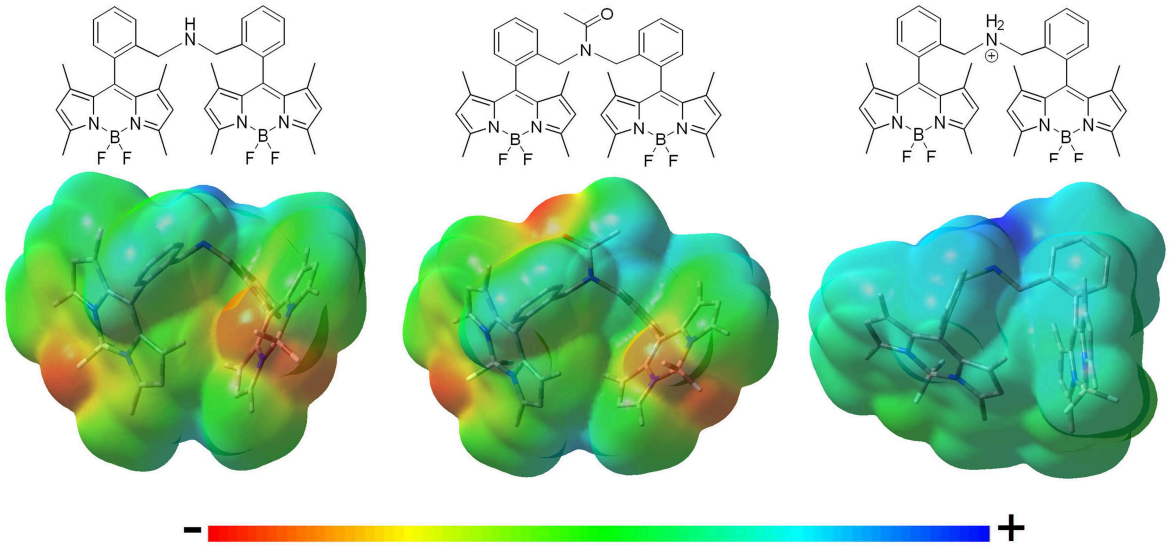

FIGURE 4 | Molecular electrostatic potential (MEP) maps of the bis-BODIPYs derived from building block **2** linked by different amine-based spacers (negative charge in red and positive charge in blue). Similar MEPs are computed for the corresponding analogs built on scaffold **3**.

on non-ethylated building block **2**, where the fluorescence efficiency decreased owing to the higher impact of the ICT, up to three exponentials were required to fit the corresponding decay curves (**Table 1**). This behavior was attributed to the inductive electron donor effect exerted by the alkyl moieties grafted to the BODIPY, which decreased the electron-withdrawing ability of the chromophoric core and consequently hampered the ICT probability from the corresponding spacer.

Effect of Solvent Polarity on ICT Stabilization

Owing to the capability of the spacer moieties to induce effective ICT processes, especially in combination with the electron-withdrawing character of the BODIPY core, the fluorescence emission of the new dyads depended markedly on the solvent polarity (**Figures 5**, **6**). Without exception, an increase of the solvent polarity led to a drastic decrease in the emission efficiency of all the dyads, so that in the most polar solvents such as acetonitrile, these systems could be considered as non-fluorescent, with quantum yields as low as 2%. Moreover, the fluorescence-quenching correlated with a drastic change in the fluorescence decay curves, since the time-resolved emission profile acquired a multi-exponential character, with the contribution of the shorter-lived component gaining prominence as the solvent polarity increased (**Tables S1**, **S2**). This trend also became modulated by the electron donor character of the molecular structure of these dyads. As we mentioned above, the full alkylation of the BODIPY core reduced its electron-withdrawing character, thereby weakening the solvent-sensitivity of the fluorescence emission (**Figures 5**, **6**). As a matter of fact, the fluorescence quantum yield of the thiourea-bridged bis-BODIPYs derived from **2** (i.e., **4b**) decreased from 51% in cyclohexane to just 8% in a more polar media such as acetonitrile, while a similar dyad derived from the fully-alkylated scaffold **3** (i.e., **5b**) retained an efficiency of 13% in the same polar solvent. Likewise, two structural factors imposed by the spacer moiety enhanced this fluorescence deactivation: (i) a further increase of the electron donor ability of the spacer, for instance, the emission quantum yield in acetonitrile on going from urea-bridged dyad **4a** to double thiourea-linked bis-BODIPY **4c** decreased from 16% to just 6% (**Figure 5**), and (ii) a shortening of the spacer bridge, activating both charge transfer mechanisms mentioned above (ICT and SBCT). Thus, the lowest fluorescence quantum yield in acetonitrile was recorded from amine-bridged bis-BODIPY dyads (2% for **4f** and **4g** arising from BODIPY **2**, and ≈10% for **5f** and **5g** derived from BODIPY **3**; **Figures 5**, **6**).

The Special Case of DMF

To obtain additional insight into the solvent-sensitive fluorescence of these dyads, we also analyzed their photophysical signatures in an electron-donating solvent such as DMF. Owing to high polarity of DMF [described by the Catalán polarity solvent scale (Catalán, 2009) as SdP = 0.977, similar to that of acetonitrile, 0.974], low fluorescence efficiency and a bi-exponential decay curve, dominated by a short lifetime component, should be expected as result of a further stabilization of the ICT process. However, the bis-BODIPYs obtained from both **2** and **3** skeletons and based on urea (**4a** and **5a**), thiourea (**4b** and **5b**), and double thiourea (**4c**) linkers exhibited fluorescence quantum yields higher than those recorded in less polar solvents like ethanol (**Figure 5**). This unusual behavior prompted by DMF should be related not only to its polarity but also to its electron-donor ability [basicity scale (Catalán, 2009)

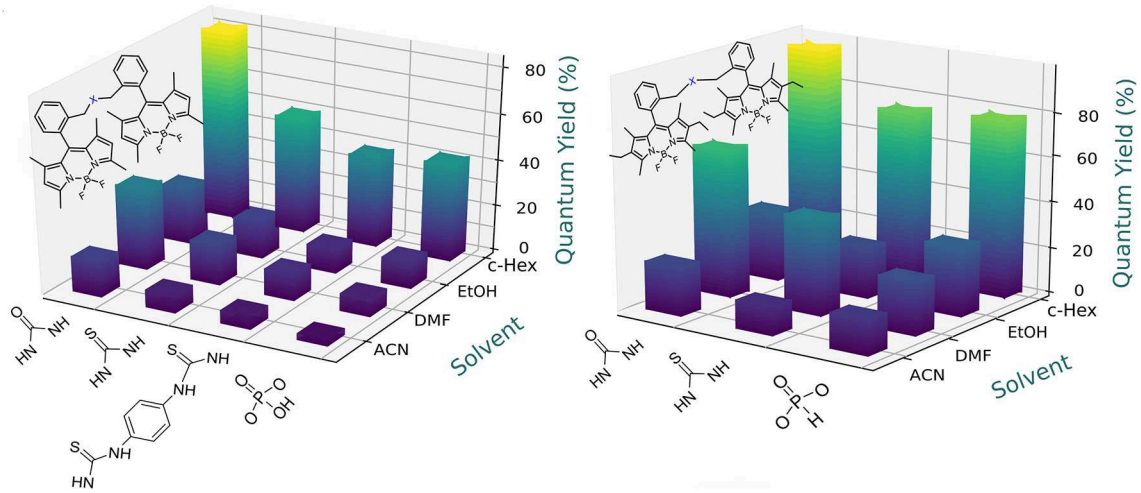

FIGURE 5 | Dependence of the fluorescence efficiency on the solvent polarity for the urea-based and phosphonate-based bridged bis-BODIPYs built on chromophoric scaffolds **2 (Left)** and fully alkylated **3 (Right)**. Full data are reported in **Tables S1**, **S2**.

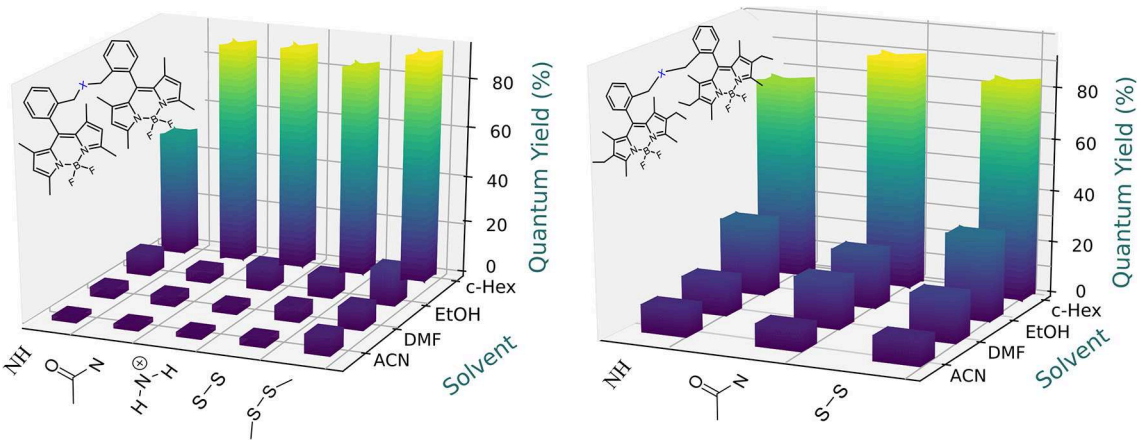

FIGURE 6 | Dependence of the fluorescence efficiency on the solvent polarity for the amine- and disulfur-based bridged bis-BODIPYs built on chromophoric scaffolds **2** (left) and **3** (right). Full data are reported in **Tables S1**, **S2**.

SB = 0.613], the highest among the solvents selected herein. The basicity of DMF could induce specific interactions between this hydrogen-bond-acceptor solvent and the proton of these linkers so long as the electron lone pair of the latter was mainly located on the amine moiety and less shifted toward the oxygen atom. In agreement with this, the positive charge (see the blue color in **Figure 3**) was mostly located around the nitrogen atoms of the spacer, highlighting this position as the most suitable for interaction with electron donor solvents. These interactions must have decreased the electron donor capacity of the urea-based bridges and, hence, have efficiently hampered the probability of the ICT process. Therefore, the fluorescence recorded in DMF arose from the balance between two opposite effects: the intrinsic polarity-induced stabilization of the charge separation counterbalanced by the high basicity of DMF. This last specific interaction hindered the ICT population and yielded higher fluorescence efficiencies and larger lifetimes than those expected in this polar solvent (**Tables S1**, **S2**). Two further experimental trends confirmed this hypothesis: on the one hand, the enhancement of the fluorescence efficiency induced by DMF decreased in the bis-BODIPYs grafted by urea > thiourea > double thiourea bridges (**Figure 5**) and, on the other hand, this enhancement was no longer recorded with the other spacer moieties selected herein (**Figure 6**). In these latter dyads, the corresponding fluorescence quantum yield decreased according to the polar character of the solvent once the specific interaction of the DMF with the spacer was no longer taking place, probably due to the absence of ionizable hydrogen atoms flanking the spacer moiety, as happened in the urea-based linkers.

Excitonic Coupling Induced by an Ether Spacer

The absorption profiles of the ether-bridged bis-BODIPYs (**4k** and **5k**) were noticeably different with respect to those

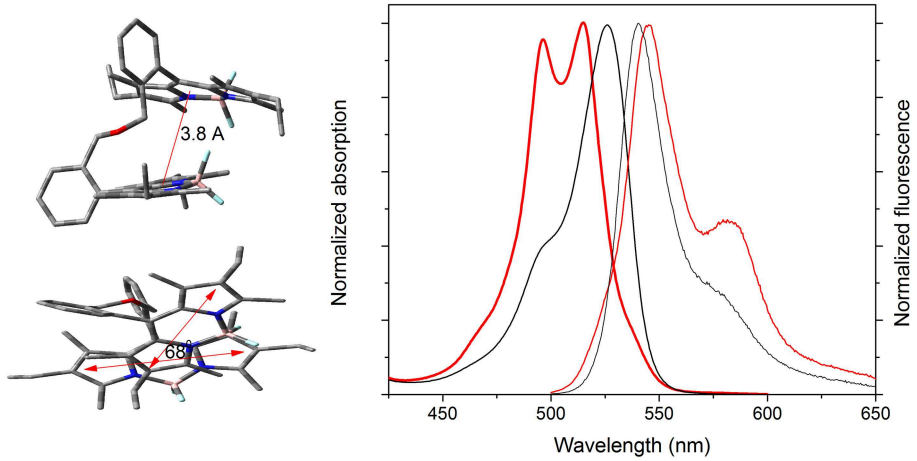

FIGURE 7 | Normalized absorption (thick line) and fluorescence (thin line) spectra of the ether-bridged bis-BODIPY **5k** and its corresponding amino-bridged analog **5f** (black line) in cyclohexane. The optimized ground state geometry of the former bis-BODIPY is also included in different views to highlight the feasible excitonic coupling between the transition dipole moments oriented along the longitudinal molecular axis.

recorded from their analog amine-bridged dyads (**Figure 7**, **Figure S1**). Regardless of the solvent, the absorption spectrum was hypsochromically shifted with respect to the rest of the bis-BODIPYs and also split into two peaks of similar intensity (**Figures S60**, **S61**). This deep disruption of the absorption profile pointed to intramolecular excitonic interaction between the BODIPY subunits. Indeed, the optimized geometry (**Figure 7**) revealed that the oxygen hybridization left the chromophoric subunits very close together (around 3.8 Å) and almost in a twisted cofacial arrangement (a dihedral angle between the transition dipole moments of 68°). This geometrical arrangement could promote excitonic interactions between the BODIPY electronic clouds (see the feasible overlap between one pyrrole and the central ring of the other BODIPY, **Figure 7**). According to the exciton theory, the growth of new absorption bands at higher energies is indicative of head-to-head interactions between the transition dipole moment (intramolecular H type aggregate), favored by the stated mutual disposition of the chromophoric units. However, this excitonic coupling provides forbidden transitions from the excited state (H aggregates are usually non-emissive). In contrast, these bis-BODIPYs displayed strong fluorescence bands, slightly red-shifted with respect to other dyads and with a marked shoulder at 580 nm (**Figure 7**). Moreover, in an apolar solvent like cyclohexane, the fluorescence turned out to be highly efficient (around 80%, **Table 2**) with surprising long lifetimes (up to 19 ns in both dyads; **Figure 8**, **Figure S2**). In this regard, the excitation and fluorescence spectra, as well as the fluorescence quantum yield and lifetime, became almost independent on the emission or/and the excitation wavelengths. All these photophysical properties could be consistent with excimer formation (long lifetimes are a fingerprint of excimer emission) upon excitation of these BODIPY dyads. Therefore, the mutual parallel and cofacial arrangement of the BODIPY units inside these dyads could enable a π-π stacking in the ground state, which led to the recorded split of the absorption bands at higher energies and, upon excitation, to subsequent geometrical rearrangement leading to the emission from intramolecular excimer species.

TABLE 2 | Photophysical properties of the ether-bridged bis-BODIPYs in different solvents.

	λ_{ab} (nm)	$\varepsilon_{max} \cdot 10^{-4}$ (M^{-1} cm^{-1})	λ_{fl} (nm)	φ	τ (ns)
4k					
ACN	475.0/490.5	14.6/13.4	520.5	0.01	0.02 (81%)–2.26 (19%)
DMF	478.0/493.0	14.7/13.2	522.5	0.01	0.03 (81%)–2.09 (11%)–3.00 (8%)
EtOH	476.5/497.5	15.1/12.8	521.0	0.03	0.13 (63%)–2.00 (37%)
c-hex	477.5/492.5	16.0/12.6	521.5	0.82	19.29
5k					
ACN	495.5/514.0	13.6/12.7	545.0	0.06	3.36 (26%)–5.52 (74%)
DMF	497.0/515.5	13.0/13.1	546.0	0.15	7.00
EtOH	496.0/514.5	14.0/13.3	545.5	0.29	10.11
c-hex	496.5/515.0	14.1/14.9	545.0	0.84	19.34

c-hex, cyclohexane; EtOH, ethanol; DMF, dimethylformamide; ACN, acetonitrile. Absorption (λ_{ab}) and fluorescence (λ_{fl}) wavelength, molar absorption at the maximum (ε_{max}), fluorescence quantum yield (φ), and lifetime (τ).

Regarding the fluorescence efficiency and lifetime, the ether-bridged dyads **4k** and **5k** exhibited similar dependence on the solvent polarity to that previously described for the other BODIPY dyads herein synthesized (**Table 2** vs. **Table 1**). Therefore, in spite of the excimer formation, the emission of the ether-dyads was still mediated by an ICT process. However, and with respect to other moieties acting as BODIPY linkers, the lower electron release of the ether bridge should significantly reduce its ability to promote ICT itself. Hence, we hypothesized that the intramolecular charge transfer had to take place mainly through other mechanisms, such as an SBCT process and the

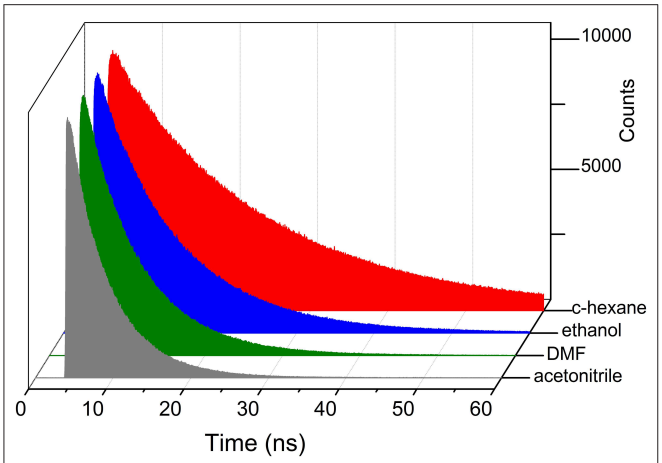

FIGURE 8 | Fluorescence decay curves of **5k** with increasing solvent polarity.

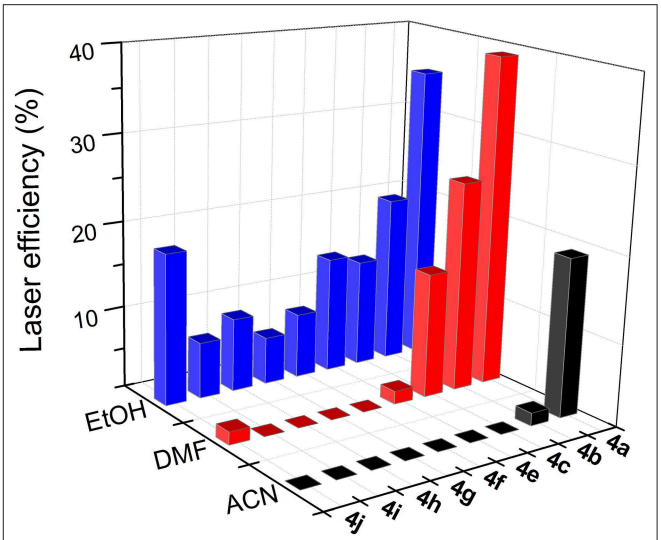

FIGURE 9 | Dependence of lasing efficiency on solvent polarity in the bis-BODIPYs derived from building block **2**.

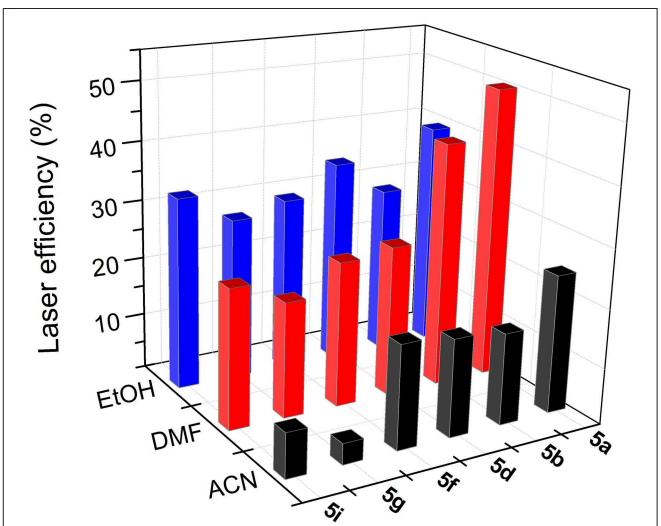

FIGURE 10 | Dependence of lasing efficiency on solvent polarity in the bis-BODIPYs derived from building block **3**.

so-called intervalence charge transfer (IVCT), invoked by some authors to account for the emission behavior recorded from closely packed intramolecular BODIPY dimers (Benniston et al., 2010), the cofacial arrangement of which led also to effective excimer formation. The significant influence of the bridging moiety on the emission behavior of BODIPY dyads, as well as its solvent-sensitivity, highlighted the complexity of the molecular dynamics upon excitation, which involved an effective excitonic coupling and the ensuing formation of an emissive excimer coexisting with an effective ICT process in polar media.

Laser Properties of Bridged bis-BODIPYs

According to the absorption properties of the new bis-BODIPYs, their lasing properties were studied under pumping at 355 nm (dyads derived from scaffold **2**) and 532 nm (dyads derived from scaffold **3**). All the dyes studied in this work exhibited broad-line-width laser emission, with a pump threshold energy of ~0.8 mJ, divergence of 5 mrad, and a pulse duration of 8 ns full-width at half maximum (FWHM), placed in a simple plane-plane non-tunable resonator cavity. The laser emission peaked at ca. 541 and 563 nm for the dyads derived from scaffolds **2** and **3**, respectively. Following the photophysical analysis, the actual effect of the solvent on the dye laser action was analyzed for solutions of polar and apolar solvents. Although the photophysical studies showed that the new derivatives exhibited their highest fluorescence capacity when dissolved in apolar solvents such as cyclohexane (**Figures 5**, **6**), the low solubility of BODIPY dyes in this solvent prevented the concentrated solutions required for laser experiments from being attained. To analyze the dependence of the laser action on the medium polarity, we then carried out the experiments in solvents of increasing polarity enabling at the same time good solubility of the new dyes, such as ethanol, DMF, and acetonitrile.

To optimize the laser action of the new dyes in the different solvents, we first analyzed the dependence of their lasing properties on dye concentration in an ethanolic solution by varying the optical densities over an order of magnitude while keeping all other experimental parameters constant (see experimental section Laser Properties). It should be noted that the optimal concentration for these bis-BODIPYs was about three-fold lower than those required to induce effective laser action in similar commercial BODIPYs (PM546 and PM567) as well as in their mono-BODIPY precursors (scaffolds **2** and **3**) (Del Río et al., 2017). The lasing behavior of the new compounds (**Figures 9**, **10**) agreed with their photophysical properties, with the fluorescence quantum yield and the lasing efficiency showing a similar dependence on the solvent polarity and the substitution pattern of the BODIPY core as well as the spacer moiety:

i) The higher the polarity of the solvent, the lower the lasing efficiency became; for the same skeleton and spacer, the lowest laser efficiency was always registered in acetonitrile.
ii) The higher the degree of substitution in the BODIPY core, the higher the emission efficiency became. Therefore, for the same solvent and spacer, the laser efficiencies recorded for dyads derived from scaffold **2** were consistently lower than those displayed by dyads built on the fully alkylated BODIPY **3**.
iii) The ability of DMF to induce specific interactions with the dyads linked by urea and thiourea bridges led to a significant increase in the laser efficiency with respect to those recorded in a less polar solvent such as ethanol. In fact, the highest lasing efficiencies among all the targets synthesized herein were recorded from the dyads **5a** (52%) and **5b** (42%) built on scaffold **3** with urea and thiourea as linkers.
iv) Shortening the spacer and/or reducing its electron donor ability impaired the laser action significantly. Thus, dyads built on scaffold **2** and linked by moieties **d-j** only showed effective laser emission in ethanol, not becoming laser emitters in more polar solvents such as acetonitrile. This is not the case of the derivatives from skeleton **3,** which maintained laser emission, even in acetonitrile, although, depending on the **d-j** spacer, the efficiency could be just 4%.

An important parameter for any practical applications of these bis-BODIPYs was their lasing photostability under hard radiation conditions and long operation times. A reasonable evaluation of the photostability of these dyads can be obtained by irradiating a small amount of ethanolic solution with exactly the same pumping energy and geometry as used in the laser experiments and monitoring the evaluation of the laser-induced fluorescence intensity with respect to the number of pump pulses under transversal excitation at 355 and 532 nm, with 5 mJ/pulse and a 10-Hz repetition rate after 100,000 pump pulses (see experimental section Laser Properties). To properly compare the behavior of the new dyads, the lasing photostabilities of commercial PM546 and PM567 as scaffolds of the new bis-BODIPY derivatives were also analyzed under otherwise identical experimental conditions. Both commercial dyes displayed good photostability under drastic pumping conditions, with the laser emission losing 50 and 25% of its efficiency, respectively, after 100,000 pump pulses at a 10-Hz repetition rate. Nevertheless, the laser action of the bis-BODIPYs derived from such commercial dyes was superior, with high lasing efficiencies and no signs of degradation under the same pumping conditions.

The main result that draws our attention is the capacity of the bis-BODIPYs to lase with high efficiency and photostability, although their fluorescence quantum yields in ethanol never exceeded 30% (see **Figures 5**, **6**). Rational design linking the BODIPY units in these bis-BODIPYS is key in accounting for their lasing behavior. On the one hand, it enables an absorption increase at the pumping wavelength, which leads to a significant decrease in the dye concentration in the active medium, drastically reducing deleterious effects such as reabsorption/reemission and aggregation processes, which becomes particularly important when highly concentrated solutions are required to induce efficient laser emission. On the other hand, the ongoing ICT process leads to a short fluorescence lifetime, which allows radiative rate constants similar to that observed for other BODIPY dyes to be reached. These facts account for the origin and unique features of the laser behavior of these bis-BODIPYs.

CONCLUSIONS

The length and stereoelectronic properties of the spacer linking the chromophoric building blocks in the symmetric bridged bis-BODIPYs designed herein played a key role in their photophysical and laser signatures. The computationally assisted spectroscopic characterization carried out herein unambiguously revealed the complex and intriguing excited state dynamics induced in these new multichromophoric systems. In fact, the photonic behavior (fluorescence and lasing efficiency) of all the tested BODIPY dyads became highly sensitive to the solvent polarity owing to the activation of ICT processes, whose effectiveness and mechanism strongly depended on the moiety acting as a spacer. We highlight that even with non-polar solvents, the connector moiety modulated the emission efficiency as follows: the higher the electron donor ability of the linker, and/or the smaller the distance between the BODIPY cores interposed by the spacer, the lower the emission efficiency and photostability became. Furthermore, up to three potential charge transfer mechanisms could be promoted by the different moieties acting as linkers in these BODIPY dyads: direct ICT between the spacer and the BODIPY core and/or a photoinduced symmetry breaking charge transfer (SBCT) and/or an intervalence charge transfer (IVCT) in closely-packed dyads, the extension and balance of which defined the final properties of these symmetric BODIPY dyads. Besides, some spacers were also able to promote intramolecular excitonic coupling, leading to an excimer-like emission. Collectively, the present work represents a breakthrough in the complex relationship between the molecular structure and the photophysical signatures of multichromophoric systems, providing key guidelines to rationalize the design of tailored photonic materials for advanced applications.

EXPERIMENTAL SECTION

General Experimental Methods

All solvents and reagents were obtained commercially and used as received unless stated otherwise. Residual water was removed from starting compounds by repeated coevaporation with toluene. Reactions were executed at ambient temperatures unless stated otherwise. All moisture-sensitive reactions were performed in dry flasks fitted with glass stoppers or rubber septa under a positive pressure of argon. Anhydrous $MgSO_4$ or Na_2SO_4 was used to dry organic solutions during workup, and evaporation of the solvents was performed under reduced pressure using a rotary evaporator. Flash column chromatography was performed using 230–400 mesh silica gel. Thin-layer chromatography was conducted on a Kieselgel 60 F254. Spots were observed under UV irradiation (254 nm). ^{1}H, ^{13}C, ^{19}F, and ^{31}P NMR spectra were recorded in $CDCl_3$

or CD_3OD at 300, 400, or 500 MHz, 75, 101, or 126, 376, and 161.97 MHz, respectively. Chemical shifts are expressed in parts per million (δ scale) downfield from tetramethylsilane and are referenced to residual protium in the NMR solvent ($CHCl_3$: δ 7.25 ppm; CD_3OD: 4.870 ppm). Mass spectra were recorded by direct injection with an Accurate Mass Q-TOF LC/MS spectrometer equipped with an electrospray ion source in positive mode.

Compounds **2**, **3, 6a, 7a**, and **7b** were prepared following the methods described in Del Río et al. (2017). A full detailed description of the synthesis protocols for the preparation of the required monomeric BODIPY units **6b**, **8a**, **8b**, **9a**, **9b**, **10b**, **11a**, **11b,** and **12**, along with the characterization and copies of NMR spectra of all products, is included in the **Supplementary Material**.

General Procedures for the Preparation of Symmetrical bis-BODIPYs

Urea-Bridged bis-BODIPYs

The appropriate azidomethyl-BODIPY **7** (0.2 mmol) was added at room temperature to a mixture of 1M triethylammonium hydrogen carbonate buffer (0.44 mmol) and 1,4-dioxane (1.0 mL). Next, triphenylphosphine (0.026 mmol) was added, and the resulting mixture was stirred at room temperature. The reaction progress was monitored by TLC. After the disappearance of the starting material, the solvent was evaporated *in vacuo* to dryness. The residue was then purified by flash chromatography on silica gel (hexane-ethyl acetate 8:2).

Thiourea-Bridged bis-BODIPYs

The appropriate BODIPY-isothiocyanate **10** (0.1 mmol) was dissolved in 1,4-dioxane (2 mL) and treated with the corresponding azidomethyl-BODIPY **7** (0.1 mmol), water (0.5 mL), and triphenylphosphine (0.15 mmol). The resulting solution was stirred under argon at room temperature for 24 h and then concentrated. The ensuing residue was then purified by chromatography on silica gel (hexane-ethyl acetate 7:3).

Phosphonate-Bridged bis-BODIPYs

The appropriate BODIPY-isothiocyanate **10** (0.1 mmol) was dissolved in 1,4-dioxane (2 mL) and treated with the corresponding azidomethyl-BODIPY **7** (0.1 mmol), water (0.5 mL), and triphenylphosphine (0.15 mmol). The resulting solution was stirred under argon at room temperature for 24 h and then concentrated. The ensuing residue was then purified by chromatography on silica gel (hexane-ethyl acetate 7:3).

Phosphate-Bridged bis-BODIPYs

Iodine (0.15 mmol) and water (30 μL) were added to a cooled solution (0°C) of H-phosphonate (0.05 mmol) in pyridine (1 mL). The reaction mixture was allowed to warm to room temperature and stirred for 1 h. The crude was then poured into a saturated solution of sodium sulfite (10 mL) and extracted with AcOEt (3 × 20 mL). The combined organic solutions were washed with HCl 5%, dried, and concentrated. The resulting crude mixture was purified by chromatography on silica gel (CH_2Cl_2-MeOH; 9:1).

Amine-Bridged bis-BODIPYs

A mixture of the corresponding aldehyde **6** (0.06 mmol) and the appropriate amine **9** (1 equiv.) was refluxed overnight in methanol (3 mL) under argon. The mixture was then concentrated *in vacuo*. The residue was dissolved in acetic acid (3 mL), and sodium cyanoborohydride (3 equiv.) was added. The reaction mixture was stirred at room temperature for 24 h and then concentrated, and the residue was purified by chromatography on silica gel (hexane-ethyl acetate 85:15).

Acetamide-Bridged bis-BODIPYs

Ac_2O (10 equiv.) was added to a stirred solution of aminomethyl dimer **4f** or **5f** (0.012 mmol) in pyridine (2 mL). The reaction mixture was stirred at room temperature overnight and then concentrated. The resulting crude mixture was purified by chromatography on silica gel (hexane-ethyl acetate; 8:2).

Ammonium-Bridged bis-BODIPYs

The corresponding ***amine-bridged bis-BODIPYs*** dissolved in diethyl ether under argon was added to a solution of tetrafluoroboric acid (0.034 mmol) in diethyl ether (3 mL). The mixture was stirred for 20 min. The precipitate was filtered and extensively washed with diethyl ether.

Disulfide-Bridged bis-BODIPYs

The appropriate thioacetate, **11a**, **11b**, or **12SAc** (see **Supplementary Material**) (0.11 mmol), was dissolved in $^{i}PrOH$ (3 mL), and K_2CO_3 (2 equiv.) was added. After stirring for 24 h, the mixture was poured into 10 mL of water and extracted with CH_2Cl_2 (3 × 20 mL); the organic layer was dried over sodium sulfate and concentrated. The crude reaction mixture was purified by flash chromatography (hexane-ethyl acetate 8:2).

Ether-Bridged bis-BODIPYs

The appropriate formyl-BODIPY **6** (0.07 mmol), dissolved in anhydrous CH_2Cl_2 (3 mL) under an argon atmosphere, was treated with triethylsilane (0.035 mmol) and indium trichloride (0.07 mmol). After stirring for 24 h, the mixture was washed with sodium bicarbonate and extracted with CH_2Cl_2 (3 × 20 mL), and the organic layer was dried over sodium sulfate and concentrated. The crude was purified by flash chromatography (hexane-ethyl acetate 98:2).

Characterization Data of bis-BODIPYs

Urea-dimer (4a): Obtained from azide **7a** according to procedure A. (Yield = 36 mg, 95 %;) m. p. 92–93°C ^{1}H NMR (300 MHz, $CDCl_3$) δ 7.57–7.29 3 (m, 6H), 7.21–7.07 (m, 2H), 5.94 (s, 4H), 4.59 (t, J = 6.2 Hz, 2H), 4.14 (d, J = 6.1 Hz, 4H), 2.51 (s, 12H), 1.33 (s, 12H). ^{13}C NMR (75 MHz, $CDCl_3$) δ 158.1, 156.1, 143.4, 140.8, 137.6, 133.2, 131.2, 130.0, 128.8, 128.8, 128.5, 128.3, 121.8, 42.5, 14.9, 14.3. HRMS (ESI-TOF): calcd for $C_{41}H_{42}B_2F_4ONaN_6$: $[M + Na]^+$ 755.3440, found 755.3382.

Urea-dimer (5a): Obtained from azide **7b** according to procedure A. (Yield = 38 mg, 90 %); m. p. 96–98°C; ^{1}H NMR (400 MHz, $CDCl_3$) δ 7.49–7.30 (m, 4H), 7.28–7.24 (m, 2H), 7.14–7.00 (m, 2H), 4.67–4.48 (m, 2H), 4.16–3.96 (m, 4H), 2.40 (s, 12H), 2.17 (q, J = 7.5 Hz, 8H), 1.16 (s, 12H), 0.86 (t, J =

7.6 Hz, 12H); ^{13}C NMR (101 MHz, $CDCl_3$) δ 157.7, 153.9, 138.8, 138.3, 137.5, 133.6, 133.0, 130.1, 129.3, 128.4, 127.8, 42.2, 17.0, 14.5, 11.1. HRMS (ESI-TOF): calcd for $C_{49}H_{58}B_2F_4N_6NaO$: $[M + Na]^+$ 867.47022, found 867.46969.

Thiourea-dimer (4b): Obtained from azide **7a** and isothiocyanate **10a** according to procedure B. (Yield = 24 mg, 65%); m. p. 152–153°C; ^{1}H NMR (300 MHz, $CDCl_3$) δ 7.44–7.39 (m, 6H), 7.19–7.12 (m, 2H), 6.02 (t, J = 6.3 Hz, 2H), 5.95 (s, 4H), 4.49 (d, J = 5.9 Hz, 4H), 2.49 (s, 12H), 1.34 (s, 12H); ^{13}C NMR (75 MHz, $CDCl_3$) δ 183.6, 155.9, 143.2, 140.1, 135.8, 133.1, 130.9, 129.7, 129.1, 128.4, 128.3, 121.6, 46.0, 14.6, 14.2. HRMS (ESI-TOF): calcd for $C_{41}H_{42}B_2F_4SNaN_6$: $[M + Na]^+$ 771.3212, found 771.3177.

Thiourea-dimer (5b): Obtained from azide **7b** and isothiocyanate **10b** according to procedure B. (Yield = 25 mg, 58%); ^{1}H NMR (400 MHz, $CDCl_3$) δ 7.48–7.31 (m, 6H), 7.17 (dt, J = 7.3, 1.0 Hz, 2H), 5.80 (t, J = 6.3 Hz, 2H), 4.45 (d, J = 6.2 Hz, 4H), 2.45 (s, 6H), 2.25 (q, J = 7.5 Hz, 4H), 1.26 (s, 6H), 0.94 (t, J = 7.5 Hz, 6H); ^{13}C NMR (126 MHz, $CDCl_3$) δ 179.1, 154.3, 154.1, 138.9, 138.7, 138.4, 137.6, 133.7, 133.4, 133.2, 130.3, 130.2, 129.5, 128.9, 128.8, 128.6, 128.1, 128.0, 42.3, 29.5, 17.2, 14.7, 11.3. HRMS (ESI-TOF): calcd for $C_{49}H_{58}B_2F_4N_6NaS$: $[M + Na]^+$ 883.4464, found 883.4437.

Thiourea-bridged bis-BODIPY (5c). Obtained from BODIPY-isothiocyanate **10a** and 1,4-phenylenediamine (1.5 equiv). (Yield = 25 mg, 45%); m. p. 175–176°C; ^{1}H NMR (500 MHz, $CDCl_3$) δ 7.74–7.69 (m, 2H), 7.48–7.41 (m, 6H), 7.38 (ddd, J = 7.8, 7.6,1.3 Hz, 2H), 7.15 (dd, J = 7.6, 1.4 Hz, 2H), 6.86–6.80 (m, 2H), 6.63–6.57 (m, 2H), 6.06–5.98 (m, 2H), 5.90 (s, 4H), 4.76 (d, J = 6.2 Hz, 4H), 2.54 (s, 12H), 1.28 (s, 12H); ^{13}C NMR (75 MHz, $CDCl_3$) δ 181.8, 156.0, 146.4, 142.8, 139.4, 135.2, 133.8, 130.8, 130.0, 129.7, 128.6, 127.5, 125.8, 116.0, 46.4, 14.8, 14.2. HRMS (ESI-TOF): calcd for $C_{48}H_{49}B_2F_4S_2N_8$: $[M + H]^+$ 899.3644, found 899.3680.

H-phosphonate-dimer (4d): Obtained from alcohol **2** and PBr_3 according to procedure C. (Yield = 175 mg, 48%); ^{1}H NMR (500 MHz, $CDCl_3$) δ 7.58–7.44 (m, 6H), 7.27–7.22 (m, 2H), 6.59 (d, J = 707 Hz, 1H), 5.95 (s, 4H), 4.96–4.82 (m, 4H), 2.54 (s, 12H), 1.30 (s, 6H), 1.29 (s, 6H); ^{13}C NMR (125 MHz, $CDCl_3$) δ 156.1, 142.9, 138.4, 133.7, 133.1, 130.9, 129.8, 129.6, 129.4, 128.5, 121.6, 121.5, 64.5, 64.4, 14.6, 13.8; ^{31}P NMR (161.97 MHz, $CDCl_3$) δ 9.18.

H-phosphonate-dimer (5d): Obtained from alcohol **3** and PBr_3 according to procedure C. (Yield = 189 mg, 52%); ^{1}H NMR (500 MHz, $CDCl_3$) 7.54–7.41 (m, 6H), 7.26–7.20 (m, 2H), 6.61 (d, J = 707.0 Hz, 1H), 5.00–4.85 (m, 4H), 2.52 (s, 12H), 2.26 (q, J = 7.5 Hz, 8H), 1.20 (s, 6H), 1.19 (s, 6H), 0.95 (t, J = 7.5 Hz, 12H). HRMS (ESI-TOF): calcd for $C_{48}H_{61}B_2F_4N_5O_3P$: $[M+NH_4]^+$ 884.46442, found: 884.46722. calcd for $C_{48}H_{57}B_2F_4N_4NaO_3P$: $[M+Na]^+$ 889.41981, found: 889.41976.

Phosphate-dimer (4e). Obtained from H-phosphonate bis-BODIPY **4d** according to procedure D. (Yield = 13.5 mg, 65%). ^{1}H NMR (500 MHz, $CDCl_3$) δ 7.62–7.51 (m, 3H), 7.34–7.24 (m, 3H), 7.13–7.05 (m, 2H), 5.81 (m, 4H), 4.69–4.49 (m, 4H), 2.47 (s, 12H), 1.18 (s, 12H); ^{31}P NMR (161.97 MHz, $CDCl_3$) δ −2.16.

Amine-dimer (4f): Obtained from aldehyde **6a** and amine **9a** according to procedure E. (Yield = 97.3 mg, 45%); ^{1}H NMR (500 MHz, $CDCl_3$) δ 7.47–7.31 (m, 6H), 7.15–7.13 (m, 2H), 5.94 (s, 4H), 3.62 (s, 4H), 2.54 (s, 12H), 1.27 (s, 12H); ^{13}C NMR (125 MHz, $CDCl_3$) δ 155.6, 142.9, 140.6, 137.8, 133.7, 131.2, 129.5, 128.3, 128.2, 127.9, 121.4, 50.8, 14.7, 13.9. HRMS (ESI-TOF): calcd for $C_{40}H_{42}B_2F_4N_5$: $[M+H]^+$ 690.35625, found: 690.35814.

Amine-dimer (5f): Obtained from aldehyde **6b** and amine **9b** according to procedure E. (Yield = 15.4 mg, 40%); ^{1}H NMR (500 MHz, $CDCl_3$) 7.45–7.30 (m, 6H), 7.14–7.12 (m, 2H), 3.62 (s, 4H), 2.51 (s, 12H), 2.27 (q, J = 7.5 Hz, 8H), 1.18 (s, 12H), 0.94 (t, J = 7.5 Hz, 12H); ^{13}C NMR (125 MHz, $CDCl_3$) 153.8, 138.9, 138.1, 138.0, 134.5, 132.9, 130.4, 129.3, 128.5, 128.0, 127.7, 50.6, 17.2, 14.7, 12.6, 11.2). HRMS (ESI-TOF): calcd for $C_{48}H_{58}B_2F_4N_5$: $[M+H]^+$ 802.48243, found: 802.48314.

Acetamide-dimer (4g): Obtained from amine-bridged bis-BODIPY **4f** according to procedure F. (Yield = 4.5 mg, 85%); ^{1}H NMR (500 MHz, $CDCl_3$) δ 7.50 (m, 1H), 7.44–7.38 (m, 2H), 7.34 (m, 1H), 7.20 (m, 1H), 7.14–7.11 (m, 2H), 5.95 (s, 2H), 5.93 (s, 2H), 4.36 (s, 2H), 4.31 (s, 2H), 2.54 (s, 6H), 2.51 (s, 6H), 1.96 (s, 3H), 1.28 (s, 6H), 1.21 (s, 6H); ^{13}C NMR (125 MHz, $CDCl_3$) δ 171.6, 156.4, 155.8, 143.1, 142.3, 139.8, 139.0, 134.2, 133.9, 133.1, 132.8, 130.7, 130.6, 130.5, 129.9, 129.2, 128.8, 128.7, 128.1, 126.5, 126.2, 121.7, 121.4, 51.5, 49.6, 21.0, 14.8, 14.7, 14.0, 13.9. HRMS (ESI-TOF): calcd for $C_{40}H_{43}B_2F_4N_5NaO$: $[M+Na]^+$ 754.34957, found: 754.35211.

Acetamide-dimer (5g): Obtained from amine-bridged bis-BODIPY **5f** according to procedure F. (Yield = 9.1 mg, 90%); ^{1}H NMR (500 MHz, $CDCl_3$) δ 7.47 (td, J = 7.6, 1.4 Hz, 1H), 7.41 (td, J = 7.6, 1.3 Hz, 1H), 7.37 (dd, J = 7.5, 1.6 Hz, 1H), 7.34 (td, J = 7.5, 1.5 Hz, 1H), 7.22 (dd, J = 7.4, 1.4 Hz, 1H), 7.19 (dd, J = 7.8, 1.2 Hz, 1H), 7.16 (dd, J = 7.3, 1.6 Hz, 1H), 7.10 (dd, J = 7.7, 1.4 Hz, 1H), 4.43 (s, 2H), 4.36 (s, 2H), 2.53 (s, 6H), 2.52 (s, 6H), 2.30–2.24 (m, 8H), 1.86 (s, 3H), 1.23 (s, 6H), 1.16 (s, 6H), 0.95 (t, J = 7.6 Hz, 12H). HRMS (ESI-TOF): calcd for $C_{50}H_{59}B_2F_4N_5NaO_2$: [M+Na]+ 882.46991, found: 882.47366.

Ammonium-dimer (4h). Obtained from amine-bridged bis-BODIPY **4f** according to procedure G. (Yield = 10 mg, 80%); ^{1}H NMR (300 MHz, CD_3OD) δ 7.70 (m, 6H), 7.52 (d, J = 7.5 Hz, 2H), 6.12 (s, 4H), 4.21 (bs, 4H), 3.32 (s, 12H), 2.99 (d, J = 8.7 Hz, 2H), 2.53 (s, 12H). HRMS (ESI-TOF) (positive mode): calcd for $C_{40}H_{42}B_2F_4N_5$: $[M+H]^+$ 690.35625, found: 690.35822; HRMS (ESI-TOF) (negative mode): $[BF_4]^-$ 87.00326, found: 86.00634.

Disulfide-dimer (4i): Obtained from thiolacetate **11a** according to procedure H. (Yield = 18 mg, 40%); ^{1}H NMR (500 MHz, $CDCl_3$) δ 7.40–7.35 (m, 6H), 7.19–7.17 (m, 2H), 5.97 (s, 4H), 3.77 (s, 4H), 2.54 (s, 12H), 1.35 (s, 12H); ^{13}C NMR (125 MHz, $CDCl_3$) δ 155.9, 143.3, 139.5, 134.9, 134.3, 131.3, 131.0, 129.7, 128.7, 128.5, 121.5, 41.1, 14.8, 14.5. HRMS (ESI-TOF): calcd for $C_{40}H_{41}B_2F_4N_4S_2$: $[M+H]^+$ 739.29027, found: 739.28922. calcd for $C_{40}H_{44}B_2F_4N_5\ S_2$: $[M+NH_4]^+$ 756.31682, found: 756.31544; calcd for $C_{40}H_{40}B_2F_4N_4NaS_2$: $[M+Na]^+$ 761.27222, found: 761.27138.

Disulfide-dimer (5i): Obtained from thiolacetate **11a** according to procedure H. (Yield = 21 mg, 45%); ^{1}H NMR (500 MHz, $CDCl_3$) δ 7.40–7.33 (m, 6H), 7.19–7.17 (m, 2H), 3.76 (s, 4H), 2.51 (s, 12H), 2.29 (q, J = 7.5 Hz, 4H), 1.24 (s, 12H), 0.96 (t, J = 7.5 Hz, 6H).^{13}C NMR (125 MHz, $CDCl_3$) δ 154.2, 138.6, 137.9, 135.2, 135.0, 133.1, 130.8, 130.6, 129.4,

129.0, 128.3, 41.2, 17.2, 14.7, 12.7, 11.8. HRMS (ESI-TOF): calcd for $C_{48}H_{57}B_2F_4N_4S_2$: $[M+H]^+$ 851.41569, found: 851.41495; calcd for $C_{48}H_{60}B_2F_4N_5S_2$: $[M+NH_4]^+$ 868.44224, found: 868.44135; calcd for $C_{48}H_{56}B_2F_4N_4NaS_2$: $[M+Na]^+$ 873.39764, found: 873.39923.

Elongated disulfide-dimer (5j): Obtained from thiolacetate **12Sac** (see **Supplementary Material**) according to procedure H. (Yield = 14.5 mg, 42%); ^{1}H NMR (500 MHz, $CDCl_3$) 7.41(dt, J = 7.5, 1.5 Hz, 2H), 7.35–7.31 (m, 4H), 7.18–7.16 (m, 2H), 5.95 (s, 4H), 2.84 (dd, J = 8.9, 6.5 Hz, 4H), 2.60 (dd, J = 8.7, 6.7 HZ, 4H), 2.52 (s, 12H), 1.34 (s, 12H).^{13}C NMR (125 MHz, $CDCl_3$) δ 155.7, 142.8, 140.6, 137.4, 134.4, 131.3, 130.3, 129.5, 128.5, 127.5, 121.4, 37.2, 32.5, 14.7, 14.3. HRMS (ESI-TOF): calcd for $C_{42}H_{45}B_2F_4N_4S_2$: $[M+H]^+$ 767.32163, found 767.32171; calcd for $C_{42}H_{48}B_2F_4N_5S_2$: $[M+NH_4]^+$ 784.34818, found 784.34983.

Ether-dimer (4k): Obtained from aldehyde **6a** according to procedure I. (Yield = 8 mg, 56%); ^{1}H NMR (300 MHz, $CDCl_3$) δ 8.07–7.96 (m, 2H), 7.53–7.41 (m, 2H), 7.30 (t, J = 7.5 Hz, 2H), 7.07 (dd, J = 7.5, 1.3 Hz, 2H), 5.80 (s, 4H), 3.78 (s, 4H, 2.46 (s, 12H), 1.21 (s, 12H). HRMS (ESI-TOF): calcd for $C_{40}H_{41}B_2F_4N_4O$: $[M+H]^+$ 691.3403, found: 691.3389.

Ether-dimer (5k): Obtained from aldehyde **6b** according to procedure I. (Yield = 5 mg, 48%); ^{1}H NMR (300 MHz, $CDCl_3$) δ 7.99 (d, J = 7.7 Hz, 2H), 7.54–7.39 (m, 2H), 7.33–7.29 (m, 2H), 7.11–7.04 (m, 2H), 3.63 (s, 4H), 2.44 (s, 12H), 2.14 (q, J = 7.5 Hz, 8H), 1.08 (s, 12H), 0.84 (t, J = 7.5 Hz, 12H). HRMS (ESI-TOF): calcd for $C_{48}H_{57}B_2F_4N_4O$: $[M+H]^+$ 803.4655, found: 803.4639.

Spectroscopic Properties

Spectroscopic properties were registered in diluted solutions (around 2×10^{-6} M) prepared by adding the corresponding solvent (spectroscopic grade) to the residue from an adequate amount of a concentrated stock solution in acetone after vacuum evaporation of this solvent. UV-Vis absorption spectra were recorded on a Varian model CARY 4E spectrophotometer, whereas the fluorescence and excitation spectra were registered in an Edinburgh Instruments spectrofluorimeter (model FLSP 920), as were the decay curves. Fluorescence quantum yields (φ) were obtained using commercial BODIPYs in ethanol (PM546 φ_r = 0.85 and PM567 φ_r = 0.84) as a reference. The values were corrected by the refractive index of the solvent. Radiative decay curves were registered with the time-correlated single-photon counting technique using a multichannel plate detector with picosecond time resolution. Fluorescence emission was monitored at the maximum emission wavelength after excitation by means of a wavelength-tunable Fianium Supercontinuum laser. The fluorescence lifetime (τ) was obtained after the deconvolution of the instrumental response signal from the recorded decay curves by means of an iterative method. The decay curve was essentially the same regardless of the excited visible absorption band. The goodness of the exponential fit was controlled by statistical parameters (chi-square and the analysis of the residuals).

Quantum Mechanical Calculations

Ground state geometries were optimized at the Density Functional Theory (DFT) level using the range-separated hybrid wB97XD method and the triple-valence basis set with one polarization functions (6–311 g*). To check that the optimized geometries correspond to a true energy minimum, the corresponding frequency analysis was conducted (no negative value). The solvent effect (ethanol) was considered in the theoretical simulations by means of the Polarizable Continuum Model (PCM). All the calculations were performed using Gaussian 16 software as implemented in the computational cluster "arina" of the UPV/EHU.

Laser Properties

Liquid solutions of dyes were contained in 1-cm optical-path rectangular quartz cells carefully sealed to avoid solvent evaporation during the experiments. The liquid solutions were transversely pumped with 5-mJ, 8-ns FWHM pulses from the second harmonic (532 nm) and the third harmonic (355 nm) of a Q-switched Nd:YAG laser (Lotis TII 2134) at a repetition rate of 1 Hz. The exciting pulses were line-focused onto the cell using a combination of positive and negative cylindrical lenses (f = 15 cm and f = −15 cm, respectively) perpendicularly arranged. The plane-parallel oscillation cavity (2 cm length) consisted of a 90%-reflectivity aluminum mirror acting as the back reflector and the lateral face of the cell acting as output coupler (4% reflectivity). The pump and output energies were detected by a GenTec powermeter. The photostability of the dyes in ethanol was evaluated by using a pumping energy and geometry exactly equal to that of the laser experiments. We used spectroscopic quartz cuvettes with a 0.1 cm optical path to allow for the minimum solution volume (40 μL) to be excited. The lateral faces were grounded, whereupon no laser oscillation was obtained. Information about photostability was obtained by monitoring the decrease in laser-induced fluorescence (LIF) intensity after 100,000 pump pulses at a 10 Hz repetition rate to speed up the running of the experiment. The fluorescence emission and laser spectra were monitored perpendicular to the exciting beam, collected by an optical fiber, imaged onto a spectrometer (Acton Research corporation), and detected with a charge-coupled device (CCD) (SpectruMM:GS128B). The fluorescence emission was recorded by feeding the signal to the boxcar (Stanford Research, model 250) to be integrated before being digitized and processed by a computer. The estimated error in the energy and photostability measurements was 10%.

DATA AVAILABILITY STATEMENT

All datasets generated for this study are included in the article/**Supplementary Material**.

AUTHOR CONTRIBUTIONS

AO-S conducted the photophysical measurements, whereas RS-L carried out the theoretical calculations. JB supervised the joint experimental and theoretical study and drafted the manuscript. IG-M performed the laser measurements and provided a critical review of the whole manuscript. JL participated in the design of the BODIPY dimers and carried out some of the synthetic work.

CU participated in the design of the BODIPY dimers and carried out most of the synthetic work. AG designed the BODIPY dimers, participated in the synthetic work, and contributed to the final writing of the manuscript.

FUNDING

We gratefully acknowledge the Spanish Ministerio de Economia y Competitividad (MINECO) (MAT2017-83856-C3-1-P and 3-P; CTQ2015-66702-R), Ministerio de Economía y Competitividad (MINECO), and Fondo Europeo de Desarrollo Regional (FEDER) (CTQ2015-66702-R, MINECO/FEDER, UE), Ministerio de Ciencia, Innovación y Universidades (MCIU), Agencia Estatal de Investigación (AEI), Fondo Europeo de Desarrollo Regional (FEDER) (RTI2018-094862-B-I00, MCIU/AEI/FEDER, UE), and Gobierno Vasco (project IT912-16) for financial support. AO-S and RS-L thank UPV/EHU and Gobierno Vasco for a predoctoral fellowship and a postdoctoral contract, respectively.

ACKNOWLEDGMENTS

The authors thank SGIker resources of UPV/EHU for technical support with the computational calculations, which were carried out in the arina informatic cluster.

SUPPLEMENTARY MATERIAL

The Supplementary Material for this article can be found online at: https://www.frontiersin.org/articles/10.3389/fchem.2019.00801/full#supplementary-material

REFERENCES

Ahrens, J., Böker, B., Brandhorst, K., Funk, M., and Bröring, M. (2013). Sulfur-bridged BODIPY DYEmers. *Chem. Eur. J.* 19, 11382–11395. doi: 10.1002/chem.201300893

Ahrens, J., Scheja, A., Wicht, R., and Bröring, M. (2016). Excitonic coupling in acyclic and cyclic dithioaryl-linked BODIPY DYEmers. *Eur. J. Org. Chem.* 2864–2870. doi: 10.1002/ejoc.201600359

Alamiry, M. A. H., Benniston, A. C., Copley, G., Harriman, A., and Howgego, D. (2011). Intramolecular excimer formation for covalently linked boron dipyrromethene dyes. *J. Phys. Chem. A* 115, 12111–12119. doi: 10.1021/jp2070419

Alberto, M. E., De Simone, B. C., Russo, N., Sicilia, E., and Toscano, M. (2018). Can BODIPY dimers act as photosensitizers in photodynamic therapy? A theoretical prediction. *Front. Phys.* 6:143. doi: 10.3389/fphy.2018.00143

Arroyo-Córdoba, I. J., Sola-Llano, R., Epelde-Elezcano, N., López-Arbeloa, I., Martínez-Martínez, V., and Peña-Cabrera, E. (2018). Fully functionalizable β,β′-BODIPY dimer: synthesis, structure, and photophysical signatures. *J. Org. Chem.* 83, 10186–10196. doi: 10.1021/acs.joc.8b01429

Avellanal-Zaballa, E., Durán-Sampedro, G., Prieto-Castañeda, A., Agarrabeitia, A. R., García-Moreno, I., López-Arbeloa, I., et al. (2017). Rational molecular design enhancing the photonic performance of red-emitting perylene bisimide dyes. *Phys. Chem. Chem. Phys.* 19, 13210–13218. doi: 10.1039/C7CP01626C

Bañuelos, J. (2016). BODIPY dye, the most versatile fluorophore ever? *Chem. Rec.* 16, 335–348. doi: 10.1002/tcr.201500238

Benniston, A. C., Copley, G., Harriman, A., Howgego, D., Harrington, R. W., and Clegg, W. (2010). Cofacial boron dipyrromethene (BODIPY) dimers: synthesis, charge delocalization, and exciton coupling. *J. Org. Chem.* 75, 2018–2027. doi: 10.1021/jo1000803

Blázquez-Moraleja, A., Cerdán, L., García-Moreno, I., Avellanal-Zaballa, E., Bañuelos, J., Jimeno, M. L., et al. (2018). Sterochemical and steric control of photophysical and chiroptical properties in bichromophoric systems. *Chem. Eur. J.* 24, 3802–3815. doi: 10.1002/chem.201705698

Boens, N., Verbelen, B., and Dehaen, W. (2015). Postfunctionalization of the BODIPY core: synthesis and spectroscopy. *Eur. J. Org. Chem.* 6577–6595. doi: 10.1002/ejoc.201500682

Cakmak, Y., Kolemen, S., Duman, S., Dede, Y., Dolen, Y., Kilic, B., et al. (2011). Designing excited states: theory-guided access to efficient photosensitizers for photodynamic action. *Angew. Chem.* 50, 11937–11941. doi: 10.1002/anie.201105736

Catalán, J. (2009). Toward a generalized treatment of the solvent effect based on four empirical scales: dipolarity (SdP, a new scale), polarizability (SP), acidity (SA), and basicity (SB) of the medium. *J. Phys. Chem. B* 113, 5951–5960. doi: 10.1021/jp8095727

De Moliner, F., Kielland, N., Lavilla, R., and Vendrell, M. (2017). Modern synthetic avenues for the preparation of functional fluorophores. *Angew. Chem. Int. Ed.* 56, 3758–3769. doi: 10.1002/anie.201609394

Del Río, M., Lobo, F., López, J. C., Oliden, A., Bañuelos, J., López-Arbeloa, I., et al. (2017). One-pot synthesis of rotationally restricted, conjugatable, BODIPY derivatives from phthalides. *J. Org. Chem.* 82, 1240–1247. doi: 10.1021/acs.joc.6b02426

Dess, B. D., and Martin, J. C. (1983). Readily accessible 12-I-5 oxidant for the conversion of primary and secondary alcohols to aldehydes and ketones. *J. Org. Chem.* 48, 4155–4156. doi: 10.1021/jo00170a070

Dumas-Verdes, C., Miomandre, F., Lépicier, E., Galangau, O., Vu, T. T., Clavier, G., et al. (2010). BODIPY-tetrazine multichromophoric devices. *Eur. J. Org. Chem.* 2010, 2525–2535. doi: 10.1002/ejoc.200900874

Fan, J., Hu, M., Zhan, P., and Peng, X. (2013). Energy transfer cassettes based on organic fluorophores: construction and applications in ratiometric sensing. *Chem. Soc. Rev.* 42, 29–43. doi: 10.1039/C2CS35273G

Galateia, Z. E., Agapi, N., Vasilis, N., Sharma, G. D., and Athanassios, C. G. (2015). "Scorpion"-shaped mono(carboxy)porphyrin-$(BODIPY)_2$, a novel triazine bridged triad: synthesis, characterization and dye sensitized solar cell (DSSC) applications. *J. Mater. Chem. C* 3, 5652–5664. doi: 10.1039/C4TC02902J

Gartzia-Rivero, L., Bañuelos, J., and López-Arbeloa, I. (2015). Excitation energy transfer in artificial antennas: from photoactive materials to molecular assemblies. *Int. Rev. Phys. Chem.* 34, 515–556. doi: 10.1080/0144235X.2015.1075279

Godoy, J., García-Lopez, V., Wang, L.-Y., Rondeau-Gagne, S., Link, S., Martí, A. A., et al. (2015). Synthesis of a fluorescent BODIPY-tagged ROMP catalyst and initial polymerization-propelled diffusion studies. *Tetrahedron* 71, 5965–5972. doi: 10.1016/j.tet.2015.04.027

Huo, Z., Ding, D., Zhang, Y., Lei, N., Gu, G., Gao, J., et al. (2018). Carbohydrate O-benzylation through trialkylsilane-mediated reductive etherification. *J. Carbohydr. Chem.* 37, 327–346. doi: 10.1080/07328303.2018.1493116

Ke, X.-S., Kim, T., Lynch, V. M., Kim, D., and Sessler, J. L. (2017). Flattened calixarene-like cyclic BODIPY array: a new photosynthetic antenna model. *J. Am. Chem. Soc.* 139, 13950–13956. doi: 10.1021/jacs.7b08611

Kesavan, P. E., Das, S., Lone, M. Y., Jha, P. C., Mori, S., and Gupta, I. (2015). Bridged bis-BODIPYs: their synthesis, structures and properties. *Dalton Trans.* 44, 17209–17221. doi: 10.1039/C5DT01925G

Kotlarska, J., Binnemans, K., and Dehaen, W. (2013). A convenient two-step synthesis of dialkylphosphate ionic liquids. *Tetrahedron* 69, 9947–9950. doi: 10.1016/j.tet.2013.09.074

Li, T., Gu, W., Lv, X., Wang, H., Hao, E., and Jiao, L. (2016). Synthesis and photophysical properties of meso-phenylene bridged boron dipyrromethene monomers, dimers and trimers. *Chin. J. Chem.* 34, 989–996. doi: 10.1002/cjoc.201600500

Li, T., Tikad, A., Pan, W., and Vincent S. P. (2014). β-stereoselective phosphorylations applied to the synthesis of ADP and

polyprenyl-β-mannopyranosides. *Org. Lett.* 16, 5628–5631. doi: 10.1021/ol5026876

Liu, Y., Zhao, J., Iagatti, A., Bussoti, A., Foggi, P., Castellucci, E., et al. (2018). A revisit to the orthogonal Bodipy dimers: experimental evidence for the symmetry breaking charge transfer-induced intersystem crossing. *J. Phys. Chem. C* 122, 2502–2511. doi: 10.1021/acs.jpcc.7b10213

López, J. C., Del Río, M., Oliden, A., Bañuelos, J., López-Arbeloa, I., García-Moreno, I., et al. (2017). Solvent-sensitive emitting urea-bridged bis-BODIPYs: ready access to one-pot tandem Staudinger/aza-wittig reaction. *Chem. Eur. J.* 23, 17511–17520. doi: 10.1002/chem.201703383

Loudet, A., and Burgess, K. (2007). BODIPY dyes and their derivatives: syntheses and spectroscopic properties. *Chem. Rev.* 107, 4891–4932. doi: 10.1021/cr078381n

Lu, H., Mack, J., Yang, Y., and Shen, Z. (2014). Structural modification strategies for the rational design of red/NIR region BODIPYs. *Chem. Soc. Rev.* 43, 4778–4823. doi: 10.1039/C4CS00030G

Misra, R., Dhokale, B., Jadhav, T., and Mobin, S. M. (2014). Meso-aryloxy and meso-arylaza linked BODIPY dimers: synthesis, structures and properties. *New J. Chem.* 38, 3579–3585. doi: 10.1039/C4NJ00354C

Patalag, L. J., Ho, L. P., Jones, P. G., and Werz, D. B. (2017). Ethylene-bridged oligo-BODIPYs: access to intramolecular J-aggregates and superfluorophores. *J. Am. Chem. Soc.* 139, 15104–15113. doi: 10.1021/jacs.7b08176

Qi, H., Teesdale, J. J., Pupillo, R. C., Rosenthal, J., and Bard, A. J. (2013). Synthesis, electrochemistry, and electrogenerated chemiluminescence of two BODIPY-appended bipyridine homologues. *J. Am. Chem. Soc.* 135, 13558–13566. doi: 10.1021/ja406731f

Sakamoto, N., Ikeda, C., Yamamura, M., and Nabeshima, T. (2012). α-bridged BODIPY oligomers with switchable near-IR photoproperties by external-stimuli-induced formation and disruption. *Chem. Commun.* 48, 4818–4820. doi: 10.1039/c2cc17513d

Speiser, S. (1996). Photophysics and mechanisms of intramolecular electronic energy transfer in bichromophoric molecular systems: solution and supersonic jet studies. *Chem Rev.* 96, 1953–1976. doi: 10.1021/cr941193

Squeo, B. M., Gregoriu, V. G., Avgeropoulos, A., Baysec, S., Allard, S., Scherf, U., et al. (2017). BODIPY-based polymeric dyes as emerging horizon materials for biological sensing and organic electronics applications. *Prog. Polym. Sci.* 71, 26–52. doi: 10.1016/j.progpolymsci.2017.02.003

Thakare, S., Stachelek, P., Mula, S., More, A. B., Chattopadhyay, S., Ray, A. K., et al. (2016). Solvent-driven conformational exchange for amide-linked bichromophoric BODIPY derivatives. *Chem. Eur. J.* 22, 14356–14366. doi: 10.1002/chem.201602354

Turksoy, A., Yildiz, D., and Akkaya, E. U. (2019). Photosensitization and controlled photosensitization with BODIPY dyes. *Coord. Chem. Rev.* 379, 47–64. doi: 10.1016/j.ccr.2017.09.029

Ulrich, G., Ziessel, R., and Harriman, A. (2008). The chemistry of fluorescent BODIPY dyes: versatility unsurpassed. *Angew. Chem. Int. Ed.* 47, 1184–1201. doi: 10.1002/anie.200702070

Wang, D.-G., Zhang, L.-N., Li, Q., Yang, Y., Wu, Y., Fan, X., et al. (2017). Dimeric BODIPYs with different linkages: a systematic investigation on structure-properties relationship. *Tetrahedron* 73, 6894–6900. doi: 10.1016/j.tet.2017.10.042

Whited, M. T., Patel, N. M., Roberts, S. T., Allen, K., Djurovich, P. I., Bradforth, S. E., et al. (2012). Symmetry-breaking intramolecular charge transfer in the excited state of meso-linked BODIPY dyads. *Chem. Commun.* 48, 284–286. doi: 10.1039/C1CC12260F

Xu, K., Sukhanov, A. A., Zhao, Y., Zhao, J., Ji, W., Peng, X., et al. (2018). Unexpected nucleophilic substitution reaction of BODIPY: preparation of the BODIPY-TEMPO triad showing radical-enhanced intersystem crossing. *Eur. J. Org. Chem.* 2018, 885–895. doi: 10.1002/ejoc.201701724

Yu, C., Jiao, L., Li, T., Wu, Q., Miao, W., Wang, J., et al. (2015). Fusion and planarization of bisBODIPY: a new family of photostable near infrared dyes. *Chem. Commun.* 51, 16852–16855. doi: 10.1039/C5CC07304A

Zhang, G., Zhao, N., Bobadova-Parvanova, P., Wang, M., Fronczek, F. R., Smith, K. M., et al. (2018). Syntheses, spectroscopic properties, and computational study of (E,Z)-ethenyl and ethynyl linked BODIPYs. *J. Phys. Chem. A* 122, 6256–6265. doi: 10.1021/acs.jpca.8b05149

Zhang, X.-F. (2017). BisBODIPYs as PCT-based halogen free photosensitizers for highly efficient excited triplet state and singlet oxygen formation: tuning the efficiency by different linking positions. *Dyes Pigm.* 146, 491–501. doi: 10.1016/j.dyepig.2017.07.051

Zhao, J., Wu, W., Sun, J., and Guo, S. (2013). Triplet photosensitizers: from molecular design to applications. *Chem. Soc. Rev.* 42, 5323–5351. doi: 10.1039/c3cs35531d

Zou, J., Yin, Z., Ding, K., Tang, Q., Li, J., Si, W., et al. (2017). BODIPY derivatives for photodynamic therapy: influence of configuration versus heavy atom effect ACS. *Appl. Mater. Interfaces* 9, 32475–32481. doi: 10.1021/acsami.7b07569

Conflict of Interest: The authors declare that the research was conducted in the absence of any commercial or financial relationships that could be construed as a potential conflict of interest.

frontiers in Chemistry

REVIEW
published: 10 December 2019
doi: 10.3389/fchem.2019.00841

Carbazole Substituted BODIPYs

Iti Gupta and Praseetha E. Kesavan*

Department of Chemistry, Indian Institute of Technology Gandhinagar, Gandhinagar, India

Difluoroboron-dipyrromethenes (BODIPYs) are highly popular fluorescent dyes with applications as NIR probes for bioimaging, fluorescent tags/sensors and as photosensitizers in cancer therapy and organic photovoltaics. This review concentrates on the synthesis and spectral properties of BODIPY dyes conjugated with carbazole heterocycle. The carbazole is an electron rich tricyclic compound and due to its excellent electronic properties, it is extensively used in the production of electroluminescent materials and polymers. This review highlights the recent progress made on the series of BODIPY derivatives containing carbazole ring at *alpha*, *beta,* and *meso*-positions of the BODIPY skeleton. Carbazole based hybrid BODIPYs, carbazole linked aza-BODIPYs and carbazole-fused BODIPYs are also discussed.

Keywords: BODIPY, carbazole, fluorescence, absorption, dyes

INTRODUCTION

Certain organic or inorganic molecules can act as fluorophores; and they can re-emit the light upon irradiation with the light source. The fluorescent organic dyes have been extensively used in the wide range of applications such as: biomolecular labels (Celli et al., 2010; Kowada and Kikuchi, 2015), chemosensors (Wu et al., 2015), energy transfer cassettes (Fan et al., 2013), organic light emitting diodes (Zampetti et al., 2017), dye-sensitized solar cells (Klfout et al., 2017), etc. Among the highly fluorescent organic molecules reported in the literature, the dyes based on 4,4-difluoro-4-bora-3α,4α-diaza-s-indacene (difluoroboron dipyrromethene, abbreviated as BODIPY, **Figure 1**); show possibly the highest potential and have become enormously popular in recent times. Although, Treibs and Kreuzer first reported these molecules in 1968 (Treibs and Kreuzer, 1968); the field was not developed much till 1980. In the 1980s, researchers reported potential use of these dyes for biological labeling (Vedamalai et al., 2018). After that, there was a clear rise in the number of reports on BODIPY dyes; making them hugely popular among chemists and biologists to develop BODIPY based fluorescent sensors (Vedamalai et al., 2016, 2018), bioimaging agents (Kesavan et al., 2019), and photosensitizers for PDT (Kamkaew et al., 2013; Zheng et al., 2018).

By mid of the 1990s BODIPY's potential applications in the area of biological sciences (Vedamalai and Gupta, 2018) and materials sciences were fully recognized and research reports in this area tremendously increased (Ulrich et al., 2008). These molecules showed remarkable properties like sharp absorption and emission, large molar absorption coefficients, high fluorescence quantum yields and high photo-stability. Thus, this group of fluorescent dyes meet the criteria for a good fluorophore; they exhibit enormous synthetic variations and versatile applications (Loudet and Burgess, 2007; Ziessel et al., 2007; Kolemen and Akkaya, 2018). Understanding the photophysical properties of these systems (Lu et al., 2014) is of principal importance, not only because of the intrinsic potential applications but, also in the design of new dyes with specific properties. The main synthetic advantage of BODIPY dye is that, the unique structure of dye skeleton provides eight positions which can be easily functionalized to fine-tune their electronic properties (Lakshmi et al., 2015, 2016). There are excellent reviews available on the BODIPYs based on the different applications, such as: fluorescent

OPEN ACCESS

Edited by:
Zhen Shen,
Nanjing University, China

Reviewed by:
Chusen Huang,
Shanghai Normal University, China
Wim Dehaen,
KU Leuven, Belgium

****Correspondence:***
Iti Gupta
iti@iitgn.ac.in

Specialty section:
This article was submitted to Supramolecular Chemistry, a section of the journal Frontiers in Chemistry

Received: *02 September 2019*
Accepted: *19 November 2019*
Published: *10 December 2019*

Citation:
Gupta I and Kesavan PE (2019) Carbazole Substituted BODIPYs. Front. Chem. 7:841. doi: 10.3389/fchem.2019.00841

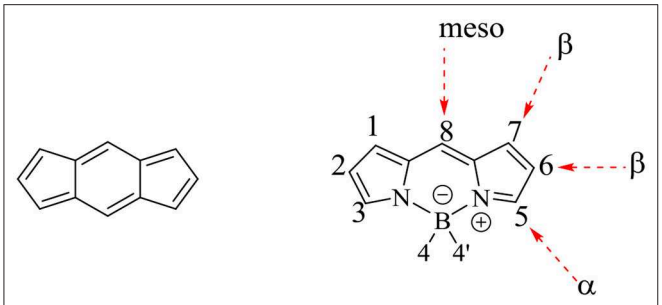

FIGURE 1 | s-indacene and basic BODIPY core structure.

NIR probes (Yuan et al., 2013), sensitizers for PDT (Kamkaew et al., 2013), organic materials for photovoltaics (Bessette and Hanan, 2014), D-A type systems with focus on energy/electron transfer (Loudet and Burgess, 2007), fluorescent sensors (Boens et al., 2012; Ni and Wu, 2014), BODIPY based multi-chromophore cassettes (Ziessel et al., 2007), etc. This review presents the structural diversity of the carbazole-BODIPY conjugates, with the emphasis on the effect of the substitution of carbazole heterocycle on the optical properties of the BODIPYs.

Carbazole is a well-known heterocyclic aromatic system. The aromatic nature of carbazole makes it chemically and thermally stable; and the ring can be easily functionalized at different positions. Carbazole and its derivatives are electron rich compounds and they exhibit good absorption and emission properties (Li et al., 2004; Barberis and Mikroyannidis, 2006; Mudadu et al., 2008). Also, due to their excellent photoluminescence and hole-transport property; these systems are used for various applications in photovoltaic systems and OLEDs. They are also employed as photosensitizers (Promarak et al., 2008; Wang et al., 2008; Tang et al., 2010) in DSSCs. Carbazole derivatives are also known for their anti-microbial, anti-tumor properties and as bioimaging agents (Głuszyńska, 2015).

In recent years, the reports on carbazole substituted BODIPYs and porphyrinoids (Das and Gupta, 2019) have significantly increased. It is observed that, the presence of electron rich carbazole moiety can alter the absorption and emission properties of BODIPYs; which depend on the position and kind of linkage through which carbazole is attached on the BODIPY skeleton. In this review, we present the overview of synthetic strategies used to prepared various kinds of carbazole substituted BODIPYs; also, the change in the electronic properties due to substitution and their applications are discussed.

Abbreviations: AIEE, aggregation induced enhanced emission; BODIPY, difluoroboron dipyrromethene; CDCA, chenodeoxycholic acid; DSSC, dye sensitized solar cell; FET, field effect transistor; FRET, fluorescence resonance energy transfer; ICT, inrtamolecular charge transfer; LHE, light harvesting efficiency; OLED, oraganic light emitting diode; OPV, organic photovoltaic; PET, photoinduced energy transfer; TPEF, two-photon emission fluorescence; TTA, triplet–triplet annihilation.

Beta-Substituted BODIPYs

Main advantage of BODPY core is that, the three available positions (α, β, and *meso*) are prone to derivetisation (**Figure 1**). But the feasibility of substitution is highly depended on the other functional groups, already present on the BODIPY core. The substitution of electron rich groups at the *beta*-positions is expected to enhancethe electronic communication between the BODIPY core and the substituents.

In 2009, Zhang et al. reported the synthesis of BODIPY **3** (**Scheme 1**); the key precursor **2** was coupled with 9-ethyl-3-(prop-1-ynyl)-9*H*-carbazole *via* Pd-catalyzed Sonogashira reaction. The ethynyl linkages present in this molecule helped to show efficient ICT process. The absorption and emission maxima of BODIPY **3** were very much red shifted (**Scheme 1**) as compared to the parent *meso*-tetraphenyl BODIPY, which reflected the effect of carbazole ring linked via rigid ethyne linker to the boron-dipyrrin core. The linear D-π-D type structure resulted in the extended conjugation along with efficient ICT process, which made this molecule to exhibit two-photon absorption properties (Zhang et al., 2009). As a result, this compound showed a sharp emission peak around 670 nm with reasonable quantum yield. This emission was attributed to two-photon emission fluorescence (TPEF). Since this emission wavelength fall in human body's therapeutic window (650–800 nm), this molecule has potential in bioimaging applications.

The BODIPYs **6** and **7** linked to carbazole via thiophene spacer were used for organic photovoltaic (OPV) applications (Lin et al., 2012). The target BODIPYs **6** and **7** were synthesized by Stille and/or Sonogashira coupling reactions between precursors BODIPY **4** and **5** with the appropriate stannyl functionalized carbazole derivative (**Scheme 2**). The studies showed that, insertion of an alkyne moiety renders flexibility between the donor carbazole and acceptor BODIPY core, which is beneficial for light harvesting. The large Stokes shift displayed by BODIPYs **6** and **7** suggests that, the excited state of the molecules have a more planar conformation, which is not favorable for solar cell applications. Both the molecules **6** and **7** showed reasonable light to current conversion efficiency of 1.8 and 2.6%, respectively. Zhao and co-workers reported BODIPYs **9** and **10** where, one *beta*-position is substituted with carbazole ring and the other *beta*-position is linked to C_{60} (**Scheme 3**) (Yang et al., 2012) or rhenium metal complex (**Chart 1**). In BODIPYs **9** and **10**, the electron rich carbazole derivative is attached through rigid ethynyl bond by Pd(0) catalyzed Sonogashira coupling. The carbazole derivative linked to the BODIPY unit, is acting as a light-harvesting antenna system. In compound **10,** intramolecular energy transfer was observed from the BODIPY based singlet excited state to the singlet excited state localized on the C60 unit.

The intrinsic intersystem crossing resulted in the triplet-excited state of the C_{60} in the absence of a heavy atom. The dyad **10** showed TTA up-conversion with quantum yield up to 2.9% (Yang et al., 2012). Complex **11** showed much weaker TTA up-conversion, which can be assigned to the weak absorption of **11** at the excitation wavelength and less efficient ISC (Yi et al., 2013).

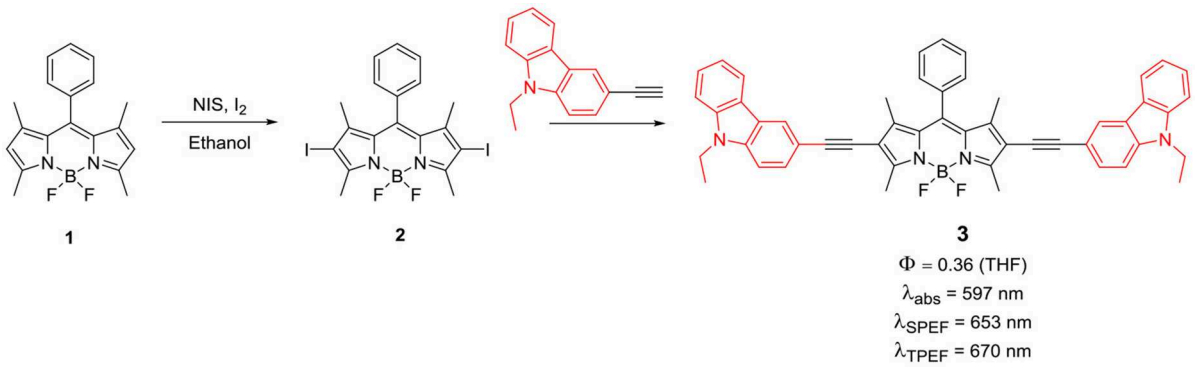

SCHEME 1 | BODIPY–carbazole conjugates inked via ethyne bridges.

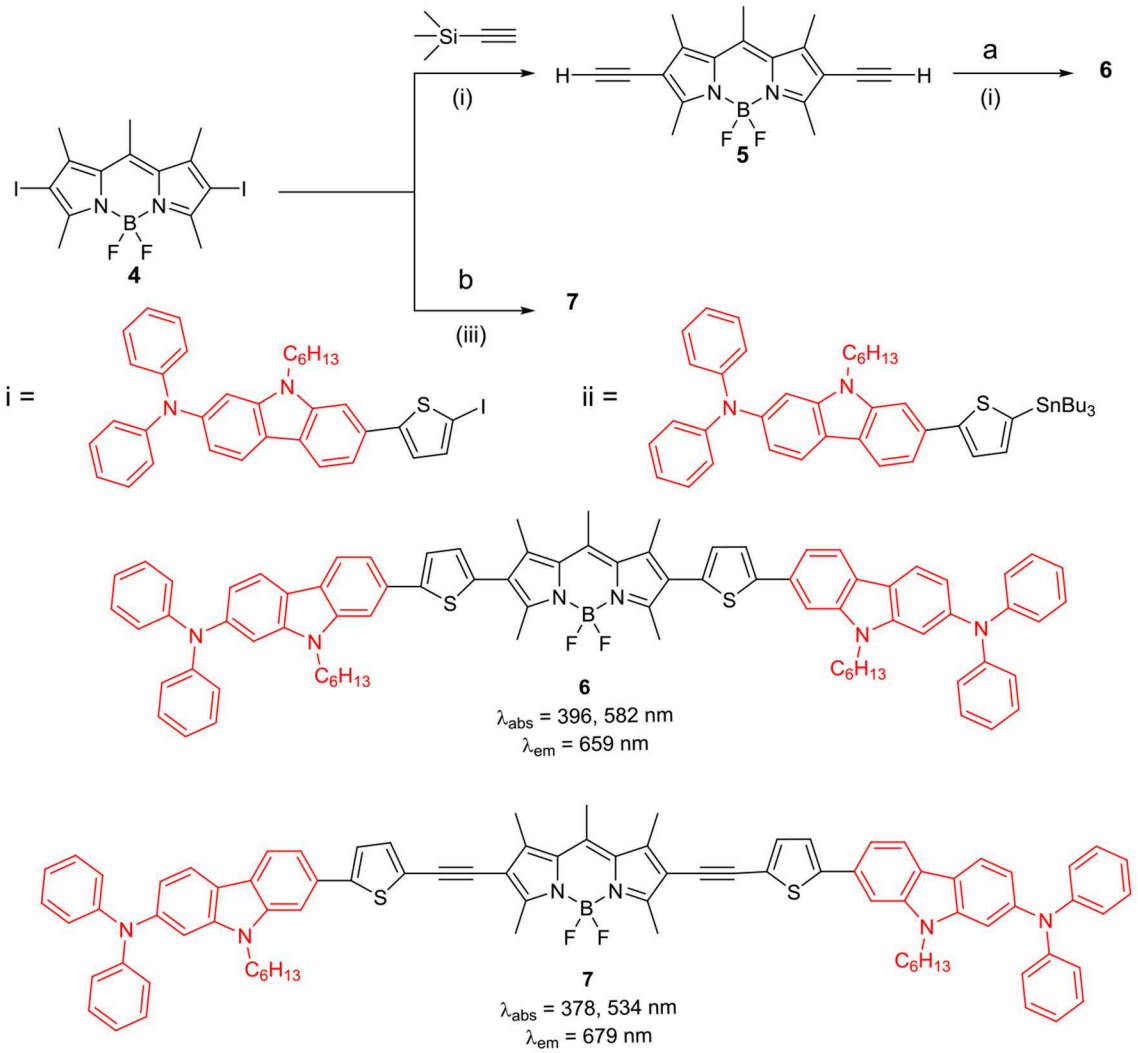

SCHEME 2 | BODIPYs linked to carbazole derivatives with thiophene spacer. (i) $Pd(PPh_3)_2Cl_2$, CuI, THF, Et_3N, TBAF, THF; (ii) $Pd(PPh_3)_2Cl_2$, CuI, THF, diisopropylamine; (iii) $Pd(PPh_3)_2Cl_2$, PPh_3, DMF.

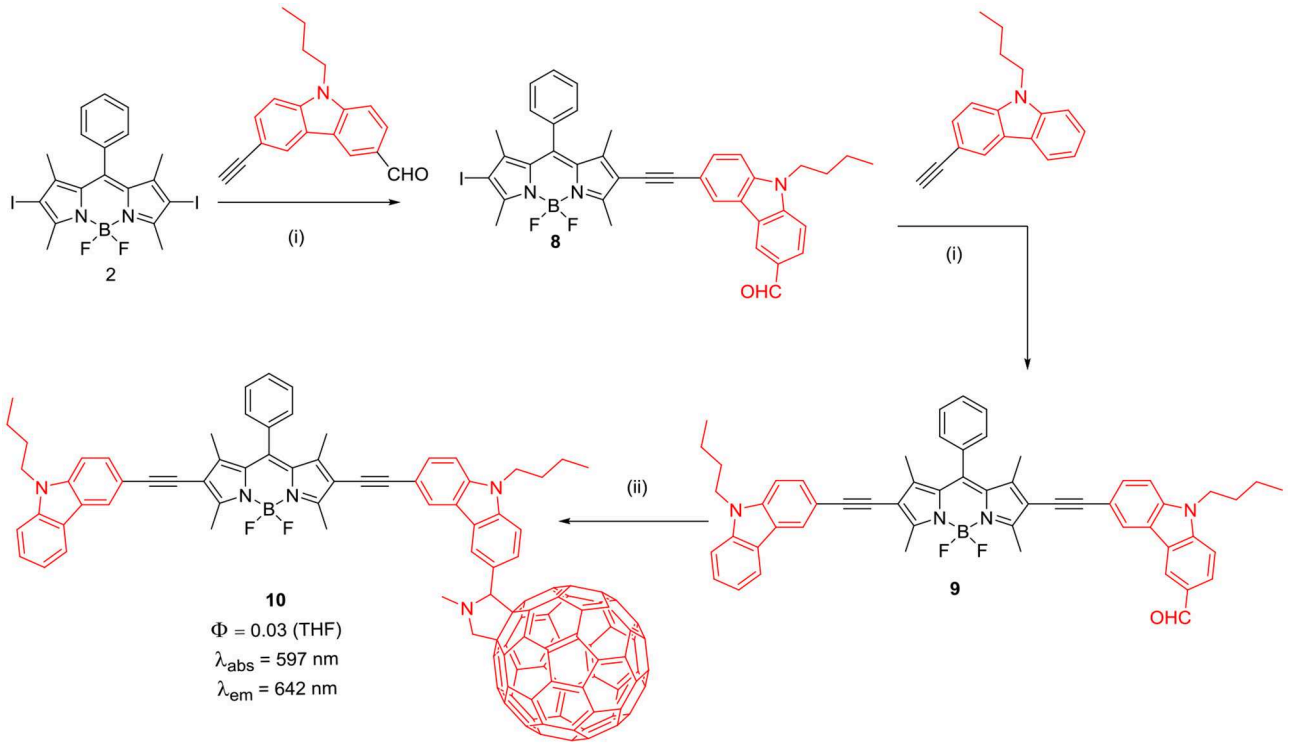

SCHEME 3 | Synthesis of BODIPY linked via ethyne linkage to carbazole and C_{60}. (i) $PdCl_2(PPh_3)_2$, PPh_3, CuI, NEt_3, THF, argon atmosphere, 60°C, 6 h; (ii) sarcosine, C_{60}, toluene, reflux.

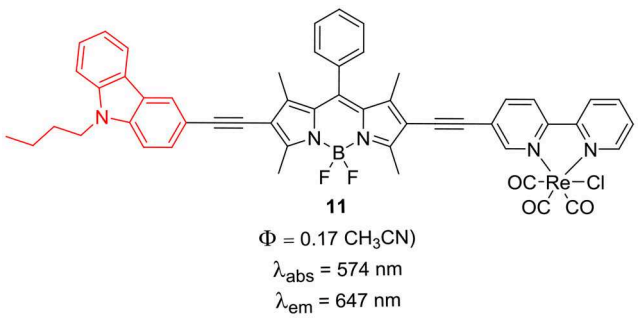

CHART 1 | Carbazole BODIPY with rhenium metal complex.

Direct substitution at the *beta*-positions of BODIPYs (**Scheme 4**) through Suzuki coupling between boronic ester derivative of carbazole and the 2,6-dibromo substituted BODIPY **12** is another method to incorporate carbazole ring on the BODIPY core. The pronounced effect of substitution of carbazole rings on the *beta*-position of the BODIPY, reflected in the increased absorption efficiency from 300 to 900 nm; thus molecule **13** acted as a panchromatic dye. This molecule showed an excellent red-shift in its emission and had high thermal stability. Photovoltaic performance studies showed that, by further engineering the molecular structure and optimization of the morphology; this type of dyes can become potential candidates for the efficient organic solar cell materials (Liao et al., 2016). Wanwong et al. reported the application of *beta* -carbazole substituted BODIPY dyad and triad (**Scheme 5**; **15** and **16**) as field effect transistors (FET). Though these derivatives provided moderate performance, modification of this structure may help to develop better dye with better performance (Wanwong et al., 2018).

Electron rich carbazole ring acts as very good electron donor and its derivatives exhibit photorefractive and hole-trasnport properties; thus they are polupar constituents of electroluminescent materials. Mao et al. reported application of *beta*-substituted BODIPYs, having D-A-π-A system (**Scheme 6**) for DSSC applications. Incorporation of the extra acceptor in between the donor moiety and π-conjugating unit decreases the HOMO-LUMO energy gap, and as a result, these BODIPYs can show an efficient photoinduced electron transfer from the donor to the BODIPY acceptor unit; which is linked to the anchor group at the opposite end (Mao et al., 2017).

BODIPY **24** with cyanoacetic acid anchoring group was used as a photosensitizer for DSSC; this linear system showed reasonable PCE efficiency of 3.1%. A series of *beta*-substituted BODIPYs **25–28** having D-π-A system were constructed for DSSC application (**Scheme 6**). The *N*-alkyl carbazole ring served as donor and BODIPY core linked to cyanoacetic acid was the acceptor unit (Liao et al., 2017b). The DSSC analysis revealed that photosensitizers **26** and **28**, having 2-carbazolyl substituent at the *beta*-position showed better J_{sc} than BODIPYs

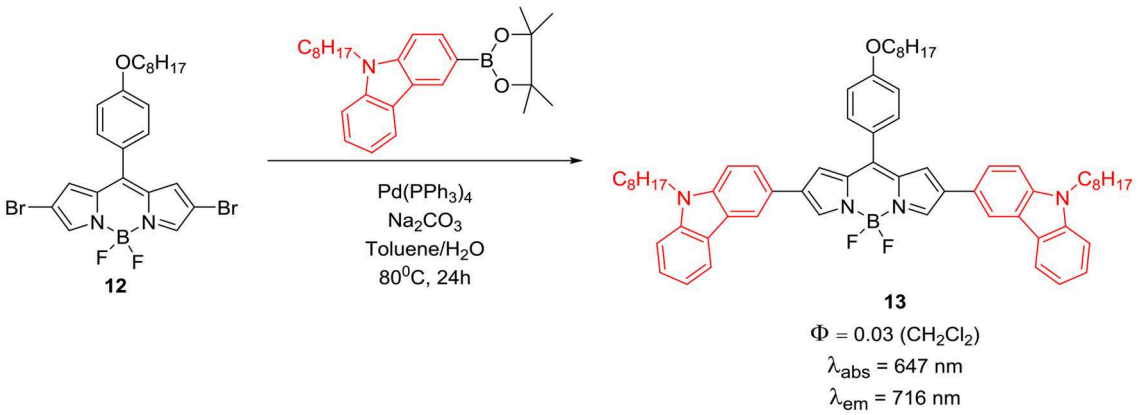

SCHEME 4 | Synthesis of directly linked carbazole-BODIPY system.

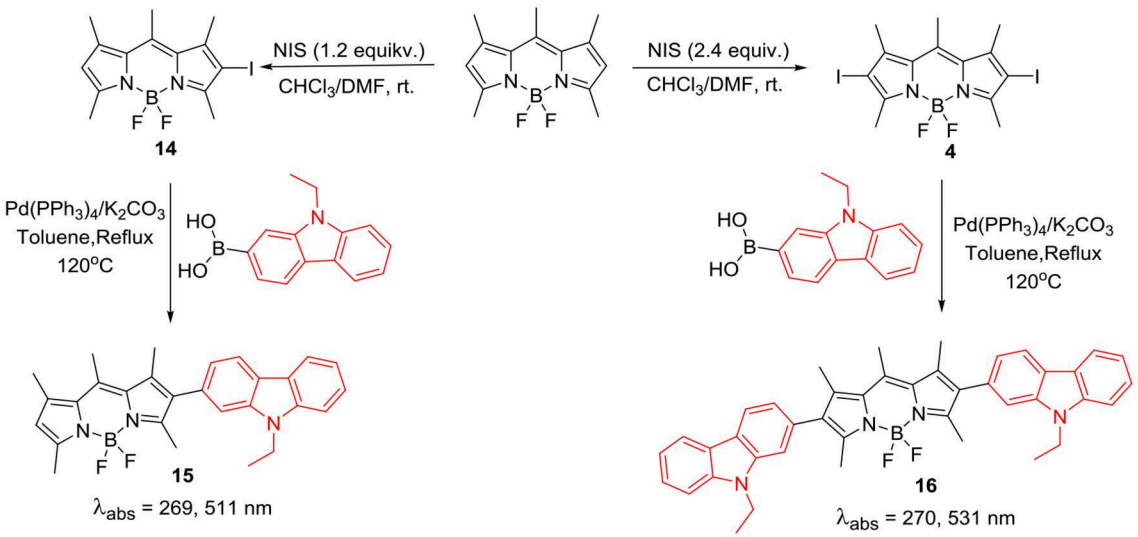

SCHEME 5 | Synthesis of 2,6-direct linked carbazole BODIPY dyad and triad.

25 and **27** where carbazole is substituted through 3-position and it was reflected in their overall efficiency (Liao et al., 2017b). BODIPY derivatives having heavy atoms such as: bromo, iodo groups on the dipyrrin core, have been used as triplet sensitizers. Such metal-free triplet sensitizers can be effectively used for singlet-oxygen generation, PDT agents and triplet-triplet annihilation upconversion (TTA-UC). Wei et al. (2017) have prepared BODIPY based organic photosensitizers connected to C_{60} and *N*-butylcarbazole at the β-positions **29** and **30** (**Chart 2**). As per the report, C_{60} has high ISC (inter system crossing) efficiency but weak absoprtion in the visible region of the solar spectrum. Thus, linking of C_{60} to the carbazole substiuted BODIPY can be useful to effectually populate the triplet excited state of the C_{60}, which in turn can transfer the energy to perylene acceptor. The calculated TTA-UC quantum yield was 4.9 for the carbazole-BODIPY—C_{60} triad **30** shown in **Chart 2** (Wei et al., 2017).

Alpha-Substituted BODIPYs

There are two alpha positions on the BODIPY skeleton which are available for derivatization after various reactions such as: nucleophilic or electrophilic substitution, cross-coupling reactions, and Knoevenagel condensation (Wood and Thompson, 2007), etc.

Ooyama et al. recently reported a new strategy to develop effective BODIPY based sensitisers possessing a good light harvesting efficiency (LHE) in the range of visible light to NIR region. They developed $(D)_2$-π-A type BODIPYs **33** and **34** (**Scheme 7**) having pyridyl and cyanoacrylic acid groups, respectively. The electron-withdrawing anchoring group (pyridyl/cyanoacetic acid) helps to bind the BODIPY on the titanium dioxide layer for photovoltaic application. The presence of strong electron-donating units of 9-butyl-*N,N*-phenyl-7-(thiophen-2-yl)-9*H*-carbazol-2-amine at *alpha*-positions of the BODIPY core, helped to obtain strong and broad absorption

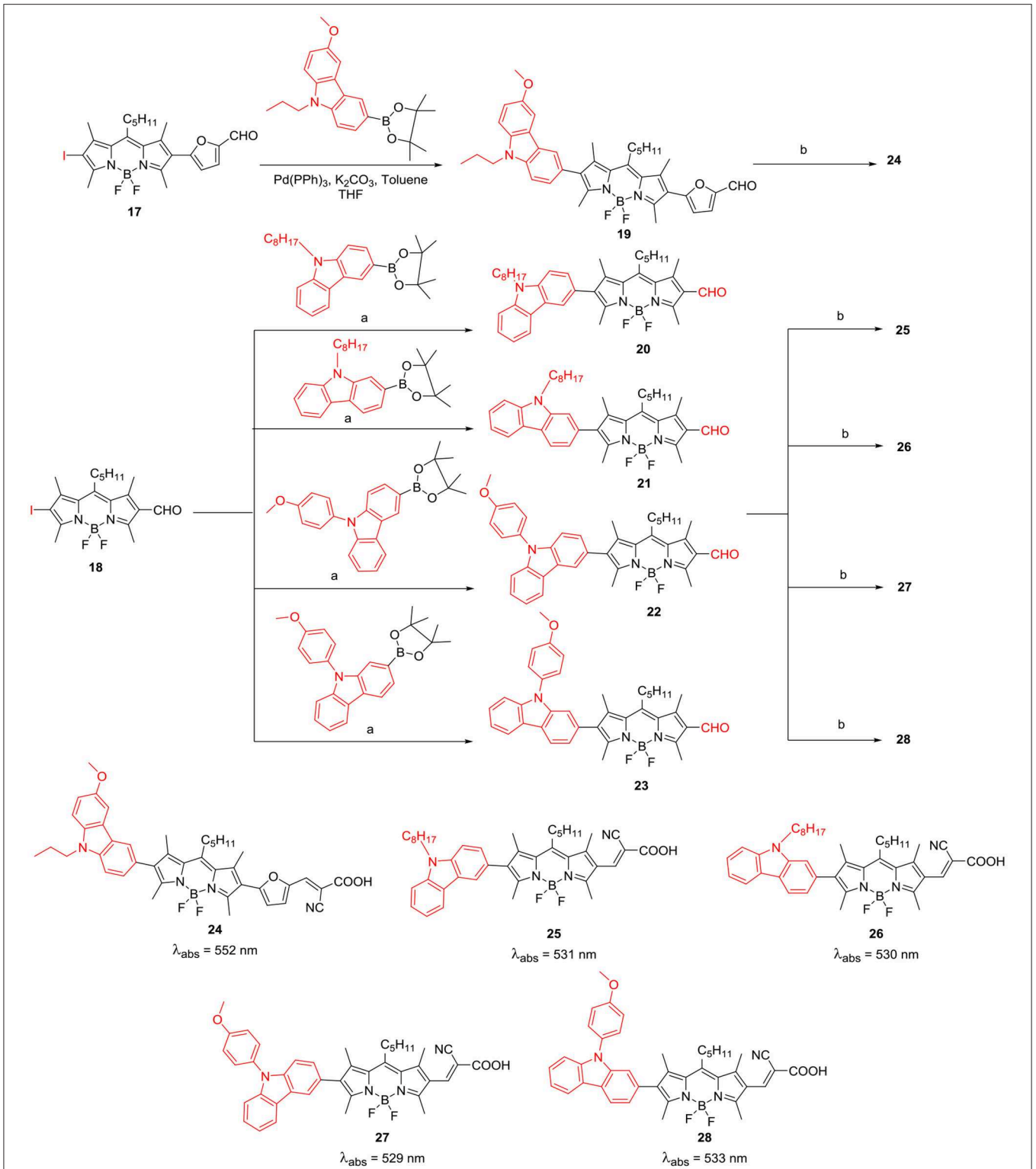

SCHEME 6 | *beta*-carbazole substituted BODIPYs for DSSC application; a: $Pd(PPh_3)_4$, K_2CO_3, toluene/THF; b: piperidine, $CNCH_2COOH$, DCM/ACN.

band ranging from 600 to 850 nm. Also, these molecules showed high LHE in the range of visible light to NIR region. Though these molecules showed good photophysical properties; these BODIPY dyes showed low photovoltaic performance in DSSC studies, which was attributed to the low lying LUMO levels (Ooyama et al., 2017).

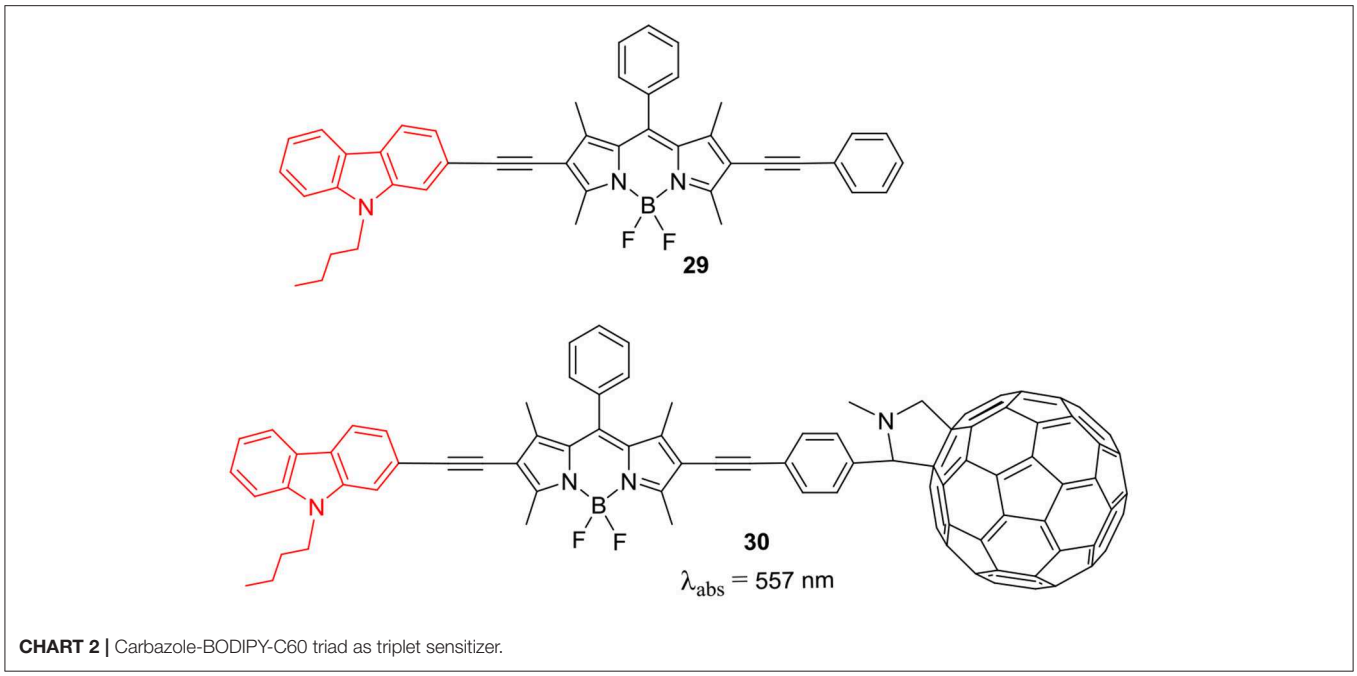

CHART 2 | Carbazole-BODIPY-C60 triad as triplet sensitizer.

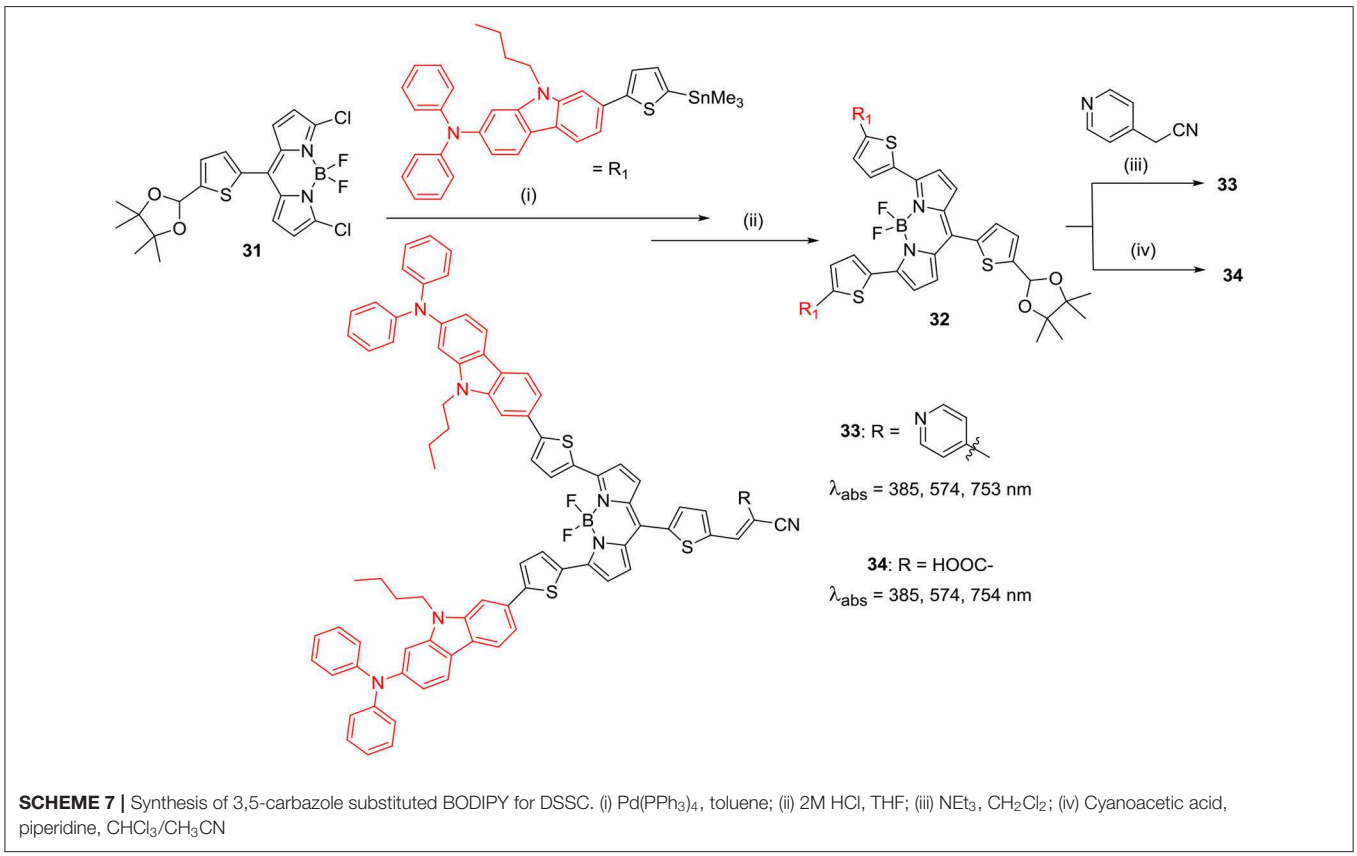

SCHEME 7 | Synthesis of 3,5-carbazole substituted BODIPY for DSSC. (i) $Pd(PPh_3)_4$, toluene; (ii) 2M HCl, THF; (iii) NEt_3, CH_2Cl_2; (iv) Cyanoacetic acid, piperidine, $CHCl_3/CH_3CN$

Knoevenagel condensation is another method to introduce carbazole unit on the BODIPY core. Zhang et al. reported mono-, di- and tetra-styryl carbazole substituted BODIPYs (**35**, **38,** and **39**). The Knoevenagel condensation between methyl-2-(2-formyl-9H-crbazole-9-yl)acetate with BODIPY **35** (**Scheme 8**) produced target styryl BODIPYs **36**, **37**, and **38** in good yields.

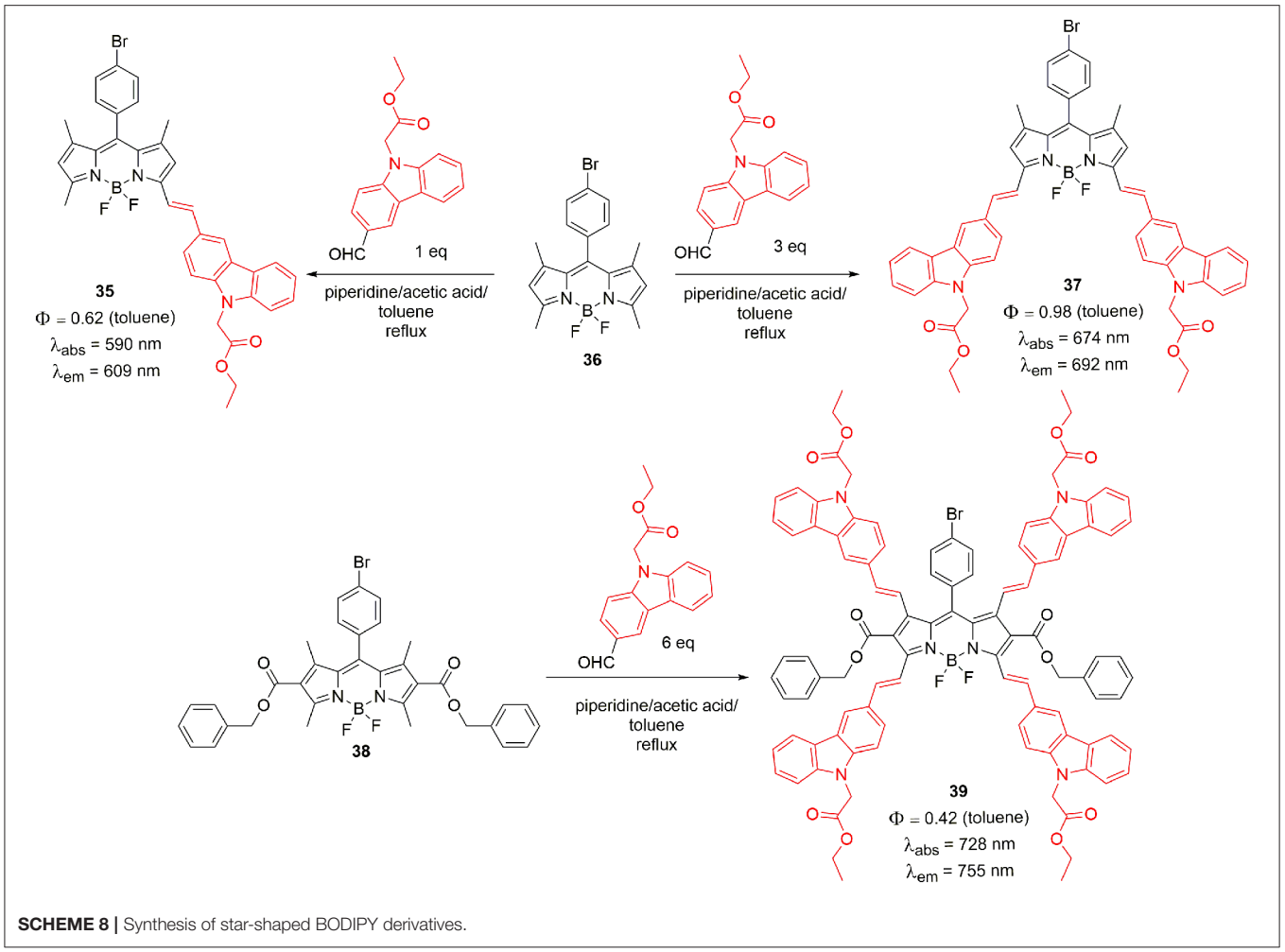

SCHEME 8 | Synthesis of star-shaped BODIPY derivatives.

The extended π-conjugation converted the simple BODIPYs to NIR dyes with strong absorption maxima in between the 600 and 727 nm range. Their corresponding emission maxima were also considerably red shifted; which reflected the increased conjugation between the carbazole units and the BODIPY core. The BODIPY **39** with four styryl-carbazole unit showed the highest PCE of 2.7% (Zhang et al., 2015).

The synthesis of *di*-styryl BODIPY based D-A and D-π-A systems (**40–44**) was reported, where thiophene served as π-linker between the *N*-alkylcarbazole unit and the BODIPY core (**Chart 3**) (Brzeczek et al., 2016; Kurowska et al., 2018). The target BODIPYs were synthesized through multistep synthetic procedure; firstly the precursor 1,3,5,7-tetramethyl-8-mesityl BODIPY was prepared by the conventional synthetic protocol. Microwave assisted Knoevenagel condensation of the precursor BODIPY with appropriate carbazole derivative afforded target BODIPYs **40–44** (**Chart 3**). The carbazole substituion at *alpha*-positions of the BODIPY core has prominent effect on the electronic properties of the dyes; the target compounds **40–44** showed markdly red shifted absorption (736–740 nm) and emission maxima (775–780 nm). Particularly, the BODIPY–carbazole conjugates with single thiophene linker showed highly red-shifted absorption and emission spectra. On increasing the number of thiophene linkers, the effect of carbazole donor on the BODIPY acceptor was diminished; the quenched emission was attributed to the stronger push-pull effect for systems with elongated conjugation framework.

Followed by this work, Cheema et al. studied the application of 3,5-di-styryl BODIPYs having *N*-alkyl carbazole units (**45–46**) for DSSC application (**Chart 3**). Carboxylic acid group on the *meso*-phenyl ring of the BODIPY acted as anchor group (Cheema et al., 2016). It was revealed that, the alkyl substitution did not change the position of absorption and emission maxima; but the intensity of these bands was altered. With the increases in the length of *N*-alkyl chain, the intensity of the lower energy absorption band decreased. DSSC performance for the dyes was much less than expected, which was attributed to the aggregation related losses (Cheema et al., 2016).

Alpha-styryl substituted BODIPY derivatives have excellent photophysical properties; they exhibit strong absorption and fluorescence in near infra-red (NIR) region. Such α-styryl substituted BODIPY derivatives have tremendous potential as bioimaging agents; particularly cell organelle

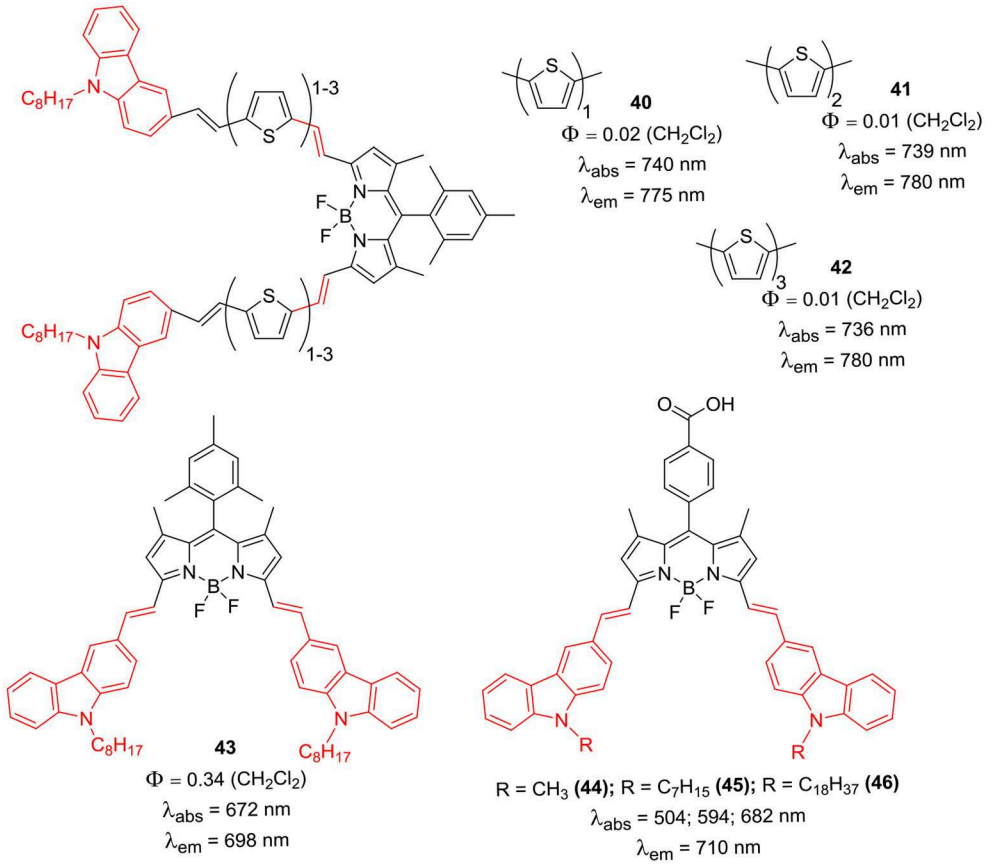

CHART 3 | α-styryl linked carbazole BODIPYs.

targeting becomes facile as their absorption and emission falls in the biological window. The α-styryl BODIPYs **48–50** (**Scheme 9**) having one or two *N*-ethynyl-carbazole groups were prepared by Zhang et al. (2013). Extended conjugation of the BODIPY core with the carbazole ring resulted in strong absorption with high extinction coefficients between 620 and 703 nm and red emission in the range of 650–730 nm. These BODIPYs showed high fluorescence quantum yields and decent two-photon absorption properties; also, the NIR probe **50** demonstrated significant localization in the mitochondria of MCF-7 cells, due to the presence of triphenylphosphonium group (Zhang et al., 2013).

An interesting system of subphthalocyanine-BODIPY scaffold containing one or two *N*-ethyl-carbaole moieties was reported by Eçik et al. (2017). Synthesis of these molecules followed multistep synthetic procedure, Knoevenagel condensation of the precursor BODIPY (**51**) with 9-ethyl-9*H*-carbazole-2-carbadehyde (**Scheme 10**) afforded **52** and **53**. Click reaction of ethyne functionalized subphthalocyanine with BODIPYs **52** and **53**, resulted in the formation of the desired target molecules **54** and **55** (**Scheme 10**). These systems (**54** and **55**) showed efficient energy transfer from subphthalocyanine unit to the BODIPY unit via fluorescence resonance energy transfer (FRET). Authors suggested that, these kinds of systems can be developed into a BODIPY-based multi-chromophore systems and this will help to reveal their energy transfer potential in efficient light-harvesting systems (Eçik et al., 2017).

Another method to introduce carbazole ring on the BODIPY core is through *N*-linkage (**Scheme 11**; **57** and **58**). Zhang et al. showed that, 4-(9*H*-carbazol-9-yl)benzaldehyde can be linked to BODIPY **56** via Knoevenagel condensation, followed by the deprotection of **57** to produce **58**. The presence of *N*-phenyl carbazolyl groups on the BODPY **58** can help to reduce the aggregation of dye to some extent; hence **58** exhibited enhanced photon to electron conversion efficiency of 4.4%. Since the electron rich carbazole ring has excellent hole-transport properties; it is widely used in optoelectronics; most of the scientists are interested in substituting carbazole to BODIPY core to enhance their photovoltaic applications (Zhang et al., 2016). A new synthetic approach for the modification of *alpha*-positions of the BODIPY with carbazole was reported by Satoh et al. (2018). As shown in the **Scheme 12**, to obtain **60,** *alpha*-positions of the BODIPY core can be substituted by nucleophilic aromatic reaction (SNAr) of carbazole with compound **59** in THF (Satoh et al., 2018). Absorption and emission spectra exhibited bathochromic shifts as compared

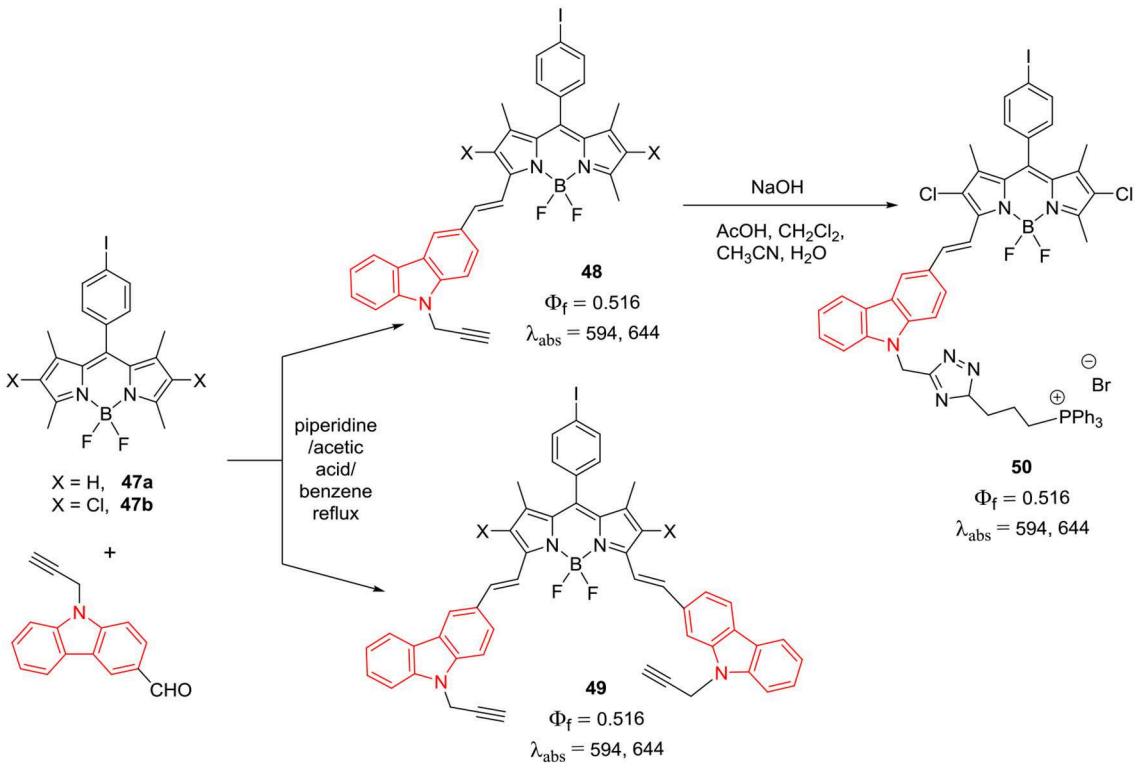

SCHEME 9 | α-styryl linked carbazole-BODIPY based probes for mitochondria imaging.

to the parent BODIPY; these molecule promises development of new BODIPY based fluorophores through this synthetic methodology (Satoh et al., 2018).

Alpha-styryl BODIPY having one *N*-alkylcarbazole substituent was prepared by Mani et al. (2017); Knoevenagel condensation of the precursor compound **61** with 7-bromo-9-butyl-9*H*-carbazole-2-carbaldehyde (**Scheme 13**) afforded **62**. The BODIPY **62** exhibited huge red shifts of 92 nm in the absorption and 118 nm in the emission w.r.t. the starting BODIPY **61** (Mani et al., 2017). Chang et al. reported donor-acceptor systems of *alpha*-styryl BODIPYs **63** and **64** (**Chart 4**) having *N*-alkylcarbazole and/or cyanuric chloride as linker group (Su et al., 2014b). BODIPYs **63** and **64** exhibited red shifted absorption and fluorescence around 617 nm and considerable pseudo Stokes shift (∼120 nm) due to intramolecular DRET (dark resonance energy transfer) in such systems (Su et al., 2014a). Significant pseudo Stokes shifts, red shifted fluorescence, and biocompatibility of cyanuric chloride linker group in **64** suggest its potential application in bioimaging of live cells (Su et al., 2014a).

Han et al. reported the *alpha*-styryl BODIPY **65** (**Chart 5**) having two carbazole rings with *N*-PEGylated chains for the deep tissue imaging and PDT application (Huang et al., 2016). The BODIPY **65** showed NIR absorption at 661 and emission at 755 nm with fluorescence quantum yield of 4%. The calculated singlet oxygen quantum efficiency 67% for compound **65** was considerably high and its water soluble nanoparticles were prepared by mixing it with the biodegradable polymer PLA-PEG-FA (comprising of poly-lactic acid, poly-ethyleneglycol, and folate). The biocompatible nanoparticles showed broad absorption and emission in the NIR region (650–800 nm) with 58% singlet oxygen quantum yield upon excitation by NIR light ∼670–800 nm; also they can be used for deep tissue imaging and for the treatment of tumors. The organic nanoparticles displayed green emission upon light irradiation in HeLA cells ∼670–800 nm and negligible cytotoxicity; making them suitable candidates for PDT studies (Huang et al., 2016). The *alpha*-distyryl BODIPYs **66–68** (**Chart 6**) having two carbazolylethynyl groups and two *beta*-bromo groups was used as photosensitizers for PDT (Zhou et al., 2018). Compound **67** exhibited strong absorption bands around 513 and 708 nm corresponding to the carbazolyl group and boron-dipyrrin core. For the BODIPY **67** containing glibenclamide analogous moiety, the fluorescene band appeared at 753 with 45 nm Stokes shift; also it demonstrated effective localization in endoplasmic reticulum (ER) of HeLa (human cervical cancer) and HepG2 (human hepatocarcinoma) cells. The compound **67** was able to generate singlet oxygen upon excitation at 610 nm; ER stress was the main reason of cell death as per the report (Zhou et al., 2018).

Meso-Substituted BODIPYs

Apart from *beta*- and *alpha*- positions of the BODIPY skeleton, the *meso*-position (C-8) can also be substituted with carbazole to prepare variety of dyes with improved absorption and

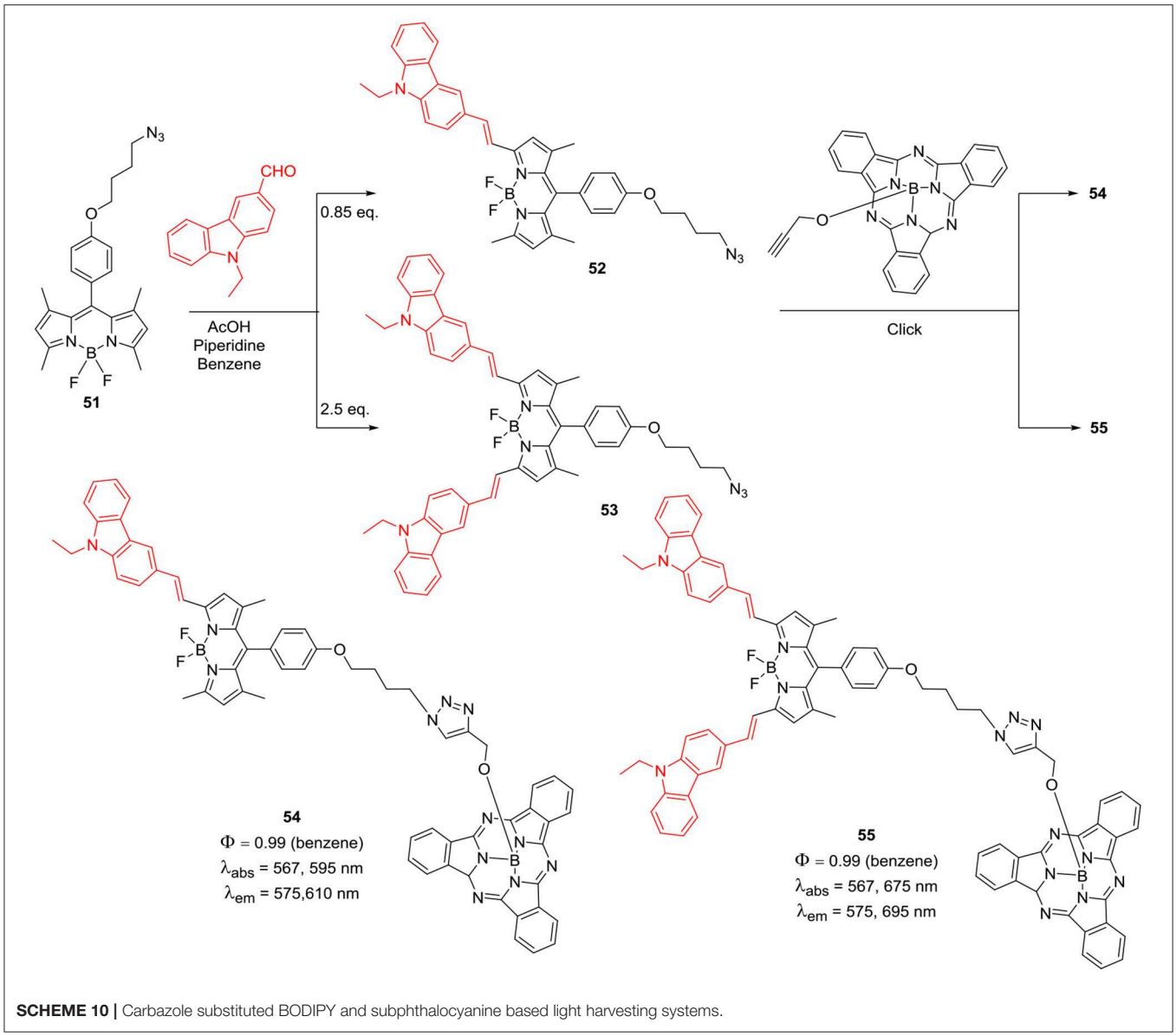

SCHEME 10 | Carbazole substituted BODIPY and subphthalocyanine based light harvesting systems.

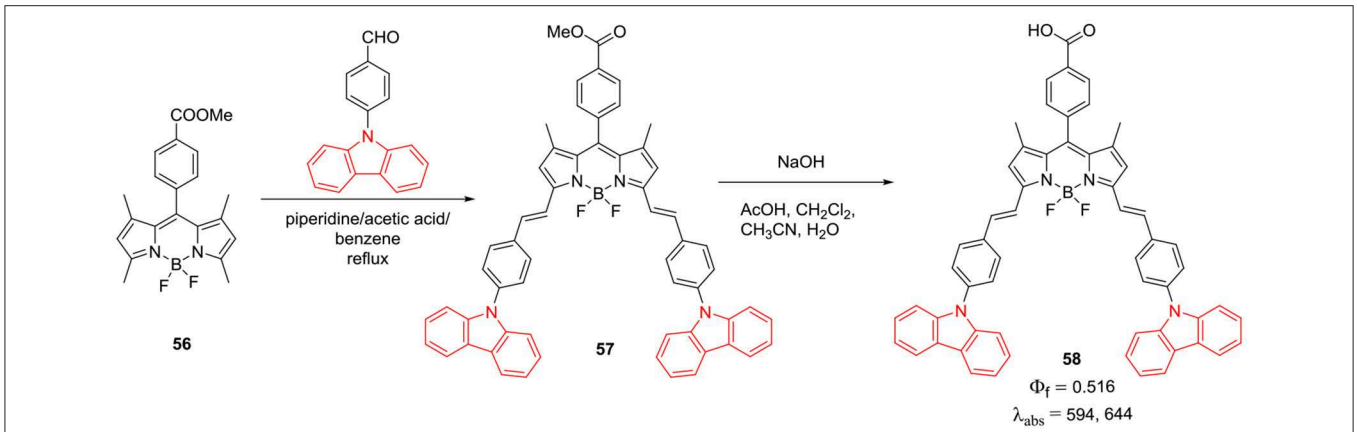

SCHEME 11 | Synthesis of α-Styryl linked *N*-phenyl carbazole BODIPY.

emission properties. Carbazole-based D–π-A type BODIPYs **69–71** were synthesized and studied for DSSC application (**Chart 7**) (Ooyama et al., 2013a). In BODIPY **69,** two 4-(thiophene-2-yl)pyridine units on the *alpha*-positions served as electron-withdrawing anchor groups and the *meso*-position was substituted with an electron donating 9-butyl-*N,N*-phenyl-7-(thiophen-2-yl)-9*H*-carbazol-2-amine group. The introduction of thiophene linkers between the donor and BODIPY core, extended the π conjugation of the entire system; which was indicated by the noticeable bathochromic shifts in absorption and emission of **69** (673, 696 nm, respectively). In BODIPYs **70** and **71** (**Chart 7**), the *meso*-substituent: 9-butyl-*N,N*-phenyl-7-(thiophen-2-yl)-9*H*-carbazol-2-amine acted as donor unit, which was linked to BODIPY core with the phenyl linker. The presence of small methyl/ethyl groups on the alpha-position of the BODIPY core in **70** and **71** does not cause much shifts in their absorption and emission maxima (Ooyama et al., 2013b).

The BODIPY **69** showed significant red shift in its absorption and emission; however, it showed moderate performance in DSSC studies. Authors attributed the low performance mainly to the following reasons: (1) Formation of strong π-stacked aggregates of BODIPY on the TiO_2 surface; (2) The lower LUMO level and the radiation less relaxation of the photoexcited dye which leads to a reduction in the electron-injection yield; (3) faster charge recombination between the injected electrons and I_3^- ions, leading to a decrease in the V_{oc} value (Ooyama et al., 2013a). Aggregation between BODIPY cores can be prevented by using co-adsorption of chenodeoxycholic acid (CDCA). One of the main reasons for radiation less relaxation is the free rotation of the aryl substituents at *alpha*- and *meso*-positions of the BODIPY skeleton. This rotation can be reduced by methyl substitution on BODIPY core (Ooyama et al., 2013b). Also, dyes **70** and **71** (**Chart 7**) showed solid-state red fluorescence and green metallic luster properties in both crystalline and amorphous states (Ooyama et al., 2014).

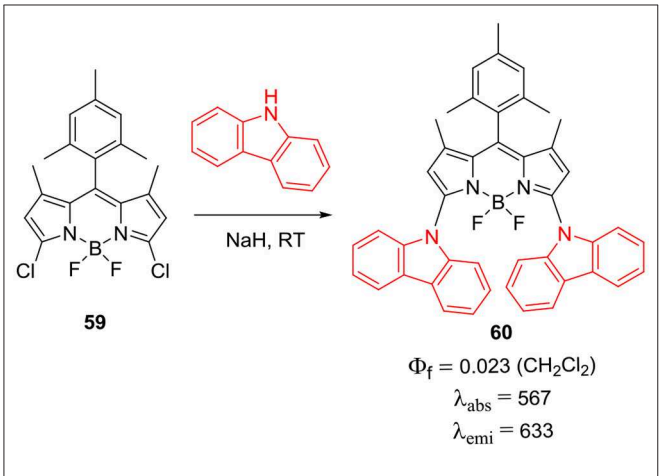

SCHEME 12 | Synthesis of *α-N*-carbazole BODIPY.

Substitution of carbazole unit on the *meso*-position of the BODIPY core through direct linkage is another method to incorporate carbazole unit on BODIPY skeleton. Gupta et al. reported synthesis and photophysical properties of *meso*-substituted carbazole-BODIPY dyad **72** (**Scheme 14**). This dyad exhibited energy transfer efficiency from donor carbazole unit to the acceptor BODIPY core. As shown in the **Scheme 14**, dyad was synthesized from the dipyrromethane having *meso*-carbazolyl unit, followed by complexation with $BF_3.OEt_2$ to obtain the desired product. BODIPY **72** was further used to make BODIPY derivatives **73–75** (**Scheme 14**). It was found that the *meso*-carbazoyl group altered the electronic properties of the four BODIPYs which was reflected in the higher extinction coefficient, red-shifted emission maxima, increased quantum yields and large Stokes shifts. Fluorescence studies indicated an efficient energy transfer from *meso*-carbazolyl moiety to the boron-dipyrrin core in all the compounds. Due to increased conjugation with the electron donor *meso*-carbazole group, anodic shifts were observed in the redox potentials of all four BODIPYs **72–75** (Kesavan and Gupta, 2014). The synthesis and photovoltaic application of *meso*-carbazolyl substituted BODIPY based photosensitizers **77** and

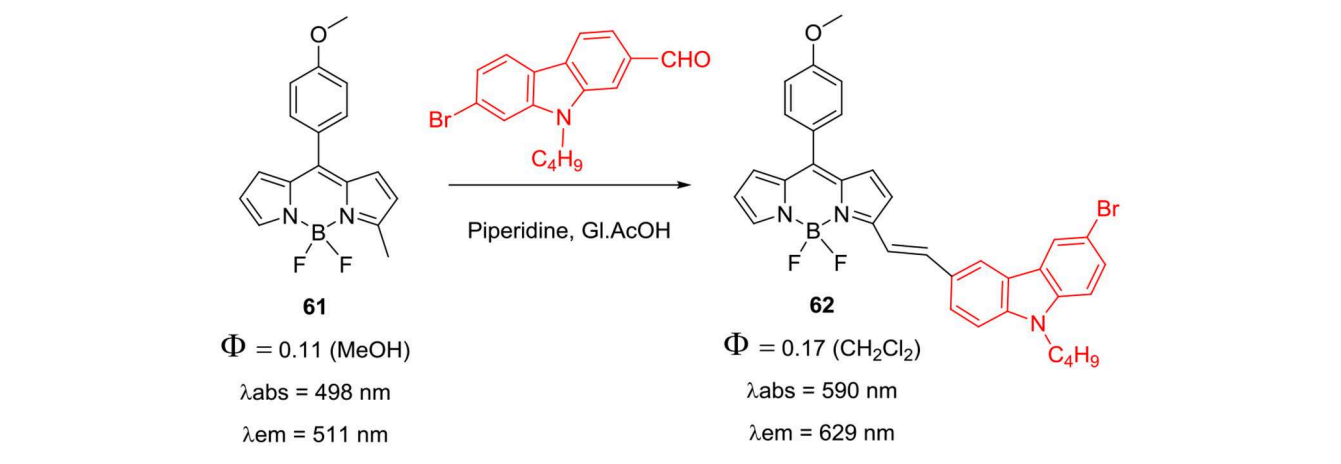

SCHEME 13 | α-Styryl BODIPY with *N*-butylcarbazole group.

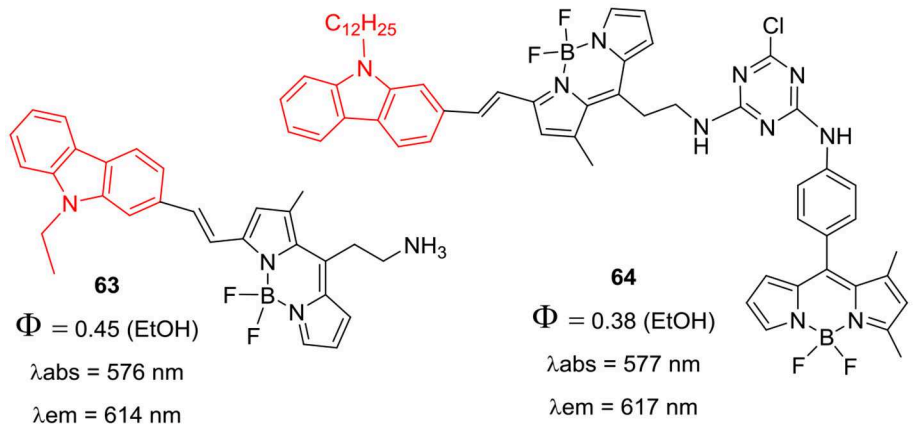

CHART 4 | Carbazole-BODIPY based systems for DRET.

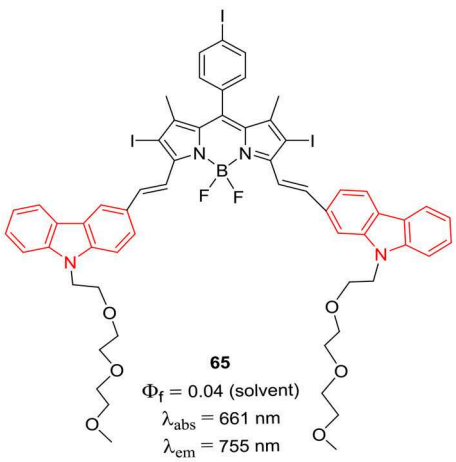

CHART 5 | α-Styryl carbazole-BODIPY based nanoparticles for PDT.

80 (**Scheme 15**) was reported. The photosensitizers were synthesized in four steps from the precursor BODIPYs **72** and **78** as shown in the **Scheme 15**. The BODIPY **80** exhibited higher photovoltaic performance than the photosensitizer **77** in DSSC studies (Kesavan et al., 2017).

Sekar et al. reported BODIPYs **81–83** having 9-ethyl-9*H*-carbazole or 9-phenyl-9*H*-carbazole group at the *meso*-position; the *alpha*- and *beta*-positions were substituted with the alkyl groups (**Chart 8**). The direct substitution of carbazole ring on the BODIPY skeleton resulted in the enhanced photostability, good lasing ability and singlet oxygen generation property of the dyes (Thorat et al., 2015; Telore et al., 2016). Misra et al. (2014) reported *meso*-ethynyl linked carbazole-BODIPYs **84–86** (**Chart 9**); efficient intramolecular charge transfer from carbazole unit to the BODIPY unit was observed (Dhokale et al., 2015). Compounds **84–86** showed high open circuit voltage and thus exhibited good application in bulk heterojunction organic solar cells (Jadhav et al., 2015).

Farfan and Correon-Castro groups (Corona-Sánchez et al., 2016) reported DFT studies of the thin films of *meso*-substituted BODIPY **87** having *N*-ethyl-carabzole ring (**Chart 10**). The thin films of BODIPY **87** were prepared by the vapor deposition on indium tin oxide; packing morphology of the films was simulated through computational methods and their semi-conductor behavior was predicted. Such kind of DFT study can be helpful when such BODIPY dyes are used in the electronic devices for OPV applications (Corona-Sánchez et al., 2016). Another interesting report by Xing et al., used BODIPYs **88** and **89** to make liposomes encapsulated fluorescent nanoparticles (Lv et al., 2017). The nanoparticles of **88** and **89** showed decent absorption in HEPES buffer at 504 nm; also their emission was centered on 525 nm with about 21 nm Stokes shift. These hydrophilic fluorescent nanoparticles were also tested for live cell imaging on HeLa cells, and the results indicated primary localization in the lysosomes (Lv et al., 2017).

Carbazole ring can also be linked to the *meso*-position of BODIPY core via *N*-linkage (**Chart 11**); Nguyen et al. (2014) revealed the OLED application of BODIPY **90**, having 9-phenyl-9*H*-carbazole group at the *meso*-position. BODIPY **90** exhibited green emission with low turn-on voltage in OLED performance, maximum brightness, current efficiency and power efficiency. Report by Li et al. revealed the AIEE ability of BODIPY **91** (**Chart 11**), which showed enhanced emission in the aggregated form. BODIPY **91** showed weak emission in THF; and the nano aggregates of **91** were prepared in THF water mixture by precipitation method. The noticeable increment in fluorescence intensity of **91** was observed with the gradual increase in the water fraction. In 90% water/THF mixture molecule **91** showed the strongest emission intensity. Similar aggregation study was carried out by preparing carbazole-BODIPY **91** loaded silica nanoparticles, and these nanoparticles demonstrated a stable uniform morphology and strong fluorescence. This AIEE effect was successfully applied for cell imaging and found that BODIPY **91** showed good cellular uptake in MCF-7 cells (Li and Qian, 2016). The recent report by Reddy et al. showed

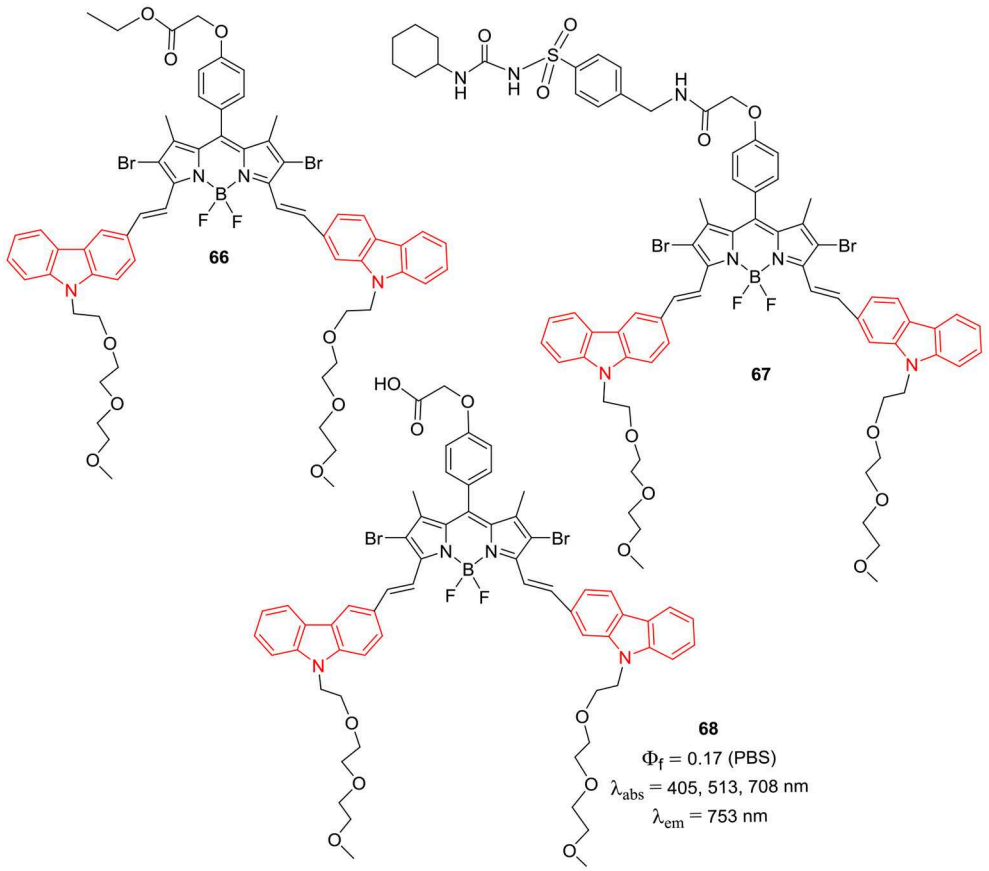

CHART 6 | α-Styryl carbazole-BODIPYs for bioimaging and PDT.

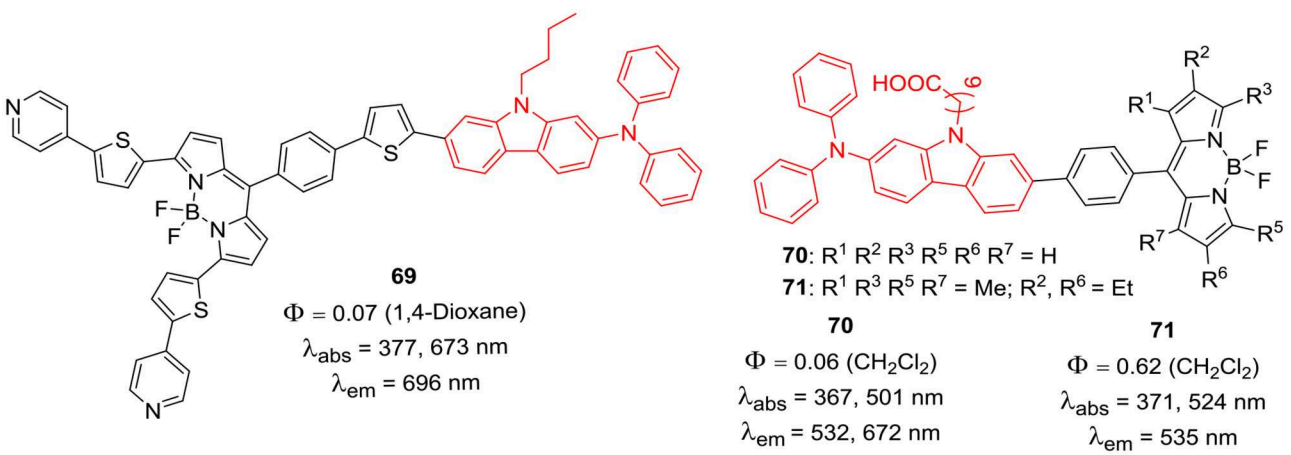

CHART 7 | *Meso N*-alkyl carbazole BODIPYs for solar cell application.

that *meso*-substitution of BODIPY with carbazole ring can be achieved through *N*-linkage; such BODIPYs **92–94** (**Chart 12**) exhibited photoinduced energy transfer (PEnT). They studied the effect of linker length on PEnT using varying lengths of bridges (phenyl, biphenyl and diphenylethyne) on the BODIPYs **92–94** (**Chart 12**). Selective excitation of these molecules at carbazole unit resulted in a very efficient energy transfer process (Reddy et al., 2018).

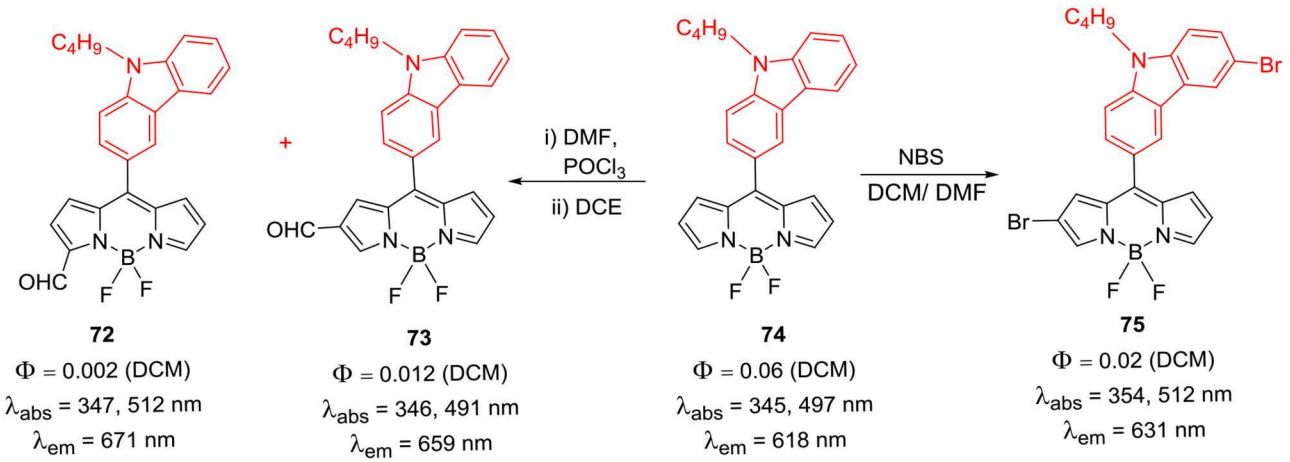

SCHEME 14 | Synthesis of *meso*-carbazole substituted BODIPYs.

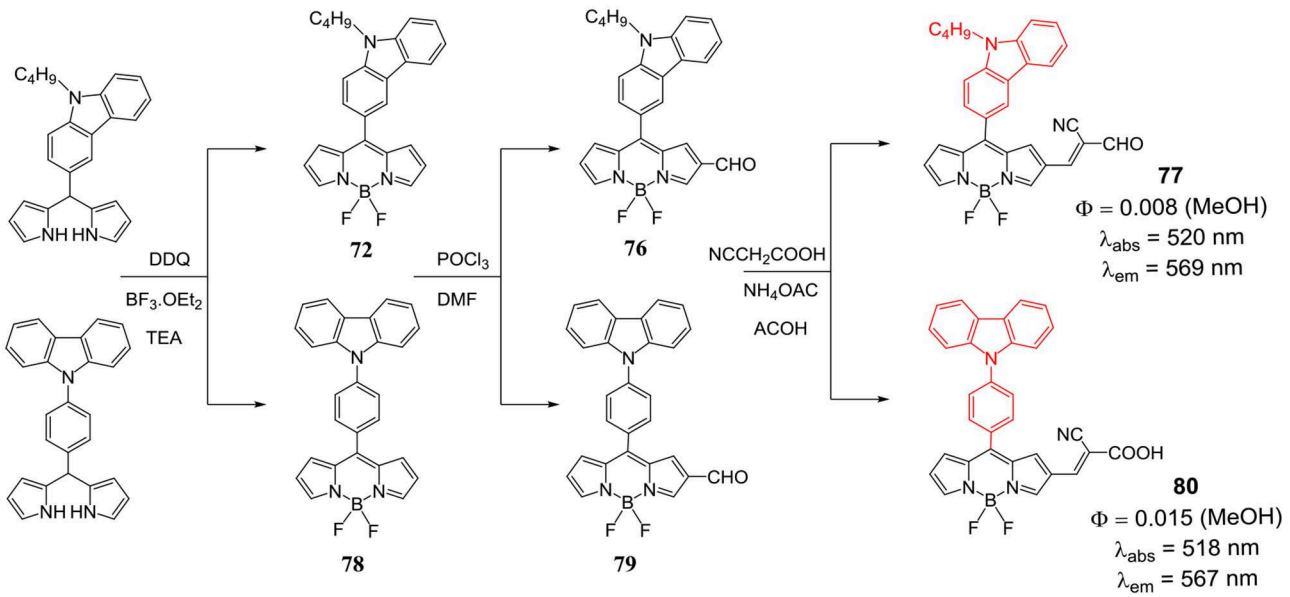

SCHEME 15 | *Meso*-carbazolyl substituted BODIPYs.

Recently, Thayumanavan et al. prepared donor-acceptor type BODIPYs **95–97** (**Chart 13**) and studied photo-induced electron transfer process for these dyes (Strahan et al., 2019). The electron rich carbazole donor group was attached at either *beta*- or *meso*-position of the BODIPYs to access intramolecular charge transfer (ICT) in the dyes **95–97** (**Chart 13**). The ICT was more facile in the BODIPY **95** as compared to the **96** and **97** in polar solvents; also the carbazole substation at *beta*-position of the BODIPY skeleton shifted the absorption of **95** toward red region with higher molar extinction coefficient than the *meso*- substituted BODIPYs **96** and **97** (Strahan et al., 2019). Qian's group had reported *meso*-*N*-ethylcarbazole substituted BODIPYs **98–100** (**Scheme 16**); the molecule **101** containing nitro-substituted benzoxadiazole (NBD) moieties, was used as fluorescent probe for biothiol detection and live cell imaging (Xia and Qian, 2018). The probe **100** also demonstrated visible color change from blue to green upon addition of biothiols in the solution; thus it can be used to develop sensor-kit for biothiols in future. In addition, **100** was successfully applied to detect Cys, Hcy, and GSH in living cells (Xia and Qian, 2018).

Carbazole Bridged BODIPY Dimers

Zong et al. reported carbazole bridged BODIPY dimers **101–103** with extended π conjugation (**Chart 14**) by introducing linker moieties in between carbazole and BODIPY units. The linkers varied from phenyl, thiophene to furan rings; all these conjugates

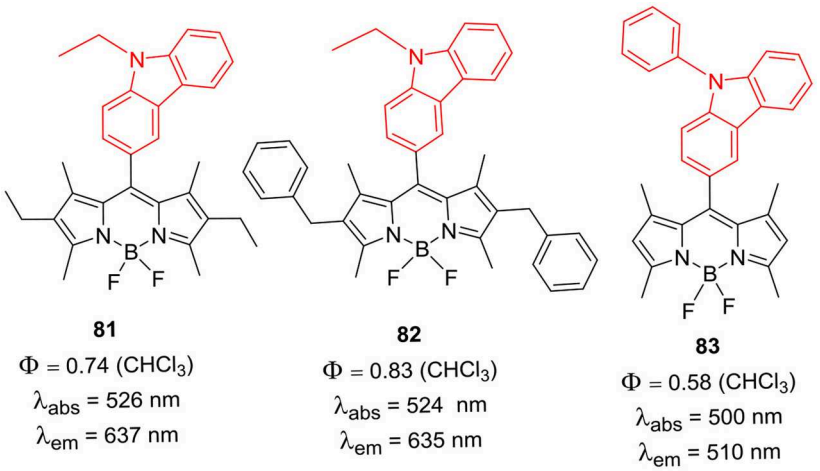

CHART 8 | *Meso*-carbazolyl substituted BODIPY derivatives.

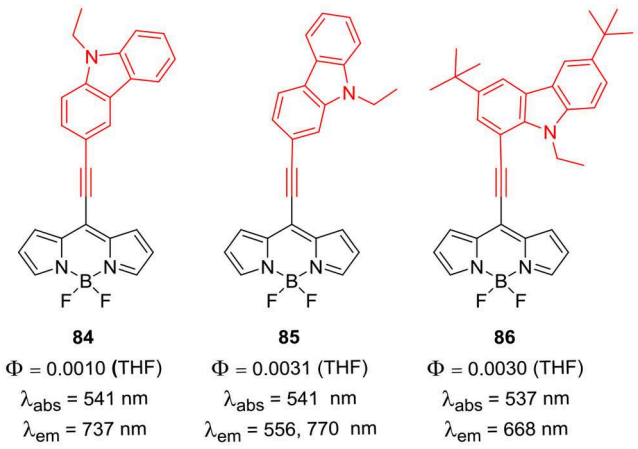

CHART 9 | *Meso*-ethynyl linked carbazole-BODIPYs.

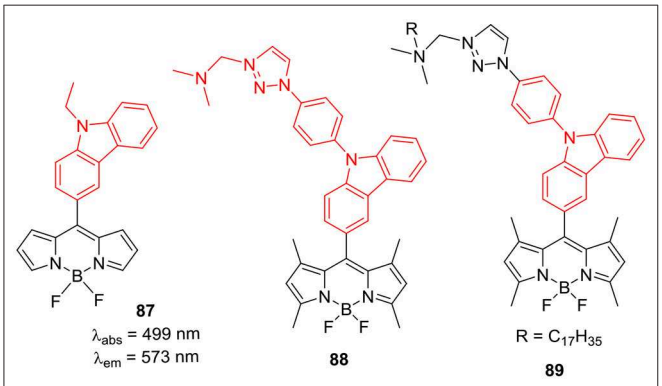

CHART 10 | *Meso*-carbazole substituted BODIPYs.

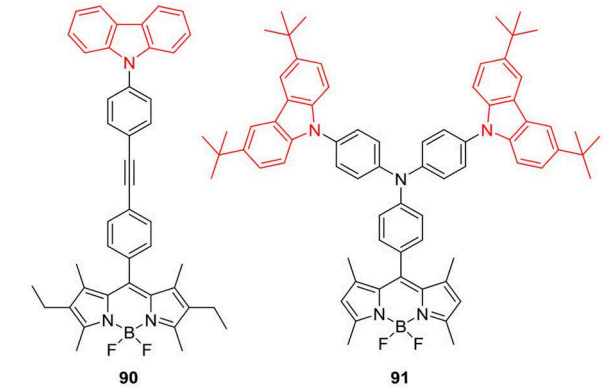

CHART 11 | *N*-Phenyl carbazole units linked to *meso*-position of BODIPYs.

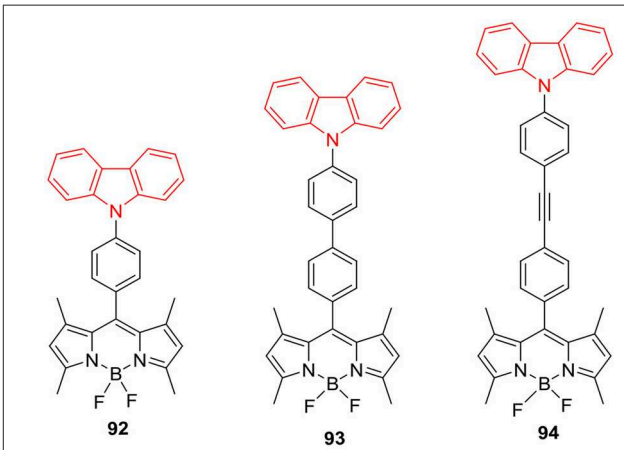

CHART 12 | *N*-Phenyl carbazole linked BODIPY with varying linker size.

possess good thermal stability. From the photophysical and electrochemical analysis, it was revealed that thiophene and furan linked carbazole-BODIPY dimers (**101**, **102**) are potential candidates for p-type semiconductor materials in organic solar cells (Zong et al., 2017). Report by Liao et al. showed that presence of alkynyl group as bridging unit (**Chart 13**; **104**) shifted the absorption and emission toward red region. BODIPY **104** exhibited average photovoltaic performance of

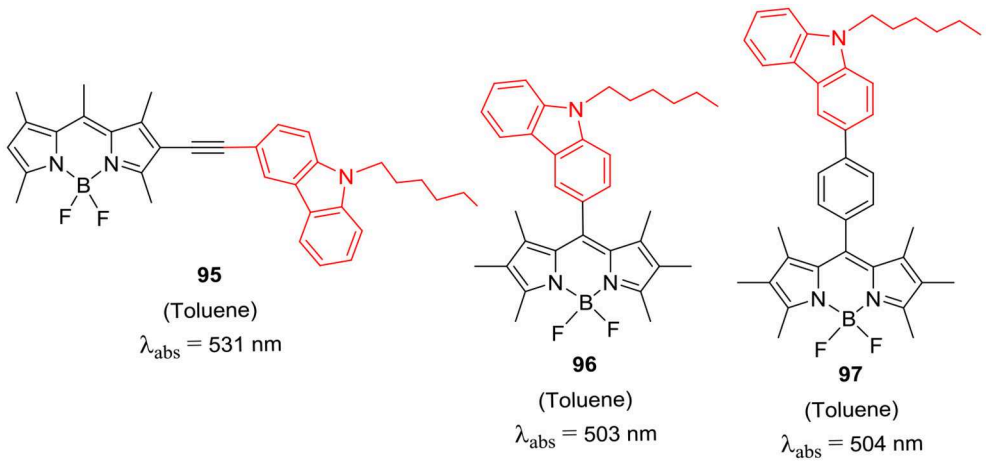

CHART 13 | β-substituted and *meso*-substituted carbazole-BODIPYs.

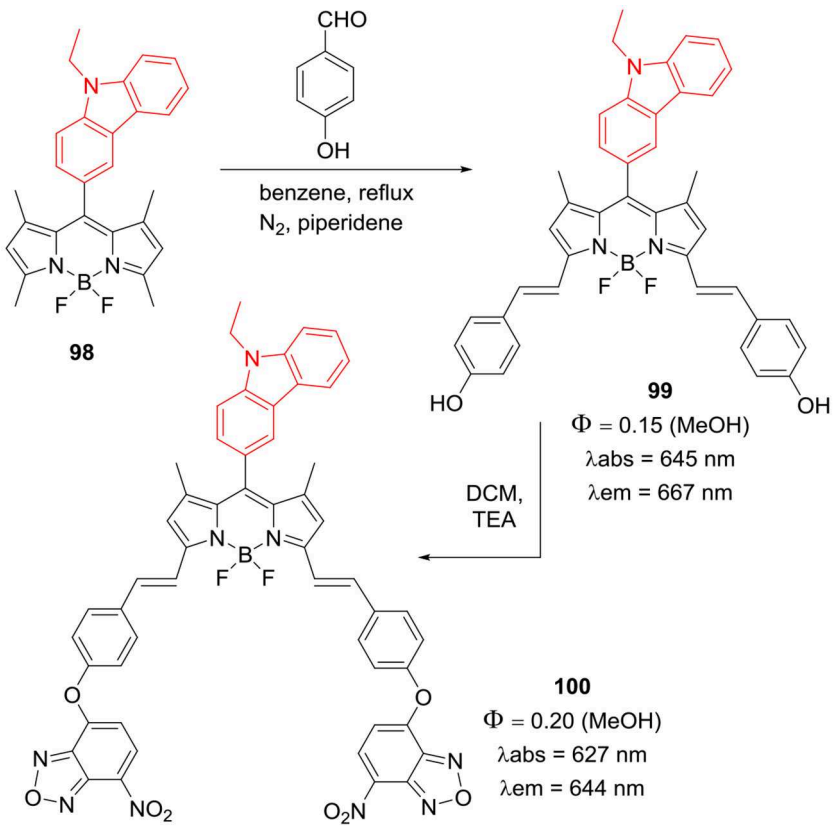

SCHEME 16 | *Meso*-carbazole substituted BODIPY for biothiol detection.

3.1% by a hole mobility mechanism (Liao et al., 2017a). Also, compound **105** (**Chart 14**) showed decent cytotoxic activity against HT29 cell lines (Sengul et al., 2015). In another report Gupta et al. synthesized *N*-butylcarbazole bridged BODIPY dimer **106** (**Chart 14**); the compound showed bathochromic shift in the emission band with good Stokes shift of 83 nm (Kesavan et al., 2015).

Meso-carbazole substituted BODIPY **107** and N-alkyl-carbazole bridged BODIPY dimer **108** (**Chart 15**) were prepared and their biological activities were tested in

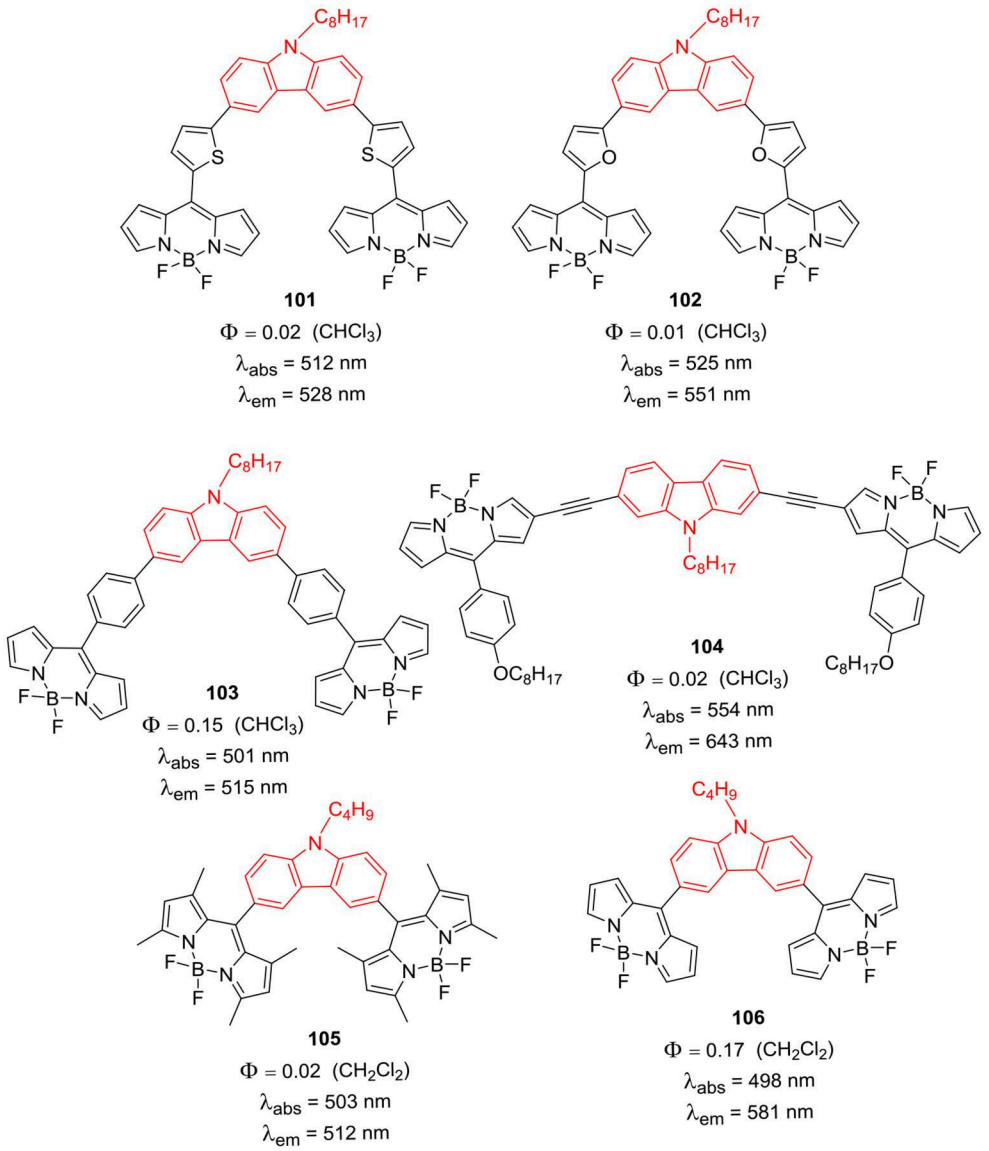

CHART 14 | Carbazole bridged BODIPY dimers.

the human colon cancer cell lines (Sengul et al., 2015). The BODIPYs **107** and **108** exhibited strong absorption around 503 nm and fluorescence at 512 nm; cytotoxicity assays in HT29 cancer cells revealed that, **108** is more toxic than **107** (**Chart 15**). The observed IC_{50} values for **107** and **108** were 21.7 ng/mL and 8.3 ng/mL, respectively (Sengul et al., 2015).

BODIPY based nanocar containing *p*-carborane wheels and central *N*-butylcarbazole moiety was prepared by Godoy et al. (2010). The BODIPY nanocar **109** (**Chart 16**), was highly emissive in nature making it ideal candidate for single molecule fluorescence spectroscopy. Such nanocars are reported to move by an average speed of 4 nm/s on the glass surface under ambient conditions due to the presence of *p*-carborane wheels (Godoy et al., 2010).

Miscellanious Systems

In 2013, Ma et al. reported NIR emissive D–π-A polymers **112**, where aza-BODIPY moiety acted as acceptor and electron rich carbazole group served as donor. The synthesis of *beta*-diiodinated derivative of aza-BODIPY **111** was prepared by treating **110** with *N*-iodosuccinimide (**Scheme 17**). The polymerization of BODIPY **111** was accomplished by a palladium-catalyzed Sonogashira coupling reaction with 3,6-diethynyl 9-octyl-9*H*-carbazole moiety (**Scheme 17**). The good advantage of such polymer systems is that, these molecules exhibit near-infrared fluorescence around 750 nm and also show tunable band gap in the range of 0.96–1.14 eV. These photophysical and electrochemical properties promises the application of this polymer **112** in device based applications (Ma et al., 2013).

Another interesting report by Patra et al. described the synthesis of porous organic polymer **113** (**Chart 17**) consisting of *N*-alkyl bridged carbazole and BODIPY units (Bandyopadhyay et al., 2018); the macromolecule was able to generate substantial singlet oxygen in solution. The porous soluble polymer **113** exhibited red shifted absorption and emission in the range of 530–610 nm; and used as fluorescent probe for superoxide anion (Bandyopadhyay et al., 2018). The π-conjugated polymers having BODIPY backbone are used as photosensitizers in organic photovoltaics (OPV); and strong absorption in the red or NIR region is desired for high performance of the devices. Combination of BODIPY unit with good electron rich donor moiety in the polymer chain can yield the copolymer with strong absorption profile in the visible-NIR region of the solar spectrum. The optical band gap can be reduced in copolymers by linking donor and acceptor units; Thayumanavan et al. have synthesized π-conjugated BODIPY copolymers **114** (**Chart 18**) having *N*-alkylcarbazole/dithienopyrrole/bithiophene/fluorene as donor moieties (Popere et al., 2012). The rationally designed copolymers exhibited lower band gap and broad absorption spectra encompassing the entire visible region; thus, making them good panchromatic dyes for OPV applications (Popere et al., 2012). Such copolymers containing π-conjugated donor-acceptor units also show interesting charge transfer and/or energy transfer properties with enhanced absorption and fluorescence in the visible to red region.

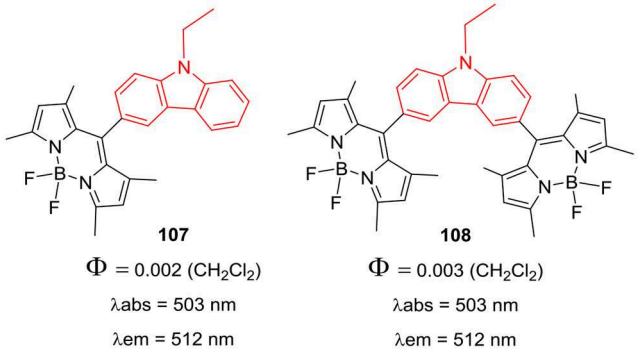

CHART 15 | *Meso*-substituted carbazole-BODIPYs.

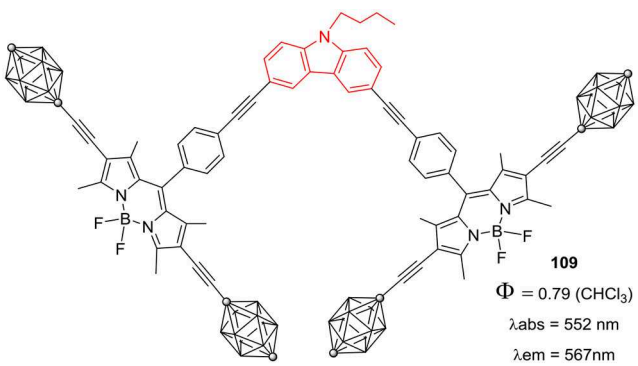

CHART 16 | BODIPY based nanocar having *p*-carbone wheels.

Another π-conjugated copolymer **116** incorporating indolo[3,2,-b]-carbazole and BODIPY units (**Chart 18**) was prepared from **115,** by Khetubol et al. (2015). Copolymer **116** showed broad and red shifted absorption and emission spectra along with the energy transfer from donor indolo[3,2,-b]-carbazole to the acceptor BODIPY unit. The electronic properties of organic π-conjugated polymers can be fine-tuned by introducing electron donor and accepter moieties in the main chain; the resultant macromolecules are popular in OPV, solar cells, and OLEDs, etc. due to light weight and flexible structures. Ma et al. (2014) had reported D-π-A type chiral copolymer **117** by joining BODIPY and *N*-alkylcarbazole via ethyne linkages (**Chart 18**). Chiral polymer **117** displayed red shifted fluorescence (624–650 nm) and small band gap of about 159–196 eV (Ma et al., 2014). Organic

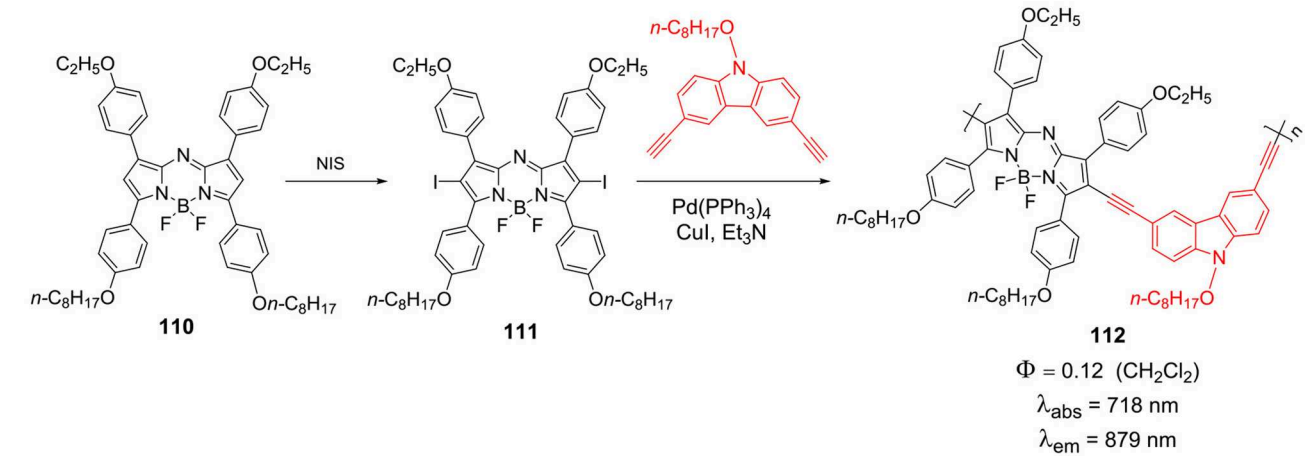

SCHEME 17 | Synthesis of carbazole aza-BODIPY polymer.

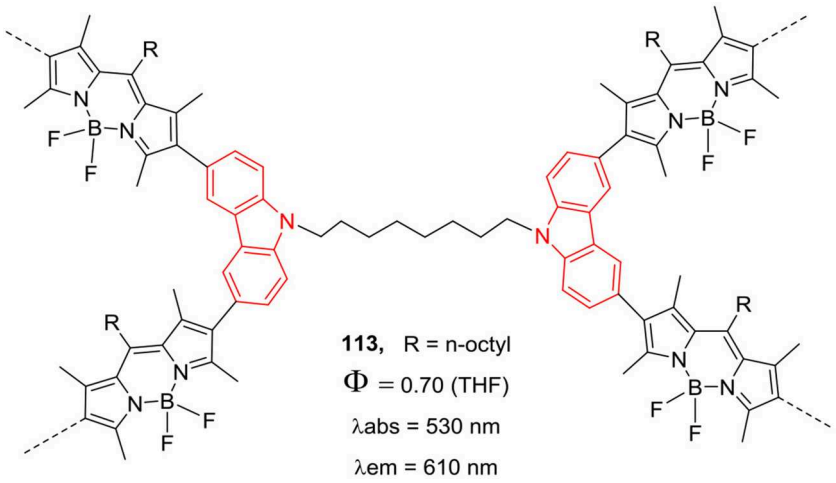

CHART 17 | Synthesis of carbazole-BODIPY based soluble polymer.

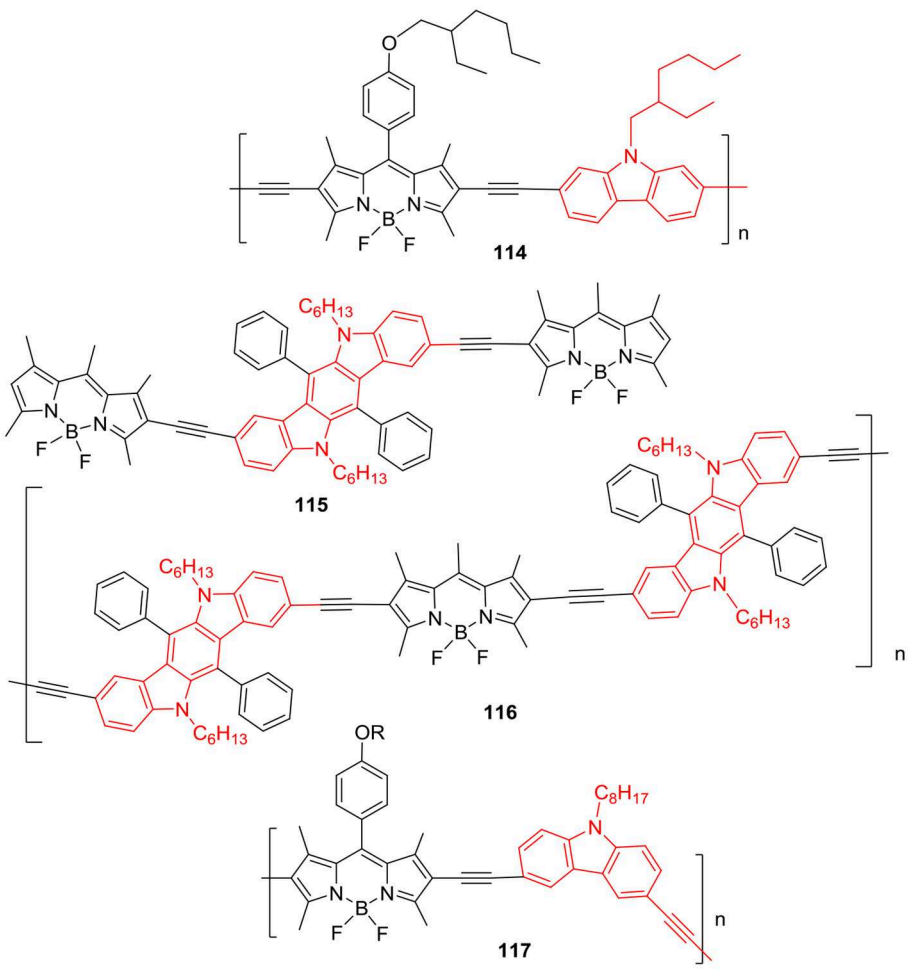

CHART 18 | Carbazole-BODIPY based polymers.

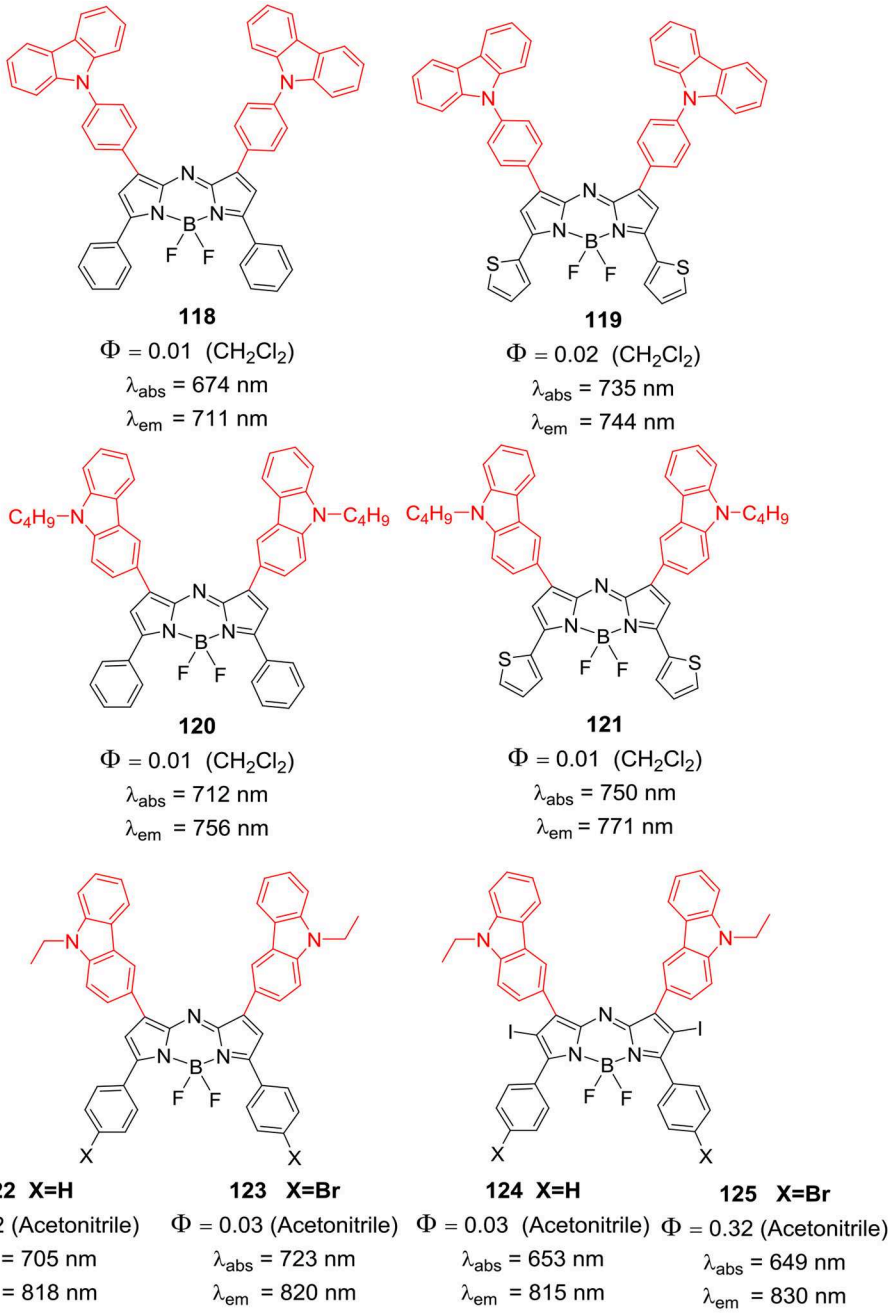

CHART 19 | 1,7 *N*-phenylcarbazole or *N*-alkylcarbazole substituted aza-BODIPYs.

conjugated copolymers are popular for their applications in OLEDs and solar cells due to low cost and light weight; and their electronic properties can be fine-tuned by altering the donor and acceptor units in the polymer backbone. Such BODIPY based macromolecules can be synthesized by replacing the electron donor moieties with different aromatic heterocycles like fluorene, phenothiazine, bithiphene, and carbazole derivatives to enhance their photophysical and electrochemical properties for various applications (Ma et al., 2014).

Aza-BODIPYs are class of BODIPYs which are obtained by substitution of the *meso*-carbon (C-8) atom by nitrogen-atom (Balsukuri et al., 2018). This alteration shifts the absorption and emission maxima of the resultant aza-BODIPY toward NIR region (600–900 nm). Aza-BODIPYs (Balsukuri et al., 2016a) are excellent candidates for the deep tissue imaging as NIR

fluorescent probes and as photosensitizers for PDT and DSSC applications. In 2016, Gupta et al. have reported synthesis and optical studies of donor-acceptor type NIR aza-BODIPYs **118–121** (**Chart 19**), having *N*-phenylcarbazole or *N*-butylcarbazole at the 1,7-positions of the BODIPY core (Balsukuri et al., 2016a). These molecules showed significantly red shifted (∼100 nm) absorption and emission relative to the parent tetraphenylaza–BODIPY (Balsukuri et al., 2016b). Also, Fluorescence studies of these molecules suggested effective energy transfer (up to 93%) from donor groups to the aza–BODIPY core. This strategy validated that, simple substitution with energy-donor groups on aza–BODIPYs can induce large red shifts in their electronic spectra, and this approach can be applied to make novel NIR dyes. In 2017, Gawale's group reported synthesis of *N*-ethylcarbazole linked aza-BODIPYs **122–125** (**Chart 19**), and studied their efficiency to produce triplet excited state and singlet oxygen generation (Gawale et al., 2017). The presence of iodo groups at the *beta*-positions of the aza-BODIPY helped in the enhancement of intersystem crossing efficiency in these molecules. Aza-BODIPYs **122–125** (**Chart 19**) were able to have sufficiently long triplet excited state and showed 70% singlet oxygen generation efficiency. Also, authors reported application of these molecules in deep tissue photo-acoustic imaging and up to 2 cm deep photoacoustic imaging was successfully demonstrated by using **122** as contrast agent; making it a potential candidate for theranostic application.

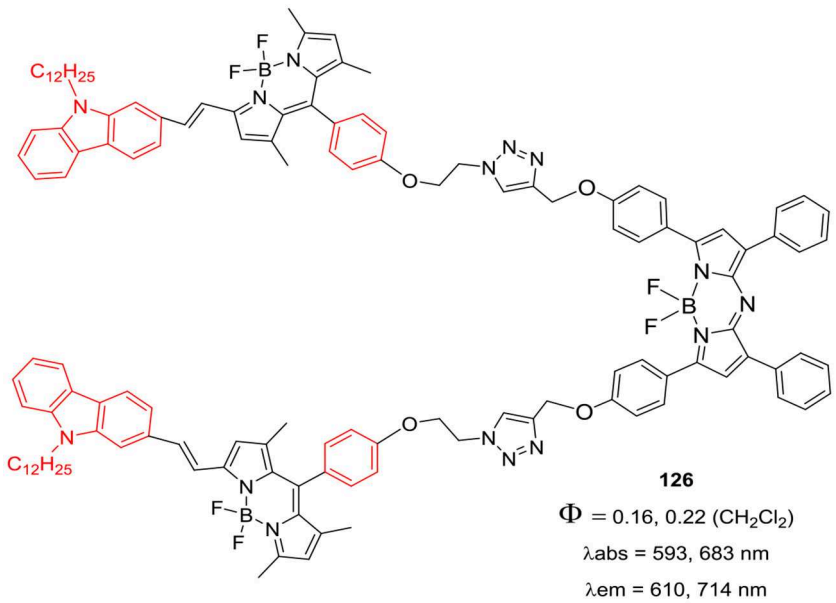

CHART 20 | BODIPY triad having Aza-BODIPY as central unit.

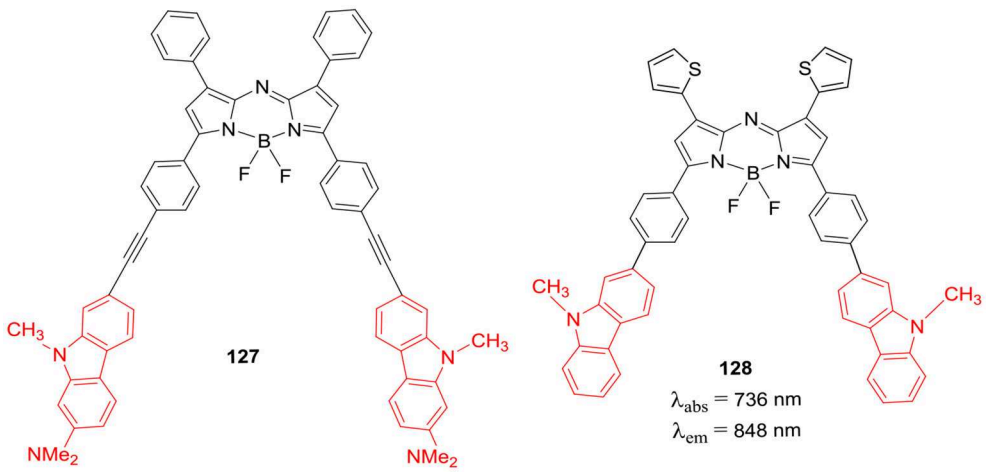

CHART 21 | Carbazole linked Aza-BODIPY model system for DFT studies.

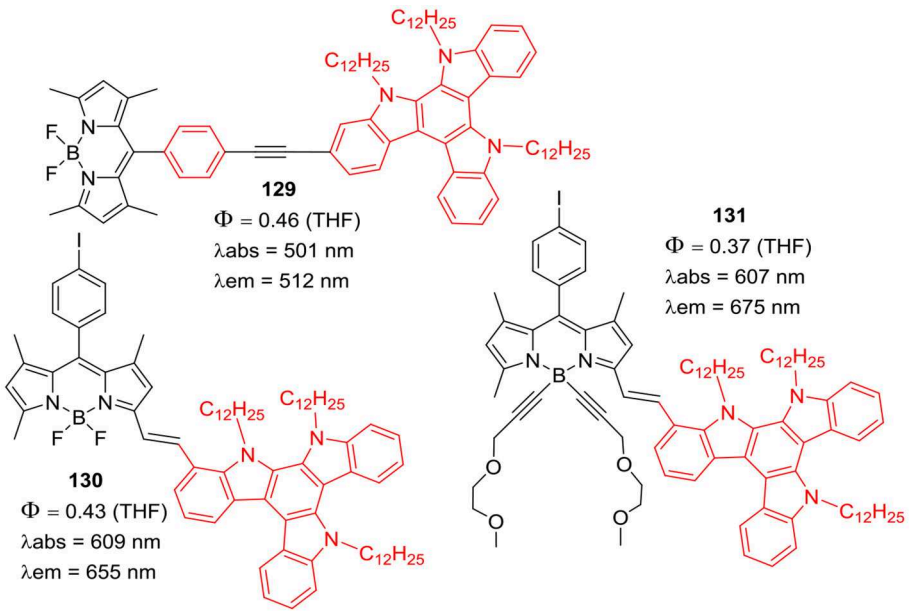

CHART 22 | Triazatruxene linked BODIPY dyes.

Triplet photosensitizers based on porphyrins and transition metal complexes are widely used in photo-catalysis of organic transformations and PDT. However, triplet sensitizers based on BODIPYs have iodo- or bromo- substituents to induce efficient ISC in such molecules. Typically, triplet sensitizers show strong absorption in the visible region, corresponding to the chromophores present in the molecule; though, panchromatic absorption of such molecules is highly desirable for various applications. Zhao and co-workers have combined the BODIPY and aza-BODIPY units to prepare a triad **126** (**Chart 20**) with interesting photophysical properties (Guo et al., 2014). The triad **126** displayed wide absorption in the visible-red region; along with the intramolecular energy transfer from donor units (BODIPY) and acceptor unit (aza-BODIPY). The resonance energy transfer (RET) in the triad **126** (**Chart 20**) was helpful to populate triplet excited state upon visible light excitation; which was further used to generate singlet oxygen with 58% quantum yield (Guo et al., 2014). Liu et al. (2013) carried out theoretical calculations for better understanding of the electronic structures and linear absorption of the series of aza-BODIPYs. DFT studies were also performed to investigate the two-photon absorption (TPA) properties of the aza-BODIPYs having various substituents viz. thiophene, phenyl, *N*-alkylcarbazole, fluorine, and pyrene, etc. Among the series of molecules investigated, the aza-BODIPY **127** (**Chart 21**) with elongated π-conjugated system was predicted to show lower HOMO-LUMO energy gap. Another interesting report by Huang's group discussed the synthesis of color tunable NIR aza-BODIPY **128** (**Chart 21**) and its application for sensing mercury ions (Liu et al., 2014). The introduction of aromatic carbazole ring induced red-shifts in the absorption and emission spectra; aza-BODIPY **128** (**Chart 21**) exhibited strong absorption peaks at 720 and 736 nm along with intense fluorescence at 848 nm. The two thienyl groups in the aza-BODIPY **128** served as binding pocket for mercury ion and its fluorescence was quenched after Hg+ binding making it a "turn-off" type fluorescent probe (Liu et al., 2014).

Ziessel et al. prepared BODIPYs **129–131** (**Chart 22**) substituted with triazatruxene (TAT) moiety at *alpha*-styryl or *meso*-phenyl positions of the BODIPY skeleton (Bura et al., 2011). TAT is a star shaped molecule consisting of three fused carbazole rings with flat aromatic structure; its derivatives have shown good two-photon absorption (TPA) properties and high hole mobility. The TAT substituted BODIPYs **129–131** exhibited large absorption coefficients and strong emission around 655–675 nm. The interesting electrochemical properties of molecules **129–131** (**Chart 22**) were examined, these blue dyes exhibited photovoltaic efficiencies in the range of 0.08–0.9% in bulk heterojunction solar cells (Bura et al., 2011).

Carbazole is an electron rich aromatic heterocycle and its derivatives are known for their good electronic and hole transport properties; therefore, carbazole conjugated systems have found application in DSSCs and OLEDs. Carbazole based dendrimers can be linked to other chromophores to enhance the absorption and emission properties of such dyes; D-π-A (Donor-π-Acceptor) type BODIPY core dendrimers **132–134** (**Chart 23**) were synthesized by Babu et al. (2018). The carbazole based dendrimers having BODIPY at the center, displayed rise in their absorption coefficients and red shifted emission upon moving from G0 to G2 generations (**Chart 24**). Compound **134** (G3 dendrimer) showed 2.7% light to energy conversion as sensitizer in DSSC, which was higher than the G0 and G1 dendrimers. Such carbazole based dendrimers are attractive alternatives for solar light

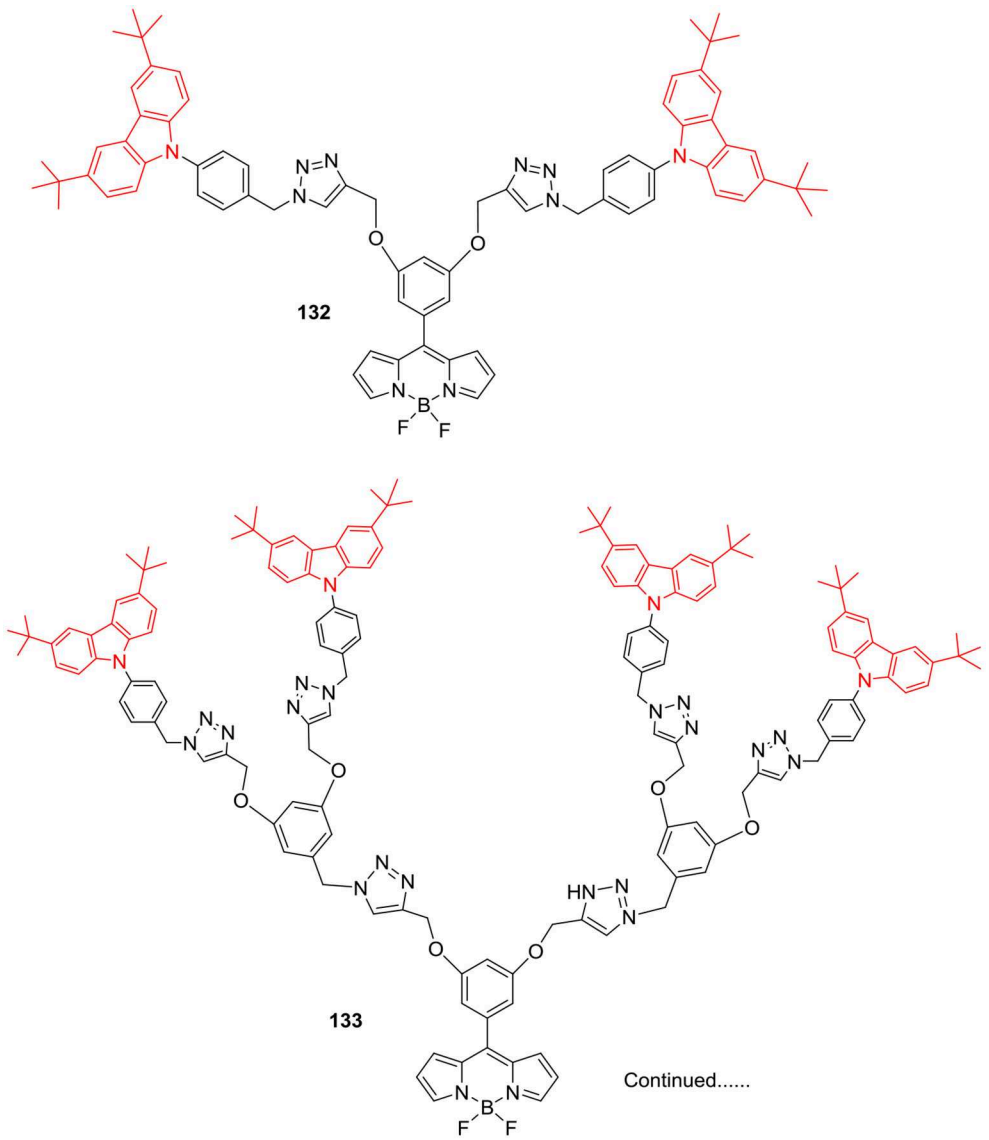

CHART 23 | Carbazole based BODIPY core dendrimers (G0, G1 series).

harvesting materials, as compared to small organic molecules (Babu et al., 2018).

Typically, BODIPY dyes have short lifetimes for singlet excited states and small Stokes shifts, which restrict their application in solar light harvesting systems. The linking of BODIPY chromophore to another metal complex can overcome such limitation; **Chart 25** shows interesting dual emission systems **135** and **136** comprising of carbazole substituted BODIPY unit and Ru(II) polypyridyl unit (Swavey et al., 2019). Compound **135** acted as precursor for the BODIPY and Ru(II)polypyridyl conjugate **136**; the major absorption band was significantly red shifted in the later (**Chart 25**). Also, the luminescence of the BODIPY unit in **136** was quenched due to the presence of Ru(II) polypyridyl unit; which could be attributed to the increased ISC and other non-radiative decay processes in such conjugates. Compound **136** generated significant singlet oxygen in acetonitrile solution, upon irradiation with long wavelength light; indicating its potential use in PDT (Swavey et al., 2019).

Sekar et al. have reported coumarin-carbazole conjugates and their BF_2 complexes **137** and **138** (**Chart 26**); such D-π-A systems displayed intramolcular charge-transfer process from donor carbazole ring to the coumarin acceptor unit (Rajeshirke et al., 2018). For conjugates **137** and **138**, the emission maxima were observed at 592 and 627 nm, respectively. The strong fluorescence of the BF_2 complexed coumarin unit in the red region was attributed to the attachment of carbazole donor group; these dyes can be potentially useful for biological applications (Rajeshirke et al., 2018). The BF_2 complexes of carbazole-benzimidazole conjugates **139** and **140** (**Chart 26**) were synthesized by Dutta et al. (2017). Both the

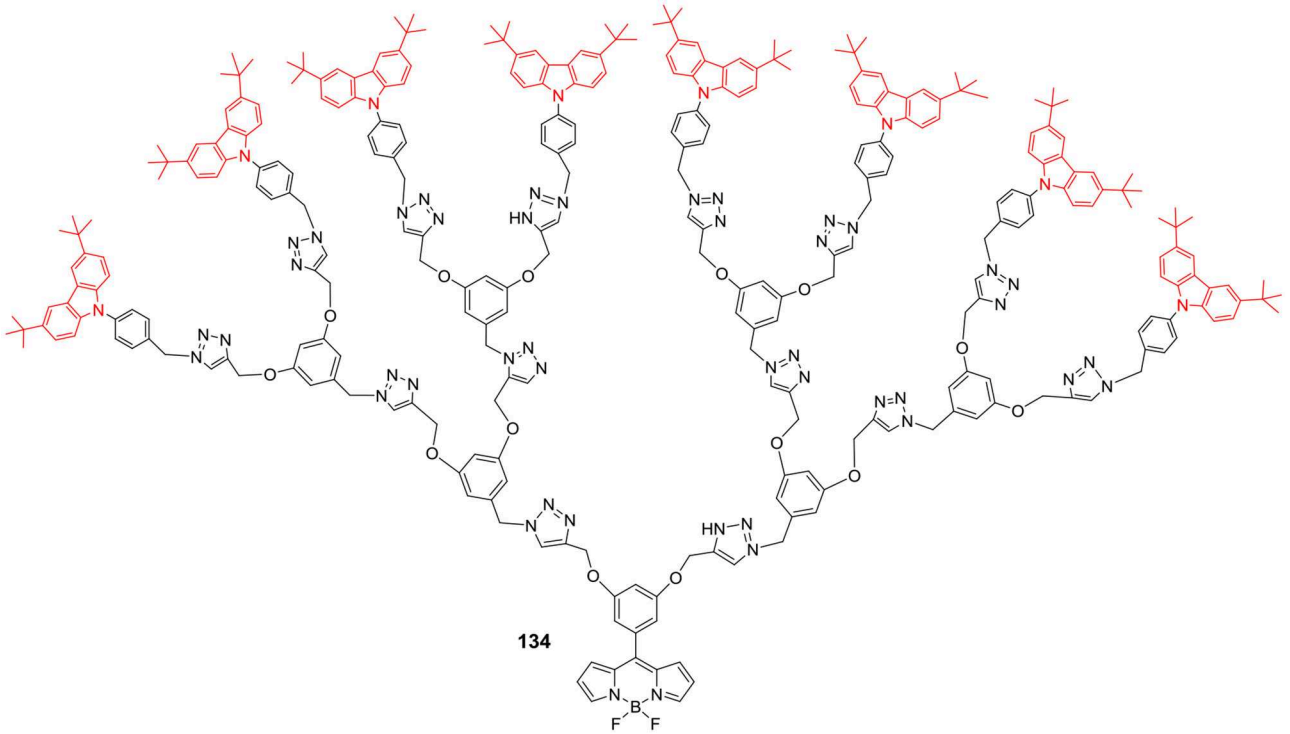

CHART 24 | Carbazole based BODIPY core dendrimer, G2 series.

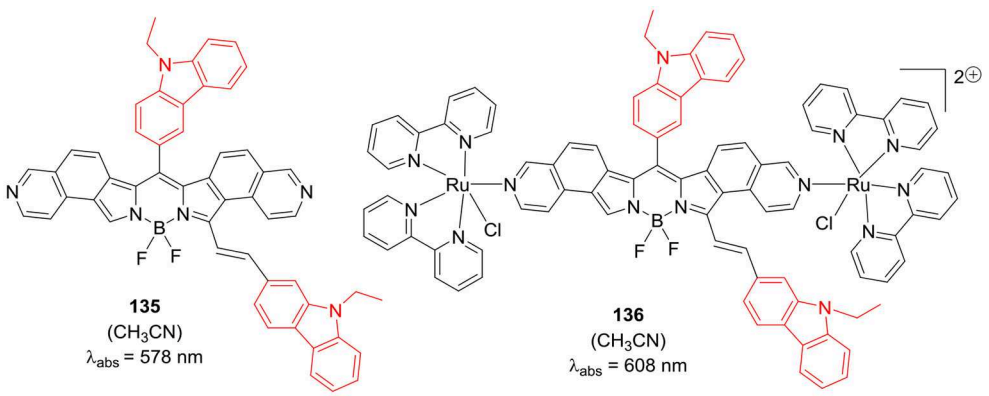

CHART 25 | Carbazole -BODIPY bridged Ru(II)polypyridyl complexes.

compounds **139** and **140** displayed relatively large Stokes shifts (34–51 nm) as compared to the typical BODIPY dyes; such molecular scaffolds can be used to develop fluorescence probes in future.

Zhu et al. (2015) have prepared very interesting BF_2 complexes **141** and **142** (**Chart 27**); where the aza-dipyrromethene skeleton was replaced by the aza-boron-diquinomethene. The aza-boron-diquinomethene scaffold was substituted with *N*-carbazolyl and/or 3,6-di-tert-butyl-*N*-carbazolyl moieties (**Chart 27**); the photoluminescence spectra of **141** and **142** showed green-yellow emission due to intramolecular charge transfer. The fluorescence quantum yields were reasonably high between 0.73 and 0.78; such BF_2 complexes may be suitable for developing pH-sensors and bioimaging probes in future (Zhu et al., 2015). Ema et al. have reported a series of exciting BF_2 complexes based on carbazole scaffold (Maeda et al., 2016); where carbazole ring was substituted with thiazole, benzothiazole, imidazole, indolone, and benzimidazole (**Chart 28**). The carbazole-based BF_2 complexes **143–148** (**Chart 28**) displayed strong absorption (382–663 nm range) and fluorescence (427–796 nm range) in dichloromethane solution; the emission quantum yield were in the range of

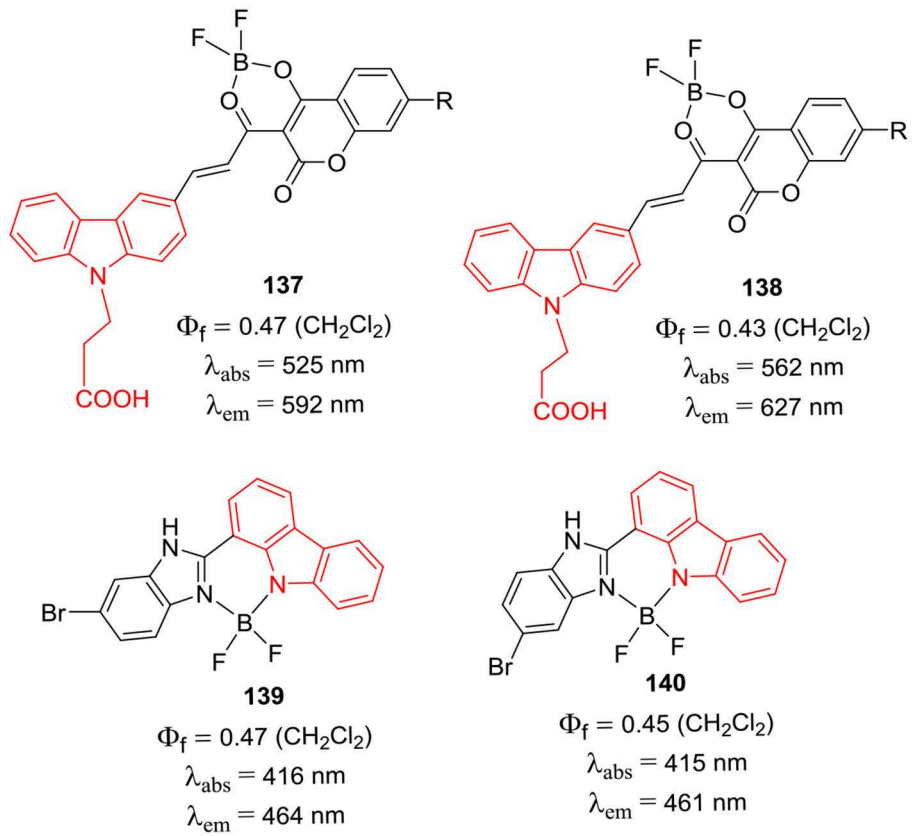

CHART 26 | BF_2 complexes of coumarin-carbazole conjugates (above); BF_2 complexes of carbazole-benzimidazole conjugates (below).

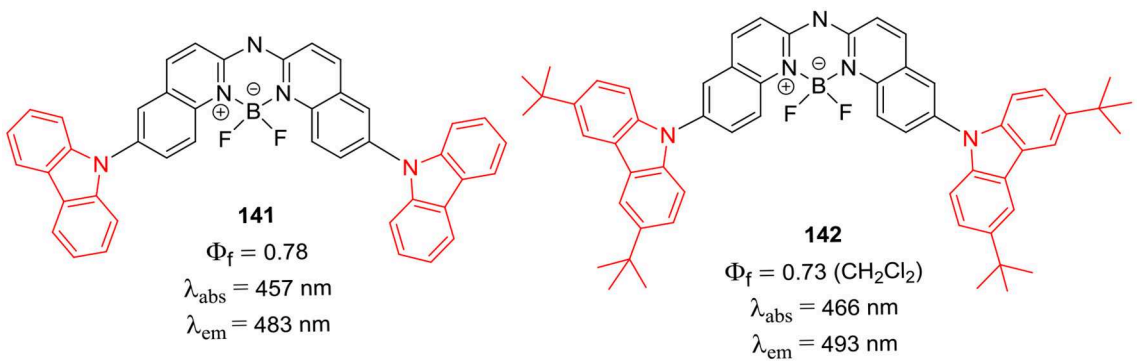

CHART 27 | Aza-boron-diquinomethene complexes.

0.074–0.547, except for molecule **145**. The molecules **143**–**148** (**Chart 28**) exhibited large Stokes shifts of about 76–130 nm in the solutions.

These dyes also showed color tunable solid state emission with emission maxima between 424 and 542 nm range; with the quantum yields around 0.13–0.21. The solid state emission maxima were slightly red shifted relative to those in solution, which was attributed to the J-type packing in the solid state (Maeda et al., 2016). Same group had prepared BF_2 complexes using organometallic approach, where carbazole was incorporated into the BODIPY framework (Maeda et al., 2015). The substitution of electron withdrawing or electron-donating groups on the carbazole skeleton altered the absorption and emission properties of **149** and **150** (**Chart 29**). The derivatives of **149** and **150** (**Chart 29**) showed absorption in the 292–493 nm range and fluorescence maxima between 508 and 650 nm. Also, the derivatives of **149** and **150** showed negligible

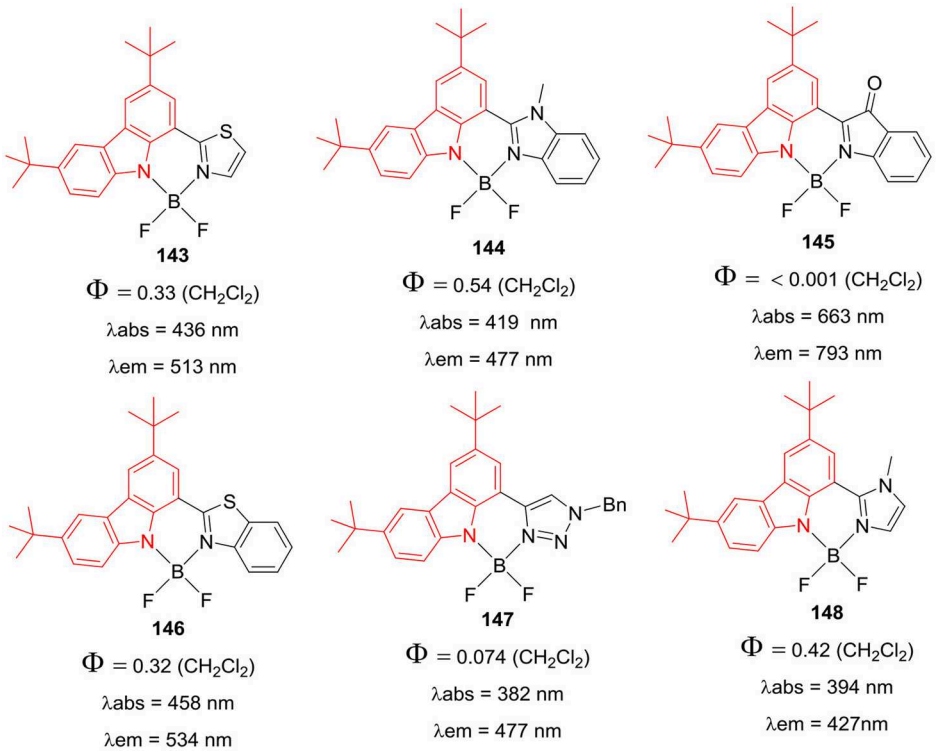

CHART 28 | Carbazole based hybrid BODIPYs.

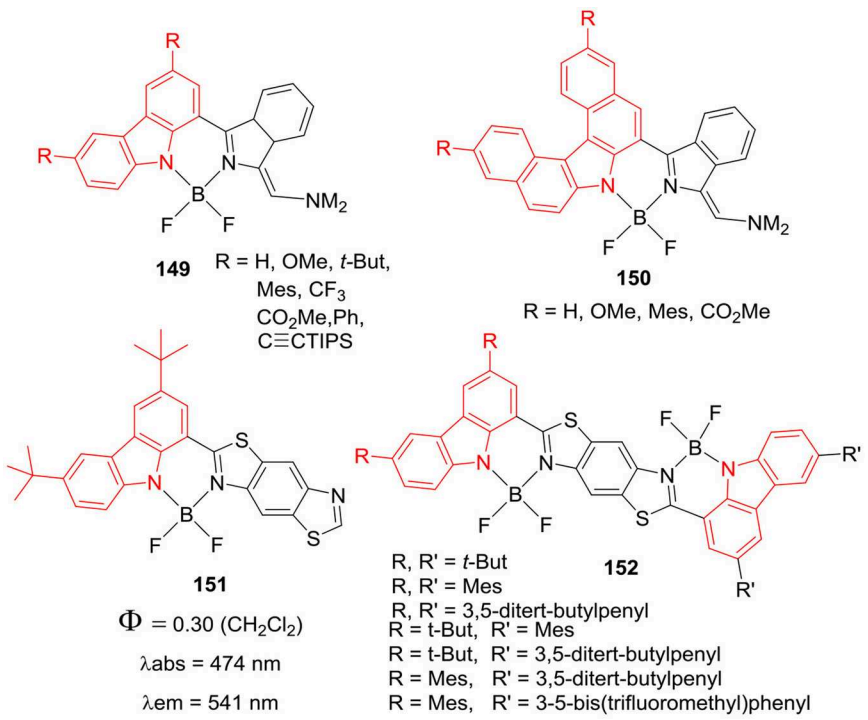

CHART 29 | Carbazole based hybrid BODIPYs.

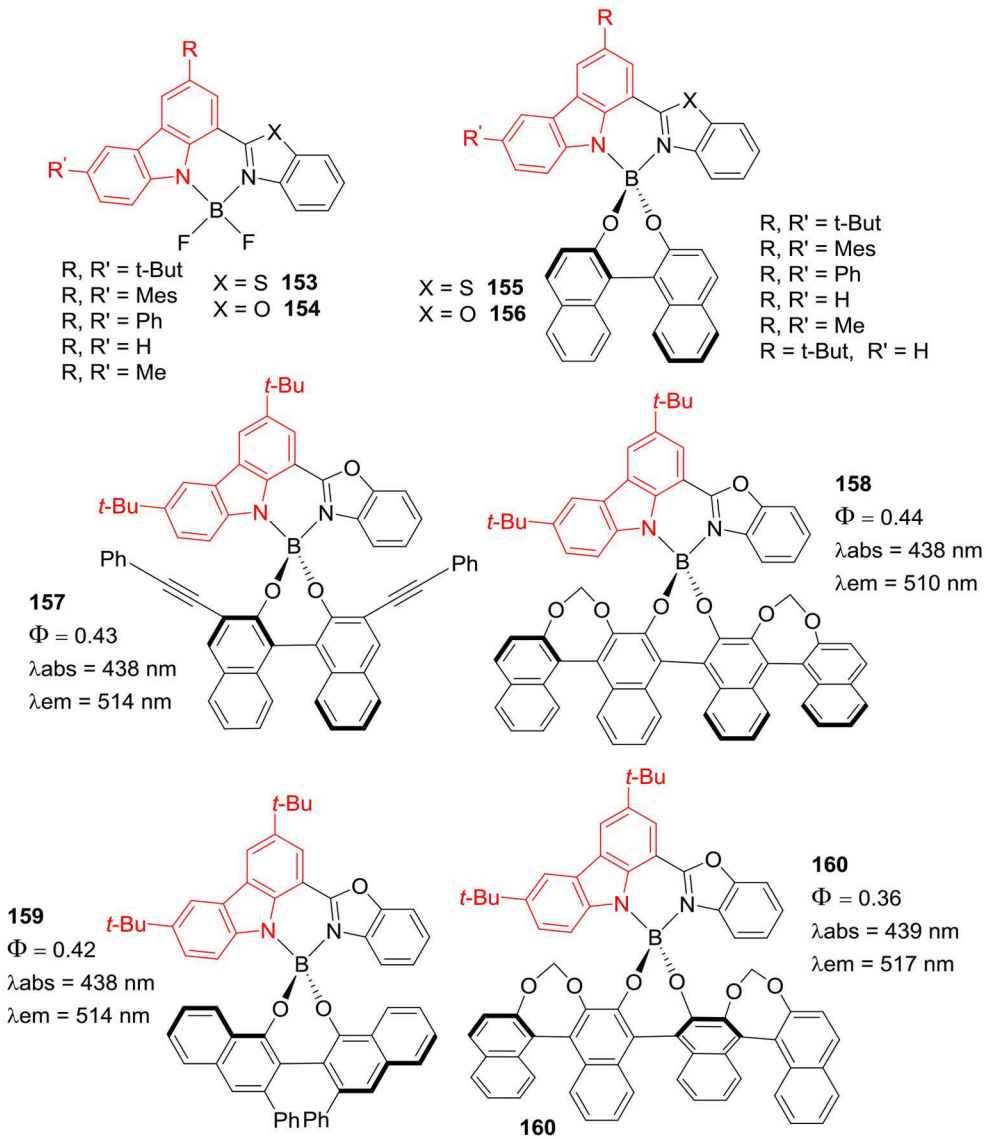

CHART 30 | Carbazole based hybrid BODIPYs; data in 1,4-dioxane.

fluorescence quantum yield with large Stokes shift of 46–142 nm (Maeda et al., 2015).

Ema et al. have also reported BF_2 complexes of carbazole-benzobisthiazole **151** and biscarbazole-benzobisthiazole **152** (**Chart 29**), these dyes displayed solid state emission in red region (Maeda et al., 2017). The compound **151** exhibited absorption and fluorescence at 474 and 541 nm, respectively; with 40 nm Stokes shift. The derivatives of dimer **152** showed absorption maxima between 516 and 523 nm range and red shifted emission in the range of 547–573 nm, with 31–47 nm Stokes shifts. Interestingly, **151** and the derivatives of **152** (**Chart 29**) exhibited solid state fluorescence around 564–639 nm, such dyes may have potential application in organic photovoltaics due to strong fluorescence in red-NIR region. Recently, same group has synthesized BF_2 complexes of carbazole-benzoxazole/carbazole-benzothiazole hybrids **153** and **154**; which were further reacted with binapthyl derivative in the Al-mediated reaction to produce **155** and **156** (**Chart 30**, Maeda et al., 2019). These chiral dyes **155–160** showed circularly polarize luminescence in solution and in solid state. The major absorption band was centered around 438–468 nm and fluorescence maxima were in between 496 and 538 nm; the emission quantum yields were in between 0.22 and 0.44 with considerable Stokes shifts of around 72–75 nm. For compounds **155–160** (**Chart 30**), the solid state emission bands appeared between 524 and 581 nm; which were red shifted as compared to those in solution. Such chiral BF_2 complexes of carbazole-benzoxoazole/carbazole-benzothiazole hybrids have potential

applications as circularly polarized luminescence materials in the chiral fields (Maeda et al., 2017).

SUMMARY

Carbazole-containing BODIPYs, carbazole-fused BODIPYs have become quite popular in the recent past; owing to their applications in live cell imaging, light harvesting systems, photovoltaics, and electroluminescent materials. The excellent hole-transport, photorefractive properties, and fluorescent nature of carbazole ring was exploited to design the BODIPY-carbazole conjugates with improved electronic and photovoltaic properties for DSSC and OLED applications. Various synthetic strategies were employed to substitute the three available positions (*alpha*, *beta* and *meso*) of the BODIPY skeleton; this resulted in the spurt of reports on carbazole substituted BODIPYs. The substitution of electron rich carbazole ring and its derivative on the BODIPY skeleton affected the spectral properties of the parent dye; which reflected in the red shifted absorption and emission maxima of the carbazole-BODIPY conjugates. Typically, direct linkage of carbazole ring on the *alpha*- and *meso*-positions of the BODIPY skeleton caused decent to large Stoke's shifts with fluorescence in the NIR region. Overall, the optical, photophysical, photoluminescent properties of the BODIPY dye can be fine- tuned for the desired application by substituting the carbazole derivatives on the BODIPY core; this knowledge can lead to the development of better more efficient BODIPY dyes in the near future.

AUTHOR CONTRIBUTIONS

All authors listed have made a substantial, direct and intellectual contribution to the work, and approved it for publication.

REFERENCES

Babu, J., Ganesan, S., Karuppusamy, M., and Rajakumar, P. (2018). Synthesis, photophysical, electrochemical properties, DFT studies and DSSC performance of BODIPY cored triazole bridged 3,6-ditertiary butyl carbazole decorated dendrimers. *Chem. Sel.* 3, 9222–9231. doi: 10.1002/slct.201801794

Balsukuri, N., Boruah, N. J., Kesavan, P. E., and Gupta, I. (2018). Near infra-red dyes based on pyrene aza-BODIPYs. *New J. Chem.* 42, 5875–5888. doi: 10.1039/C7NJ03408C

Balsukuri, N., Lone, M. Y., Jha, P. C., Mori, S., and Gupta, I. (2016a). Synthesis, structure, and optical studies of donor-acceptor-type near-infrared (NIR) aza-boron-dipyrromethene (BODIPY) dyes. *Chem. Asian J.* 11, 1572–1587. doi: 10.1002/asia.201600167

Balsukuri, N., Mori, S., and Gupta, I. (2016b). Donor acceptor type ferrocene substituted aza-BODIPYs: synthesis, optical and electrochemical studies. *J. Porphy. Phthaloc.* 20, 719–729. doi: 10.1142/S1088424616500693

Bandyopadhyay, S., Kundu, S., Giri, A., and Patra, A. (2018). A smart photosensitizer based on a red emitting solution processable porous polymer: generation of reactive oxygen species. *Chem. Com.* 54, 9123–9126. doi: 10.1039/C8CC04328K

Barberis, V. P., and Mikroyannidis, J. A. (2006). Novel blue luminescent twin molecules containing fluorene, carbazole or phenothiazine units. *Synth. Met.* 156, 1408–1414. doi: 10.1016/j.synthmet.2006.11.007

Bessette, A., and Hanan, G. S. (2014). Design, synthesis and photophysical studies of dipyrromethene-based materials: insights into their applications in organic photovoltaic devices. *Chem. Soc. Rev.* 43, 3342–3405. doi: 10.1039/C3CS60411J

Boens, N., Leen, V., and Dehaen, W. (2012). Fluorescent indicators based on BODIPY. *Chem. Soc. Rev.* 41, 1130–1172. doi: 10.1039/C1CS15132K

Brzeczek, A., Piwowar, K., Domagala, W., Mikolajczyk, M. M., Walczak, K., and Wagner, P. (2016). Systematic elongation of thienyl linkers and their effect on optical and electrochemical properties in carbazole-BODIPY donor-acceptor systems. *RSC Adv.* 6, 36500–36509. doi: 10.1039/C6RA04984B

Bura, T., Leclerc, N., Fall, S., Lévêque, P., Heiser, T., and Ziessel, R. (2011). Absorption tuning of monosubstituted triazatruxenes for bulk heterojunction solar cells. *Org. Lett.* 13, 6030–6033. doi: 10.1021/ol202443g

Celli, J. P., Spring, B. Q., Rizvi, I., Evans, C. L., Samkoe, K. S., Verma, S., et al. (2010). Imaging and photodynamic therapy: mechanisms, monitoring, and optimization. *Chem. Rev.* 110, 2795–2838. doi: 10.1021/cr900300p

Cheema, H., Younts, R., Gautam, B., Gundogdu, K., and El-Shafei, A. (2016). Design and synthesis of BODIPY sensitizers with long alkyl chains tethered to N-carbazole and their application for dye sensitized solar cells. *Mater. Chem. Phys.* 184, 57–63. doi: 10.1016/j.matchemphys.2016.09.024

Corona-Sánchez, R., Arcos-Ramos, R., Maldonado-Domínguez, M., Amelines-Sarria, O., Jerezano-Domínguez, A., García-Ortega, H., et al. (2016). Structural and morphological studies of *meso*-ethylcarbazole F-BODIPY thin films. *Monatsh. Fur Chem.* 147, 1915–1923. doi: 10.1007/s00706-016-1760-4

Das, S., and Gupta, I. (2019). Synthetic aspects of carbazole containing porphyrins and porphyrinoids. *J. Porphy. Phthaloc.* 23, 367–409. doi: 10.1142/S1088424619300052

Dhokale, B., Jadhav, T., Mobin, S. M., and Misra, R. (2015). *Meso* enyne substituted BODIPYs: synthesis, structure and properties. *Dalton Trans.* 44, 15803–15812. doi: 10.1039/C5DT00565E

Dutta, R., Firmansyah, D., Yoo, J., Kumar, R., Mulugeta, E., Jo, H., et al. (2017). BF2-complexes of carbazole–benzimidazole conjugates: synthesis, structures, and spectroscopic properties. *Bull. Korean Chem. Soc.* 38, 1163–1168. doi: 10.1002/bkcs.11240

Eçik, E. T., Özcan, E., Kandemir, H., Sengul, I. F., and Çoşut, B. (2017). Light harvesting systems composed of carbazole based subphthalocyanine-BODIPY enhanced with intramolecular fluorescence resonance energy transfer (FRET). *Dyes Pigmen.* 136, 441–449. doi: 10.1016/j.dyepig.2016.09.003

Fan, J., Hu, M., Zhan, P., and Peng, X. (2013). Energy transfer cassettes based on organic fluorophores: construction and applications in ratiometric sensing. *Chem. Soc. Rev.* 42, 29–43. doi: 10.1039/C2CS35273G

Gawale, Y., Adarsh, N., Kalva, S. K., Joseph, J., Pramanik, M., Ramaiah, D., et al. (2017). Carbazole-linked near-infrared aza-BODIPY dyes as triplet sensitizers and photoacoustic contrast agents for deep-tissue imaging. *Chem. Eur. J.* 23, 6570–6578. doi: 10.1002/chem.201605702

Głuszyńska, A. (2015). Biological potential of carbazole derivatives. *Eur. J. Med. Chem.* 94, 405–426. doi: 10.1016/j.ejmech.2015.02.059

Godoy, J., Vives, G., and Tour, J. M. (2010). Synthesis of highly fluorescent BODIPY-based nanocars. *Org. Lett.* 12, 1464–1467. doi: 10.1021/ol100108r

Guo, S., Ma, L., Zhao, J., Küçüköz, B., Karatay, A., Hayvali, M., et al. (2014). BODIPY triads triplet photosensitizers enhanced with intramolecular resonance energy transfer (RET): broadband visible light absorption and application in photooxidation. *Chem. Sci.* 5, 489–500. doi: 10.1039/C3SC52323C

Huang, L., Li, Z., Zhao, Y., Zhang, Y., Wu, S., Zhao, J., et al. (2016). Ultralow-power near infrared lamp light operable targeted organic nanoparticle photodynamic therapy. *J. Am. Chem. Soc.* 138, 14586–14591. doi: 10.1021/jacs.6b05390

Jadhav, T., Misra, R., Biswas, S., and Sharma, G. D. (2015). Bulk heterojunction organic solar cells based on carbazole-BODIPY conjugate small molecules as donors with high open circuit voltage. *Phys. Chem. Chem. Phys.* 17, 26580–26588. doi: 10.1039/C5CP04807A

Kamkaew, A., Lim, S. H., Lee, H. B., Kiew, L. V., Chung, L. Y., and Burgess, K. (2013). BODIPY dyes in photodynamic therapy. *Chem. Soc. Rev.* 42, 77–88. doi: 10.1039/C2CS35216H

Kesavan, P. E., Behera, R. N., Mori, S., and Gupta, I. (2017). Carbazole substituted BODIPYs: synthesis, computational, electrochemical and DSSC studies. *J. Fluoresc.* 27, 2131–2144. doi: 10.1007/s10895-017-2152-9

Kesavan, P. E., Das, S., Lone, M. Y., Jha, P. C., Mori, S., and Gupta, I. (2015). Bridged bis-BODIPYs: their synthesis, structures and properties. *Dalton Trans.* 44, 17209–17221. doi: 10.1039/C5DT01925G

Kesavan, P. E., and Gupta, I. (2014). Carbazole substituted boron dipyrromethenes. *Dalton Trans.* 43, 12405–12413. doi: 10.1039/C4DT01160K

Kesavan, P. E., Pandey, V., Raza, M. K., Mori, S., and Gupta, I. (2019). Water soluble thioglycosylated BODIPYs for mitochondria targeted cytotoxicity. *Bioorg. Chem.* 91:103139. doi: 10.1016/j.bioorg.2019.103139

Khetubol, A., Van Snick, S., Clark, M. L., Fron, E., Coutiño-González, E., Cloet, A., et al. (2015). Improved spectral coverage and fluorescence quenching in donor-acceptor systems involving indolo[3-2-b]carbazole and boron-dipyrromethene or diketopyrrolopyrrole. *Photochem. Photobiol.* 91, 637–653. doi: 10.1111/php.12437

Klfout, H., Stewart, A., Elkhalifa, M., and He, H. (2017). BODIPYs for dye-sensitized solar cells. *ACS Appl. Mater. Interfaces* 9, 39873–39889. doi: 10.1021/acsami.7b07688

Kolemen, S., and Akkaya, E. U. (2018). Reaction-based BODIPY probes for selective bio-imaging. *Coord. Chem. Rev.* 354, 121–134. doi: 10.1016/j.ccr.2017.06.021

Kowada, T., and Kikuchi, K. (2015). BODIPY-based probes for the fluorescence imaging of biomolecules in living cells. *Chem. Soc. Rev.* 44, 4953–4972. doi: 10.1039/C5CS00030K

Kurowska, A., Brzeczek-Szafran, A., Zassowski, P., Lapkowski, M., Domagala, W., Wagner, P., et al. (2018). Mono and di-substituted BODIPY with electron donating carbazole, thiophene, and 3,4-ethylenedioxythiophene units. *Electrochim. Acta* 271, 685–698. doi: 10.1016/j.electacta.2018.03.044

Lakshmi, V., Rajeswara Rao, M., and Ravikanth, M. (2015). Halogenated boron-dipyrromethenes: synthesis, properties and applications. *Org. Biomol. Chem.* 13, 2501–2517. doi: 10.1039/C4OB02293A

Lakshmi, V., Sharma, R., and Ravikanth, M. (2016). Functionalized boron-dipyrromethenes and their applications. *Rep. Org. Chem.* 6, 1–24. doi: 10.2147/ROC.S60504

Li, Q., and Qian, Y. (2016). Aggregation-induced emission enhancement and cell imaging of a novel (carbazol-N-yl)triphenylamine–BODIPY. *New J. Chem.* 40, 7095–7101. doi: 10.1039/C6NJ01495J

Li, Y., Ding, J., Day, M., Tao, Y., Lu, J., and D'iorio, M. (2004). Synthesis and properties of random and alternating fluorene/carbazole copolymers for use in blue light-emitting devices. *Chem. Mater.* 16, 2165–2173. doi: 10.1021/cm030069g

Liao, J., Xu, Y., Zhao, H., Zong, Q., and Fang, Y. (2017a). Novel A-D-A type small molecules with β -alkynylated BODIPY flanks for bulk heterojunction solar cells. *Org. Electron.* 49, 321–333. doi: 10.1016/j.orgel.2017.06.054

Liao, J., Zhao, H., Xu, Y., Cai, Z., Peng, Z., Zhang, W., et al. (2016). Novel D–A–D type dyes based on BODIPY platform for solution processed organic solar cells. *Dyes Pigm.* 128, 31–140. doi: 10.1016/j.dyepig.2016.01.020

Liao, J., Zhao, H., Xu, Y., Zhou, W., Peng, F., Wang, Y., et al. (2017b). Novel BODIPY dyes with electron donor variety for dye-sensitized solar cells. *RSC Adv.* 7, 33975–33985. doi: 10.1039/C7RA04402J

Lin, H. Y., Huang, W. C., Chen, Y. C., Chou, H. H., Hsu, C. Y., Lin, J. T., et al. (2012). BODIPY dyes with β-conjugation and their applications for high-efficiency inverted small molecule solar cells. *Chem. Commun.* 48, 8913–8915. doi: 10.1039/c2cc34286c

Liu, S., Shi, Z., Xu, W., Yang, H., Xi, N., Liu, X., et al. (2014). A class of wavelength-tunable near-infrared aza-BODIPY dyes and their application for sensing mercury ion. *Dyes Pigmen.* 103, 145–153. doi: 10.1016/j.dyepig.2013.12.004

Liu, X., Zhang, J., Li, K., Sun, X., Wu, Z., Ren, A., et al. (2013). New insights into two-photon absorption properties of functionalized aza-BODIPY dyes at telecommunication wavelengths: a theoretical study. *Phy. Chem. Chem. Phys.* 15, 4666–4676. doi: 10.1039/c3cp44435j

Loudet, A., and Burgess, K. (2007). BODIPY dyes and their derivatives: syntheses and spectroscopic properties. *Chem. Rev.* 107, 4891–4932. doi: 10.1021/cr078381n

Lu, H., Mack, J., Yang, Y., and Shen, Z. (2014). Structural modification strategies for the rational design of red/NIR region BODIPYs. *Chem. Soc. Rev.* 43, 4778–4823. doi: 10.1039/C4CS00030G

Lv, H. J., Zhang, X. T., Wang, S., and Xing, G. W. (2017). Assembly of BODIPY-carbazole dyes with liposomes to fabricate fluorescent nanoparticles for lysosomal bioimaging in living cells. *Analyst* 142, 603–607. doi: 10.1039/C6AN02705A

Ma, X., Azeem, E. A., Liu, X., Cheng, Y., and Zhu, C. (2014). Synthesis and tunable chiroptical properties of chiral BODIPY-based D-π-A conjugated polymers. *J. Mater. Chem. C* 2, 1076–1084. doi: 10.1039/C3TC32029D

Ma, X., Mao, X., Zhang, S., Huang, X., Cheng, Y., and Zhu, C. (2013). Aza-BODIPY-based D–π-A conjugated polymers with tunable band gap: synthesis and near-infrared emission. *Polym. Chem.* 4, 520–527. doi: 10.1039/C2PY20677C

Maeda, C., Nagahata, K., Takaishi, K., and Ema, T. (2019). Synthesis of chiral carbazole-based BODIPYs showing circularly polarized luminescence. *Chem. Com.* 55, 3136–3139. doi: 10.1039/C9CC00894B

Maeda, C., Todaka, T., and Ema, T. (2015). Carbazole-based boron dipyrromethenes (BODIPYs): facile synthesis, structures, and fine-tunable optical properties. *Org. Lett.* 17, 3090–3093. doi: 10.1021/acs.orglett.5b01363

Maeda, C., Todaka, T., Ueda, T., and Ema, T. (2016). Color-tunable solid-state fluorescence emission from carbazole-based BODIPYs. *Chem. Eur. J.* 22, 7508–7513. doi: 10.1002/chem.201505150

Maeda, C., Todaka, T., Ueda, T., and Ema, T. (2017). Synthesis of carbazole-based BODIPY dimers showing red fluorescence in the solid state. *Org. Biomol. Chem.* 15, 9283–9287. doi: 10.1039/C7OB02419C

Mani, V., Krishnakumar, V. G., Gupta, S., Mori, S., and Gupta, I. (2017). Synthesis and characterization of styryl-BODIPY derivatives for monitoring *in vitro* Tau aggregation. *Sens. Actuators B Chem.* 244, 673–683. doi: 10.1016/j.snb.2016.12.104

Mao, M., Li, Q. S., Zhang, X. L., Wu, G. H., Dai, C. G., and Ding, Y. (2017). Effects of donors of bodipy dyes on the performance of dye-sensitized solar cells. *Dyes Pigm.* 141, 148–160. doi: 10.1016/j.dyepig.2017.02.017

Misra, R., Jadhav, T., Dhokale, B., Gautam, P., Sharma, R., Maragani, R., et al. (2014). Carbazole-BODIPY conjugates: design, synthesis, structure and properties. *Dalton Trans.* 43:13076. doi: 10.1039/C4DT00983E

Mudadu, M. S., Singh, A. N., and Thummel, R. P. (2008). Preparation and study of 1,8-Di(pyrid-2′-yl)carbazoles. *J. Org. Chem.* 73, 6513–6520. doi: 10.1021/jo801132w

Nguyen, Q. P. B., Hwang, H. M., Song, M. -S., Song, H. J., Kim, G. H., Kwon, J. H., et al. (2014). Synthesis and electroluminescent properties of OLED green dopants based on BODIPY derivatives. *Bull. Korean Chem. Soc.* 35, 1247–1250. doi: 10.5012/bkcs.2014.35.4.1247

Ni, Y., and Wu, J. (2014). Far-red and near infrared BODIPY dyes: synthesis and applications for fluorescent pH probes and bio-imaging. *Org. Biomol. Chem.* 12, 3774–3791. doi: 10.1039/c3ob42554a

Ooyama, Y., Hagiwara, Y., Mizumo, T., Harima, Y., and Ohshita, J. (2013a). Photovoltaic performance of dye-sensitized solar cells based on D–π-A type BODIPY dye with two pyridyl groups. *New J. Chem.* 37, 2479–2485. doi: 10.1039/c3nj00456b

Ooyama, Y., Hagiwara, Y., Mizumo, T., Harima, Y., and Ohshita, J. (2013b). Synthesis of diphenylamino-carbazole substituted BODIPY dyes and their photovoltaic performance in dye-sensitized solar cells. *RSC Adv.* 3, 18099–18106. doi: 10.1039/c3ra43577f

Ooyama, Y., Hagiwara, Y., Oda, Y., Fukuoka, H., and Ohshita, J. (2014). BODIPY dye possessing solid-state red fluorescence and green metallic luster properties in both crystalline and amorphous states. *RSC Adv.* 4, 1163–1167. doi: 10.1039/C3RA45785K

Ooyama, Y., Kanda, M., EnoKi, T., Adachi, Y., and Ohshita, J. (2017). Synthesis, optical and electrochemical properties, and photovoltaic performance of a panchromatic and near-infrared (D)2–π-A type BODIPY dye with pyridyl group or cyanoacrylic acid. *RSC Adv.* 7, 13072–13081. doi: 10.1039/C7RA00799J

Popere, B. C., Pelle, A. M. D., Poe, A., Balaji, G., and Thayumanavan, S. (2012). Predictably tuning the frontier molecular orbital energy levels of panchromatic low band gap BODIPY-based conjugated polymers. *Chem. Sci.* 3, 3093–3102. doi: 10.1039/c2sc20731a

Promarak, V., Ichikawa, M., Sudyoadsuk, T., Saengsuwan, S., Jungsuttiwong, S., and Keawin, T. (2008). Thermally and electrochemically stable amorphous hole-transporting materials based on carbazole dendrimers for electroluminescent devices. *Thin Solid Films* 516, 2881–2888. doi: 10.1016/j.tsf.2007.05.062

Rajeshirke, M., Tathe, A. B., and Sekar, N. (2018). Viscosity sensitive fluorescent coumarin-carbazole chalcones and their BF 2 complexes containing carboxylic acid – synthesis and solvatochromism. *J. Mol. Liq.* 264, 358–366. doi: 10.1016/j.molliq.2018.05.074

Reddy, G., Duvva, N., Seetharaman, S., DSouza, F., and Lingamallu, G. (2018). Photoinduced energy transfer in carbazole-BODIPY dyads. *Phys. Chem. Chem. Phy*. 20, 27418–27428. doi: 10.1039/C8CP05509B

Satoh, T., Fujii, K., Kimura, Y., and Matano, Y. (2018). Synthesis of 3,5-disubstituted BODIPYs bearing N-containing five-membered heteroaryl groups via nucleophilic C–N bond formation. *J. Org. Chem.* 83, 5274–5281. doi: 10.1021/acs.joc.8b00087

Sengul, I. F., Okutan, E., Kandemir, H., Astarci, E., and Çoşut, B. (2015). Carbazole substituted BODIPY dyes: synthesis, photophysical properties and antitumor activity. *Dyes Pigm.* 123, 32–38. doi: 10.1016/j.dyepig.2015.07.025

Strahan, J., Popere, B. C., Khomein, P., Pointer, C. A., Martin, S. M., Oldacre, A. N., et al. (2019). Modulating absorption and charge transfer in bodipy-carbazole donor-acceptor dyads through molecular design. *Dalton Trans.* 48, 8488–8501. doi: 10.1039/C9DT00094A

Su, D., Oh, J., Lee, S. C., Lim, J. M., Sahu, S., Yu, X., et al. (2014a). Dark to light! a new strategy for large stokes shift dyes: coupling of a dark donor with tunable high quantum yield acceptors. *Chem. Sci.* 5, 4812–4818. doi: 10.1039/C4SC01821D

Su, D., Teoh, C. L., Sahu, S., Das, R. K., and Chang, Y. T. (2014b). Live cells imaging using a turn-on FRET-based BODIPY probe for biothiols. *Biomaterials* 35, 6078–6085. doi: 10.1016/j.biomaterials.2014.04.035

Swavey, S., Wertz, A., and Erb, J. (2019).Bichromophoric properties of ruthenium(II) polypyridyl complexes bridged by boron dipyrromethenes: synthesis, electrochemical, spectroscopic, computational evaluation, and plasmid DNA photoreactions. *Chem. Eur. J.* 2019, 3690–3698. doi: 10.1002/ejic.201900527

Tang, J., Hua, J., Wu, W., Li, J., Jin, Z., Long, Y., et al. (2010). New starburst sensitizer with carbazole antennas for efficient and stable dye-sensitized solar cells. *Energy. Environ. Sci.* 3, 1736–1745. doi: 10.1039/c0ee00008f

Telore, R. D., Jadhav, A. G., and Sekar, N. (2016). NLOphoric and solid state emissive BODIPY dyes containing N -phenylcarbazole core at *meso* position – synthesis, photophysical properties of and DFT studies. *J. Lumin.* 179, 420–428. doi: 10.1016/j.jlumin.2016.07.035

Thorat, K. G., Kamble, P., Ray, A. K., and Sekar, N. (2015). Novel pyrromethene dyes with N-ethyl carbazole at the *meso* position: a comprehensive photophysical, lasing, photostability and TD-DFT study. *Phys. Chem. Chem. Phys*. 17, 17221–17236. doi: 10.1039/C5CP01741F

Treibs, A., and Kreuzer, F. H. (1968). Difluorboryl-komplexe von Di- und tripyrrylmethenen. *Justus Liebigs Ann. Chem.* 718, 208–223. doi: 10.1002/jlac.19687180119

Ulrich, G., Ziessel, R., and Harriman, A. (2008). The chemistry of fluorescent bodipy dyes: versatility unsurpassed. *Angew. Chem. Int. Ed.* 47, 1184–1201. doi: 10.1002/anie.200702070

Vedamalai, M., and Gupta, I. (2018). Design and synthesis of the BODIPY–BSA complex for biological applications. *Luminescence* 33, 10–14. doi: 10.1002/bio.3365

Vedamalai, M., Kedaria, D., Vasita, R., and Gupta, I. (2018). Oxidation of phenothiazine based fluorescent probe for hypochlorite and its application to live cell imaging. *Sens. Actu. B Chem.* 263, 137–142. doi: 10.1016/j.snb.2018.02.071

Vedamalai, M., Kedaria, D., Vasita, R., Mori, S., and Gupta, I. (2016). Design and synthesis of BODIPY-clickate based Hg2+ sensors: The effect of triazole binding mode with Hg2+ on signal transduction. *Dalton Trans.* 45, 2700–2708. doi: 10.1039/C5DT04042F

Wang, Z.-S., Koumura, N., Cui, Y., Takahashi, M., Sekiguchi, H., Mori, A., et al. (2008). Hexylthiophene-functionalized carbazole dyes for efficient molecular photovoltaics: tuning of solar-cell performance by structural modification. *Chem. Mater.* 20, 3993–4003. doi: 10.1021/cm8003276

Wanwong, S., Khomein, P., and Thayumanavan, S. (2018). BODIPY dyads and triads: synthesis, optical, electrochemical and transistor properties. *Chem. Cent. J.* 12:60. doi: 10.1186/s13065-018-0430-5

Wei, Y., Zhou, M., Zhou, Q., Zhou, X., Liu, S., Zhang, S., et al. (2017). Triplet-triplet annihilation upconversion kinetics of C 60 -Bodipy dyads as organic triplet photosensitizers. *Phy. Chem. Chem. Phy.* 19, 22049–22060. doi: 10.1039/C7CP03840B

Wood, T. E., and Thompson, A. (2007). Advances in the chemistry of dipyrrins and their complexes. *Chem. Rev.* 107, 1831–1861. doi: 10.1021/cr050052c

Wu, J., Kwon, B., Liu, W., Anslyn, E. V., Wang, P., and Kim, J. S. (2015). Chromogenic/fluorogenic ensemble chemosensing systems. *Chem. Rev.* 115, 7893–7943. doi: 10.1021/cr500553d

Xia, X., and Qian, Y. (2018). NIR two-photon fluorescent probe for biothiol detection and imaging of living cells *in vivo*. *Analyst* 143, 5218–5224. doi: 10.1039/C8AN01605D

Yang, P., Wu, W., Zhao, J., Huang, D., and Yi, X. (2012). Using C60-bodipy dyads that show strong absorption of visible light and long-lived triplet excited states as organic triplet photosensitizers for triplet–triplet annihilation upconversion. *J. Mater. Chem.* 22, 20273–20283. doi: 10.1039/c2jm34353c

Yi, X., Zhao, J., Sun, J., Guo, S., and Zhang, H. (2013). Visible light-absorbing rhenium(i) tricarbonyl complexes as triplet photosensitizers in photooxidation and triplet–triplet annihilation upconversion. *Dalton Trans.* 42, 2062–2074. doi: 10.1039/C2DT32420B

Yuan, L., Lin, W., Zheng, K., He, L., and Huang, W. (2013). Far-red to near infrared analyte-responsive fluorescent probes based on organic fluorophore platforms for fluorescence imaging. *Chem. Soc. Rev.* 42, 622–661. doi: 10.1039/C2CS35313J

Zampetti, A., Minotto, A., Squeo, B. M., Gregoriou, V. G., Allard, S., and Scherf, U. (2017). Highly efficient solid-state near-infrared organic light-emitting diodes incorporating ADA dyes based on α, β-unsubstituted "BODIPY" moieties. *Sci. Rep.* 7:1611. doi: 10.1038/s41598-017-01785-2

Zhang, D., Wang, Y., Xiao, Y., Qian, S., and Qian, X. (2009). Long-wavelength boradiazaindacene derivatives with two-photon absorption activity and strong emission: versatile candidates for biological imaging applications. *Tetrahedron* 65, 8099–8103. doi: 10.1016/j.tet.2009.08.002

Zhang, J., Lu, F., Qi, S., Zhao, Y., Wang, K., Zhang, B., et al. (2016). Influence of various electron-donating triarylamine groups in BODIPY sensitizers on the performance of dye-sensitized solar cells. *Dyes Pigm.* 128, 296–303. doi: 10.1016/j.dyepig.2016.02.008

Zhang, X., Xiao, Y., Qi, J., Qu, J., Kim, B., Yue, X., et al. (2013). Long-wavelength, photostable, two-photon excitable BODIPY fluorophores readily modifiable for molecular probes. *J. Org. Chem.* 78, 9153–9160. doi: 10.1021/jo401379g

Zhang, X., Zhang, Y., Chen, L., and Xiao, Y. (2015). Star-shaped carbazole-based BODIPY derivatives with improved hole transportation and near-infrared absorption for small-molecule organic solar cells with high open-circuit voltages. *RSC Adv.* 5, 32283–32289. doi: 10.1039/C5RA02414E

Zheng, Z., Zhang, T., Liu, H., Chen, Y., Kwok, R. T. K., Ma, C., et al. (2018). Bright near-infrared aggregation-induced emission luminogens with strong two-photon absorption, excellent organelle specificity, and efficient photodynamic therapy potential. *ACS Nano* 12, 8145–8159. doi: 10.1021/acsnano.8b03138

Zhou, Y., Cheung, Y. K., Ma, C., Zhao, S., Gao, D., Lo, P. C., et al. (2018). Endoplasmic reticulum-localized two-photon-absorbing boron dipyrromethenes as advanced photosensitizers for photodynamic therapy. *J. Med. Chem.* 61, 3952–3961. doi: 10.1021/acs.jmedchem.7b01907

Zhu, X., Huang, H., Liu, R., Jin, X., Li, Y., Wang, D., et al. (2015). Aza-boron-diquinomethene complexes bearing N-aryl chromophores: synthesis, crystal structures, tunable photophysics, the protonation effect and their application as pH sensors. *J. Mater. Com. C* 3, 3774–3782. doi: 10.1039/C4TC02955K

Ziessel, R., Ulrich, G., and Harriman, A. (2007). The chemistry of bodipy: a new El Dorado for fluorescence tools. *New J.Chem.* 31, 496–501. doi: 10.1039/b617972j

Zong, Q., Zhao, H., Zhou, W., Zhang, W., Liao, J., and Yang, N. (2017). Novel dual BODIPY-carbazole conjugates with various linkers. *Aust. J. Chem.* 70:806. doi: 10.1071/CH16704

Conflict of Interest: The authors declare that the research was conducted in the absence of any commercial or financial relationships that could be construed as a potential conflict of interest.

frontiers in Chemistry

REVIEW
published: 12 December 2019
doi: 10.3389/fchem.2019.00821

Bodipy Derivatives as Triplet Photosensitizers and the Related Intersystem Crossing Mechanisms

Kepeng Chen[1†], *Yu Dong*[1†], *Xiaoyu Zhao*[1,2], *Muhammad Imran*[1], *Geliang Tang*[1], *Jianzhang Zhao*[1,2*] *and Qingyun Liu*[3*]

[1] State Key Laboratory of Fine Chemicals, School of Chemical Engineering, Dalian University of Technology, Dalian, China, [2] Key Laboratory of Energy Materials Chemistry, School of Chemistry and Chemical Engineering, Institute of Applied Chemistry, Xinjiang University, Ürümqi, China, [3] College of Chemical and Environmental Engineering, Shandong University of Science and Technology, Qingdao, China

Recently varieties of Bodipy derivatives showing intersystem crossing (ISC) have been reported as triplet photosensitizers, and the application of these compounds in photocatalysis, photodynamic therapy (PDT), and photon upconversion are promising. In this review we summarized the recent development in the area of Bodipy-derived triplet photosensitizers and discussed the molecular structural factors that enhance the ISC ability. The compounds are introduced based on their ISC mechanisms, which include the heavy atom effect, exciton coupling, charge recombination (CR)-induced ISC, using a spin converter and radical enhanced ISC. Some transition metal complexes containing Bodipy chromophores are also discussed. The applications of these new triplet photosensitizers in photodynamic therapy, photocatalysis, and photon upconversion are briefly commented on. We believe the study of new triplet photosensitizers and the application of these novel materials in the abovementioned areas will be blooming.

Keywords: Bodipy, intersystem crossing, photocatalysis, triplet photosensitizers, upconversion

OPEN ACCESS

Edited by:
Zhen Shen,
Nanjing University, China

Reviewed by:
Wei Lu,
Southern University of Science and Technology, China
Wanhua Wu,
Sichuan University, China

***Correspondence:**
Jianzhang Zhao
zhaojzh@dlut.edu.cn
Qingyun Liu
qyliu@sdust.edu.cn

[†] *These authors have contributed equally to this work*

Specialty section:
This article was submitted to Supramolecular Chemistry, a section of the journal Frontiers in Chemistry

Received: *14 August 2019*
Accepted: *12 November 2019*
Published: *12 December 2019*

Citation:
Chen K, Dong Y, Zhao X, Imran M, Tang G, Zhao J and Liu Q (2019) Bodipy Derivatives as Triplet Photosensitizers and the Related Intersystem Crossing Mechanisms. Front. Chem. 7:821. doi: 10.3389/fchem.2019.00821

INTRODUCTION

Triplet Photosensitizers (PSs) are compounds showing strong absorption of UV or visible light, efficient intersystem crossing (ISC), appropriate excited state redox potential, and long triplet-state lifetimes. These compounds are widely used for photo-driven energy transfer or electron transfer processes, which are the fundamental photophysical processes in photocatalysis, such as catalytic H_2 evolution by water splitting (DiSalle and Bernhard, 2011; Gärtner et al., 2011, 2012), photocatalytic redox synthetic organic reactions (Shi and Xia, 2012; Xuan and Xiao, 2012; Hari and König, 2013), photoreduction of CO_2 (Sato et al., 2013), photodynamic therapy (PDT) (Awuah and You, 2012; Kamkaew et al., 2013; Stacey and Pope, 2013; Jiang et al., 2016; Li et al., 2017), photon upconversion (triplet-triplet annihilation upconversion) (Singh-Rachford and Castellano, 2010; Ceroni, 2011; Zhao et al., 2011; Monguzzi et al., 2012; Simon and Weder, 2012; Zhou et al., 2015), photovoltaics (Guo et al., 2006; Dai et al., 2012; Bittner et al., 2014; Cheema et al., 2014; Etzold et al., 2015), and photo-initiated polymerizations (Goessl et al., 2001; Ho et al., 2010; Rivard, 2012; Cengiz et al., 2017). It is highly desired to find a chromophore to develop a series of triplet PSs to meet these requirements. Concerning this aspect, Boron dipyrromethene (Bodipy) is of particular interest due to its robust photostability and feasible derivatization (Ulrich et al., 2008; Ziessel and Harriman, 2011; Lu et al., 2014; Miao et al., 2019).

The ISC process is electron spin forbidden, and a mechanism is thus required to enhance the electron spin flipping, which requires a magnetic torque. Recently, a variety of Bodipy-based triplet PSs have been reported, and the application of these novel triplet PSs in the abovementioned areas is promising. In this review, we have summarized the recent development of the Bodipy-derived triplet PSs, ranging from the molecular structure design to the applications of these materials.

$S_n \rightarrow T_m$ ISC is a non-radiative transition, during which the electron spin flips or rephrases. A magnetic torque acting on the electron spin is therefore required. The most commonly encountered mechanisms are the spin-orbital coupling (SOC) and hyperfine interaction. For the SOC, the orbital angular momentum interacts with the spin angular momentum (also known as the magnetic angular momentum interaction), and the typical examples are the heavy atom effect, the El Syed's rule ($n\pi^* \leftrightarrow \pi\pi^*$ transition), the spin orbital charge transfer, etc. Hyperfine interaction refers to the magnetic coupling between the electron and the magnetic nucleus, which is responsible for the radical pair ISC (RP ISC) in electron donor/acceptor dyads. Other ISC mechanisms do exist; for instance, the exciton coupling and singlet fission. In the following sections we have introduced the exemplars of application of Bodipy derivatives as triplet photosensitizers (Lakshmi et al., 2015). The challenge in the designing of heavy atom-free triplet photosensitizers were also introduced.

HEAVY ATOM EFFECT IN BODIPY DERIVATIVES

Nagano et al. reported that the 2,6-diiodoBodipy (**Supplementary Figure 1**) showed the ISC ability (Yogo et al., 2005). The ISC was confirmed with the photosensitizing of singlet oxygen (confirmed with the near IR luminescence of $^1O_2$), and the relative efficiency of $^1O_2$ generation is up to 6-fold of that of Rose Bengle under the same conditions. The photostability of the diiodoBodipy is better than the Rose Bengle. Intracellular phototoxicity was also confirmed. However, the triplet-state lifetime of the diiodoBodipy was not reported.

Based on the feasible derivatization of the Bodipy framework, we prepared a library of iodinated Bodipy derivatives (**Figure 1**); the absorption wavelength ranged from 510 to 629 nm, and the T_1 state energy level of the derivatives varied from 1.5 to 1.15 eV (based on TDDFT computations) (Wu et al., 2011). The visible light absorbing of these derivatives was strong (59,400–180,000 M^{-1} cm^{-1}). With nanosecond transient absorption spectra of the diiodoBodipy derivatives, the triplet-state lifetimes of the compounds were determined to be in the range of 26–66 μs. It is worth mentioning that these *apparent* triplet-state lifetimes were shorter than the *intrinsic* triplet-state lifetimes as a result of the triplet-triplet-annihilation (TTA) self-quenching effect. Later, Zhao and Dick reported a kinetic model with the TTA effect that was considered to determine the intrinsic triplet-state lifetimes, and the triplet-state lifetime of the diiodoBodipy was up to 276 μs (Lou et al., 2018; Wang et al., 2019b). To the best of our knowledge, this was the first report of the intrinsic triplet-state lifetime of Bodipy derivatives.

Since these diiodoBodipy derivatives showed strong absorption of visible light, an efficient ISC, and a long-lived triplet state, we used these triplet PSs for TTA upconversion (Wu et al., 2011). For instance, upon 532 nm cw-laser excitation, strong upconverted blue emission of ca. 450 nm was observed with perylene as the triplet acceptor/emitter, and the upconversion quantum yields were up to 6% (Wu et al., 2011). Other excitation wavelengths can be also used for TTA upconversion with these compounds.

In **Figure 1**, the methyl groups at the 1,7-position of the Bodipy core restrict the rotation of the phenyl ring at the

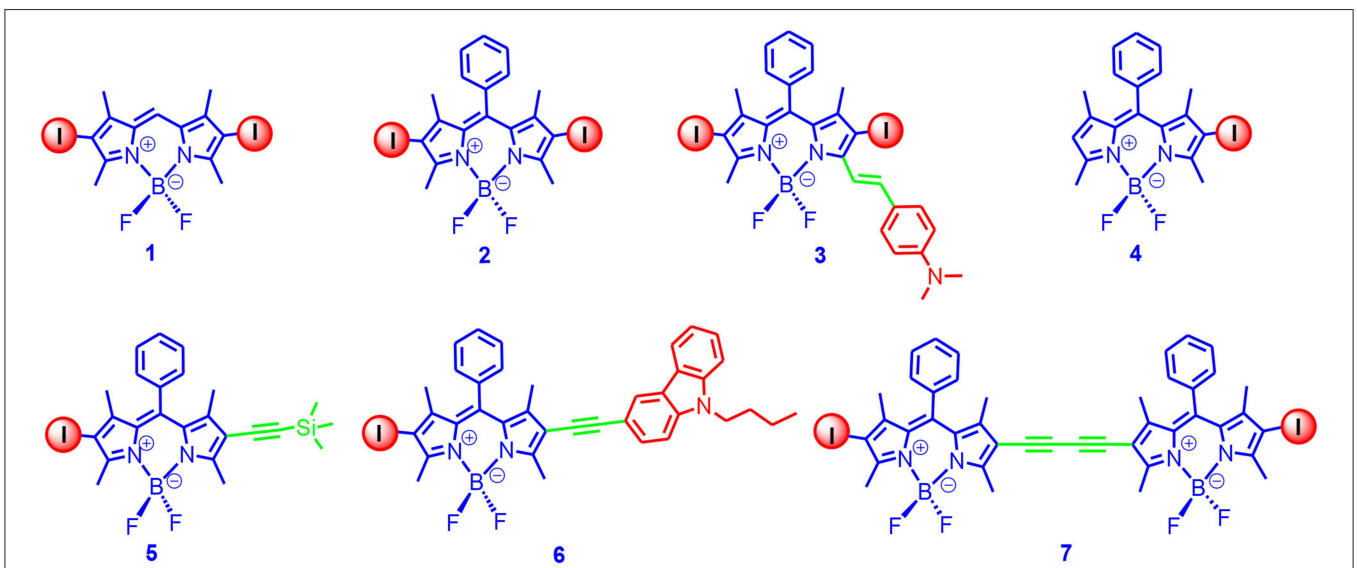

FIGURE 1 | Mono- and DiiodoBodipy derivatives showing variable absorption wavelengths and efficient ISC.

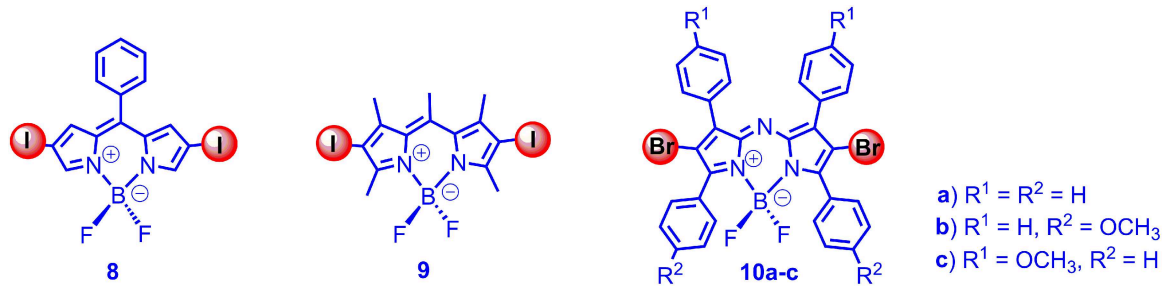

FIGURE 2 | DiiodoBodipy derivatives (8, 9), which are devoid of free rotor effect on the triplet states and dibromoAzaBodipy (10a-c), showing absorption at 650–690 nm.

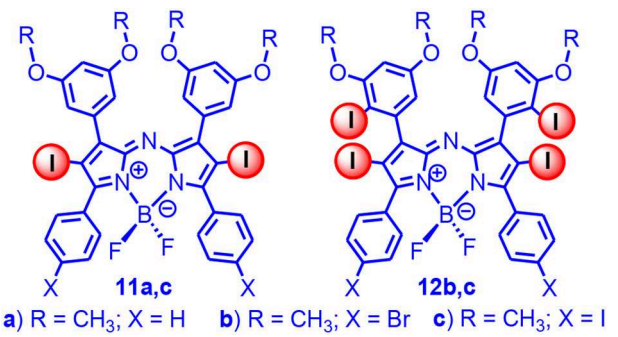

FIGURE 3 | Di- and tetraiodoAzaBodipy showing absorption at 650–690 nm.

meso-position. Without the iodination and the methyl groups at the 1,7-positions, the rotation of the phenyl ring will induce the free rotor effect, and the fluorescence of the Bodipy core is significantly quenched. A fluorescence sensor for detection of the viscosity of the microenvironment has been developed based on this property because the rotation of the phenyl ring will be inhibited in a viscous solvent (Kuimova et al., 2008). With theoretical computation, it was proposed that the quenching of the fluorescence of the Bodipy core was not due to rotation of the phenyl ring at the meso-positions, but rather that it was the bending of the Bodipy core at the excited state that quenched the fluorescence (Suhina et al., 2017).

With the initial intention to develop a viscosity-sensitive triplet photosensitizer, we studied the triplet-state property of the diiodoBodipy without methyl groups at 1,7-position (**8**, **9** in **Figure 2**). Interestingly, we found that the triplet state in **8** was not quenched, as compared to that of **9**, in both aspects of triplet-state lifetimes (126 μs for **8**, 241 μs for **9**) and ISC quantum yields (approximated with the O.D. values of the nanosecond transient absorption) (Lou et al., 2018). The non-quenched triplet state of **8** was also confirmed with the TTA upconversion with this triplet PS (upconversion quantum yield was up to 6.3%).

With theoretical computation, we found that, with torsion of the molecule at excited state, there is a crossing for S_1/S_0 at the energy minimum on the S_1 state energy curve. For T_1 state, however, there is not such crossing point for the potential energy curves (Lou et al., 2018), which can be used to rationalize the un-quenched T_1 state of **8** and the quenched S_1 state of the same molecule. The electron spin-forbidden feature of the $T_1 \rightarrow S_0$ may also play a role in the observation of the non-quenched T_1 state of **8**. These results indicated the triplet-state property was different from the singlet excited state property for the same molecule.

While the normal Bodipy showed absorption in the green range (ca. 500 nm), the azaBodipy showed much red-shifted absorption in the range of 680 nm. O'shea et al. prepared dibromoazaBodipy (**10** in **Figure 2**), and the compounds showed strong absorption in the near IR spectral region (the molar absorption coefficients were up to 80,000 M^{-1} cm^{-1}) (Gorman et al., 2004; Palma et al., 2009). The fluorescence quantum yields of the dibromoazaBodipy were low (1–10%). The ISC ability of the compounds were confirmed by singlet oxygen photosensitizing, and the PDT effect was studied with cancer cells (Gorman et al., 2004). However, the triplet-state lifetimes of the compounds were not reported.

Ramaiah et al. prepared a series of iodinated analogs (**Figure 3**; Adarsh et al., 2012), and the absorption wavelength and the absorptivity were similar to the brominated analogs. With nanosecond transient absorption spectra, the triplet-state lifetimes of the diiodoazaBodipys were determined as *ca.* 2 μs, and triplet-state quantum yields were determined as 70–80% (Adarsh et al., 2012). Besides the azaBodipy derivatives, the styryl Bodipy also showed absorption in the red spectral region (Deniz et al., 2008; Lu et al., 2014). We studied the triplet-state property of the 2,6-diiodobisstyrylBodipy; the triplet-state lifetime was determined as 1.8 μs, and the singlet oxygen quantum yield was determined as 69% (Huang et al., 2013b). Notably, the triplet-state lifetime was much shorter than the normal diiodoBodipy (*ca.* 270 μs). We proposed that the energy gap law alone is not the reason for the short triplet-state lifetimes (Liu and Zhao, 2012; Sun et al., 2013b; Yang et al., 2016). To the best of our knowledge, this was the first time that the triplet-state property of the styryl substituted Bodipy was studied. We also used the 2,6-diiodoBodipy as a novel photocatalyst for an Aza Henry reaction (oxidative coupling of benzylamine); the reaction was more efficient than the conventional photocatalysts, such as the $Ru(bpy)_3$ or $Ir(ppy)_3$ (Huang et al., 2013b). We attributed the

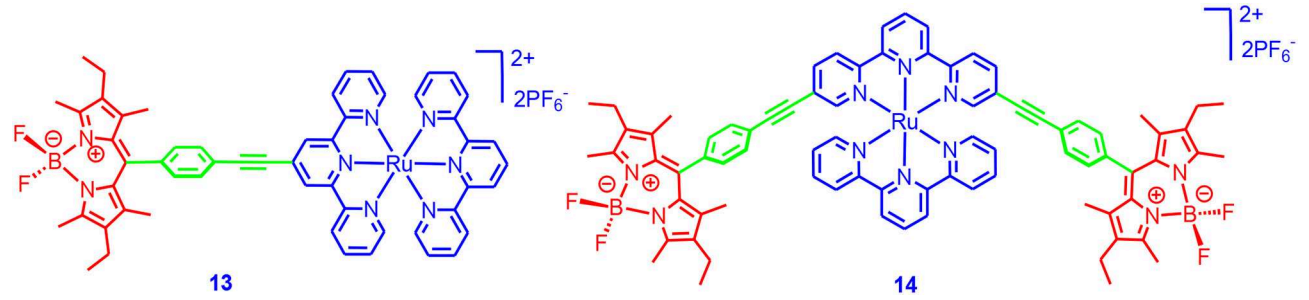

FIGURE 4 | Ru(II) complex containing Bodipy appendants.

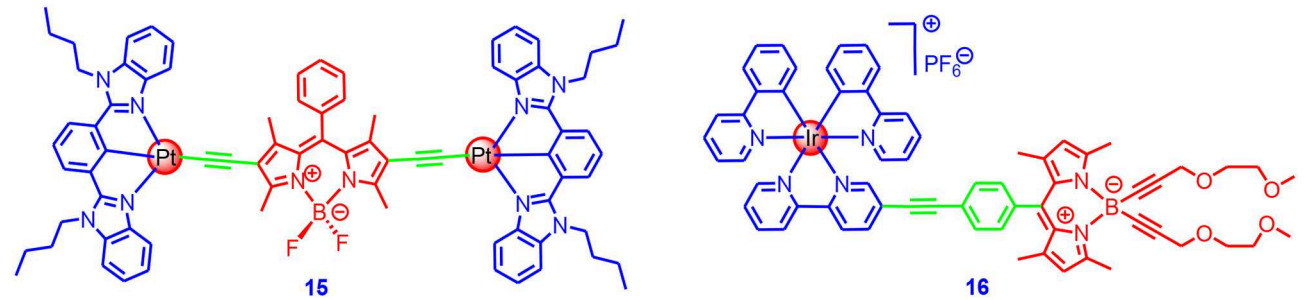

FIGURE 5 | N^C^N Pt(II)–acetylide complex and Ir(III)(ppy)(bpy) complex contains Bodipy chromophore.

efficient photocatalysis to the strong absorption of visible light by the diiodostyrylBodipy.

The heavy atom effect for enhancing spin–orbit coupling is a common mechanism to facilitate the ISC of Bodipy compounds (**Supplementary Figure 2**; Wu et al., 2011; Chen et al., 2012; Nakashima et al., 2018). Furthermore, Eisenberg and MaCamant studied the ISC kinetics of the 2,6-dibromoBodipy and the 2,6-diiodoBodipy (Sabatini et al., 2011). Based on the decay of the stimulated emission (SE) band, the ISC time constants of the 2,6-dibromoBodipy and the 2,6-diiodoBodipy were determined as 1.3 ns and 127 ps, respectively. This result indicated that the iodine atom was more efficient in inducing ISC. It is worth mentioning that the heavy atoms should be attached to the π-conjugation framework of the Bodipy, not to the peripheral moieties, as otherwise the heavy atom effect-induced ISC would not be efficient (Singh-Rachford et al., 2008).

TRANSITION METAL COMPLEXES CONTAINING BODIPY MOIETIES

Transient metal complexes normally show partially forbidden $S_0 \rightarrow {}^1$MLCT transition; as a result, the absorption in the visible range is normally weak. Moreover, because of the significant involvement of the transition metal in the transitions, the T_1 state is actually strongly quenched, manifested by its short triplet-state lifetime (Williams, 2007; Wong and Yam, 2007). Incorporation of a visible light-harvesting chromophore in the transition metal complex will have at least two possible benefits: to strengthen the visible light harvesting and to prolong the triplet-state lifetimes. The achievement of these goals, however, is dependent on the molecular structure design.

Campagna and Ziessel et al. reported Ru(II) terpyridine complexes containing a Bodipy chromophore (**Figure 4**; Galletta et al., 2005). A population of the Bodipy-localized triplet state (lifetimes are 8 and 30 μs, respectively) were observed for both complexes. Phosphorescence of the ^{3*}Bodipy was observed at 77 K. However, we hypothesized that the ISC, upon excitation of the Bodipy unit, was probably not efficient due to the large distance between the Ru(II) center and the Bodipy moiety. It should be noted that the triplet-state lifetime of the parent Ru(II) $(terpyridine)_2$ was short (250 ps), and the long triplet-state lifetimes of **13** and **14** were due to the energy transfer and the localization of triplet state on the Bodipy part. This is a typical example for manipulation of the triplet-state property of transition metal complexes with ligand modification (McClenaghan et al., 2005; Campagna et al., 2007).

Inspired by the molecular structures in the literature (Nastasi et al., 2008), we theorized that directly linking the π-conjugation framework to a metal center may greatly enhance the ISC of the chromophore as this will ensure the excitation energy harvested by the complexes will be efficiently transformed into triplet-state energy (**15** in **Figure 5**; Wu et al., 2012a). Complex **15** was based on a N^C^N Pt(II)–acetylide coordination profile, which showed high phosphorescence quantum yields (19%) (Tam et al., 2011). The absorption of **15** was redshifted (absorption maximum was at 574 nm), as compared to the free Bodipy ligands (absorption band was centered at 543 nm), indicating

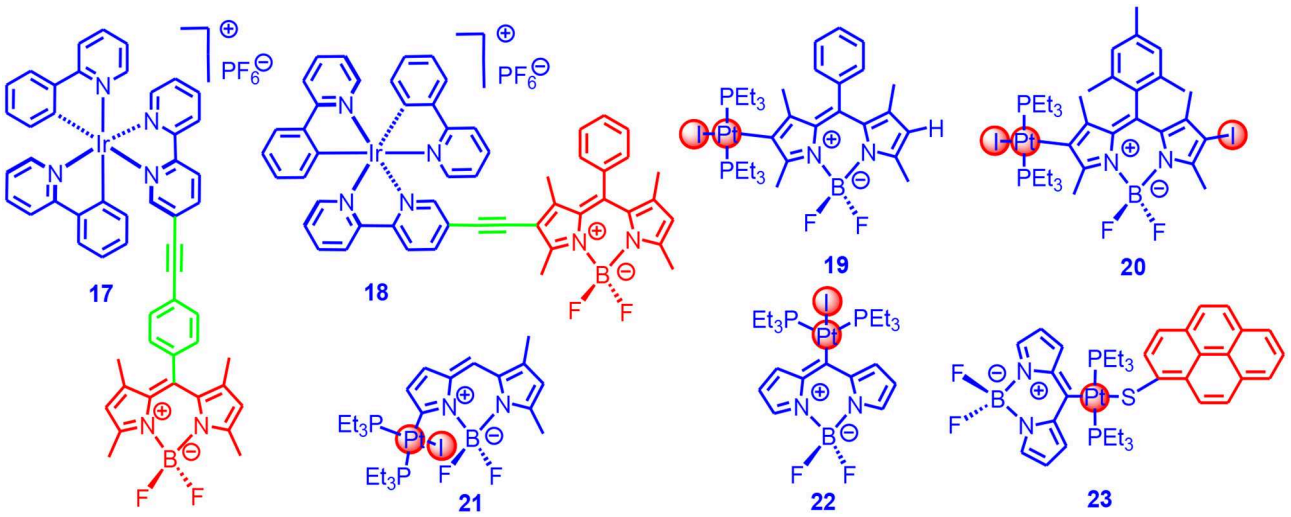

FIGURE 6 | Ir(III)(ppy)(bpy) complex (17, 18) contains Bodipy chromophores via conjugated and non-conjugated linkers and σ-Pt-BODIPY complexes (19–23) with the Bodipy carbon directly metalated.

strong electronic interaction between the Pt(II) coordination center and the Bodipy chromophore. Room temperature near IR phosphorescence band centered at 770 nm was observed, and the phosphorescence quantum yield was up to 3.5%. The triplet-state lifetime was determined as 128 μs by nanosecond transient absorption spectroscopy (Wu et al., 2012a). To the best of our knowledge, this was the first report of the strong near-IR phosphorescence of Bodipy at room temperature. This property indicated the efficiency of the ISC. The complex was used as a triplet photosensitizer for TTA upconversion, and upconversion of the quantum yield up to 5.2% was observed.

Bodipy chromophores were also attached to Ir(III) coordination frameworks. Castellano and Ziessel prepared complex **16**, in which the Bodipy chromophore was attached to the Ir(III) coordination center via an ethynyl linker at the meso-phenyl moiety (**16** in **Figure 5**; Rachford et al., 2010). The complex showed a strong absorption band centered at 501 nm, and it showed the same for the Bodipy ligand, indicating limited electronic interaction between the Ir(III) coordination center and the Bodipy chromophore at the ground state. This is also supported by the redox potentials of the complex and the free ligands. Nanosecond transient absorption spectroscopy showed the Bodipy-localized triplet state with a lifetime of 25 μs. The residual fluorescence of the Bodipy ligand was observed for the complex, and a phosphorescence band centered at 730 nm was observed at 77 K.

We studied the effect of π-conjugated and non-conjugated linkers on the photophysical properties of the Ir(III) complexes (**17**, **18** in **Figure 6**; Sun et al., 2013a). The molecular structure of **17** was similar to complex **16**. In complex **18**, however, the π-conjugated framework of the Bodipy chromophore was connected to the Ir(III) coordination center, which was different from that in **17**. Although **18** showed the same absorption wavelength as compared to the free ligand, room temperature phosphorescence at 742 nm was observed (phosphorescence quantum yield: 0.03%), although with the residual fluorescence of the Bodipy unit at 553 nm (yield 0.3%). We noted the residual fluorescence of the Bodipy unit in **17** was higher (1.8%), and no phosphorescence was observed for **17**. These results indicated the ISC in **18** was more efficient than **17**. This conclusion was supported by the singlet oxygen photosensitizing studies; for **18**, the singlet oxygen quantum yield (Φ_Δ) was 97%, whereas, for **17**, the Φ_Δ was 52%. These results demonstrated that the structure of the linker must be taken into account in order to ensure an efficient ISC.

The triplet-state lifetimes of **17** and **18** were determined as 23.7 and 87.2 μs, respectively. We used the photosensitizer for photocatalytic oxidation of 1,5-dihydroxylnaphthalene, and results showed that the Ir(III) complexes containing the Bodipy units were much more efficient than the conventional $Ir(ppy)_2bpy$ complex. The complexes were also used as triplet photosensitizers for TTA upconversion, with perylene as the triplet acceptor/emitter. The TTA upconversion efficiency with **18** was 2.8%, whereas it was 1.2% for **17**. The parent complex $Ir(ppy)_2bpy$ showed an upconversion quantum yield of 0.3%. We expect that the transition metal complexes showing strong absorption of visible light and a long-lived triplet state will be promising for applications in photocatalysis (Sun et al., 2012, 2013b; Guo et al., 2018; Wang et al., 2019a).

Winter et al. directly attached the Bodipy chromophore to the Pt (**19**-**23** in **Figure 6**) without the ethyne linker, and thus the ISC was supposed to be maximized for these so-called σ-Pt-BODIPY complexes (Irmler and Winter, 2016, 2018; Irmler et al., 2019a,b). The photophysical properties, as well as the electrochemical properties, are substitution position dependent. Dual emission bands centered at 588 and 797 nm were observed for the complexes, with the phosphorescence quantum yield up to 0.364%. The singlet oxygen quantum yields were *ca*. 50%

for the complexes with metalation at the 2- or 3-positions, and it reached 95% for the complex with metalation at the 8-position (Irmler and Winter, 2018). Complexes containing both Bodipy and pyrene ligands (**23**) were prepared (Irmler and Winter, 2016; Irmler et al., 2019a,b), and charge separation (CS) and energy transfer were observed with the complexes. The CT phosphorescence emission band was at 724 nm, and the singlet and triplet emissions of the Bodipy-localized excited state were at 470 and 635 nm, respectively. The phosphorescence lifetimes were up to 500 μs. Interestingly, the complexes with 8-metalation show blueshifted emission as compared to the complexes with metalation at 2-positions (Leen et al., 2012). The ISC mechanism of σ-Pt-BODIPY complexes is presented in **Supplementary Figure 3**.

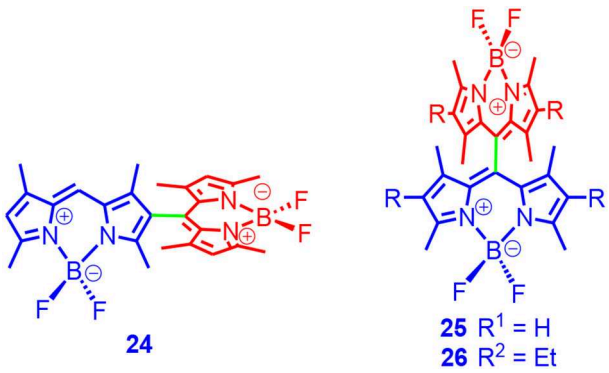

FIGURE 7 | Orthogonal Bodipy dimers showing efficient ISC.

ORTHOGONAL BODIPY DIMERS: THE ISC MECHANISM

Previously, some Bodipy dimers were reported to show the exciton coupling effect (**Supplementary Figure 4**; Bröring et al., 2008; Ventura et al., 2009), which requires specific orientation of the two chromophores (Kasha et al., 1965). These compounds have been revised recently, and readers are suggested to refer those review articles (Zhao et al., 2013, 2015). The manifestation of the exciton coupling is normally a significant splitting of the absorption band of the monomer chromophore in the dimers or dyads (Bröring et al., 2008; Ventura et al., 2009). In this case, one singlet state may share similar energy levels with a triplet state, and thus the ISC will be enhanced.

Recently, orthogonal Bodipy dimers were reported (dimers **24**, **25,** and **26** in **Figure 7**; Cakmak et al., 2011). In this case, there is no splitting of the absorption band, which is different from the exciton coupling effect. The absorption maxima of the compounds are close to the absorption of the monomer. The fluorescence quantum yields of dimers **24**, **25,** and **26** were 3, 31, and 49%, respectively. The singlet oxygen quantum yields of the compounds were 51, 46, and 21%, respectively. Phototoxicity was confirmed with cancer cells. However, the triplet-state property, such as the triplet-state lifetimes, were not studied. Later, Akkya and Dede et al. proposed that the ISC was due to a doubly excited state mechanism (Duman et al., 2012).

We prepared an orthogonal Bodipy dimer **27**, and two hetero-Bodipy dimers, **28** and **29**. The aim was to extend the absorption wavelength (**Figure 8**; Wu et al., 2013). Dimer **27** showed one major absorption band centered at 506 nm, indicating that the two subunits in **27** were identical. For **28** and **29**, however, two absorption bands centered at 509 and 541 nm were observed, which indicated that the two parts were not identical. The fluorescence quantum yields of **27, 28,** and **29** were determined as 2.2, 17.6, and 2.3%, respectively (in DCM). The Φ_Δ values were 64 and 42% for **27** and **28**; no singlet oxygen production was observed for **29**. With nanosecond transient absorption spectroscopy, we determined the triplet-state lifetime of **27** and **28** as 115.6 and 140.9 μs, respectively. Note these apparent triplet-state lifetimes were shorter than the intrinsic triplet-state lifetimes as a result of TTA quenching effect. To the best of our knowledge, this is the first time that the triplet excited state of Bodipy dimers was reported. We proposed that the heavy atom-free triplet photosensitizers were superior, and that the triplet-state lifetime was long, which made it beneficial for intermolecular electron transfer or the charge transfer processes. Thus, we used the dimers as triplet photosensitizers for TTA upconversion, and perylene was used as triplet acceptor/emitter. The upconversion quantum yield was determined as 3.7%. This example demonstrated that the heavy atom-free triplet photosensitizer based on the Bodipy dimers were applicable to intermolecular triplet energy transfers like TTA upconversion.

The ISC mechanisms of these orthogonal Bodipy dimers are controversial. Initially, it was proposed the doubly excited state was responsible for the ISC (Duman et al., 2012). Later, it was proposed that charge transfers between the two units are involved, and that the charge recombination induced the ISC. This was based on an observation of the charge transfer state with the femtosecond transient absorption spectroscopy (Epelde-Elezcano et al., 2017; Liu et al., 2018). It was proposed that the spin–orbital charge-transfer ISC (SOCT-ISC) was responsible for the ISC. Recently, it was proposed the ISC of these orthogonal Bodipy dimers was due to singlet fission (Montero et al., 2018). However, the time-resolved electron paramagnetic resonance (TREPR) spectroscopy study of the dimers does not support this postulation because no quartet state was observed (the spin–spin interaction was as a result of the triplet–triplet pair) (Kandrashkin et al., 2019).

Moreover, the donor/acceptor dyads with large separation distances between the electron donor and acceptor have been studied for a long time. The radical pair ISC (RP ISC) was found to be responsible for the ISC (Wiederrecht et al., 2000; Dance et al., 2006; Kc et al., 2014). However, the synthesis of these electron donor/acceptor dyads is difficult because of the rigid and long linkers in these compounds. Interestingly, some electron donor/acceptor dyads with simple molecular structures were reported recently to show ISC ability; these compounds are promising candidates for heavy atom-free triplet photosensitizers.

Harriman and Ziessel reported a Bodipy derivative with pyridium moiety at the meso position (**Figure 9**). For the analog containing a neutral pyridyl moiety, the fluorescence quantum

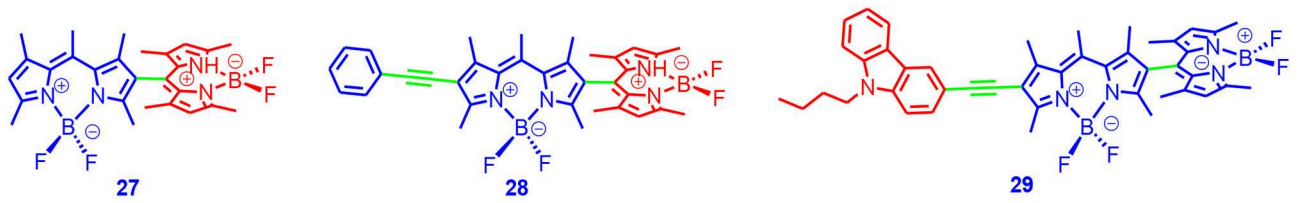

FIGURE 8 | Orthogonal Bodipy dimer 27 and heteroBodipy dimers 28 and 29 showing efficient ISC.

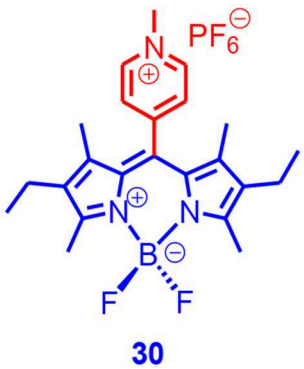

FIGURE 9 | Bodipy derivative with pyridium electron acceptor unit.

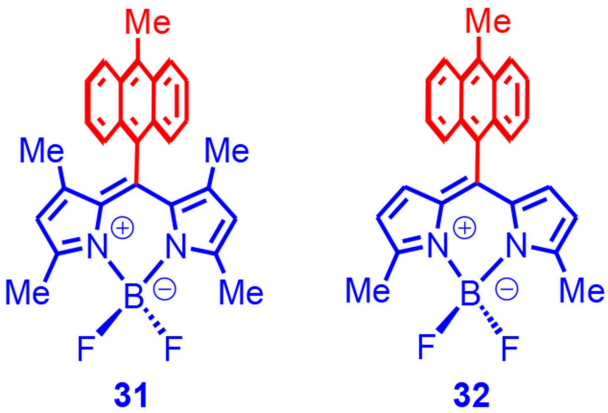

FIGURE 10 | Bodipy derivative with anthryl moiety as electron donor.

yield was high (78%) and the formation of triplet state was negligible (Harriman et al., 2007).

For compound **30**, however, the fluorescence quantum yield decreased to 0.5%, triplet-state formation upon photoexcitation was conformed with nanosecond transient absorption spectroscopy, the ISC quantum yield was determined as 75%, and the triplet-state lifetime was determined as 2.0 ± 0.5 μs. Based on picosecond transient absorption spectroscopy, the charge separation process had a time constant of 5 ps, and the charge recombination (CR)-induced ISC had a time constant of 0.7 ns (Harriman et al., 2007). The ISC should belong to the SOCT-ISC mechanism (**Supplementary Figure 5**) of the compact electron donor/acceptor dyads; the electron donor and acceptor should adopt orthogonal geometry, and the angular momentum conservation would thus be satisfied for the ISC (van Willigen et al., 1996; Dance et al., 2008). Energy levels of the Bodipy dimers do not support the singlet fission mechanism (excitation energy is 2.44 eV, whereas the T_1 state energy of the Bodipy chromophore is ca. 1.70 eV) (Rachford et al., 2010). It should be pointed out that some Bodipy dimers do not show any ISC (Liu et al., 2018), although the so-called symmetry-breaking charge transfer (SBCT) still occurs (Whited et al., 2012).

CHARGE RECOMBINATION-INDUCED ISC IN BODIPY DERIVATIVES

Charge recombination (CR)-induced ISC in electron donor/acceptor dyads with large separation distance between the electron donor and acceptor has been studied for a long time. Radical pair ISC (RP ISC) has been found to be responsible for the ISC (Wiederrecht et al., 2000; Dance et al., 2006; Kc et al., 2014). However, the synthesis of these electron donor/acceptor dyads is difficult because of the rigid and long linkers in these compounds. Interestingly, some electron donor/acceptor dyads with simple molecular structures were reported recently to show ISC ability; these compounds are promising candidates for heavy atom-free triplet photosensitizers (Filatov et al., 2017; Hou et al., 2019).

Filatov and Senge reported feasibly prepared Bodipy–anthryl electron donor/acceptor dyads, in which the anthryl was used as an electron donor (**Figure 10**; Filatov et al., 2017). The fluorescence of the Bodipy moiety in the dyads was quenched to a large extent, and the CS in both dyads was confirmed with femtosecond transient absorption spectroscopy. The singlet oxygen quantum yields of the two dyads were determined as 67 and 38%, respectively. Among other factors, the orthogonal geometry in the dyad was beneficial for the higher singlet oxygen quantum yields. For **31**, the triplet-state lifetime was determined as 41 μs with nanosecond transient absorption spectroscopy. The same researchers prepared a series of analog Bodipy-derived electron donor/acceptor dyads. The dyads generally showed satisfactory SOCT-ISC (Filatov et al., 2018). Zhang also prepared Bodipy-based electron donor/acceptor dyads, and the SOCT-ISC was observed (Zhang and Feng, 2017; Zhang et al., 2017; Hu et al., 2019).

We prepared a series of Bodipy–anthryl dyads, in which the anthryl and the Bodipy units adopted orthogonal geometry, but

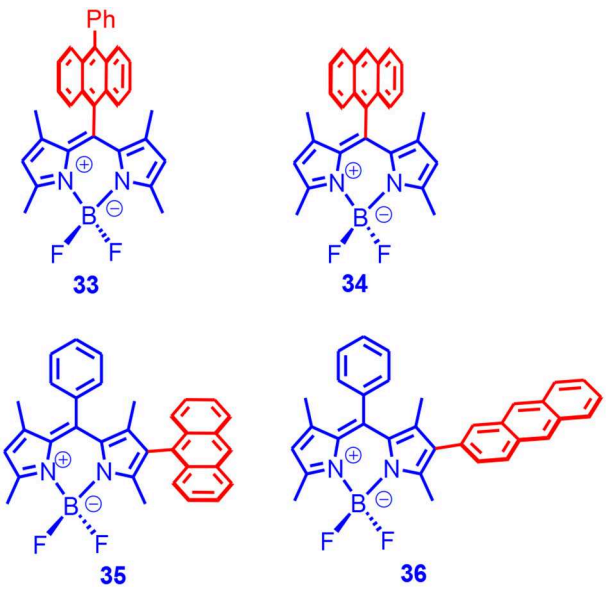

FIGURE 11 | Bodipy derivative with anthryl moiety as electron donor and the dipole moments of the subunits are with parallel or perpendicular.

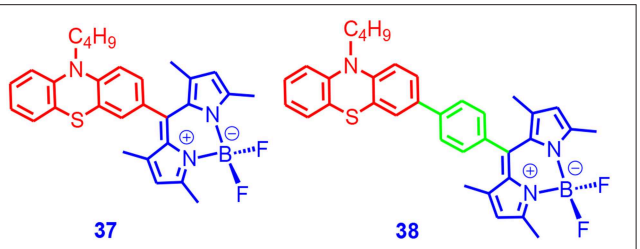

FIGURE 12 | Bodipy derivative with phenothiazine (PTZ) moiety as electron donor.

the dipole moments of the two subunits were either in parallel or perpendicular (**Figure 10**; Wang and Zhao, 2017; Wang et al., 2019b), which was different from the previous reports of the anthryl–Bodipy dyads (Filatov et al., 2017).

We found that, although the fluorescence of the Bodipy unit was all quenched in the dyads, the singlet oxygen quantum yield varied drastically. For **33** and **34**, the singlet oxygen quantum yield can be up to 90%, whereas for **35** and **36**, the singlet oxygen quantum yields were much lower (at most ca. 20% **Figure 11**). Delayed fluorescence was observed for the dyads (P-type, i.e., TTA mechanism). We observed a long triplet-state lifetime for the dyads (up to 82 μs). These dyads were used for TTA upconversion, and an upconversion quantum yield up to 15.8% was observed (Wang and Zhao, 2017). To the best of our knowledge, this was the first time that electron donor/acceptor dyads showing SOCT-ISC and strong absorption of visible light were used for TTA upconversion.

Moreover, we used TREPR spectroscopy to study the electron spin polarization (ESP) of the triplet state of the dyads. The purpose of this kind of study was to study the ISC mechanisms, e.g., to discriminate the radical pair ISC and the SOCT-ISC mechanisms. We observed an ESP of (*e, e, e, a, a, a*) for **33** and **34**, which was similar to that of 2,6-diiodoBodipy (Wang et al., 2019b). This finding was different from the previous reports that the ESP of the triplet state accessed with SOCT-ISC should be always different from the SO ISC (Dance et al., 2008). Interestingly, **35** and **36** showed an ESP of (*a, e, a, e, a, e*), which was different from that of **33** and **34**. The ESP ruled out the RP ISC mechanism. Interestingly, for **34**, three triplet states were simultaneously observed, i.e., the ^{3}CT state, ^{3}An state, and ^{3}Bodipy states. It was proposed that the CR was inhibited to some extent at low temperatures. We have proposed that it is more convincing to use the potential energy curve of the torsion to study the molecular conformation rather than the single point optimization.

We also used phenothiazine as a strong electron donor to construct SOCT-ISC dyads based on Bodipy (**37** and **38**, **Figure 12**; Chen et al., 2017). PTZ had an oxidation potential of +0.3 V (vs. Fc/Fc$^+$), which was more negative than anthryl (ca. +1.0 V, vs. Fc/Fc$^+$). One of the effects of using a stronger electron donor was the decreasing of the CT state energy levels, which may lead to changes of the energy level match profile between the CT state and the LE triplet state.

In other words, the solvent polarity dependency of the ISC quantum yields may change for **37** and **38**, as compared to that fluorescence. This was observed for the Bodipy–anthryl dyads (Filatov et al., 2017). The fluorescence of the Bodipy moiety in **37** (2.7%) was weaker than **38** (7.2%). Efficient singlet oxygen photosensitizing was observed for **37** (67% in toluene, much weaker in other solvents). The singlet oxygen photosensitizing of **38** was weaker (24.6%). Note for the Bodipy–anthryl dyads, high singlet oxygen photosensitizing was observed in acetonitrile (Wang et al., 2019b). An apparent triplet-state lifetime of 116 μs was observed with nanosecond transient absorption spectroscopy. We used **38** as triplet photosensitizer for TTA upconversion, and an upconversion quantum yield of 3.2% was observed.

ISC OF THE C_{60}-BODIPY DYADS: C_{60} AS THE ELECTRON SPIN CONVERTER FOR ACHIEVING ISC

Fullerene C_{60} has been widely used as an electron acceptor in organic photovoltaics materials (Yamazaki et al., 2004; Chen et al., 2011; Izawa et al., 2011; Tamura et al., 2014). It was also used in electron transfer because of its small reorganization energy (Turro et al., 2009). However, we believe one of its photophysical properties has not been fully exploited, i.e., the efficient ISC (Arbogast et al., 1991). The ISC efficiency is close to a unit; however, C_{60} itself is not an ideal triplet photosensitizer because the absorption in the visible spectral region is very weak. We proposed that this drawback could be addressed by attaching a visible light-harvesting chromophore to C_{60}. The energy transfer from the organic chromophore to the C_{60} would thus produce the S_1 state of C_{60}, then, via the ISC of the C_{60} unit, the triplet

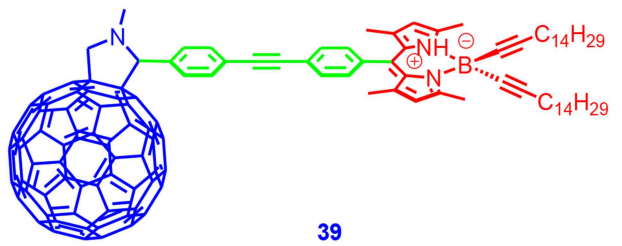

FIGURE 13 | Bodipy–C_{60} dyad derivative with Bodipy moiety as electron donor.

state would be populated. The final localization of the triplet state would be dependent on the relative triplet energy levels of the chromophore and the C_{60} unit. Moreover, charge separation cannot be excluded for the C_{60}-Bodipy dyads, especially in highly polar solvents.

Ziessel and Harriman prepared a C_{60}-Bodipy dyad (**39** in **Figure 13**; Ziessel et al., 2009). The fluorescence of the Bodipy unit was strongly quenched in the dyad. Based on picosecond transient absorption as well as electrochemical studies, it was found the singlet energy transfer was dominant upon photoexcitation of the C_{60} unit in non-polar solvents. Finally, the triplet state on the C_{60} unit was populated. In polar solvent benzonitrile, the CT state contained lower energy than the $^{3*}C_{60}$ state. The CT state had a lifetime of 430 ps. In DCM, the formation of the CT state was observed; the lifetime was 160 ps, the CR lead to the formation of the $^{3*}C_{60}$ state and not the ^{3*}Bodipy state (Ziessel et al., 2009). The triplet-state quantum yields of the dyad were not studied. The main photophysical processes is presented in **Supplementary Figure 6**.

D'Souza and Ng et al. prepared a PTZ–AzaBodip—C_{60} triad (Shi et al., 2013; Bandi et al., 2015; Collini et al., 2017). Photoexcitation of the Bodipy unit lead to the formation of $PTZ^{+\bullet}-azaBodipy^{-\bullet}$-$C_{60}$ and $PTZ^{+\bullet}-azaBODIPY-C_{60}^{-\bullet}$ CT states. The CR lead to the formation of the ^{3*}AzaBodipy state. The ISC quantum yield was not reported.

Inspired by these studies, we prepared a Bodipy–C_{60} dyad (**Figure 14**), and the photophysical property was studied (Wu et al., 2012b). The absorption wavelength of the dyads can be easily changed by using different organic chromophores; **40** showed an absorption band at 515 nm, whereas **41** showed absorption at 590 nm. Note that the S_1 state energy level of C_{60} moiety was 1.77 eV. Thus, singlet energy transfer from the Bodipy unit to the C_{60} unit is possible, although this is not a typical scenario for Förest resonance energy transfer (FRET), since the $S_0 \rightarrow S_1$ transition of the C_{60} unit is very weak (Lakowicz, 1999).

The fluorescence of the Bodipy units in the dyads was strongly quenched, indicating either singlet energy transfer or electron transfer from the Bodipy units to the C_{60} unit. With nanosecond transient absorption spectroscopy, an excited state absorption band centered at 720 nm was observed, which was the characteristic absorption of the $^3C_{60}^*$ state. The triplet-state lifetime was determined as 33.3 μs (Wu et al., 2012b). Since the dyads showed strong absorption in the visible spectral region and long-lived triplet excited states, we used the dyads for TTA

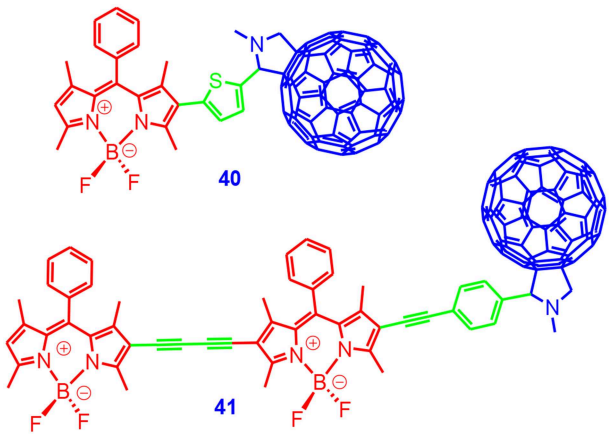

FIGURE 14 | Bodipy–C_{60} dyads 40 and 41 as triplet photosensitizers.

upconversion. The upconversion quantum yields were up to 2.9% (**40**) and 7.0% (**41**). We determined the singlet oxygen quantum yield of an analog of **40** as 81%, thus indicating the ISC of the C_{60}-Bodipy dyads was efficient (Huang et al., 2013a). To the best of our knowledge, this was the first application of C_{60}-organic chromophore dyads for TTA upconversion. Following this line, we prepared a C_{60}-Bodipy–styrylBodipy triad, which showed broadband absorption in the visible spectral region, to enhance the photocatalytic efficiency with a white light source (Huang et al., 2013a). We also prepared C_{60}-dyads containing the chromophore of perylenebisimide (Liu and Zhao, 2012), styrylBodipy (Huang et al., 2012b), and ethyne-linked Bodipy (Huang et al., 2012a; Yang et al., 2012); an efficient ISC was observed for the dyads. We proposed that these C_{60}-organic chromophore dyads that showed strong absorption of visible light and a long-lived triplet state are promising triplet photosensitizers for PDT, photocatalysis, and photon upconversion.

RADICAL ENHANCED ISC

It has been known that the fluorescence of organic chromophores can be quenched by stable radicals (Likhtenstein et al., 2007; Li et al., 2010; Yapici et al., 2012). With TREPR spectroscopy, it was shown that there existed a spin–spin interaction between the persistent radical and the chromophore (Corvaja et al., 1995; Ishii et al., 1996, 1999, 2001; Likhtenstein et al., 2007; Dyar et al., 2015). The overall spin of the dyad may facilitate the ISC of the chromophore (Dyar et al., 2015). However, this property was rarely used for designing visible light-harvesting triplet photosensitizers. One critical issue was to fine-tune the spin–spin interaction magnitude between the radical and the chromophore in order to attain efficient ISC and a long-lived triplet state at the same time. Strong spin–spin interactions will quench the triplet state of the chromophore (Dyar et al., 2015).

We prepared two Bodipy–TEMPO dyads (**Figure 15**), which contain different linkers (Wang et al., 2017). The purpose of varying the linker was to tune the electron spin–spin interaction

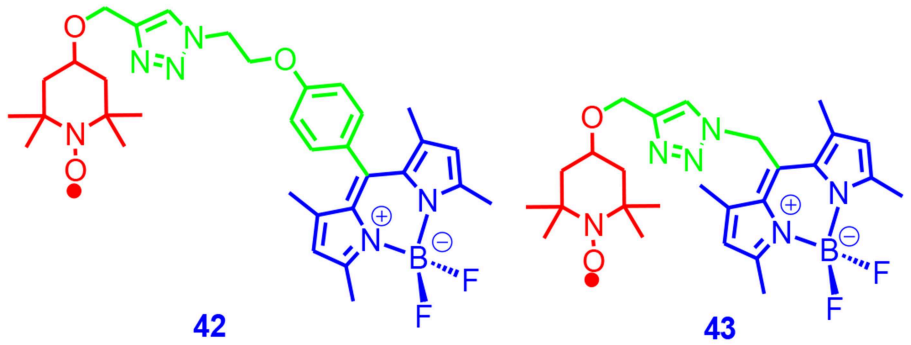

FIGURE 15 | Bodipy-TEMPO dyads showing radical enhanced ISC.

in the dyads to achieve the goal to have efficient ISC and also a long-lived triplet state. The results showed that the fluorescence of the Bodipy unit was quenched in the dyads; the fluorescence quantum yield of **42** was 29%, and the fluorescence of **43** was 5%. With nanosecond transient absorption spectroscopy, we confirmed the ISC and the formation of the ^{3*}Bodipy state upon photoexcitation. The triplet-state lifetimes of the dyads were 190 and 62 μs, respectively. The singlet oxygen quantum yields of the dyads were determined as 14 and 56% for **42** and **43**, respectively. These results show that the linker length in **43** is optimal to achieve both efficient ISC and a long-lived triplet state. With TREPR spectroscopy, we observed the quartet state in a frozen solution at 80 K, indicating that the spin–spin interaction between the radical and the chromophore. In a fluid solution at 185 K, we observed the electron spin polarization of the TEMPO changed from absorption to emission with a longer delay time after the laser flash. The initial absorptive signal was due to the radical-triplet pair mechanism having a doublet precursor, and the later emissive signal was due to RTPM having a triplet precursor. The Bodipy–TEMPO dyads were used for TTA upconversion, and the upconversion quantum yield for **43** was 6.7%, but it was much lower for **42** (0.2%). The radical enhanced ISC mechanism is presented in **Supplementary Figure 7**.

CONCLUSION

In summary, in recent years, varieties of Bodipy derivatives have been reported as having an intersystem crossing (ISC) ability, and the applications of these compounds in photocatalysis, photodynamic therapy, and photon upconversion are promising. One of the critical photophysical properties of the triplet photosensitizers is the efficient ISC ability. In this review article, we summarized the recent development in the area of Bodipy-derived triplet photosensitizers. The compounds have been introduced based on their ISC mechanisms, which include the heavy atom effect, exciton coupling, charge recombination induced ISC, using a spin converter, and radical enhanced ISC. Some transition metal complexes containing Bodipy chromophores are also introduced. The designing rationales of the molecular structures are discussed. We believe the research on the designing of new triplet photosensitizers and the application of these novel materials in the abovementioned areas will flourish.

AUTHOR CONTRIBUTIONS

JZ conceived the topic of the review article and wrote most of the draft. QL took part in the writing and the discussion. KC, YD, XZ, MI, and GT wrote sections of the review and prepared the figures. All the authors made comments and suggestions for the writing of the review.

ACKNOWLEDGMENTS

We thank the NSFC (21673031, 21761142005, 21911530095, and 21421005) and the State Key Laboratory of Fine Chemicals (ZYTS201901) for financial support.

SUPPLEMENTARY MATERIAL

The Supplementary Material for this article can be found online at: https://www.frontiersin.org/articles/10.3389/fchem.2019.00821/full#supplementary-material

REFERENCES

Adarsh, N., Shanmugasundaram, M., Avirah, R. R., and Ramaiah, D. (2012). Aza-BODIPY derivatives: enhanced quantum yields of triplet excited states and the generation of singlet oxygen and their role as facile sustainable photooxygenation catalysts. *Chem. Eur. J.* 18, 12655–12662. doi: 10.1002/chem.201202438

Arbogast, J. W., Darmanyan, A. P., Foote, C. S., Diederich, F. N., Whetten, R. L., Rubin, Y., et al. (1991). Photophysical properties of sixty atom carbon molecule (C_{60}). *J. Phys. Chem.* 95, 11–12. doi: 10.1021/j100154a006

Awuah, S. G., and You, Y. (2012). Boron dipyrromethene (BODIPY)-based photosensitizers for photodynamic therapy. *RSC Adv.* 2, 11169–11183. doi: 10.1039/c2ra21404k

Bandi, V., Gobeze, H. B., Lakshmi, V., Ravikanth, M., and D'Souza, F. (2015). Vectorial charge separation and selective triplet-state formation during charge recombination in a pyrrolyl-bridged BODIPY–fullerene dyad. *J. Phys. Chem. C* 119, 8095–8102. doi: 10.1021/acs.jpcc.5b02712

Bittner, E. R., Lankevich, V., Gélinas, S., Rao, A., Ginger, D. A., and Friend, R. H. (2014). How disorder controls the kinetics of triplet charge recombination in semiconducting organic polymer photovoltaics. *Phys. Chem. Chem. Phys.* 16, 20321–20328. doi: 10.1039/C4CP01776E

Bröring, M., Krüger, R., Link, S., Kleeberg, C., Köhler, S., Xie, X., et al. (2008). Bis(BF_2)-2,2′-bidipyrrins (bisBODIPYs): highly fluorescent BODIPY dimers with large stokes shifts. *Chem. Eur. J.* 14, 2976–2983. doi: 10.1002/chem.200701912

Cakmak, Y., Kolemen, S., Duman, S., Dede, Y., Dolen, Y., Kilic, B., et al. (2011). Designing excited states: theory-guided access to efficient photosensitizers for photodynamic action. *Angew. Chem. Int. Ed.* 50, 11937–11941. doi: 10.1002/anie.201105736

Campagna, S., Puntoriero, F., Nastasi, F., Bergamini, G., and Balzani, V. (2007). "Photochemistry and photophysics of coordination compounds: ruthenium," in *Photochemistry and Photophysics of Coordination Compounds I*, eds V. Balzani and S. Campagna (Heidelberg: Springer Berlin Heidelberg), 117–214.

Cengiz, N., Gevrek, T. N., Sanyal, R., and Sanyal, A. (2017). Orthogonal thiol–ene 'click' reactions: a powerful combination for fabrication and functionalization of patterned hydrogels. *Chem. Commun.* 53, 8894–8897. doi: 10.1039/C7CC02298K

Ceroni, P. (2011). Energy up-conversion by low-power excitation: new applications of an old concept. *Chem. Eur. J.* 17, 9560–9564. doi: 10.1002/chem.201101102

Cheema, H., Islam, A., Han, L., Gautam, B., Younts, R., Gundogdu, K., et al. (2014). Influence of mono versus bis-electron-donor ancillary ligands in heteroleptic Ru(II) bipyridyl complexes on electron injection from the first excited singlet and triplet states in dye-sensitized solar cells. *J. Mater. Chem. A* 2, 14228–14235. doi: 10.1039/C4TA01942C

Chen, K., Yang, W., Wang, Z., Iagatti, A., Bussotti, L., Foggi, P., et al. (2017). Triplet excited state of BODIPY accessed by charge recombination and its application in triplet-triplet annihilation upconversion. *J. Phys. Chem. A.* 121, 7550–7564. doi: 10.1021/acs.jpca.7b07623

Chen, T. L., Zhang, Y., Smith, P., Tamayo, A., Liu, Y., and Ma, B. (2011). Diketopyrrolopyrrole-containing oligothiophene-fullerene triads and their use in organic solar cells. *ACS Appl. Mater. Inter.* 3, 2275–2280. doi: 10.1021/am200145t

Chen, Y., Zhao, J., Xie, L., Guo, H., and Li, Q. (2012). Thienyl-substituted bodipys with strong visible light-absorption and long-lived triplet excited states as organic triplet sensitizers for triplet–triplet annihilation upconversion. *RSC Adv.* 2, 3942–3953. doi: 10.1039/c2ra01064j

Collini, M. A., Thomas, M. B., Bandi, V., Karr, P. A., and D'Souza, F. (2017). Directly attached bisdonor-BF_2 chelated azadipyrromethene-fullerene tetrads for promoting ground and excited state charge transfer. *Chem. Eur. J.* 23, 4450–4461. doi: 10.1002/chem.201700200

Corvaja, C., Maggini, M., Prato, M., Scorrano, G., and Venzin, M. (1995). C_{60} derivative covalently linked to a nitroxide radical: time-resolved EPR evidence of electron spin polarization by intramolecular radical-triplet pair interaction. *J. Am. Chem. Soc.* 117, 8857–8858. doi: 10.1021/ja00139a022

Dai, F. R., Zhan, H. M., Liu, Q., Fu, Y. Y., Li, J. H., Wang, Q. W., et al. (2012). Platinum(II)–bis(aryleneethynylene) complexes for solution-processible molecular bulk heterojunction solar cells. *Chem. Eur. J.* 18, 1502–1511. doi: 10.1002/chem.201102598

Dance, Z. E., Mi, Q., McCamant, D. W., Ahrens, M. J., Ratner, M. A., and Wasielewski, M. R. (2006). Time-resolved EPR studies of photogenerated radical ion pairs separated by *p*-phenylene oligomers and of triplet states resulting from charge recombination. *J. Phys. Chem. B* 110, 25163–25173. doi: 10.1021/jp063690n

Dance, Z. E. X., Mickley, S. M., Wilson, T. M., Ricks, A. B., Scott, A. M., Ratner, M. A., et al. (2008). Intersystem crossing mediated by photoinduced intramolecular charge transfer: julolidine–anthracene molecules with perpendicular π systems. *J. Phys. Chem. A* 112, 4194–4201. doi: 10.1021/jp800561g

Deniz, E., Isbasar, G. C., Bozdemir, O. A., Yildirim, L. T., Siemiarczuk, A., and Akkaya, E. U. (2008). Bidirectional switching of near IR emitting boradiazaindacene fluorophores. *Org. Lett.* 10, 3401–3403. doi: 10.1021/ol801062h

DiSalle, B. F., and Bernhard, S. (2011). Orchestrated photocatalytic water reduction using surface-adsorbing iridium photosensitizers. *J. Am. Chem. Soc.* 133, 11819–11821. doi: 10.1021/ja201514e

Duman, S., Cakmak, Y., Kolemen, S., Akkaya, E. U., and Dede, Y. (2012). Heavy atom free singlet oxygen generation: doubly substituted configurations dominate S_1 states of bis-BODIPYs. *J. Org. Chem.* 77, 4516–4527. doi: 10.1021/jo300051v

Dyar, S. M., Margulies, E. A., Horwitz, N. E., Brown, K. E., Krzyaniak, M. D., and Wasielewski, M. R. (2015). Photogenerated quartet state formation in a compact ring-fused perylene-nitroxide. *J. Phys. Chem. B* 119, 13560–13569. doi: 10.1021/acs.jpcb.5b02378

Epelde-Elezcano, N., Palao, E., Manzano, H., Prieto-Castañeda, A., Agarrabeitia, A. R., Tabero, A., et al. (2017). Rational design of advanced photosensitizers based on orthogonal BODIPY dimers to finely modulate singlet oxygen generation. *Chem. Eur. J.* 23, 4837–4848. doi: 10.1002/chem.201605822

Etzold, F., Howard, I. A., Forler, N., Melnyk, A., Andrienko, D., Hansen, M. R., et al. (2015). Sub-ns triplet state formation by non-geminate recombination in PSBTBT:PC_{70}BM and PCPDTBT:PC_{60}BM organic solar cells. *Energy Environ. Sci.* 8, 1511–1522. doi: 10.1039/C4EE03630A

Filatov, M. A., Karuthedath, S., Polestshuk, P. M., Callaghan, S., Flanagan, K. J., Telitchko, M., et al. (2018). Control of triplet state generation in heavy atom-free BODIPY–anthracene dyads by media polarity and structural factors. *Phys. Chem. Chem. Phys.* 20, 8016–8031. doi: 10.1039/C7CP08472B

Filatov, M. A., Karuthedath, S., Polestshuk, P. M., Savoie, H., Flanagan, K. J., Sy, C., et al. (2017). Generation of triplet excited states via photoinduced electron transfer in meso-anthra-BODIPY: fluorogenic response toward singlet oxygen in solution and *in vitro*. *J. Am. Chem. Soc.* 139, 6282–6285. doi: 10.1021/jacs.7b00551

Galletta, M., Campagna, S., Quesada, M., Ulrich, G., and Ziessel, R. (2005). The elusive phosphorescence of pyrromethene–BF_2 dyes revealed in new multicomponent species containing Ru(II)–terpyridine subunits. *Chem. Commun.* 4224. doi: 10.1039/b507196h

Gärtner, F., Cozzula, D., Losse, S., Boddien, A., Anilkumar, G., Junge, H., et al. (2011). Synthesis, characterisation and application of iridium(III) photosensitisers for catalytic water reduction. *Chem. Eur. J.* 17, 6998–7006. doi: 10.1002/chem.201100235

Gärtner, F., Denurra, S., Losse, S., Neubauer, A., Boddien, A., Gopinathan, A., et al. (2012). Synthesis and characterization of new iridium photosensitizers for catalytic hydrogen generation from water. *Chem. Eur. J.* 18, 3220–3225. doi: 10.1002/chem.201103670

Goessl, A., Bowen-Pope, D. F., and Hoffman, A. S. (2001). Control of shape and size of vascular smooth muscle cells *in vitro* by plasma lithography. *J. Biomed. Mater. Res.* 57, 15–24. doi: 10.1002/1097-4636(200110)57:1<15::AID-JBM1136>3.0.CO;2-N

Gorman, A., Killoran, J., O'Shea, C., Kenna, T., Gallagher, W. M., and O'Shea, D. F. (2004). *In vitro* demonstration of the heavy-atom effect for photodynamic therapy. *J. Am. Chem. Soc.* 126, 10619–10631. doi: 10.1021/ja047649e

Guo, F., Kim, Y. G., Reynolds, J. R., and Schanze, K. S. (2006). Platinum–acetylide polymer based solar cells: involvement of the triplet state for energy conversion. *Chem. Commun.* 1887–1889. doi: 10.1039/B516086C

Guo, S., Chen, K., Dong, R., Zhang, Z., Zhao, J., and Lu, T. (2018). Robust and long-lived excited state Ru(II) polyimine photosensitizers boost hydrogen production. *ACS Catalysis* 8, 8659–8670. doi: 10.1021/acscatal.8b02226

Hari, D. P., and König, B. (2013). The photocatalyzed meerwein arylation: classic reaction of aryl diazonium salts in a new light. *Angew. Chem. Int. Ed.* 52, 4734–4743. doi: 10.1002/anie.201210276

Harriman, A., Mallon, L. J., Ulrich, G., and Ziessel, R. (2007). Rapid intersystem crossing in closely-spaced but orthogonal molecular dyads. *ChemPhysChem* 8, 1207–1214. doi: 10.1002/cphc.200700060

Ho, K. M., Li, W. Y., Wong, C. H., and Li, P. (2010). Amphiphilic polymeric particles with core–shell nanostructures: emulsion-based

syntheses and potential applications. *Colloid Polym. Sci.* 288, 1503–1523. doi: 10.1007/s00396-010-2276-9

Hou, Y., Zhang, X., Chen, K., Liu, D., Wang, Z., Liu, Q., et al. (2019). Charge separation, charge recombination, long-lived charge transfer state formation and intersystem crossing in organic electron donor/acceptor dyads. *J. Mater. Chem. C* 7, 12048–12074. doi: 10.1039/C9TC04285G

Hu, W., Liu, M., Zhang, X., Wang, Y., Wang, Y., Lan, H., et al. (2019). Can BODIPY-electron acceptor conjugates act as heavy atom-free excited triplet state and singlet oxygen photosensitizers via photoinduced charge separation-charge recombination mechanism? *J. Phys. Chem. C* 123, 15944–15955. doi: 10.1021/acs.jpcc.9b02961

Huang, D., Zhao, J., Wu, W., Yi, X., Yang, P., and Ma, J. (2012a). Visible-light-harvesting triphenylamine ethynyl C_{60}-BODIPY dyads as heavy-atom-free organic triplet photosensitizers for triplet-triplet annihilation upconversion. *Asian J. Org. Chem.* 1, 264–273. doi: 10.1002/ajoc.201200062

Huang, L., Cui, X., Therrien, B., and Zhao, J. (2013a). Energy-funneling-based broadband visible-light-absorbing bodipy–C60 triads and tetrads as dual functional heavy-atom-free organic triplet photosensitizers for photocatalytic organic reactions. *Chem. Eur. J.* 19, 17472–17482. doi: 10.1002/chem.201302492

Huang, L., Yu, X., Wu, W., and Zhao, J. (2012b). Styryl bodipy-C_{60} dyads as efficient heavy-atom-free organic triplet photosensitizers. *Org. Lett.* 14, 2594–2597. doi: 10.1021/ol3008843

Huang, L., Zhao, J., Guo, S., Zhang, C., and Ma, J. (2013b). Bodipy derivatives as organic triplet photosensitizers for aerobic photoorganocatalytic oxidative coupling of amines and photooxidation of dihydroxylnaphthalenes. *J. Org. Chem.* 78, 5627–5637. doi: 10.1021/jo400769u

Irmler, P., Gogesch, F. S., Larsen, C. B., Wenger, O. S., and Winter, R. F. (2019a). Four different emissions from a Pt(Bodipy)$(PEt_3)_2$(S-Pyrene) dyad. *Dalton Trans.* 48, 1171–1174. doi: 10.1039/C8DT04823A

Irmler, P., Gogesch, F. S., Mang, A., Bodensteiner, M., Larsen, C. B., Wenger, O. S., et al. (2019b). Directing energy transfer in Pt(bodipy)(mercaptopyrene) dyads. *Dalton Trans.* 48, 11690–11705. doi: 10.1039/C9DT01737B

Irmler, P., and Winter, R. F. (2016). Complexes trans-Pt(BODIPY)X$(PEt_3)_2$: excitation energy-dependent fluorescence and phosphorescence emissions, oxygen sensing and photocatalysis. *Dalton Trans.* 45, 10420–10434. doi: 10.1039/C6DT01623E

Irmler, P., and Winter, R. F. (2018). σ-Pt-BODIPY complexes with platinum attachment to carbon atoms C2 or C3: spectroscopic, structural, and (spectro)electrochemical studies and photocatalysis. *Organometallics* 37, 235–253. doi: 10.1021/acs.organomet.7b00806

Ishii, K., Fujisawa, J., Ohba, Y., and Yamauchi, S. (1996). A time-resolved electron paramagnetic resonance study on the excited states of tetraphenylporphinatozinc(II) coordinated by *p*-pyridyl nitronyl nitroxide. *J. Am. Chem. Soc.* 118, 13079–13080. doi: 10.1021/ja961661s

Ishii, K., Hirose, Y., Fujitsuka, H., Ito, O., and Kobayashi, N. (2001). Time-resolved EPR, fluorescence, and transient absorption studies on phthalocyaninatosilicon covalently linked to one or two TEMPO radicals. *J. Am. Chem. Soc.* 123, 702–708. doi: 10.1021/ja002780h

Ishii, K., Hirose, Y., and Kobayashi, N. (1999). Electron spin polarizations of phthalocyaninatosilicon covalently linked to one TEMPO radical in the excited quartet and doublet ground states. *J. Phys. Chem. A* 103, 1986–1990. doi: 10.1021/jp983624o

Izawa, S., Hashimoto, K., and Tajima, K. (2011). Efficient charge generation and collection in organic solar cells based on low band gap dyad molecules. *Chem. Commun.* 47, 6365–6367. doi: 10.1039/c1cc11387a

Jiang, X. J., Lau, J. T., Wang, Q., Ng, D. K., and Lo, P. C. (2016). pH- and thiol-responsive BODIPY-based photosensitizers for targeted photodynamic therapy. *Chem. Eur. J.* 22, 8273–8281. doi: 10.1002/chem.201600452

Kamkaew, A., Lim, S. H., Lee, H. B., Kiew, L. V., Chung, L. Y., and Burgess, K. (2013). BODIPY dyes in photodynamic therapy. *Chem. Soc. Rev.* 42, 77–88. doi: 10.1039/C2CS35216H

Kandrashkin, Y. E., Wang, Z., Sukhanov, A. A., Hou, Y., Zhang, X., Liu, Y., et al. (2019). Balance between triplet states in photoexcited orthogonal bodipy dimers. *J. Phys. Chem. Lett.* 10, 4157–4163. doi: 10.1021/acs.jpclett.9b01741

Kasha, M., Rawls, H. R., and Ashraf El-Bayoumi, M. (1965). The exciton model in molecular spectroscopy. *Pure Appl. Chem.* 11, 371–392. doi: 10.1351/pac196511030371

Kc, C. B., Lim, G. N., Nesterov, V. N., Karr, P. A., and D'Souza, F. (2014). Phenothiazine–BODIPY–fullerene triads as photosynthetic reaction center models: substitution and solvent polarity effects on photoinduced charge separation and recombination. *Chem. Eur. J.* 20, 17100–17112. doi: 10.1002/chem.201404863

Kuimova, M. K., Yahioglu, G., Levitt, J. A., and Suhling, K. (2008). Molecular rotor measures viscosity of live cells via fluorescence lifetime imaging. *J. Am. Chem. Soc.* 130, 6672–6673. doi: 10.1021/ja800570d

Lakowicz, J. R. (1999). *Principles of Fluorescence Spectroscopy*. New York, NY: Kluwer Academic.

Lakshmi, V., Rao, M. R., and Ravikanth, M. (2015). Halogenated boron-dipyrromethenes: synthesis, properties and applications. *Org. Biomol. Chem.* 13, 2501–2517. doi: 10.1039/C4OB02293A

Leen, V., Yuan, P., Wang, L., Boens, N., and Dehaen, W. (2012). Synthesis of meso-halogenated BODIPYs and access to meso-substituted analogues. *Org. Lett.* 14, 6150–6153. doi: 10.1021/ol3028225

Li, P., Xie, T., Duan, X., Yu, F., Wang, X., and Tang, B. (2010). A new highly selective and sensitive assay for fluorescence imaging of ·OH in living cells: effectively avoiding the interference of peroxynitrite. *Chem. Eur. J.* 16, 1834–1840. doi: 10.1002/chem.200901514

Li, X., Kolemen, S., Yoon, J., and Akkaya, E. U. (2017). Activatable photosensitizers: agents for selective photodynamic therapy. *Adv. Funct. Mater.* 27:1604053. doi: 10.1002/adfm.201604053

Likhtenstein, G. I., Ishii, K., and Nakatsuji, S. (2007). Dual chromophore-nitroxides: novel molecular probes, photochemical and photophysical models and magnetic materials. *Photochem. Photobiol.* 83, 871–881. doi: 10.1111/j.1751-1097.2007.00141.x

Liu, Y., and Zhao, J. (2012). Visible light-harvesting perylenebisimide–fullerene (C_{60}) dyads with bidirectional "ping-pong" energy transfer as triplet photosensitizers for photooxidation of 1,5-dihydroxynaphthalene. *Chem. Commun.* 48, 3751–3753. doi: 10.1039/c2cc30345k

Liu, Y., Zhao, J., Iagatti, A., Bussotti, L., Foggi, P., Castellucci, E., et al. (2018). A revisit to the orthogonal bodipy dimers: experimental evidence for the symmetry breaking charge transfer-induced intersystem crossing. *J. Phys. Chem. C* 122, 2502–2511. doi: 10.1021/acs.jpcc.7b10213

Lou, Z., Hou, Y., Chen, K., Zhao, J., Ji, S., Zhong, F., et al. (2018). Different quenching effect of intramolecular rotation on the singlet and triplet excited states of Bodipy. *J. Phys. Chem. C* 122, 185–193. doi: 10.1021/acs.jpcc.7b10466

Lu, H., Mack, J., Yang, Y., and Shen, Z. (2014). Structural modification strategies for the rational design of Red/NIR region BODIPYs. *Chem. Soc. Rev.* 43, 4778–4823. doi: 10.1039/C4CS00030G

McClenaghan, N. D., Leydet, Y., Maubert, B., Indelli, M. T., and Campagna, S. (2005). Excited-state equilibration: a process leading to long-lived metal-to-ligand charge transfer luminescence in supramolecular systems. *Coord. Chem. Rev.* 249, 1336–1350. doi: 10.1016/j.ccr.2004.12.017

Miao, W., Feng, Y., Wu, Q., Sheng, W., Li, M., Liu, Q., et al. (2019). Phenanthro[b]-fused bodipys through tandem suzuki and oxidative aromatic couplings: synthesis and photophysical properties. *J. Org. Chem.* 84, 9693–9704. doi: 10.1021/acs.joc.9b01425

Monguzzi, A., Tubino, R., Hoseinkhani, S., Campione, M., and Meinardi, F. (2012). Low power, non-coherent sensitized photon up-conversion: modeling and perspectives. *Phys. Chem. Chem. Phys.* 14, 4322–4332. doi: 10.1039/c2cp23900k

Montero, R., Martínez-Martínez, V., Longarte, A., Epelde-Elezcano, N., Palao, E., Lamas, I., et al. (2018). Singlet fission mediated photophysics of bodipy dimers. *J. Phys. Chem. Lett.* 9, 641–646. doi: 10.1021/acs.jpclett.7b03074

Nakashima, M., Iizuka, K., Karasawa, M., Ishii, K., and Kubo, Y. (2018). Selenium-containing bodipy dyes as photosensitizers for triplet–triplet annihilation upconversion. *J. Mater. Chem. C* 6, 6208–6215. doi: 10.1039/C8TC00944A

Nastasi, F., Puntoriero, F., Campagna, S., Diring, S., and Ziessel, R. (2008). Photoinduced intercomponent processes in multichromophoric species made of Pt(II)-terpyridine-acetylide and dipyrromethene-BF_2 subunits. *Phys. Chem. Chem. Phys.* 10, 3982–3986. doi: 10.1039/b805972a

Palma, A., Tasior, M., Frimannsson, D. O., Vu, T. T., Méallet-Renault, R., and O'Shea, D. F. (2009). New on-bead near-infrared fluorophores and fluorescent sensor constructs. *Org. Lett.* 11, 3638–3641. doi: 10.1021/ol901413u

Rachford, A. A., Ziessel, R., Bura, T., Retailleau, P., and Castellano, F. N. (2010). Boron dipyrromethene (Bodipy) phosphorescence revealed in $[Ir(ppy)_2$(bpy-C=C-Bodipy)$]^+$. *Inorg. Chem.* 49, 3730–3736. doi: 10.1021/ic901996u

Rivard, E. (2012). Inorganic and organometallic polymers. *Annu. Rep. Sect. A Inorgan. Chem.* 108, 315–329. doi: 10.1039/c2ic90001g

Sabatini, R. P., McCormick, T. M., Lazarides, T., Wilson, K. C., Eisenberg, R., and McCamant, D. W. (2011). Intersystem crossing in halogenated Bodipy chromophores used for solar hydrogen production. *J. Phys. Chem. Lett.* 2, 223–227. doi: 10.1021/jz101697y

Sato, S., Morikawa, T., Kajino, T., and Ishitani, O. (2013). A highly efficient mononuclear iridium complex photocatalyst for CO_2 reduction under visible light. *Angew. Chem. Int. Ed.* 52, 988–992. doi: 10.1002/anie.201206137

Shi, L., and Xia, W. (2012). Photoredox functionalization of C–H bonds adjacent to a nitrogen atom. *Chem. Soc. Rev.* 41, 7687–7697. doi: 10.1039/c2cs35203f

Shi, W. J., El-Khouly, M. E., Ohkubo, K., Fukuzumi, S., and Ng, D. K. (2013). Photosynthetic antenna-reaction center mimicry with a covalently linked monostyryl boron-dipyrromethene–aza-boron-dipyrromethene–C_{60} triad. *Chem. Eur. J.* 19, 11332–11341. doi: 10.1002/chem.201300318

Simon, Y. C., and Weder, C. (2012). Low-power photon upconversion through triplet–triplet annihilation in polymers. *J. Mater. Chem.* 22, 20817–20830. doi: 10.1039/c2jm33654e

Singh-Rachford, T. N., and Castellano, F. N. (2010). Photon upconversion based on sensitized triplet–triplet annihilation. *Coord. Chem. Rev.* 254, 2560–2573. doi: 10.1016/j.ccr.2010.01.003

Singh-Rachford, T. N., Haefele, A., Ziessel, R., and Castellano, F. N. (2008). Boron dipyrromethene chromophores: next generation triplet acceptors/annihilators for low power upconversion schemes. *J. Am. Chem. Soc.* 130, 16164–16165. doi: 10.1021/ja807056a

Stacey, O. J., and Pope, S. J. A. (2013). New avenues in the design and potential application of metal complexes for photodynamic therapy. *RSC Adv.* 3, 25550–25564. doi: 10.1039/c3ra45219k

Suhina, T., Amirjalayer, S., Woutersen, S., Bonn, D., and Brouwer, A. M. (2017). Ultrafast dynamics and solvent-dependent deactivation kinetics of BODIPY molecular rotors. *Phys. Chem. Chem. Phys.* 19, 19998–20007. doi: 10.1039/C7CP02037F

Sun, J., Zhao, J., Guo, H., and Wu, W. (2012). Visible-light harvesting iridium complexes as singlet oxygen sensitizers for photooxidation of 1,5-dihydroxynaphthalene. *Chem. Commun.* 48, 4169–4171. doi: 10.1039/c2cc16690a

Sun, J., Zhong, F., Yi, X., and Zhao, J. (2013a). Efficient enhancement of the visible-light absorption of cyclometalated Ir(III) complexes triplet photosensitizers with Bodipy and applications in photooxidation and triplet–triplet annihilation upconversion. *Inorg. Chem.* 52, 6299–6310. doi: 10.1021/ic302210b

Sun, J., Zhong, F., and Zhao, J. (2013b). Observation of the long-lived triplet excited state of perylenebisimide (PBI) in C∧N cyclometalated Ir(III) complexes and application in photocatalytic oxidation. *Dalton Trans.* 42, 9595–9605. doi: 10.1039/c3dt33036b

Tam, A. Y., Tsang, D. P., Chan, M. Y., Zhu, N., and Yam, V. W. (2011). A luminescent cyclometalated platinum(II) complex and its green organic light emitting device with high device performance. *Chem. Commun.* 47, 3383–3385. doi: 10.1039/c0cc05538g

Tamura, Y., Saeki, H., Hashizume, J., Okazaki, Y., Kuzuhara, D., Suzuki, M., et al. (2014). Direct comparison of a covalently-linked dyad and a 1:1 mixture of tetrabenzoporphyrin and fullerene as organic photovoltaic materials. *Chem. Commun.* 50, 10379–10381. doi: 10.1039/C4CC03801K

Turro, N. J., Ramamurthy, V., and Scaiano, J. C. (2009). *Principles of Molecular Photochemistry: An Introduction.* Sausalito, CA: University Science Books.

Ulrich, G., Ziessel, R., and Harriman, A. (2008). The chemistry of fluorescent bodipy dyes: versatility unsurpassed. *Angew. Chem. Int. Ed.* 47, 1184–1201. doi: 10.1002/anie.200702070

van Willigen, H., Jones, G., and Farahat, M. S. (1996). Time-resolved EPR study of photoexcited triplet-state formation in electron-donor-substituted acridinium ions. *J. Phys. Chem.* 100, 3312–3316. doi: 10.1021/jp953176+

Ventura, B., Marconi, G., Bröring, M., Krüger, R., and Flamigni, L. (2009). Bis(BF_2)-2,2′-bidipyrrins, a class of BODIPY dyes with new spectroscopic and photophysical properties. *New J. Chem.* 33, 428–438. doi: 10.1039/B813638F

Wang, P., Guo, S., Wang, H., Chen, K., Zhang, N., Zhang, Z., et al. (2019a). A broadband and strong visible-light-absorbing photosensitizer boosts hydrogen evolution. *Nat. Commun.* 10:3155. doi: 10.1038/s41467-019-11099-8

Wang, Z., Sukhanov, A. A., Toffoletti, A., Sadiq, F., Zhao, J., Barbon, A., et al. (2019b). Insights into the efficient intersystem crossing of Bodipy-anthracene compact dyads with steady-state and time-resolved optical/magnetic spectroscopies and observation of the delayed fluorescence. *J. Phys. Chem. C* 123, 265–274. doi: 10.1021/acs.jpcc.8b10835

Wang, Z., and Zhao, J. (2017). Bodipy–anthracene dyads as triplet photosensitizers: effect of chromophore orientation on triplet-state formation efficiency and application in triplet-triplet annihilation upconversion. *Org. Lett.* 19, 4492–4495. doi: 10.1021/acs.orglett.7b02047

Wang, Z., Zhao, J., Barbon, A., Toffoletti, A., Liu, Y., An, Y., et al. (2017). Radical-enhanced intersystem crossing in new bodipy derivatives and application for efficient triplet-triplet annihilation upconversion. *J. Am. Chem. Soc.* 139, 7831–7842. doi: 10.1021/jacs.7b02063

Whited, M. T., Patel, N. M., Roberts, S. T., Allen, K., Djurovich, P. I., Bradforth, S. E., et al. (2012). Symmetry-breaking intramolecular charge transfer in the excited state of meso-linked BODIPY dyads. *Chem. Commun.* 48, 284–286. doi: 10.1039/C1CC12260F

Wiederrecht, G. P., Svec, W. A., Wasielewski, M. R., Galili, T., and Levanon, H. (2000). Novel mechanism for triplet state formation in short distance covalently linked radical ion pairs. *J. Am. Chem. Soc.* 122, 9715–9722. doi: 10.1021/ja000662o

Williams, J. A. G. (2007). "Photochemistry and photophysics of coordination compounds: platinum," in *Photochemistry and Photophysics of Coordination Compounds II*, eds V. Balzani and S. Campagna (Heidelberg: Springer Berlin Heidelberg), 205–268.

Wong, K. M. C., and Yam, V. W. W. (2007). Luminescence platinum(II) terpyridyl complexes—from fundamental studies to sensory functions. *Coord. Chem. Rev.* 251, 2477–2488. doi: 10.1016/j.ccr.2007.02.003

Wu, W., Cui, X., and Zhao, J. (2013). Hetero Bodipy-dimers as heavy atom-free triplet photosensitizers showing a long-lived triplet excited state for triplet-triplet annihilation upconversion. *Chem. Commun.* 49, 9009–9011. doi: 10.1039/c3cc45470c

Wu, W., Guo, H., Wu, W., Ji, S., and Zhao, J. (2011). Organic triplet sensitizer library derived from a single chromophore (BODIPY) with long-lived triplet excited state for triplet-triplet annihilation based upconversion. *J. Org. Chem.* 76, 7056–7064. doi: 10.1021/jo200990y

Wu, W., Zhao, J., Guo, H., Sun, J., Ji, S., and Wang, Z. (2012a). Long-lived room-temperature near-IR phosphorescence of bodipy in a visible-light-harvesting N∧C∧N Pt^{II}-acetylide complex with a directly metalated BODIPY chromophore. *Chem. Eur. J.* 18, 1961–1968. doi: 10.1002/chem.201102634

Wu, W., Zhao, J., Sun, J., and Guo, S. (2012b). Light-harvesting fullerene dyads as organic triplet photosensitizers for triplet-triplet annihilation upconversions. *J. Org. Chem.* 77, 5305–5312. doi: 10.1021/jo300613g

Xuan, J., and Xiao, W. (2012). Visible-light photoredox catalysis. *Angew. Chem. Int. Ed.* 51, 6828–6838. doi: 10.1002/anie.201200223

Yamazaki, T., Murata, Y., Komatsu, K., Furukawa, K., Morita, M., Maruyama, N., et al. (2004). Synthesis and electrolytic polymerization of the ethylenedioxy-substituted terthiophene-fullerene dyad. *Org. Lett.* 6, 4865–4868. doi: 10.1021/ol048081h

Yang, P., Wu, W., Zhao, J., Huang, D., and Yi, X. (2012). Using C_{60}-bodipy dyads that show strong absorption of visible light and long-lived triplet excited states as organic triplet photosensitizers for triplet–triplet annihilation upconversion. *J. Mater. Chem.* 22, 20273–20283. doi: 10.1039/c2jm34353c

Yang, W., Zhao, J., Sonn, C., Escudero, D., Karatay, A., Yaglioglu, H. G., et al. (2016). Efficient intersystem crossing in heavy-atom-free perylenebisimide derivatives. *J. Phys. Chem. C* 120, 10162–10175. doi: 10.1021/acs.jpcc.6b01584

Yapici, N. B., Jockusch, S., Moscatelli, A., Mandalapu, S. R., Itagaki, Y., Bates, D. K., et al. (2012). New rhodamine nitroxide based fluorescent probes for intracellular hydroxyl radical identification in living cells. *Org. Lett.* 14, 50–53. doi: 10.1021/ol202816m

Yogo, T., Urano, Y., Ishitsuka, Y., Maniwa, F., and Nagano, T. (2005). Highly efficient and photostable photosensitizer based on BODIPY chromophore. *J. Am. Chem. Soc.* 127, 12162–12163. doi: 10.1021/ja0528533

Zhang, X. F., and Feng, N. (2017). Photoinduced electron transfer-based halogen-free photosensitizers: covalent meso-aryl (phenyl, naphthyl, anthryl, and pyrenyl) as electron donors to effectively induce the formation of the excited triplet state and singlet oxygen for BODIPY compounds. *Chem. Asian J.* 12, 2447–2456. doi: 10.1002/asia.201700794

Zhang, X. F., Yang, X., and Xu, B. (2017). PET-based bisBODIPY photosensitizers for highly efficient excited triplet state and singlet oxygen generation: tuning

photosensitizing ability by dihedral angles. *Phys. Chem. Chem. Phys.* 19, 24792–24804. doi: 10.1039/C7CP02645E

Zhao, J., Ji, S., and Guo, H. (2011). Triplet–triplet annihilation based upconversion: from triplet sensitizers and triplet acceptors to upconversion quantum yields. *RSC Adv.* 1, 937–950. doi: 10.1039/c1ra00469g

Zhao, J., Wu, W., Sun, J., and Guo, S. (2013). Triplet photosensitizers: from molecular design to applications. *Chem. Soc. Rev.* 42, 5323–5351. doi: 10.1039/c3cs35531d

Zhao, J., Xu, K., Yang, W., Wang, Z., and Zhong, F. (2015). The triplet excited state of Bodipy: formation, modulation and application. *Chem. Soc. Rev.* 44, 8904–8939. doi: 10.1039/C5CS00364D

Zhou, J., Liu, Q., Feng, W., Sun, Y., and Li, F. (2015). Upconversion luminescent materials: advances and applications. *Chem. Rev.* 115, 395–465. doi: 10.1021/cr400478f

Ziessel, R., Allen, B. D., Rewinska, D. B., and Harriman, A. (2009). Selective triplet-state formation during charge recombination in a fullerene/Bodipy molecular dyad (Bodipy=borondipyrromethene). *Chem. Eur. J.* 15, 7382–7393. doi: 10.1002/chem.200900440

Ziessel, R., and Harriman, A. (2011). Artificial light-harvesting antennae: electronic energy transfer by way of molecular funnels. *Chem. Commun.* 47, 611–631. doi: 10.1039/C0CC02687E

Conflict of Interest: The authors declare that the research was conducted in the absence of any commercial or financial relationships that could be construed as a potential conflict of interest.

Advantages of publishing in Frontiers

OPEN ACCESS
Articles are free to read for greatest visibility and readership

FAST PUBLICATION
Around 90 days from submission to decision

HIGH QUALITY PEER-REVIEW
Rigorous, collaborative, and constructive peer-review

TRANSPARENT PEER-REVIEW
Editors and reviewers acknowledged by name on published articles

Frontiers
Avenue du Tribunal-Fédéral 34
1005 Lausanne | Switzerland

Visit us: www.frontiersin.org
Contact us: info@frontiersin.org | +41 21 510 17 00

REPRODUCIBILITY OF RESEARCH
Support open data and methods to enhance research reproducibility

DIGITAL PUBLISHING
Articles designed for optimal readership across devices

FOLLOW US
@frontiersin

IMPACT METRICS
Advanced article metrics track visibility across digital media

EXTENSIVE PROMOTION
Marketing and promotion of impactful research

LOOP RESEARCH NETWORK
Our network increases your article's readership